ELECTROMECHANICAL STREAMING INSTABILITIES

by

FREDERICK DAVID KETTERER

B.A., University of Pennsylvania
(1954)

M.S., University of Pennsylvania
(1960)

SUBMITTED IN PARTIAL FULFILLMENT OF THE

REQUIREMENTS FOR THE DEGREE OF

DOCTOR OF PHILOSOPHY

at the

MASSACHUSETTS INSTITUTE OF TECHNOLOGY
August, 1965

Signature of Author_____
Department of Electrical Engineering, September 1, 1965

Certified by_____
Thesis Supervisor

Accepted by_____
Chairman, Departmental Committee on Graduate Students

ELECTROMECHANICAL STREAMING INSTABILITIES

by

FREDERICK DAVID KETTERER

Submitted to the Department of Electrical Engineering on September 3, 1965 in partial fulfillment of the requirements for the degree of Doctor of Philosophy.

ABSTRACT

The problem of two highly conducting, finite length streams in relative motion, stressed by a transverse electric or longitudinal magnetic field is examined in detail. The system may be mathematically described by two second order coupled hyperbolic partial differential equations. Four classes of flow exist (1) subcapillary, (2) supercapillary co-streaming, (3) supercapillary counter-streaming, and (4) subcapillary-supercapillary flow. Causal boundary conditions are distinct for each class.

The behavior of the infinitely long system is examined from the dispersion relation and the Bers-Briggs stability criterion. The eigenvalue problem is formulated for class (1), (3) and (4) flows (no eigenvalues exist for class (2) flow) and the complex eigenfrequencies are computed. Experiments on each of these systems are performed and good agreement is obtained between theory and experiment. In addition, the eigenfunctions are computed and agree with the observed trajectories of the streams. Physical explanations are given for the instabilities observed for each class of flow. Complex eigenfrequencies for the specific cases of counter-streaming electron beams and an extended region klystron are presented to point out the analogy which exists between a degenerate form of the magnetically coupled surface waves and electron beams.

Thesis Supervisor: James R. Melcher
Title: Assistant Professor

ACKNOWLEDGEMENTS

This thesis is a continuation of work pioneered by Professor James R. Melcher, in the area of continuum electromechanical surface phenomena.

To him I wish to express my sincerest thanks, as my thesis superviser and good friend. For his untiring patience and understanding during difficulties, his setting a personal example of excellence, and for his enthusiasm and the excitement which he stimulates in others for research, I will always be indebted.

The author wishes to extend his thanks to Professors A. Bers and D. Benney for their interest in this work and for their useful suggestions during the latter part of the thesis. The author had the benefit of many enlightening discussions with other members of the continuum electromechanical energy conversion group; in particular with Professor G. L. Wilson, Dr. A. T. Lewis, Dr. J. Crowley, and Misters E. Devitt, P. Warren, and H. Arndt.

The computor programming and debugging was often facilitated by the help of Miss Martha Pennell and also by Dr. R. Lucchetta. Mr. Felipe Herba was most helpful in providing experimental assistance during much of the experimental work. Special thanks go to Misses Barbara Smith and Susan Johnson for typing the thesis. Miss Diane Staples typed part of the rough draft.

The author would like to thank Educational Services Inc. and Mr. Victor Komow in particular, for providing the author with a copy of the movies and the time sequence photographs used in Chapter 8. The movies were taken for use in the film " Electromechical Waves and Instabilities ", sponsored by the National Science Foundation under the supervision of the National Committee on Electrical Engineering Films. This research was performed under NASA Contract NsG 368. The numerical work was performed at the M.I.T. Computational Center.

TABLE OF CONTENTS

LIST OF FIGURES

LIST OF TABLE

CHAPTER 1

INTRODUCTION

Background

The field of continuum electromechanics is an area of current interest. Magnetohydrodynamics, in particular, has received much recent attention. In this work, the model of a magnetic field interacting with a conducting fluid is of interest. However, the interactions of electric fields with fluids have received comparatively little attention. Those areas in electrohydrodynamics which are of interest include dynamical effects of free charges entrained in fluids and induced effects due to free charges and polarization. Often, problems are encountered in both electrohydrodynamics and magnetohydrodynamics which are similar. This fact will be exploited in the work presented here.

The wave picture provides a useful means of describing the dynamics of continuous media. For example, a fluid interface stressed by an electric field can be conveniently described in this manner. Similarly, Alfven waves are essential to the shearing motions of a conducting fluid in a magnetic field. The usual starting point for studying complicated wave motions is to first consider the medium at rest. One then proceeds to investigate the effect of fluid convection on the dynamical behaviour. This thesis is devoted to a detailed consideration of a class of such phenomena, namely the interaction of two streams of conducting fluid by means of an electric or magnetic field. Quite often the effect of relative motion is to produce instability. Examples of streaming instabilities are found in fluid mechanics (Kelvin-Helmholtz instability), electron dynamics and plasma physics.

One of the difficulties common to almost all streaming instabilities is the complicated model that is required to adequately describe the dynamics. For example, the Kelvin-Helmholtz instability, which arises from the relative motion of adjacent layers of fluid, can be modeled by an inviscid fluid, but gives a naive picture of real fluid dynamics. Experiments involving counterstreaming electron beams are complicated by the presence of a background plasma and are currently the subject of research.

The continuum electromechanical situations considered here can be modeled by a relatively simple theory which provides good agreement with experiment. The electrohydrodynamic model consists of two highly conducting streams in relative motion and coupled by an electric field. Electrical coupling eliminates the difficulty encountered in modeling two real fluids in physical contact. An analogous situation exists in magnetohydrodynamics, in which the electric field is replaced by a magnetic field. Here, the coupling is produced by a magnetic field trapped between two perfectly conducting fluid streams. These situations complement each other and both will be considered here in the same context.

Although this thesis is devoted to a detailed consideration of this seemingly small class of phenomena, yet the implications of the results are broad. Waves are considered to be propagating in the direction of streaming (the longitudinal direction). In general, the imposition of transverse boundaries produces an infinite set of modes of propagation. To solve for these modes, with both longitudinal and transverse boundaries imposed, is an immense problem. The

conventional technique is to assume that wavelengths of interest (in the longitudinal direction) are short compared to the length of the system, so that the effect of longitudinal boundaries is small. Quite often, and in all of the cases examined in this thesis, the long waves are the most significant and play a more important role in determining the dynamics than higher order transverse modes. For this reason, the effects of longitudinal boundaries will be carefully considered. It is possible then to provide a complete picture of the system dynamics. The correct model for the longitudinal boundary conditions can be unambiguously specified. This is not possible in general, since boundary conditions consistent with causality may not be clearly defined.

Related Topics

The equations of an electron beam are the same as the degenerate form of the magnetically coupled surface waves considered here. The problem of counter-streaming electron beams has been experimentally studied by Kofoid[27] to test the theory of Bohm and Gross[8]. With longitudinal boundaries, standing waves of longitudinal plasma electron oscillations were produced. These results are as yet not completely explained.

Chandrasekhar[10] offers an introduction to the classical Kelvin-Helmholtz instabilities. Some recent work has been done on the effect of electric and magnetic fields. Special cases of the hydromagnetic version have been considered by Fejer[16], Michael[37], Northrop[42], Alterman[3], and Sen[44]. The only work done on the electrohydrodynamic Kelvin-Helmholtz instability is by Lyon[32]

who derived the dispersion relation for two streaming dielectric fluids (in contact) stressed by an electric field.

Preview

Because the area of surface-wave electromechanics has not received wide attention, it is well to review the recent work of Melcher[34] on the study of the basic field-coupled surface waves. This work really serves as the starting point in this study of two stream field-coupled systems. Chapter 2 will briefly review the basic waves, particularly the highly conducting field-coupled models. Only these two basic wave types will be considered throughout the thesis. In addition, attention will be focused almost exclusively on the long-wave model and the kink modes of the streams.

In Chapter 3, the two-stream equations of motion are derived. The selection of proper boundary conditions is discussed and the various flow configurations classified. The infinite system behavior for each is discussed from the dispersion relation and the stability determined by the Bers-Briggs[6] criterion. Both electric and magnetic coupling are considered. The remainder of the thesis will be devoted to studying each of these classes in detail with the effect of longitudinal boundaries included. Experiments are performed for three of the classes and compared with theory.

Chapter 4 is devoted to subcapillary flow, and to supercapillary co-streaming flow. The eigenvalue problem is solved and an experiment consisting of two springs in an electric field is described. This experiment allows for the calibration of the field coupling parameters to provide for a quantitative comparison with later experiments. The supercapillary co-streaming class is then discussed.

Chapter 5 is a study of counterstreaming jets. The eigenvalue problem is formulated for the two modes of symmetry and analytical expressions for special cases derived. The eigenvalue equation is solved numerically for the complex eigenfrequencies as a function of system parameters.

In order to better understand the nature of the counter-streaming instability, a degenerate counter-streaming jet problem is formulated and solved for the eigenfrequencies and the eigenfunctions. Comparisons are then made with the electric and the magnetic field coupled cases. Physical arguments are given to explain the static instabilities observed. To obtain a more physical picture of the dynamics, the linear transient response is computed for an initial pulse under both stable and unstable conditions. Finally, the problem of counter-streaming electron beams is considered and the complex eigenfrequencies computed.

An experiment for the electric field coupled counter-streaming jets is described in Chapter 6. The complex eigenfrequency for the lowest mode is measured and the results are compared with theory.

Chapter 7 is a theoretical analysis of Class 4, or stream-structure interactions. The eigenvalue equation is formulated and solved numerically for the complex eigenfrequencies in both the electric and magnetic field cases. The eigenfunctions are computed and discussed. As in the case of counter-streaming jets, the degenerate stream-structure problem is formulated and solved for the eigenfrequencies and compared with the electric and magnetic field cases. A physical argument is given to explain the observed

overstability. Finally, the example of an electron beam-cavity device (klystron) is considered, the eigenfrequencies computed and compared with the magnetic field case.

In Chapter 8, experiments are described which quantitatively verify the electric field coupled stream-structure model of the previous chapter.

CHAPTER 2

ONE STREAM INTERACTIONS

2.1 Introduction

This chapter will be primarily concerned with the effects of electric and magnetic field coupling to a highly conducting, moving, deformable mechanical body. The structure will be modeled very simply to emphasize the electromechanical coupling effects. Part of the material to be presented in this chapter has been developed by J.R. Melcher[†], whose active interest in the area of continuum electromechanics has provided the background and incentive for this thesis. It is worthwhile to review part of it here to provide the foundation for a discussion of two stream phenomena in subsequent chapters.

The various types of field coupled surface interactions will be reviewed to place the scope of the present work in perspective. The linearized equations of motion for the highly conducting models will be derived and dispersion relations discussed. The infinite system stability will be considered by means of a recently developed stability criterion due to Bers and Briggs.[6,9] In order to determine the existance of eigenvalue problems, the method of characteristics will be introduced and appropriate boundary conditions established for the two possible flow conditions. The eigenvalue problems will be solved and an example will be given to show that under certain circumstances, boundaries can produce instabilities. The long wave nonlinear equations of motion will be derived and the nonlinear transient reponse foran electric field coupled system presented. Finally, the equation of motion for the longitudinal oscillations of a cold electron beam will be presented and the close analogy between parallel field magnetically coupled surface waves and longitudinal waves in an electron beam discussed.

---

†For an introduction to the subject of electromechanical surface waves, the reader is encouraged to read J.R. Melcher Field-Coupled Surface Waves, M.I.T. Press, 1963.

The various types of field coupled surface waves have been classified by Melcher[†] as being due to either electric or magnetic fields interacting with surface charges or surface currents. The charges and currents may be either free or bound, so that polarizable and magnetizable media as well as conducting media are included in the classification. This classification is illustrated in Fig. 2.1; the nomenclature is that used by Melcher.

In the EH1f interaction, a transverse electric field is coupled to free charges residing on the surface of the media. This implies a sufficiently high electrical conductivity so that the relaxation time ε/σ is small compared to the time scale of the problem. In this limit, the surface charges are completely mobile and no electric field exists in the bulk of the material. The electrical traction exerted on the surface is destabilizing in character, in that a small upward displacement of the interface increases the electric field, exerting an increase in the upward traction.

The EH1p model is similar to the free charge model except that the surface charges are bound polarization charges. An electric field exists in the media, but if the pressure is suitably redefined, it has been shown[††] that the mechanical equations of motion are uncoupled from the field equations except at the interface. Since the surface charge is proportional to the discontinuity in normal electric field, the polarization surface charge density is weaker than the free charge density for the same conditions, resulting in similar but weaker coupling.

The EH2 configuration couples a tangential electric field to a dielectric media. Although the equilibrium electric field is the same on each side of the interface, there is a traction exerted on the interface due to the discontinuity in polarization. This surface traction can be modeled as a surface

[†]See Reference 34, Chapter 3.

[††]See Reference 34, p. 23.

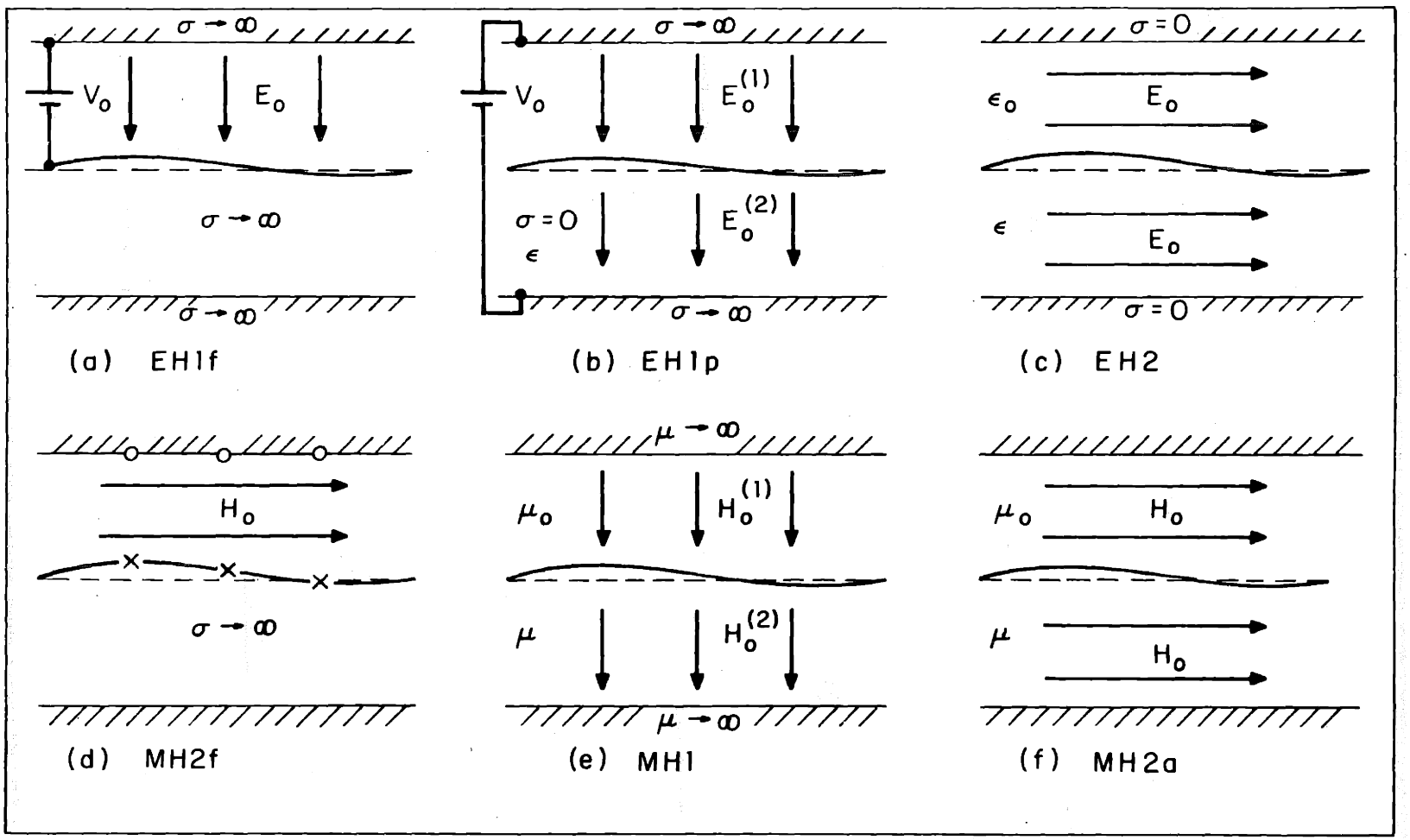

FIGURE 2.1 CLASSIFICATION OF FIELD COUPLED SURFACE WAVES

polarization current, called the Korteweg current, interacting with an electric field in much the same way as Amperian currents interact with magnetic fields in magnetic systems. The perturbation electric traction is stabilizing. Again the mechanical and electrical equations decouple.

The MH2f system couples a tangential magnetic field to a highly conducting media. In this case the currents are assumed to reside on the surface, which puts a lower bound on conductivity as in the EH1f model. Here, however, the diffusion time for the magnetic field (or currents) into the bulk of the material must be long compared to the time scale of the model. The surface traction is stablizing in character by contrast with the EH1f model.

The MH1 model couples a transverse magnetic field to a magnetic media. This system is analogous to the EH1p perpendicular field polarization charge case, and we may consider the surface interaction to be between the transverse magnetic field and bound magnetic charges. The surface traction is destabilizing as in the EH1p model and the equations describing the two systems are identical.

Finally the MH2a case may be modeled by using Amperian currents flowing on the surface of the magnetic media interacting with a parallel magnetic field. Comparison with the EH2 model shows them to be duals, not only in their configuration, but the describing equations and surface tractions are identical in form.

These six basic wave types have been studied by Melcher[††] and others[40,15,49] and all of the models except the MH1 have been verified experimentally. The problem of considering all of the two stream interactions for each of the six field coupled models would indeed be a major task. Some progress has been made on the effect of a magnetic field on the classical Kelvin-Helmholtz instability.[†]

[†]See Chandrasekhar for a general discussion of the Kelvin-Helmholtz instability. Reference 10, Chapter 11.

[††]Reference 34, Chapters 3 and 4.

Chandrasekhar[10] has considered the case of an incompressible fluid with a discontinuity across the interface in density and velocity but not in magnetic field. Some of the restrictions have been removed more recently by Michael[37], Northrop[42], Alterman[3], and Sen.[44] Lyon[32] has considered the electric field Kelvin-Helmholtz instability to the extent of deriving dispersion relations for the case where no free charge is present.

If the fluid-fluid interface is replaced by two fluid streams coupled by an electric or magnetic field, much of the original character of the Kelvin-Helmholtz interaction is preserved. The advantage gained is that simple nondegenerate models can be formulated which can be solved exactly with both transverse and longitudinal boundaries imposed, shedding light on the nature of the Kelvin-Helmholtz instability, the role of electric and magnetic field coupling, and the effect of boundaries. Quantitative experimental verification of the electric field coupled case will be demonstrated to validate the use of these models. The present work will be restricted to a detailed description of the two stream EH1f and the antidual MH2f models. Let us begin, then, with a derivation of the linearized one stream equations of motion.

2.2 Electromechanical Equations

The model of a highly conducting planar fluid surface stressed by a transverse electric field or a longitudinal magnetic field was shown in Fig. 2.1. The equations of motion have been derived by Melcher[†], but because of their use in considering two stream interactions they will be derived here. The model assumes the fluid to be incompressible, homogeneous, and nonviscous.

The fluid equations of motion may be written

$$\nabla\cdot\bar{V} = 0 \tag{2.1a}$$

$$\rho[\frac{\partial\bar{V}}{\partial f} \times (\bar{V}\cdot\nabla)\bar{V}] + \nabla p = \bar{f} \tag{2.1b}$$

[†]See Reference 34, Chapter 2.

where $\bar{f}$ is the body force density.

Since fluid motions are very slow on the time scale of electromagnetic wave propagation, the usual magnetohydrodynamic and electrohydrodynamic approximations will be made. For the quasistatic electric field model, magnetic fields are unimportant and we may write,

$$\nabla \times \bar{E} = 0 \tag{2.2a}$$

$$\nabla \cdot \varepsilon_o E = \rho_f \tag{2.2b}$$

$$\nabla \cdot \bar{J}_f + \frac{\partial \rho_f}{\partial t} = 0 \tag{2.2c}$$

For quasistatic magnetic field processes, the displacement current may be ignored in Ampere's Law and the equations become

$$\nabla \cdot \mu_o \bar{H} = 0 \tag{2.3a}$$

$$\nabla \times \bar{H} = \bar{J}_f \tag{2.3b}$$

$$\nabla \cdot \bar{J}_f = 0 \tag{2.3c}$$

$$\nabla \times \bar{E} = - \frac{\partial \mu_o \bar{H}}{\partial t} \tag{2.3d}$$

2.2.1 Surface conditions

An interface between two fluids is physically a surface that is always composed of the same particles. If $F(x_1,x_2,x_3,t) = 0$ is the equation which defines the position of this surface, then $\frac{dF}{dt} = 0$ is the equation of motion of the surface, or in an Eulerian description,

$$\frac{\partial F}{\partial t} + \bar{V} \cdot \nabla F = 0 \tag{2.4}$$

From (2.4) the equation for the unit normal may be obtained. Since this vector depends only on the orientation of the surface and not on dynamical considerations $\hat{n}$ is purely a function of F. We may write, then

$$\hat{n} = \frac{\nabla F}{|\nabla F|} \tag{2.5}$$

An important consequence of (2.4) and (2.5) is

$$\hat{n} \cdot [\bar{V}^{(1)} - \bar{V}^{(2)}] = 0 \tag{2.6}$$

i.e., the normal velocity is continuous across the interface.

The remaining boundary conditions are shown in Table 2.1 and are found by integrating the bulk equations, (2.1) to (2.3), across an interface.

Table 2.1 Boundary Conditions on a Material Surface

Mechanical		Electrical
$\hat{n} \cdot [\bar{V}] = 0$	Electric	$\hat{n} \times [\bar{E}] = 0$
$\hat{n}\,[p] - \hat{n}\cdot[\bar{\bar{T}}] = 0$		$\hat{n} \cdot [\epsilon\bar{E}] = \sigma_f$
	Magnetic	$\hat{n} \cdot [\mu\bar{H}] = 0$
		$\hat{n} \times [\bar{H}] = \bar{K}_f$
		$\hat{n} \times [\bar{E}] = (V\cdot\hat{n})[\mu\bar{H}]$

where $[Q] = Q^{(2)} - Q^{(1)}$.

In integrating the momentum equation (2.1b), it is convenient to consider the body force $\bar{f}$ as derived from the divergence of a stress tensor. We may write, then[†]

$$f_\alpha = \frac{\partial T_{\alpha\beta}}{\partial x_\beta} \tag{2.7}$$

The quantity $T_{\alpha\beta}$ includes the Maxwell stress tensor and stresses of mechanical origin. The writer has found it useful for physical understanding of the behavior of streaming interactions to take the point of view that electric and magnetic fields exert tractions on surfaces with the surface charges or currents that set up the fields of secondary importance. In this way, the electrical traction plays a role similar to mechanical pressure. The Maxwell stress tensor may be written

[†]Repeated subscripts connotes summation.

$$\underline{\text{Electric}} \quad T_{\alpha\beta} = \varepsilon E_\alpha E_\beta - \frac{1}{2}\delta_{\alpha\beta}\varepsilon E_\gamma E_\gamma$$

$$\underline{\text{Magnetic}} \quad T_{\alpha\beta} = \mu H_\alpha H_\beta - \frac{1}{2}\delta_{\alpha\beta}\mu H_\gamma H_\gamma \tag{2.8}$$

where $$\delta_{\alpha\beta} = \begin{cases} 1 & \alpha=\beta \\ 0 & \alpha\neq\beta \end{cases}$$

The only surface traction of mechanical origin which will be considered in what follows is due to surface tension, which may be written

$$T_{\alpha\beta}^{\,m} = \delta_{\alpha\beta}\, T\left[\frac{1}{R_1} + \frac{1}{R_2}\right] \tag{2.9}$$

where R_1 and R_2 are the radii of curvature of two orthogonal curves lying in the interface.

2.3 The EHlf Planar Jet (free surface charge-electric field model)

The equations derived in the previous section will now be applied to the problem of a highly conducting fluid† jet stressed by a transverse electric field (Fig. 2.2). Gravitational effects will be ignored as will variations in the direction normal to the plane of the paper. The analysis will be further restricted to small perturbations from an equilibrium configuration, so that the equations of motion may be linearized. Equations (2.1) to (2.5) become

$$\underline{\text{Mechanical}} \qquad \nabla \cdot \bar{V} = 0$$

$$\rho_o \left(\frac{\partial \bar{V}}{\partial t} + V_o \frac{\partial \bar{V}}{\partial x_1}\right) + \nabla p = 0 \tag{2.10}$$

$$\underline{\text{Electrical}} \qquad \nabla \times \bar{E} = 0$$

$$\nabla \cdot \bar{E} = 0 \tag{2.11}$$

Since the electrical and mechanical equations are independent, the coupling takes place at the interface. Taking the curl of the momentum equation

†"Highly conducting" here means that the relaxation time ε/σ for free charge to the surface of a conductor is short compared to the shortest characteristic time of the phenomena being considered.

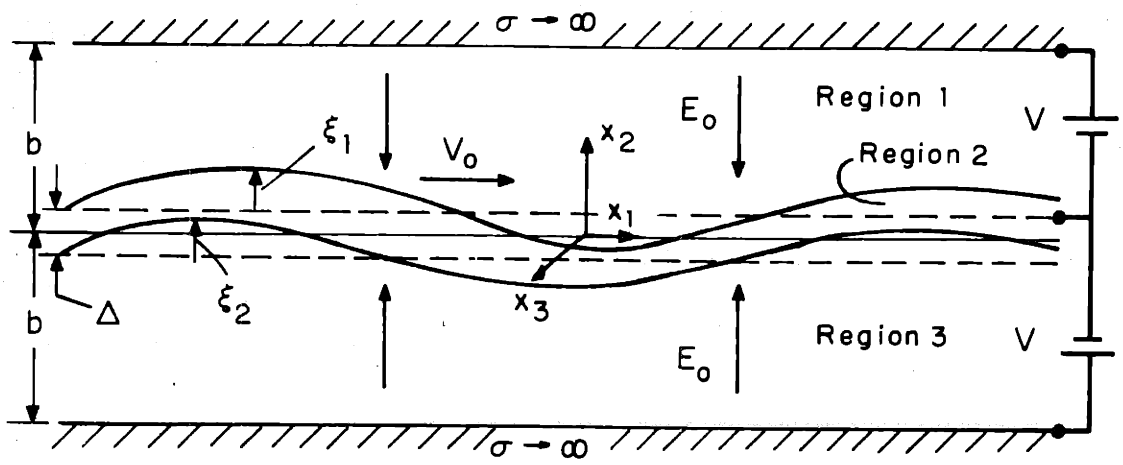

(a) EH1f

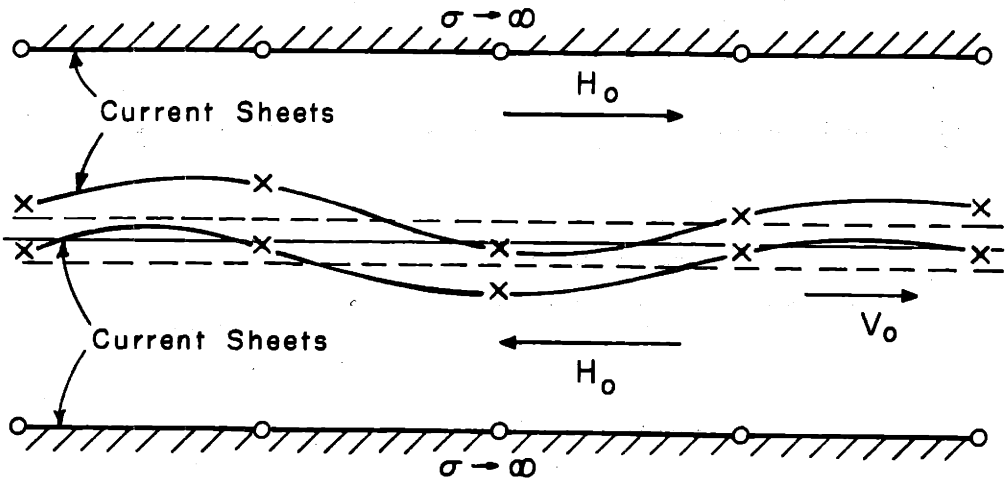

(b) MH2f

FIGURE 2.2 PLANAR MODEL OF A FIELD COUPLED FLUID STREAM

$$\left(\frac{\partial}{\partial t} + V_o \frac{\partial}{\partial x_1}\right)\nabla \times \bar{V} = 0$$

Physically this equation states that the vorticity of any fluid element is time invariant. If the fluid jet exits the nozzle irrotationally, then $\nabla x\bar{V} = 0$. In this case the mechanical and the electrical equations of motion independently satisfy the Laplace equation

$$\nabla^2\bar{V} = 0$$

$$\text{or} \qquad \nabla^2\bar{E} = 0 \tag{2.12}$$

If wavelike solutions are assumed, the variables may be written

$$Q(x_1,x_2,t) = \text{Re}[\tilde{Q}(x_2)e^{j(\omega t-kx_1)}]$$

The solutions to (2.12) may then be written

$$\left(\frac{d^2}{dx_2^2} - k^2\right)\begin{pmatrix}\tilde{V}_2\\ \tilde{E}_1\end{pmatrix} = 0 \tag{2.13}$$

From the solution of (2.13) for $\tilde{V}_2$ and $\tilde{E}_1$, the remaining variables may be obtained from (2.10) and (2.11). For the three regions of Fig. 2.2 the solutions are

<u>Region I</u>

$$\tilde{E}_1(x_2) = A_1 \sinh k(b-x_2) + B_1 \sinh k(x_2-\Delta/2)$$

$$\tilde{E}_2(x_2) = -j[-A_1 \cosh k(b-x_2) + B_1 \cosh k(x_2-\Delta/2)]$$

<u>Region II</u>

$$\tilde{V}_2(x_2) = A_2 \sinh k(\Delta/2-x_2) + B_2 \sinh k(x_2+\Delta/2)$$

$$\tilde{V}_1(x_2) = -j[-A_2 \cosh k(x_2-\Delta/2) + B_2 \cosh k(x_2-\Delta/2)]$$

$$\tilde{p}(x_2) = -j\,\frac{\rho_o(\omega-V_o k)}{k}[-A_2 \cosh k(x_2-\Delta/2) + B_2 \cosh k(x_2+\Delta/2)]$$

<u>Region III</u>

$$\tilde{E}_1(x_2) = A_3 \sinh k(b+x_2) + B_3 \sinh k(-\Delta/2-x_2)$$

$$\tilde{E}_2(x_2) = -j[A_3 \cosh k(b+x_2) - B_3 \cosh k(-x_2-\Delta/2)]$$

The equation of an interface is simply

$$F(x_1,x_2,t) = x_2-\xi(x_1,t) = 0$$

from which we obtain the normal vector using (2.5)

$$\hat{n} = \frac{\hat{i}_2-\hat{i}_1 \frac{\partial \xi}{\partial x_1}}{\sqrt{1+\left(\frac{\partial \xi}{\partial x_1}\right)^2}} \tag{2.15a}$$

or to linear terms,

$$\hat{n} \approx \hat{i}_2 - \hat{i}_1 \frac{\partial \xi}{\partial x_1} \tag{2.15b}$$

The linearized equation of motion of the interface from (2.4) may be written

$$-\frac{\partial \xi}{\partial t} - V_o \frac{\partial \xi}{\partial x_1} + \tilde{V}_2 = 0$$

where $\tilde{V}_2$ is evaluated at the equilibrium position of the interface. Since $\xi(x_1,t) = \mathrm{Re}[\xi_o e^{j(\omega t-kx_1)}]$ we have

$$\tilde{V}_2 = j(\omega-V_o k)\xi_o \tag{2.16}$$

The electrical boundary conditions are obtained from $\hat{n} \times [\bar{E}] = 0$ at each surface. Expanding and linearizing (E_o is the equilibrium electric field)

$$-\frac{\partial \xi}{\partial x_1} E_o - E_1 = 0$$

so that at the boundaries:

$$\begin{aligned} \tilde{E}_1(\pm b) &= 0 \\ \tilde{E}_1(\Delta/2) &= -jkE_o\xi_{o1} \\ \tilde{E}_1(-\Delta/2) &= jkE_o\xi_{o2} \end{aligned} \tag{2.17}$$

Substituting (2.14) into (2.17) and (2.16) the arbitrary constants in terms of the interface displacements ξ_{01} and ξ_{02} are

$$A_1 = \frac{-jkE_o\xi_{o1}}{\sinh k(b-\Delta/2)} \qquad A_2 = \frac{-j(\omega-V_o k)\xi_{o2}}{\sinh k\Delta} \qquad A_3 = \frac{jkE_o\xi_{o2}}{\sinh k(b-\Delta/2)}$$

$$B_1 = 0 \qquad B_2 = \frac{j(\omega-V_o k)\xi_{o1}}{\sinh k\Delta} \qquad B_3 = 0 \tag{2.18}$$

The problem of determining the dispersion equation is now reduced to obtaining two relations involving ξ_{01} and ξ_{02}. These are obtained from the transverse momentum boundary condition at each interface.

$$-\tilde{p}(\tfrac{\Delta}{2}) = T\frac{\partial^2\xi_1}{\partial x_1^2} + T_{21}\left|n_1\right|_{\Delta/2} + T_{22}\left|n_2\right|_{\Delta/2}$$

and

$$\tilde{p}(-\tfrac{\Delta}{2}) = T\frac{\partial^2\xi_2}{\partial x_1^2} - T_{21}\left|n_1\right|_{-\Delta/2} - T_{22}\left|n_2\right|_{-\Delta/2} \tag{2.19}$$

From the Maxwell stress tensor,

$$T_{21} = \varepsilon_o E_1 E_2$$

$$T_{22} = \tfrac{1}{2}\varepsilon_o[E_2^2 - E_1^2]$$

To linear terms the shear traction $T_{21}n_1$ is negligible, and the normal traction becomes

$$T_{22}n_2 \tilde{\sim} \tfrac{1}{2}\varepsilon_o[E_o^2 + 2E_oE_2]$$

The equilibrium electric traction on the surfaces of the jet is accounted for by a reduction of equilibrium pressure in the jet from the surrounding environment by an amount $\frac{1}{2}\varepsilon_o E_o^2$.

Substituting (2.14) and (2.18) into (2.19) and simplifying,

$$\left[(\omega-V_o k)^2 \coth k\Delta - \frac{Tk^3}{\rho_o} + \frac{\varepsilon_o E_o^2 k^2 \coth k(b-\Delta/2)}{\rho_o}\right]\xi_{01} = -\frac{(\omega-V_o k)^2}{\sinh k\Delta}\xi_{02}$$

$$\left[(\omega-V_o k)^2 \coth k\Delta - \frac{Tk^3}{\rho_o} + \frac{\varepsilon_o E_o^2 k^2 \coth k(b-\Delta/2)}{\rho_o}\right]\xi_{02} = -\frac{(\omega-V_o k)^2}{\sinh k\Delta}\xi_{01} \tag{2.20}$$

From (2.20) and Fig. 2.1 it is evident that the x_2 plane is a plane of symmetry. If we define the symmetric and antisymmetric modes as $\xi_{01} = \bar{+}\ \xi_{02} = \xi_{\substack{S\\A}}$, (2.20) becomes

$$(\omega - V_o k)^2 = \left[\frac{k^3 T}{\rho_o} - \frac{\varepsilon_o E_o^2 k^2 \coth k(b-\Delta/2)}{\rho_o}\right] \left[\begin{matrix}\coth(\frac{k\Delta}{2}) \\ \tanh \frac{k\Delta}{2}\end{matrix}\right] ; \left[\begin{matrix}S \\ A\end{matrix}\right] \qquad (2.21)$$

The consequences of this dispersion equation will be discussed after a similar relation is derived for the magnetic field coupled model.

2.4 The MH2f Planar Jet (free surface current-magnetic field model)

The analysis for the MH2f interaction is similar to the EH1f case just considered if the electrical boundary conditions are appropriately modified. In particular (2.14) to (2.16) and (2.19) are unchanged if we simply replace $\tilde{E}_1$ by $\tilde{H}_2$ and $\tilde{E}_2$ by $\tilde{H}_1$.

The electrical boundary condition is $\hat{n}\cdot[\bar{H}] = 0$, applied at each surface. Expanding and linearizing,

$$\tilde{H}_2 - H_o \frac{\partial \xi}{\partial x} = 0$$

where H_o is the equilibrium magnetic field at the boundaries then,

$$\tilde{H}_2(\pm b) = 0$$
$$\tilde{H}_2(\Delta/2) = + jkH_o\xi_{o1}$$
$$\tilde{H}_2(-\Delta/2) = - jkH_o\xi_{o2}$$

This changes the sign of the arbitrary constants A_1 and A_3, the others remaining unchanged. From the Maxwell stress tensor

$$T_{21} = \mu_o H_1 H_2$$
$$T_{22} = \frac{1}{2}\varepsilon_o[H_2^2 - H_1^2]$$

so that to linear terms, the surface traction is

$$T_{21}n_1 \tilde{\approx} 0$$
$$T_{22}n_2 \tilde{\approx} -\frac{1}{2}\mu_o H_o^2 - \mu_o H_o H_1$$

In contrast to the electric field case, the equilibrium magnetic traction increases the static pressure inside the jet above the ambient value. Qualitatively speaking, one could state that transverse electric fields pull while longitudinal magnetic fields push on a highly conducting surface, but these facts are as much connected with the constraints imposed on the fields as with the type of field.

Making the necessary substitutions into (2.19) the following dispersion relation is obtained

$$(\omega - V_o k)^2 = \left[\frac{k^3 T}{\rho_o} + \frac{\mu_o H_o^2 k^2 \coth k(b-\Delta/2)}{\rho_o}\right] \begin{bmatrix} \coth \frac{k\Delta}{2} \\ \tanh \frac{k\Delta}{2} \end{bmatrix} ; \begin{bmatrix} S \\ A \end{bmatrix} \qquad (2.22)$$

2.5 The Dispersion Equations

It is evident that the symmetric and antisymmetric modes for each configuration are of the same form, except for the term tanh $k\Delta/2$, which depends only on the ratio of jet thickness to perturbation wavelength. For $\frac{k\Delta}{2} >> 1$, (short wave limit) the S and A modes become identical and the interfaces of the jet become uncoupled in their motion. The jet, then is effectively infinitely thick.

If the thickness Δ is made much smaller than wavelengths of interest, $\tanh \frac{k\Delta}{2} \longrightarrow \frac{k\Delta}{2}$ and the interfaces couple strongly.. The right hand side of the above dispersion equations becomes much larger for the antisymmetric mode (commonly called kink mode) than the symmetric (or sausage) mode. The symmetric mode is highly dispersive, even without electric or magnetic field coupling. An investigation of the modes on a thin sheet of fluid without field coupling has been carried out by G.I. Taylor[50].

On physical grounds, one would expect that the kink mode should exhibit much larger deflections than the sausage mode, since for a thin jet, the largest deflection which the latter mode can experience before being pinched off is $\Delta/2$. It is quite advantageous from the observational point of view to allow the deflections to become large. Whether linear theory can predict the proper

behavior for deflections larger than $\Delta/2$ remains to be seen. Experiments and nonlinear analysis indicate that the important measure of nonlinearity is $[\xi/b-\Delta/2]$ and that deflections considerably larger than $\Delta/2$ can be predicted by linear theory. As a result our main concern will be with the antisymmetric mode.

If the wavelengths of interest are much longer than the transverse plate spacing (more precisely $k(b-\Delta/2)<<1$) then the dispersion relations (2.21) and (2.22) take on a simple form.

$$\begin{aligned} &\text{EH1f} \qquad (\omega-V_o k)^2 = V_t^2 k^2 - \omega_e^2 \\ &\text{EH2f} \qquad (\omega-V_o k)^2 = V_t^2 k^2 + \omega_h^2 \end{aligned} \tag{2.23}$$

where

$$V_t = \frac{2T}{\rho\Delta} \ , \ \omega_e = \frac{2\varepsilon_o E_o^2 (b-\Delta/2)}{\rho\Delta} \ , \ \omega_h = \frac{2\mu_o H_o^2 (b-\Delta/2)}{\rho\Delta}$$

Without an applied field the jet behaves as a vibrating string travelling with a velocity V_o. To examine the effects of field coupling the dispersion relations (2.23) are plotted in Fig. 2.3. At high frequencies, the effect of the field coupling is weak and becomes negligible as $\omega \longrightarrow \infty$ independent of the type of field coupling or the jet velocity. The wavelength at high frequencies is short and the surface tension restoring force, proportional to the curvature of the jet is strong and dominates the traction exerted by the field. As the frequency is reduced, the electrical traction is unaltered, but the restring force becomes weaker, and the effect of the field becomes important.

For EH1f subcapillary systems ($V_o<V_t$) the wavelength is real for all real frequencies, indicating a propagating wave response <u>if the system can be excited in the sinusoidal steady state</u>. For decreasing wave number, a critical value is reached at which the frequency becomes complex, indicating an instability (the type of instability will be determined in the next section). The growth

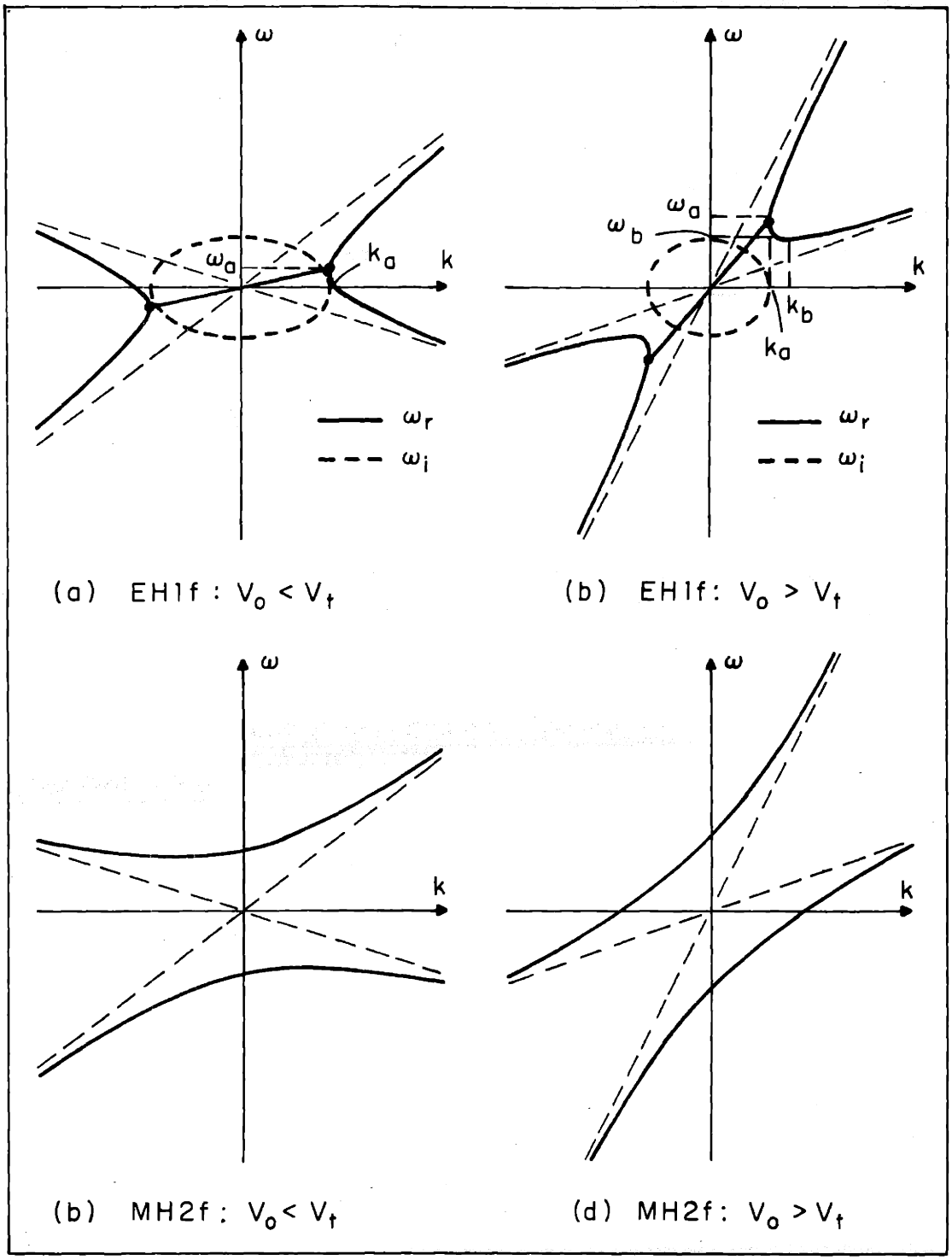

FIGURE 2.3 DISPERSION CURVES FOR A FIELD COUPLED STREAM

rate of this instability increases to a maximum value of ω_e as $k \rightarrow 0$.

The EH1f supercapillary case, Fig. 2.3b, also exhibits an instability at the same wavelength and has the same maximum growth rate as for subcapillary flow, but an important difference is that if a steady state exists, the system exhibits a spatial growth or decay for frequencies below $\omega = \omega_b$. Whether the system exhibits spatial amplification or evanescence (decay) will also be taken up in the next section. The nature of the instability should be evident; since the electric traction is destabilizing in character, if the wavelength becomes too large, the mechanical force is no longer able to provide a sufficient force to restore equilibrium.

The MH2f subcapillary flow mode also exhibits either spatial growth or decay for low frequency; the supercapillary case, however shows only propagating behavior. No instabilities are present. This fact is also clear since the magnetic traction exerts a stabilizing force on the jet. We should now try to specify more precisely the type of instability and to distinguish between spatial growth and decay mentioned above.

2.6 The Bers Briggs Criterion for Infinite System Stability

While this thesis is primarily concerned with electromechanical streaming instabilities with finite longitudinal dimensions, it is useful, although certainly not necessary, to have knowledge about the limiting case when the boundaries are removed to infinity. Mathematical criteria have been developed which enable one to distinguish absolute and convective instabilities, evanescent waves, and the direction of signal flow in propagating waves. The proof will be omitted, only the procedure and physical interpretation will be discussed.†

†For a clear brief description of the criteria, the reader is encouraged to read A. Bers, R.J. Briggs "Criteria for Determining Absolute Instabilities and Distinguishing Between Amplifying and Evanescent Waves", QPR #71 RLE,MIT, October 15, 1963 pp. 122-130. For a more complete treatment, see Briggs Electron Stream Interaction with Plasmas, MIT Press, 1964.

Consider a linear, time invariant system, uniform in the spatial dimension x. If solutions of the form $e^{j(\omega t-kx)}$ are assumed, the solution is described by the resulting dispersion relation $D(\omega,k) = 0$ where ω,k are in general complex. The problem then is to determine the meaning of the various dispersion equation solutions. The procedure consists of two parts: (1) the complex frequencies are computed from $D(\omega,k)$ for values of k along the real k axis. Those frequencies having a negative imaginary part represent, in principle, potentially unstable waves. Let the most negative value be ω_{is}. This represents the maximum possible growth rate the system can have.

The second part of the procedure consists in plotting the complex k loci for complex frequencies $\omega = \omega_r + j\omega_i$, ω_r is fixed and ω_i is increased from a point below ω_{is} to zero. The behavior of the system at the frequency ω_r is determined by the behavior of the k loci. The frequency ω_r is then incremented and ω_i varied as before. In this way the system behavior is determined for all ω_r. The interpretation of the loci is as follows: for large $-\omega_i$, the k values represent waves decaying away from some finite source, so that those k's lying below the k_r axis are waves existing to the right of the source, those above, to the left of the source. As ω_i is increased to zero, the k's will also move. For k's originating below the k_r axis, if a k locus remains below the k_r axis when $\omega_i = 0$ it remains a decaying or evanescent wave; if it lies on the axis, it is a purely propagating wave to the right, and if it crosses the axis, it becomes an amplifying wave or convective instability. For k's originating above the k_r axis, the same statement is valid, but now they represent waves to the left of the source. Whether k's from the same side of the k_r axis join and split, or cross the k_r axis and return is not important.

The one situation which has not been mentioned is the merging of a k from above and one from below and splitting apart, forming a saddle point in the

complex k plane. This behavior is characteristic of an absolute instability. The imaginary part of the frequency is the temporal growth rate; if the real part of the saddle frequency is zero, the instability is said to be a static instability; otherwise it is an over stability. The saddle wave number describes the spatial character of the instability.

As an illustration of the procedure, the dispersion relations for the EH1f and MH2f single jet will be examined for stability. There are four plots to be considered, since the jet may be subcapillary or supercapillary.

Applying the Bers-Briggs criterion, three appropriate values of ω_r have been selected and the k loci plotted in Fig. 2.4. From symmetry the plots for $\pm\omega_r$ are identical. From Fig. 2.4a the subcapillary electric field coupled jet is statically unstable at infinite wavelength. This should be expected on physical grounds, since for k = 0, the surface tension provides no restoring force and hence the slightest electric field makes the system unstable.

If however the jet is moving with a velocity $V_o > V_t$, then while the displacement of a particle on the jet will grow exponentially in time in the reference frame of the jet, in the laboratory frame there will be a spatial growth or convective instability, as observed in Fig. 2.4b.

Contrasting the transverse electric field systems, which are destabilizing in character, longitudinal magnetic fields are stabilizing, exerting a restoring traction on the jet. If the wavelength is sufficiently long, the magnetic restoring force effectively overpowers the wave to produce evanescent waves for subcapillary flow. If the jet is supercapillary however, (Fig. 2.4d) the evanescent wave will appear as a propagating wave in the laboratory frame.

It might be pointed out that for subcapillary flow there exists a saddle point, but it occurs at $\omega = \frac{\omega_h}{V_t}\sqrt{V_t^2 - V_o^2}$, so that the system is purely propagating. This is the natural frequency at which the infinite system would

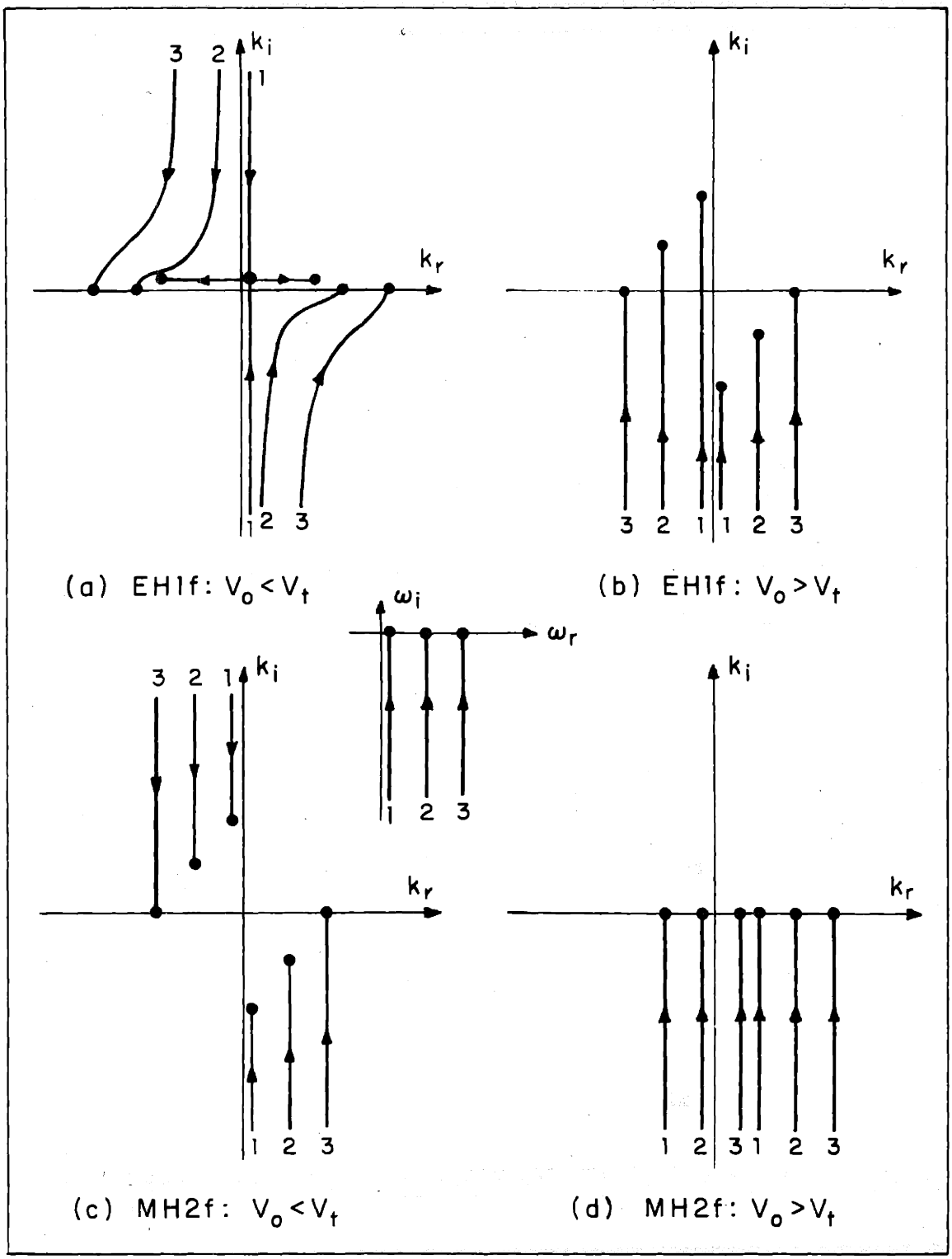

FIGURE 2.4 INFINITE SYSTEM STABILITY CURVES FOR A FIELD COUPLED STREAM USING THE BERS-BRIGGS CRITERION.

resonate if excited.

2.6.1 Physical interpretation

A physical argument for the Bers-Briggs criterion may help to clarify the situation. Consider that the system is driven in a small region of space at a complex frequency with a large temporal growth rate. If this growth rate is larger than the growth rate of any absolute instabilities of the system, then all waves must decay away from the source. This means that the k loci below the k_r axis represent waves to the right of the source, those k's above the axis represent waves to the left of the source. If the source growth rate is reduced to zero without the system exhibiting any absolute instabilities, then the system can be driven in the sinusoidal steady state. Since the identity of each k locus has been maintained, the final positions corresponding to $\omega = \omega_r + j0$ determines whether the system is convectively unstable, propagating, or evanescent, by the values of k_i.

If the system exhibits an absolute instability, the saddle point may be interpreted as taking place when a wave to the right and a wave to the left of the source assume the same k value. When this happens, the source may be removed and the waves joined smoothly to form a natural mode of the system. If this occurs for $\omega_i < 0$, the natural mode is unstable.

2.7 The Method of Characteristics

The method of characteristics is a very powerful mathematical tool for propagating systems since it answers two fundamental questions: (1) what type of boundary conditions does one have a right to impose on a system and insure that the solutions be valid as time progresses and (2) what is the transient behavior, for either a linear or nonlinear system, to an arbitrary initial or driven input. In particular, once the question of boundary conditions has been

settled, one may wish to investigate the stability of the model in a situation where it might be quite difficult or impossible to handle analytically. What will be said below is not intended to be a general discussion of the method of characteristics, but rather an application to the problem at hand.

Consider the second order partial differential equation

$$A \frac{\partial^2 \xi}{\partial x^2} + B \frac{\partial^2 \xi}{\partial x \partial t} + C \frac{\partial^2 \xi}{\partial t^2} = D \tag{2.24}$$

where A, B, C, D may be functions of $x,t,\xi, \frac{\partial \xi}{\partial x_1} \frac{\partial \xi}{\partial t}$ but not higher derivatives, and we pose the following question: do there exist solution curves in the x,t plane such that the partial differential equation may be reduced to the solution of ordinary differential equations. Such lines are called characteristic lines.

To examine this, factor the left hand side of (2.24)

$$C \left[\frac{\partial}{\partial t} + g_1 \frac{\partial}{\partial x}\right]\left[\frac{\partial}{\partial t} + g_2 \frac{\partial}{\partial x}\right]\xi = D \tag{2.25}$$

where g_1 and g_2 are for the moment assumed to be real functions and define a dummy variable u equal to one of the factors

$$u = \frac{\partial \xi}{\partial t} + g_2 \frac{\partial \xi}{\partial x} \tag{2.26}$$

The right hand side of (2.26) can be written as an exact differential if $g_2 = \frac{dx}{dt}$ so that we may write

$$u = \frac{\partial \xi}{\partial t} + \frac{\partial \xi}{\partial x} \frac{dx}{dt} = \frac{d\xi}{dt} \tag{2.27}$$

The quantity g_2 defines a family of lines in the x,t plane and will be designated the physical or type I characteristics. Integrating

$$x = \int g_2 \, dt + C_I^+ \tag{2.28}$$

Specifying the constant C_I^+, then determines which one of the family of type I characteristics is being considered.

Equation (2.27) may also be integrated, using the restriction imposed by (2.28)

$$\xi = \int u\,dt + C_{II}^{+} \qquad \text{along } C^{+} \tag{2.29}$$

In general (2.28) and (2.29) must be solved simultaneously.

While we have focused our attention on the second factor of (2.26) it is clear that either factor exhibits the same behavior, so that there are two families of type I characteristics and correspondingly two families of type II characteristics. Summarizing,

$$x = \int g_2\,dt + C_I^{+} \qquad \xi = \int u\,dt + C_{II}^{+} \quad \text{along } C_I^{+}$$

$$x = \int g_1\,dt + C_I^{-} \qquad u = \int D/C\,dt + C_{II}^{-} \quad \text{along } C_I^{-}$$

The solution has thus formally been obtained; although not in a very suitable analytic form, it is quite amenable to numerical calculation.

Returning to (2.24), if g_1 and g_2 are real, then $(g_1-g_2)^2 > 0$, or in terms of the original coefficients

$$B^2 - 4AC \geq 0$$

The reverse procedure can also be demonstrated. This is the inequality commonly written which must be satisfied to guarantee that real characteristics exist.

2.7.1 Causality and Specification of Boundary Conditions

If the functions g_1 and g_2 are functions of x and t only, the problem simplifies substantially, for then the type I characteristics can be found directly, and hence the type II characteristics. If we anticipate the derivation of the long wave nonlinear equation of motion in section 2.10 (equation 2.37) the above equations become very simple.

$$x = (V_o + V_t)t + C_I^{+} \qquad \frac{\xi}{b-\Delta/2} = \int u\,dt + C_{II}^{+} \quad \text{along } C_I^{+}$$

$$x = (V_o - V_t)t + C_I^{-} \qquad u = \omega_e^2 \int \left[\frac{1}{\left(1-\frac{\xi}{b-\Delta/2}\right)^2} - \frac{1}{\left(1+\frac{\xi}{b-\Delta/2}\right)^2}\right]dt + C_{II}^{-}$$

along C_I^{-}

where $V_1(t) = V_o$.

The type I characteristics are simply two families of straight lines in the x,t plane and can be constructed independently of the type II characteristics.

If one carries out the necessary integrations of (2.30), what kind of boundary conditions are required to uniquely specify the problem will become apparent. Let the type I characeristics be as shown in Fig. 2.5. The type II equations will be approximately integrated, assuming the time interval $dt \approx \Delta t$ and the integrand may be approximated as the average of the values at the ends of the characteristic line segment. Along the C_I^+ characteristic we may write

$$\frac{\xi(C) - \xi(B)}{b-\Delta/2} \approx \frac{1}{2}[u(C) + u(B)]\Delta t$$

and along the C_I^- characteristic $u(C) - u(A) \approx \frac{1}{2}[f(C) + f(A)]\Delta t$

$$\text{where} \qquad f(P) = \omega_e^2 \left[\frac{1}{\left[1 - \frac{\xi(P)}{b-\Delta/2}\right]^2} - \frac{1}{\left[1 + \frac{\xi(P)}{b-\Delta/2}\right]^2}\right]$$

These equations may be solved numerically to obtain $\xi(C)$ and $u(C)$. It is assumed that ξ and u are known along the axis $t = 0$; in other words, two initial conditions are required to start the solution. Note that in order to have causal solutions one must integrate forward in time. It is clear that the values of the variables at C are completely determined from a knowledge of the variables at A and B. The triangle ABC is commonly called the domain of dependence for point C and is bounded by the characteristic lines passing through C going backward in time. Since the solution is generated by integrating along characteristic lines, a given point, say A, can affect all points in space at a later time which lie within the characteristic lines passing through A. Such region is called the range of influence of point A.

One might get the feeling that the characteristic lines are related to the propagation of pulses in a system. Such is in fact a valid interpretation.

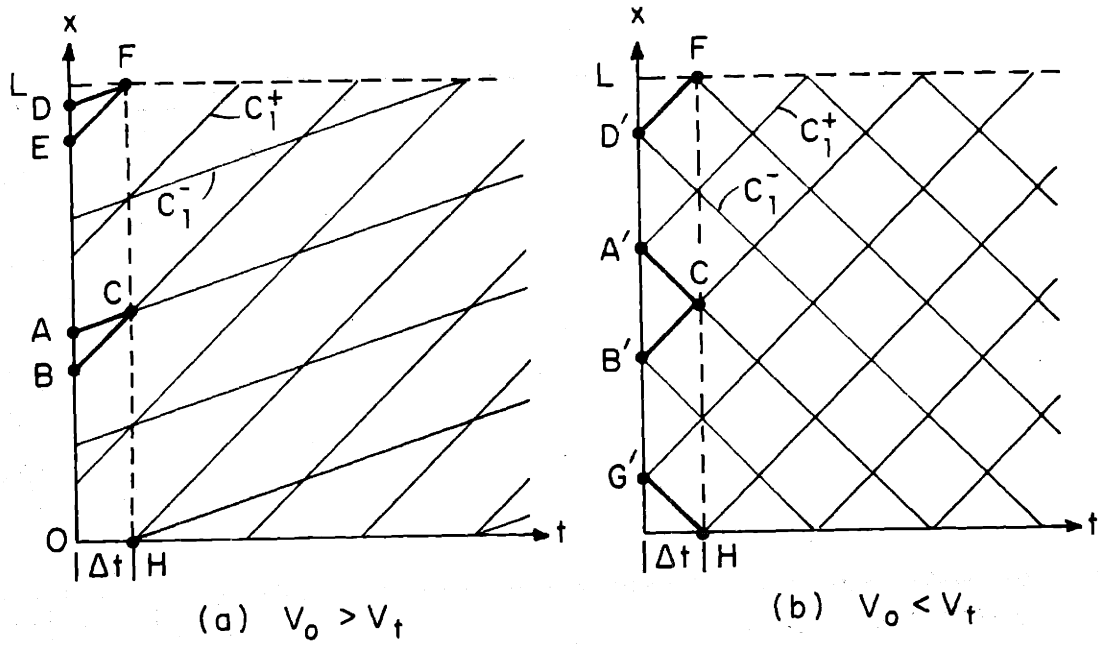

FIGURE 2.5 CHARACTERISTIC LINES IN THE x,t PLANE FOR A (a) SUPERCAPILLARY AND (b) SUBCAPILLARY JET.

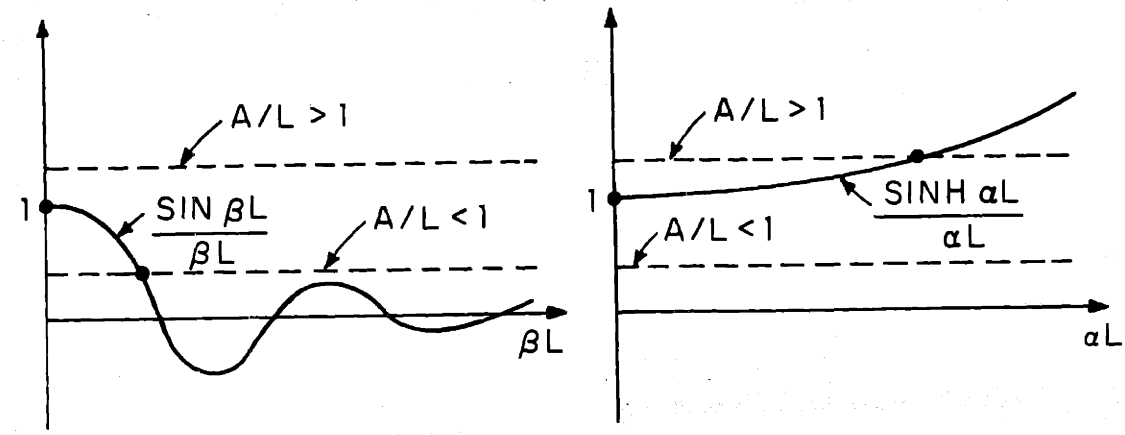

FIGURE 2.6 GRAPHICAL REPRESENTATION OF THE EIGENVALUE EQUATION FOR THE EXAMPLE OF AN ACTIVE BOUNDARY.

In Fig. 2.5 a pulse originating at point A will spread out affecting all points lying within the characteristic lines passing through A for increasing time and continuing until a boundary is reached. The pulse thus propagates both upstream and downstream, typical of subcapillary flow ($V_o < V_t$). If on the other hand $V_o > V_t$ (supercapillary flow), the pulse at A spreads out as before, but this region of influence lies downstream of the original point A. The information at point A has thus been swept downstream and has no means of returning to point A except possibly by means of the external constraints, which shall now be considered.

Consider in Fig. 2.5b that we wish to find the solution at point F ($x = L$) at which a boundary exists (point D having been specified). Because of the boundary, no solution exists for $x > L$. From (2.38), along the C_I^+ characteristic

$$\xi(F) - \xi(D') \overset{\sim}{\sim} \frac{1}{2}[u(F) + u(D')]\Delta t$$

but there is no corresponding equation for the C_I^- characteristic. In order to have a unique solution, either $\xi(F)$ or $u(F)$ (or some combination) must be specified. Only one such specification is allowed, else the problem be over determined. Therefore one boundary condition is required at $x = L$. If we now consider the solution at point H, it is evident that the same argument is valid as for F, and again one boundary condition is required. One can state quite generally that for subcapillary flow the necessary and sufficient boundary conditions are one condition at each end of the system.

For supercapillary flow the situation is quite different. To compute the solution at point F on the boundary $x = L$ from points D and E is straight forward and follows in the same way as the calculation for point C. Since F is then determined, no boundary conditions may be imposed at $x = L$. Finally consider the solution for point H. This point cannot be reached by any

characteristic lines originating along the x axis between $0 \leq x \leq L$. This means point H must be specified. We may conclude therefore that for supercapillary flow the necessary and sufficient boundary conditions are specified with two upstream and none downstream.

2.8 The Eigenvalue Problem

In the previous section the stability of the infinite system was discussed, and from the remarks made concerning boundary conditions, a subcapillary jet possesses boundary conditions at two points in space and hence represents an eigenvalue problem. From the long wave linearized equations for the electric and magnetic field coupled systems,

$$\underline{\text{Electric}} \qquad \left(\frac{\partial}{\partial t} + V_o \frac{\partial}{\partial x}\right)^2 \xi = V_t^2 \frac{\partial^2 \xi}{\partial x^2} + \omega_e^2 \xi \qquad \underline{\text{Magnetic}} \qquad \left(\frac{\partial}{\partial t} + V_o \frac{\partial}{\partial x}\right)^2 \xi = V_t^2 \frac{\partial^2 \xi}{\partial x^2} - \omega_h^2 \xi \tag{2.31}$$

Assuming solutions of the form $\xi(x,t) = \mathrm{Re}\hat{\xi}(x)e^{j\omega t}$, the equation in k is second order and has the solution

$$\hat{\xi}(x) = A\, e^{-jk_1 x} + Be^{-jk_2 x}$$

For rigid ends, $\hat{\xi}(0) = \hat{\xi}(L) = 0$ so that $e^{-jk_1 L} = e^{-jk_2 L}$

The only solution is $k_1 = k_2 + \frac{2n\pi}{L}$ (2.32)

If (2.32) is combined with the dispersion equation, we obtain a single equation involving ω and L.

$$\underline{\text{Electric}} \qquad \omega^2 = \frac{(V_t^2 - V_o^2)^2}{V_t^2}\left(\frac{n\pi}{L}\right)^2 - \frac{\omega_e^2(V_t^2 - V_o^2)}{V_t^2} \qquad \underline{\text{Magnetic}} \qquad \omega^2 = \frac{(V_t^2 - V_o^2)}{V_t^2}\left(\frac{n\pi}{L}\right)^2 + \frac{\omega_h^2(V_t^2 - V_o^2)}{V_t^2} \tag{2.33}$$

It is clear from (2.33) that the end conditions exert a stabilizing effect on the electric system. In the limit as $L \to \infty$, we obtain the saddle frequency mentioned earlier. As L is decreased for fixed electric field, each mode becomes

stable in turn for

$$\frac{\omega_e L}{\sqrt{V_t^2 - V_o^2}} = n\pi$$

and the lowest mode (n = 1) is the most difficult one to stabilize. The effect of boundaries on the magnetic coupled jet is to raise the resonant frequency above the saddle frequency; the system is stable.

These results could have been predicted on physical grounds. If the field is turned off both electric and magnetic jets degenerate to the same mechanical system. As field is applied, since the electric traction acts in the direction of displacement, it opposes the spring restoring force, effectively making it a weaker spring, and the resonant frequency is decreased. The wavelength of course is unaffected, since the ends are fixed. The opposite effect takes place for magnetic coupling, the traction aids the spring tension, effectively stiffening the spring, and the resonant frequency is increased.

One might wonder if the effect of boundaries is always stabilizing in nature; i.e, is it possible that boundaries could produce instabilities where none existed or increase the growth rate of an instability above the saddle point growth rate? A simple example helps to answer this question.

2.9 Example of a Destabilizing Boundary

Consider a vibrating string with one end tied down and the other end given a displacement $\xi(\ell) = A \frac{\partial \xi}{\partial x}(0)$. In other words, the slope of the fixed end is deflected and used to fix the position of the opposite end. The constant A is a measure of the gain of the feedback loop. The equation of motion is simply

$$\frac{\partial^2 \xi}{\partial t^2} = V_t^2 \frac{\partial^2 \xi}{\partial x^2}$$

and the solutions are $\hat{\xi}(x) = B_1 \cos kx + B_2 \sin kx$

Applying the boundary conditions, $B_1 = 0$ and $\frac{\sin k\ell}{k\ell} = A/\ell$ (2.34)

Equation (2.34) is plotted graphically in Fig. 2.6 for k real and k imaginary. For $A/\ell < 1$, there is at least one intersection point indicating these modes to be stable, but we should expect to find an infinite set of eigen modes. The answer is that higher modes have complex k, with one unstable, since $\omega = \pm V_t k$ from the dispersion relation. For $A/\ell > 1$, even the lowest mode is unstable, since k is imaginary.

To show that solutions of (2.34) exist for complex k, let $k\ell = \beta + j\alpha$. Equation (2.34) then splits into the real and imaginary parts

$$\frac{\sin\beta}{\beta}\cosh\alpha = A/\ell \text{ (a) and } \cos\beta\,\frac{\sinh\alpha}{\alpha} = A/\ell \quad \text{(b)} \qquad (2.35)$$

Consider the higher modes, so that β and α are large. For large α, $\frac{\sinh\alpha}{\alpha} \to e^{\alpha}/\alpha$ is large and $\cos\beta \approx (n + \frac{1}{2})\pi$. Then from (2.35a),

$$\frac{\sin(n + \frac{1}{2})\pi}{(n + \frac{1}{2})\pi}\; e^{\alpha} \approx A/\ell$$

or

$$\alpha \approx \ln[(2m + \tfrac{1}{2})\pi\,\frac{A}{\ell}] \quad \text{and} \quad n = 2m$$

The argument may be extended for $A < 0$ as well, so that the system is unstable for any real value of A. Since there is a saddle point which is not unstable without boundaries, we have a case where the saddle point growth rate is exceeded by growth rates found with boundaries.

To preview the results of later chapters when the effects of passive boundaries on two stream systems will be considered, the author has found no instances of temporal growth rates larger than the saddle point growth rate, provided an unstable saddle point exists. This is not to suggest that passive boundaries cannot produce an absolute instability; indeed examples will be given where a

convective instability in the infinite system is transformed into an over-stability when the system is of finite length.

2.10 The Nonlinear Long Wave Jet

We would like at this time to go back and take up the question of how large displacements can become for a valid linear theory, and to consider what effects nonlinearities have on the dynamics. To derive meaningful expressions for the two dimensional model is untractable; but if the analysis is restricted to the lowest transverse eigen mode, it is possible to obtain useful quasi-one-dimensional equations. In this limit the perturbation wavelength is long compared to all transverse dimensions, so that variations in the x_1 direction are small compared to variations in the transverse (x_2) direction.

The derivation is somewhat simplified if we take advantage of the symmetry discussed earlier. Only the nonlinear long wave equation of motion for the antisymmetric mode will be derived. The results for the symmetric mode indicate that the system is not hyperbolic and the method of characteristics is not applicable for the nonlinear transient response.

Since the two interfaces move in unison for the antisymmetric mode, the transverse velocity is independent of the transverse coordinate for long waves. In addition we should expect that the transverse electric field be independent of the transverse coordinate because of the very gradual slope of the interface. The longitudinal field component is small compared to the transverse component. We shall assume therefore,

$$V_2 \neq V_2(x_2)$$

$$E_2 \neq E_2(x_2)$$

and

$$\left|\frac{E_1}{E_2}\right| \ll 1, \quad \left|\frac{n_1}{n_2}\right| \ll 1$$

The equation of motion may be conveniently derived by using the integral form of (1.1) and (1.2), which may be written

$$\frac{\partial}{\partial t}\int_{CV}\rho dV + \oint_{CS}\rho\bar{V}\cdot\hat{n}\,dA = 0$$

and

$$\frac{\partial}{\partial t}\int_{CV}\rho\bar{V}dV + \oint_{CS}\rho\bar{V}(\bar{V}\cdot\hat{n})dA + \oint_{CS}p\hat{n}dA = \oint_{CS}\bar{\bar{T}}\cdot ndA$$

The control volume to be used is fixed in space. Carrying out the integration of the continuity equation

$$0 = \rho(V_1(x_1+\delta x_1) - V_1(x_1))$$

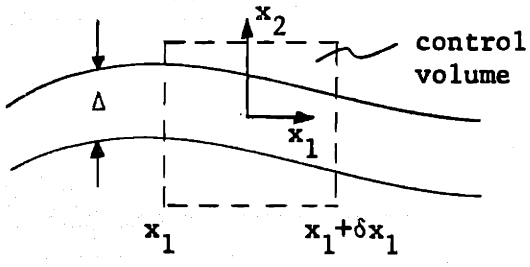

or V_1 is independent of x_1.

Next consider the normal component of momentum equation, using the assumption on the normal velocity.

$$\rho\Delta\,\delta x_1\frac{\partial V_2}{\partial t} + \rho\Delta V_1[V_2(x_1+\delta x_1) - V_2(x_1)] = 2T\frac{\partial^2\xi}{\partial x_1^2}\delta x_1 + ([T_{21}]n_1+[T_{22}]n_2)\delta x_1$$

The factor 2T arises because the surface tension of each interface makes an equal contribution. Using the equation of motion of an interface, (2.4), the above equation may be rewritten

$$\left(\frac{\partial}{\partial t} + V_1\frac{\partial}{\partial x_1}\right)^2\xi = \frac{2T}{\rho\Delta}\frac{\partial^2\xi}{\partial x_1^2} + \frac{1}{\rho\Delta}\{[T_{21}]n_1 + [T_{22}]n_2\} \qquad (2.36)$$

The transverse electric field component may be found simply in the long wave limit if the field region is viewed as a pair of capacitor plates one of which is slightly deformable. The field is then

$$V = -\int_{\Delta/2+\xi}^{b} E_2 \, dx_2$$

or

$$E_2 = \frac{-V}{b-\frac{\Delta}{2}-\xi} \quad \text{upper field region}$$

and

$$E_2 = \frac{V}{b-\frac{\Delta}{2}+\xi} \quad \text{lower field region}$$

The normal electric traction $[T_{22}]n_2$ becomes

$$[T_{22}]n_2 = \frac{1}{2}\,\epsilon_o V^2 \left[\frac{1}{(b-\frac{\Delta}{2}-\xi)^2} - \frac{1}{(b-\frac{\Delta}{2}+\xi)^2}\right] \frac{1}{\sqrt{1+|\frac{\partial \xi}{\partial x_1}|^2}}$$

Since the slope of the interface is assumed very small $|\frac{\partial \xi}{\partial x_1}| \ll 1$ and may be ignored. The shear traction $[T_{21}]n_1$ is clearly of no consequence in the problem. Equation (2.37) then becomes

$$[\frac{\partial}{\partial t} + V_1 \frac{\partial}{\partial x_1}]^2 \frac{\xi}{b-\Delta/2} = V_t^2 \frac{\partial^2 \xi/b-\Delta/2)}{\partial x_1^2} + \omega_e^2 \left[\frac{1}{(1-\frac{\xi}{b-\Delta/2})^2} - \frac{1}{(1+\frac{\xi}{b-\Delta/2})^2}\right]$$

where as before $V_t^2 = \frac{2T}{\rho\Delta}$ and $\omega_e^2 = \frac{2\epsilon_o V^2}{\rho\Delta(b-\frac{\Delta}{2})^3}$

We observe that the only nonlinear term is the field coupling. The velocity $V_1(t)$ is really a decoupled variable and would be specified in the problem. From (2.37) it is evident that for $\frac{\xi}{b-\Delta/2} \to 1$, the field coupling term can be quite large and exert a strong destabilizing force on the system. If (2.37) is linearized, then

$$(\frac{\partial}{\partial t} + V_1 \frac{\partial}{\partial x_1})^2 \xi = V_t^2 \frac{\partial^2 \xi}{\partial x_1^2} + \omega_e^2 \qquad (2.38)$$

As an example, a transient solution will be computed for both the linear and nonlinear cases to show the nonlinear effects.

It should be pointed out that a nonlinear analysis for the highly conducting magnetic field coupled case follows the same development as above, the only modification is replace ω_e^2 by $-\omega_h^2$ in (2.37) and (2.38).†

2.10.1 Transient solution

Equations (2.37) and (2.38) were programmed to obtain the transient buildup using the method of characteristics described above. The jet velocity was chosen $V_o/V_t = 3$. A sizable electric field was applied ($\frac{\omega_e(b-\Delta/2)}{V_t} = 1$) to accentuate the convective instability, and the jet was sinusoidally driven at the upstream end of the jet. The solution was continued until the jet collided with the rigid plate. Comparing the linear and nonlinear solutions shown in Fig. 2.7, for $\frac{\xi}{b-\Delta/2} < \frac{1}{4}$ the dynamics is predicted by linear theory. As the disturbance propagates and amplifies, only the crest of the wave is enhanced by the nonlinearity. It may seem surprising that such large displacements are predicted correctly by a linear theory which assumes the displacement to be small compared to the jet thickness and to all wavelengths of interest, but observations of a jet excited in the kink mode experimentally bear this out.

If the magnetic antidual of (2.37) is computed for both the linear and nonlinear equation of motion, virtually no differences are observed since the magnetic MH2f single jet system is stable, the only nonlinear effect is to flatten out the peaks for amplitudes $\frac{\xi}{b-\Delta/2} > \frac{1}{4}$.

2.11 Electron Beam Analogy to MH2f Surface Waves

It is well to point out that the techniques employed in studying electromechanical surface waves and the resulting equations of motion are not restricted to that area. An interesting analogy exists between the free surface current magnetic field coupled surface wave and the longitudinal oscillations of an electron beam. In fact the cold electron beam in ideal geometry is a special case of the MH2f model, and the results described in this chapter and those to follow

†See reference 34, p.53

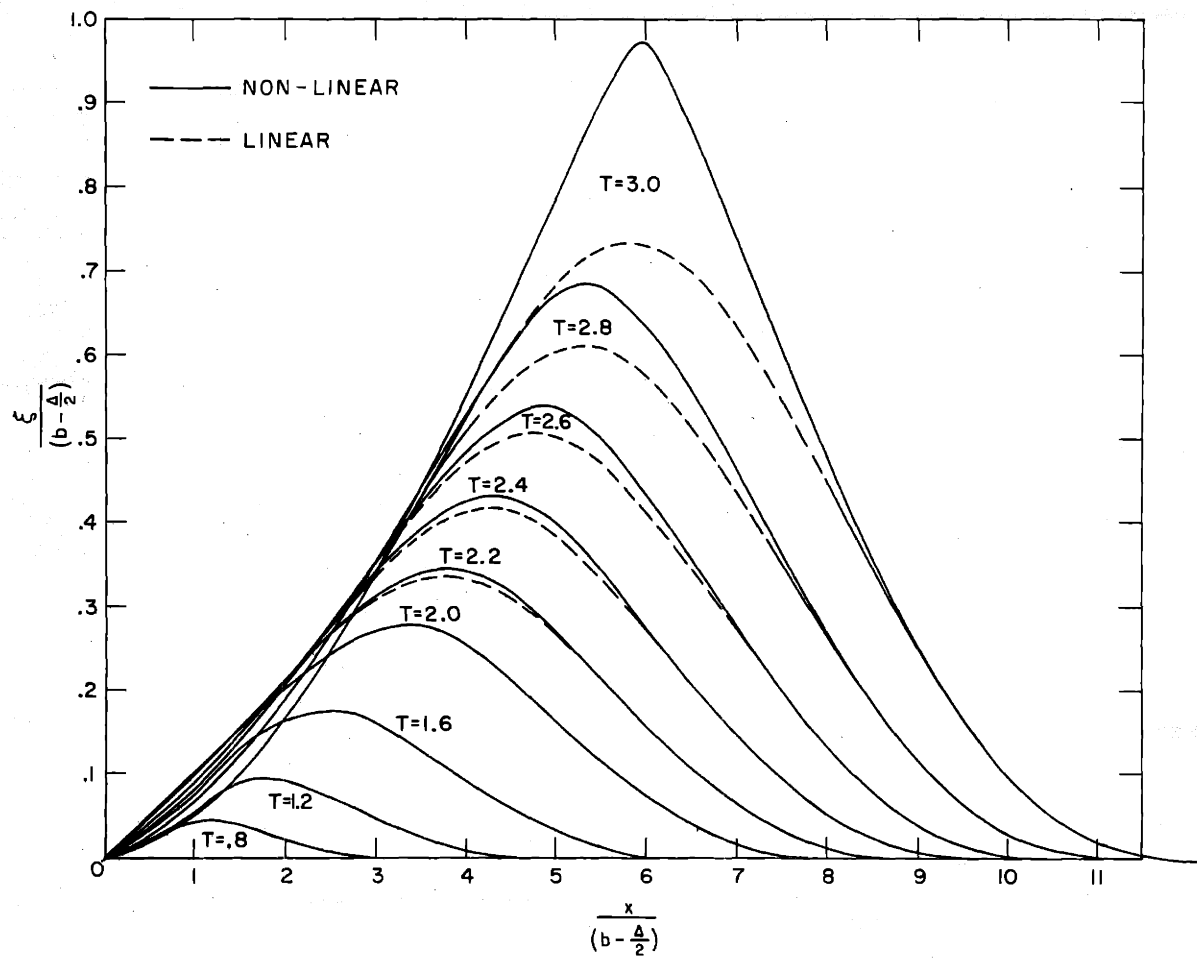

FIGURE 2.7 TRANSIENT BUILDUP OF AN ELECTRIC FIELD COUPLED JET SHOWING NON-LINEAR EFFECTS. THE JET IS SINUSOIDALLY DRIVEN AT x= 0 .

are applicable to the analogous electron beam problem. The equation of motion for a cold electron beam of infinite extent travelling with a velocity V_o may be written[30]

$$\left(\frac{\partial}{\partial t} + V_o \frac{\partial}{\partial x}\right)^2 u = - \omega_p^2 u$$

where u is the longitudinal perturbation velocity of the electrons and ω_p is the plasma frequency, given by $\omega_p^2 = \frac{e\rho_o}{m\varepsilon_o}$. Comparing this equation with the magnetic form of (2.38)

$$\left(\frac{\partial}{\partial t} + V_o \frac{\partial}{\partial x}\right)^2 \xi = V_t^2 \frac{\partial^2 \xi}{\partial x^2} - \omega_h^2 \xi$$

We observe they are identical in form if the surface tension is suppressed. However, setting $V_t = 0$ eliminates the subcapillary region, so that only supercapillary flow is meaningful. The above analogy will be shown to be valid for two streaming electron beams as well.

Some of the standard techniques used in electron beam theory will not be used in this thesis, such as coupling of modes and small signal power theorems. The reason simply is that they are not applicable or of little value when considering the coupling of complex waves, which is the case for most of the electric field coupled systems. For this reason the author has abandoned the techniques of obtaining approximate analytical answers for the magnetic systems in favor of exact numerical values for both electric and magnetic systems. Where the mathematics is tractable, however, analytical expressions will be given whenever possible.

CHAPTER 3

TWO STREAM INTERACTIONS FOR THE INFINITE SYSTEM

3.1 Introduction

In the previous chapter the interaction of a fluid jet with rigid boundaries by means of an electric or magnetic field was considered. It was found that two distinct flow regimes existed: supercapillary and subcapillary. For subcapillary flow, surface waves propagate both upstream and downstream, and physically meaningful boundary conditions are imposed, one each at the upstream and downstream end of the jet. A consequence of this fact is that an infinite discrete set of eigenfrequencies and eigenvalues (wavenumbers) exist for this system. This is by contrast with the supercapillary flow regime in which both waves propagate in the direction of flow. This means that two boundary conditions are imposed at the upstream end of the jet and that an eigenvalue problem does not exist.

We would now like to take up questions as to what basically different flow regimes exist when two jets in relative motion are allowed to be coupled by an electric or magnetic field, and what are the properties of each regime? In order to answer these questions the equations of motion will be derived using the long wave model to eliminate the transverse dependence from the problem. Later in the chapter the equations will be rederived without this restriction. The main effect of not assuming long waves is that the coupling between the jets is reduced as the wavelength of the disturbance is decreased.

The different flow regimes will be classified making use of the theory of characteristics again, to determine the conditions necessary for causal solutions. It will be shown that there are four basically different flow regimes: (1) subcapillary jets,(2) supercapillary jets - co-streaming, (3) supercapillary jets - counter-streaming, (4) one jet supercapillary, one jet subcapillary. Cases

1, 3, and 4 pose an eigenvalue problem; case 2 does not. The dispersion relations of each case will be derived and stability studied using the Bers-Briggs criterion.

As mentioned in the previous chapter, only the highly conducting electric field and magnetic field surface wave models will be discussed in detail. A small effort at considering the two stream polarization interactions and the corresponding magnetization interactions indicates the mutual interaction between the two jets to be quite a small effect,especially for thin jets. To the author's knowledge, no experiments have been done on even the single jet polarization interaction. Experiments on any of the magnetically coupled jets at the present time are not feasible. The remainder of the work to follow will be devoted exclusively to the behavior of two stream highly conducting jets coupled by an electric or magnetic field. In addition, because of the much larger interactions possible, the analysis will for the most part be restricted to an investigation of the kink modes on the jets, i.e. with both interfaces of a jet moving essentially in phase.

3.2 The Long Wave Equations of Motion

The long wave model for the two stream EH1f and MH2f interaction is shown in Fig. 3.1. Only the equations for the EH1f system will be derived, since the MH2f equations of motion are obtained by replacing E^2 by $-H^2$ in the field coupling terms. The basic equations and assumptions are the same as in the single jet problem.

The $\bar{E}$ field under the long wave assumption may be computed simply as:

Region I: $$E_2^{(1)} = \frac{-V_1}{b-a-\frac{\Delta}{2}-\xi_1}$$

Region II: $$E_2^{(2)} = \frac{V_2}{2a-\Delta+\xi_2-\xi_3}$$

Region III: $$E_2^{(3)} = \frac{-V_3}{b-a-\frac{\Delta}{2}+\xi_4} \qquad (3.1)$$

The voltages V_1, V_2, V_3 will be adjusted so that the equilibrium field in each region is E_o, and (3.1) then becomes

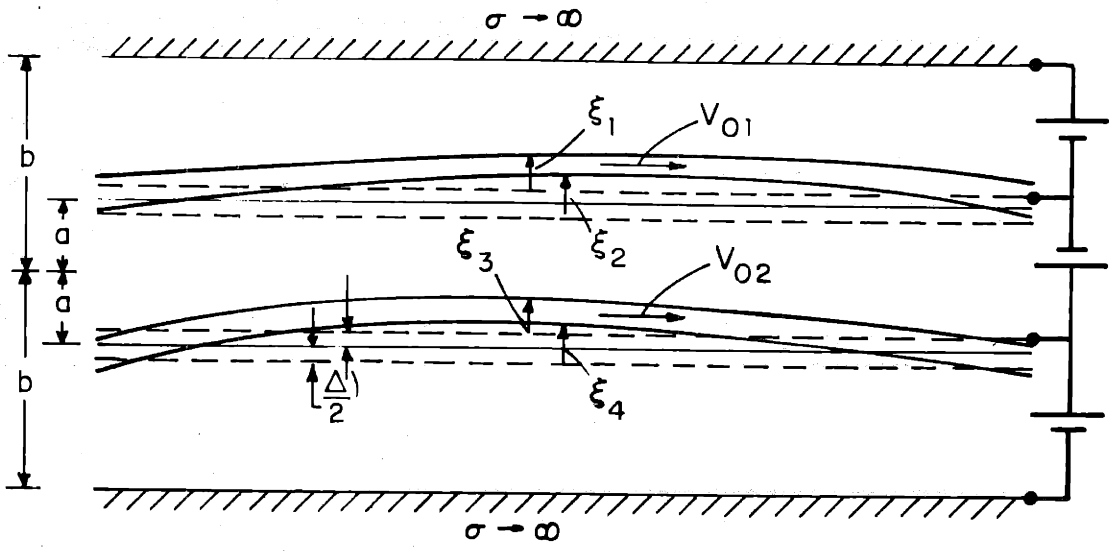

FIGURE 3.1 LONG WAVE MODEL OF A TWO-STREAM FIELD COUPLED SYSTEM

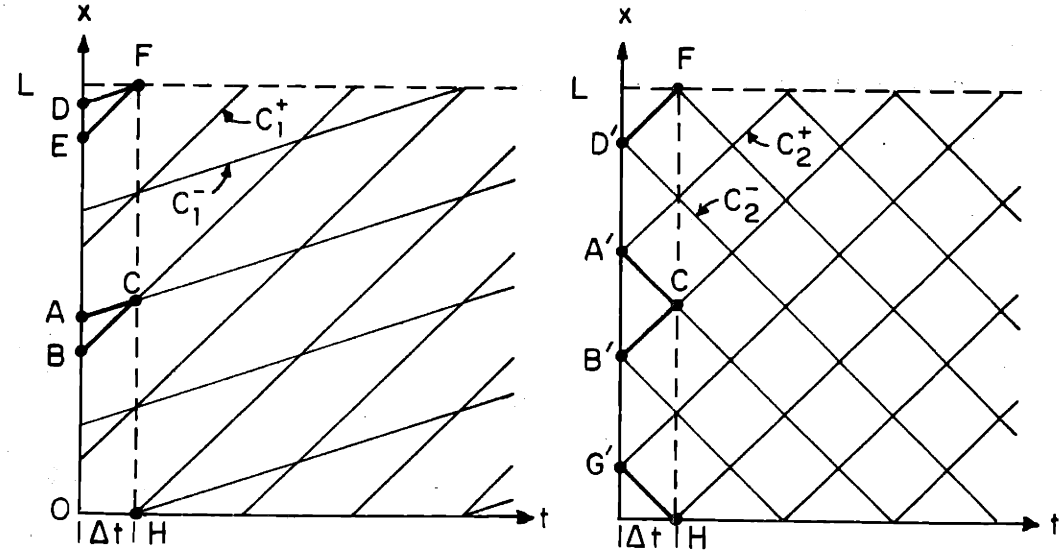

FIGURE 3.2 CHARACTERISTIC CURVES IN THE x,t PLANE FOR A TWO-STREAM SYSTEM

$$E_2^{(1)} = \frac{-E_o}{1 - \frac{\xi_1}{b-a-\frac{\Delta}{2}}} \qquad E_2^{(2)} = \frac{E_o}{1 + \frac{\xi_2-\xi_3}{2a-\Delta}} \qquad E_2^{(3)} = \frac{-E_o}{1 + \frac{\xi_4}{b-a-\frac{\Delta}{2}}} \tag{3.2}$$

If we restrict our attention to the kink modes, $\xi_+ \tilde{\wedge} \xi_1 \tilde{\wedge} \xi_2$ and $\xi_- \tilde{\wedge} \xi_3 \tilde{\wedge} \xi_4$, the jets behave essentially like elastic membranes, each having a surface tension 2T. The equations of motion are:

$$\begin{aligned} \rho_1 \Delta [\frac{\partial}{\partial t} + V_{o1} \frac{\partial}{\partial x_1}]^2 \xi_+ &= 2T_1 \frac{\partial^2 \xi_+}{\partial x_1^2} + T_{22}^{(1)} - T_{22}^{(2)} \\ \rho_2 \Delta [\frac{\partial}{\partial t} + V_{o2} \frac{\partial}{\partial x_1}]^2 \xi_- &= 2T_2 \frac{\partial^2 \xi_-}{\partial x_1^2} + T_{22}^{(2)} - T_{22}^{(3)} \end{aligned} \tag{3.3}$$

where the jets are allowed to have different surface tensions and densities.

Equation (3.3) is valid for both the EH1f and MH2f systems. The Maxwell stress T_{22} is given simply by

$$T_{22} = \frac{1}{2} \varepsilon_o E_2^2$$

so that

$$T_{22}^{(1)} - T_{22}^{(2)} = \frac{1}{2} \varepsilon_o E_o^2 \left[\frac{1}{(1 - \frac{\xi_+}{b-a-\frac{\Delta}{2}})^2} - \frac{1}{(1 - \frac{\xi_+-\xi_-}{2a-\Delta})^2} \right]$$

$$T_{22}^{(2)} - T_{22}^{(3)} = \frac{1}{2} \varepsilon_o E_o^2 \left[\frac{1}{(1 - \frac{\xi_+-\xi_-}{2a-\Delta})^2} - \frac{1}{(1 + \frac{\xi_-}{b-a-\frac{\Delta}{2}})^2} \right]$$

Since our analysis will be limited to small amplitudes, the above equations may be linearized and combined with Equation 3.3 to yield the following second order set of equations.

$$\left[\frac{\partial}{\partial t} + V_{o1}\frac{\partial}{\partial x_1}\right]^2 \xi_+ - V_{t_1}^2 \frac{\partial^2 \xi_+}{\partial x_1^2} - \frac{\eta}{2}\omega_{e_1}^2 \xi_+ = -\frac{1}{2}\omega_{e_1}^2 \xi_-$$

$$\left[\frac{\partial}{\partial t} + V_{o2}\frac{\partial}{\partial x_1}\right]^2 \xi_- - V_{t_2}^2 \frac{\partial^2 \xi_-}{\partial x_1^2} - \frac{\eta}{2}\omega_{e_2}^2 \xi_- = -\frac{1}{2}\omega_{e_2}^2 \xi_+ \qquad (3.4)$$

where

$$V_{t_{1,2}} = \sqrt{\frac{2T_{1,2}}{\rho_{1,2}\Delta}}\,, \quad \omega_{e_{1,2}} = \sqrt{\frac{2\varepsilon_o E_o^2}{(2a-\Delta)\rho_{1,2}\Delta}}\,, \quad \eta = \frac{b+a-\frac{3\Delta}{2}}{b-a-\frac{\Delta}{2}}$$

If solutions of the form $\xi(x_1,t) = \mathrm{Re}\{\xi e^{j(\omega t - kx_1)}\}$ are assumed, we obtain directly the following dispersion relation.

$$[(\omega - V_{o1}k)^2 - V_{t_1}^2 k^2 + \frac{\eta}{2}\omega_{e_1}^2][(\omega - V_{o2}k) - V_{t_2}^2 k^2 + \frac{\eta}{2}\omega_{e_2}^2] - \frac{1}{4}\omega_{e_1}^2\omega_{e_2}^2 = 0 \qquad (3.5)$$

Equation (3.4) is in essence two coupled wave equations, the coupling being provided by the zeroth derivative term. The self coupling term we have seen before and may be thought of as representing a distributed spring of negative spring constant attached between each jet and its adjacent boundaries, assuming the boundaries to be fixed in space. If one of the boundaries (jet) is free to move, however, then an additional spring term appears, which is the mutual coupling term.

We observe in comparing the self and mutual coupling terms of a given jet that the ratio is simply η, which depends only on the transverse geometry. If the spacing between jets and between jet and boundary are the same, and if $\Delta << a$, then $\eta = 2$. This is physically reasonable since if jet 1 (say) is given a small positive displacement, the field is enhanced above the jet and diminished below the jet, by an equal amount, while if jet 2 is given the same small displacement, the effect on jet 1 is produced by the change in the field region between the jets only. This is not to suggest that the self

coupling term is always more important than the mutual term. It will be shown in Chapter 5, in fact, that in the case of counter-streaming supercapillary jets the mutual term can produce an absolute instability in spite of the fact that the self coupling term (in the MH2f configuration) produces a stabilizing effect on the jets.

Probably the most judicious way of classifying the flow regimes is by the specification of the boundary conditions. The boundary conditions cannot be specified arbitrarily, as shown in the previous chapter, but must satisfy causality. The method of characteristics is appropriate for handling the systems to be considered here, since they are hyperbolic in character and possess real characteristics. The type of boundary conditions that may be imposed, then, is uniquely determined.

3.3 Two Stream Boundary Conditions: Classification of Flow Regimes

In Chapter 2 the method of characteristics was introduced and it was shown that for solutions to advance forward in time, the proper specification of boundary conditions was determined by the direction of the characteristic lines $V_o \pm V_t$. These lines were independent of the field coupling. If two jets of arbitrary flow velocity are field coupled it is not immediately clear that the mutual coupling does not alter these lines. If (3.4) are split into first order equations as in Chapter 2 we have:

$$
\begin{aligned}
&[\frac{\partial}{\partial t} + (V_{o1} + V_{t_1}) \frac{\partial}{\partial x}]\xi_1 = u_1 \\
&[\frac{\partial}{\partial t} + (V_{o1} - V_{t_1}) \frac{\partial}{\partial x}]u_1 - \omega_{e_1}^2 \frac{\eta}{2} \xi_1 = - \omega_{e_1}^2 \frac{1}{2} \xi_2 \qquad (3.7) \\
&[\frac{\partial}{\partial t} + (V_{o2} + V_{t_2}) \frac{\partial}{\partial x}]\xi_2 = u_2 \\
&[\frac{\partial}{\partial t} + (V_{o2} - V_{t_2}) \frac{\partial}{\partial x}]u_2 - \omega_{e_2}^2 \frac{\eta}{2} \xi_2 = - \omega_{e_2}^2 \frac{1}{2} \xi_1
\end{aligned}
$$

The physical (type I) characteristic lines are evidently

$$\frac{dx}{dt} = V_{o1} + V_{t_1} \quad \text{along } C_1^+ \qquad \frac{dx}{dt} = V_{o2} + V_{t_2} \quad \text{along } C_2^+$$

$$\frac{dx}{dt} = V_{o1} - V_{t_1} \quad \text{along } C_1^- \qquad \frac{dx}{dt} = V_{o2} - V_{t_2} \quad \text{along } C_2^-$$

and the type II characteristics become:

$$\frac{d\xi_1}{dt} = u_1 \quad \text{along } C_1^+ \qquad \frac{d\xi_2}{dt} = u_2 \quad \text{along } C_2^+$$

$$\frac{du_1}{dt} = \omega_{e_1}^2 [\frac{\eta}{2} \xi_1 - \frac{\xi_2}{2}] \quad \text{along } C_1^- \qquad \frac{du_2}{dt} = \omega_{e_2}^2 [\frac{\eta}{2} \xi_2 - \frac{\xi_1}{2}] \quad \text{along } C_2^-$$

The type I characteristics might look as shown in Fig. 3.2. In order to begin the computation moving forward in time, it is necessary to specify 2 initial conditions on each jet, say ξ and u, and we wish to compute point C. If the increments are made sufficiently small, we may replace the differentials by differences and we get:

$$\begin{aligned}
&\xi_1(C) - \xi_1(B) \approx \frac{1}{2}[u_1(C) + u_1(B)]\Delta t \\
&u_1(C) - u_1(A) \approx \omega_{e_1}^2 \{\frac{\eta}{2}\left[\frac{\xi_1(C) + \xi_1(A)}{2}\right] - \frac{1}{2}\left[\frac{\xi_2(C) + \xi_2(A)}{2}\right]\}\Delta t \\
&\xi_2(C) - \xi_2(B') \approx \frac{1}{2}[u_2(C) + u_2(B')]\Delta t \\
&u_2(C) - u_2(A') \approx \omega_{e_2}^2 \{\frac{\eta}{2}\left[\frac{\xi_2(C) + \xi_2(A')}{2}\right] - \frac{1}{2}\left[\frac{\xi_1(C) + \xi_1(A')}{2}\right]\}\Delta t
\end{aligned} \tag{3.8}$$

From (3.8) the ξ's and u's may be found by solving the system of 4 coupled linear equations.

Since the A's and B's are arbitrary points along the t = 0 line, this method is valid for any interior point C at a time $t = \Delta t$. To continue one step further in time, the C's now become the new A's and B's and new C's are computed for $t = 2\Delta t$, and so on. Once a boundary is reached however, the above process must be modified. Consider the calculation of point F. Equation (3.8) becomes:

$$\xi_1(F) - \xi_1(E) = \frac{1}{2}[u_1(F) + u_1(E)]\Delta t$$

$$u_1(F) - u_1(D) = \omega_{e_1}^2 \left\{\frac{n}{4}[\xi_1(F) + \xi_1(D)] - \frac{1}{4}[\xi_2(F) + \xi_2(D)]\right\}\Delta t$$

$$\xi_2(F) - \xi_2(D') = \frac{1}{2}[u_2(F) + u_2(D')]\Delta t$$

We observe two facts: first the equation corresponding to the C_2^- line is absent, since the C_2^- line segment has degenerated to a point. This means that to have a unique solution it is necessary to specify one boundary condition for jet 2 at $x = L$. Secondly, since ξ_1 and u_1 are now completely determined at point F, no boundary conditions may be specified along $x = L$, or else the variables would be overspecified. Finally consider a point H, (which lies along $x = 0$). Both C_1^+ and C_1^- line segments have degenerated to points, and the jet 1 variables are undetermined so that two boundary conditions must be specified on jet 1 at $x = 0$. Along the C_2^- characteristic we may write

$$u_2(H) - u_2(G') = \omega_{e_2}^2 \left\{\frac{n}{4}[\xi_2(H) + \xi_2(G')] - \frac{1}{4}[\xi_1(H) + \xi_1(G')]\right\}\Delta t$$

Since the C_2^+ characteristic does not produce a condition, one jet 2 variable is unspecified and 1 boundary condition must be specified at $x = 0$. With points F and H determined, the computation can proceed without difficulty for later time.

While the selection of characteristic lines was specific, to illustrate the procedure, namely $V_{o1} > V_t$ and $V_{o2} < V_t$, the same technique holds regardless of the flow conditions. The specifications of boundary conditions for the various flow conditions is shown in Table 3.1. The method of characteristics is more powerful than illustrated: the type 1 characteristics need not be straight lines, so that the method applies to nonlinear problems as well. Further, while the coupling between the jets was proportional to the jet displacement, the results are unchanged for first derivative coupling in space or time.

since the type I characteristics are unchanged. Other flow conditions may be placed in one of the four classes specified, by suitable symmetry arguments, as seen in Fig. 3.3.

TABLE 3.1

Class	Flow Conditions	No. Boundary Conditions			
		Jet 1		Jet 2	
		x=0	x=L	x=0	x=L
I	$\|V_{o1}\|<V_{T_1}$, $\|V_{o2}\|<V_{T_2}$	1	1	1	1
II	$V_{o1} > V_{T_1}$, $V_{o2} > V_{T_2}$	2	0	2	0
III	$V_{o1} > V_{T_1}$, $V_{o2} < V_{T_2}$	2	0	0	2
IV	$V_{o1} > V_{T_1}$, $\|V_{o2}\|<V_{T_2}$	2	0	1	1

It should also be evident that the above arguments are independent of whether the coupling is to an electric or to a magnetic field.

With appropriate boundary conditions formulated, the dynamics of field coupled two jet systems, may be solved. These constitute the main body of this thesis. Class I and class II systems will be discussed in the next chapter, class III, counter-streaming jets, in Chapters 5 and 6, and class IV systems in Chapters 7 and 8. It is usually not possible to draw general conclusions about the dynamics of these systems in an actual physical situation of finite length without actually solving the boundary value problem. Nevertheless, useful information concerning the behavior of a system can be obtained from a discussion of the infinite system. In the sections to follow, a brief discussion of the dispersion relations and stability for the infinite system using the Bers-Briggs criterion will be made.

3.4 Dispersion Relations and Stability for the Infinite System

In order to simplify the discussion we shall consider only the case of

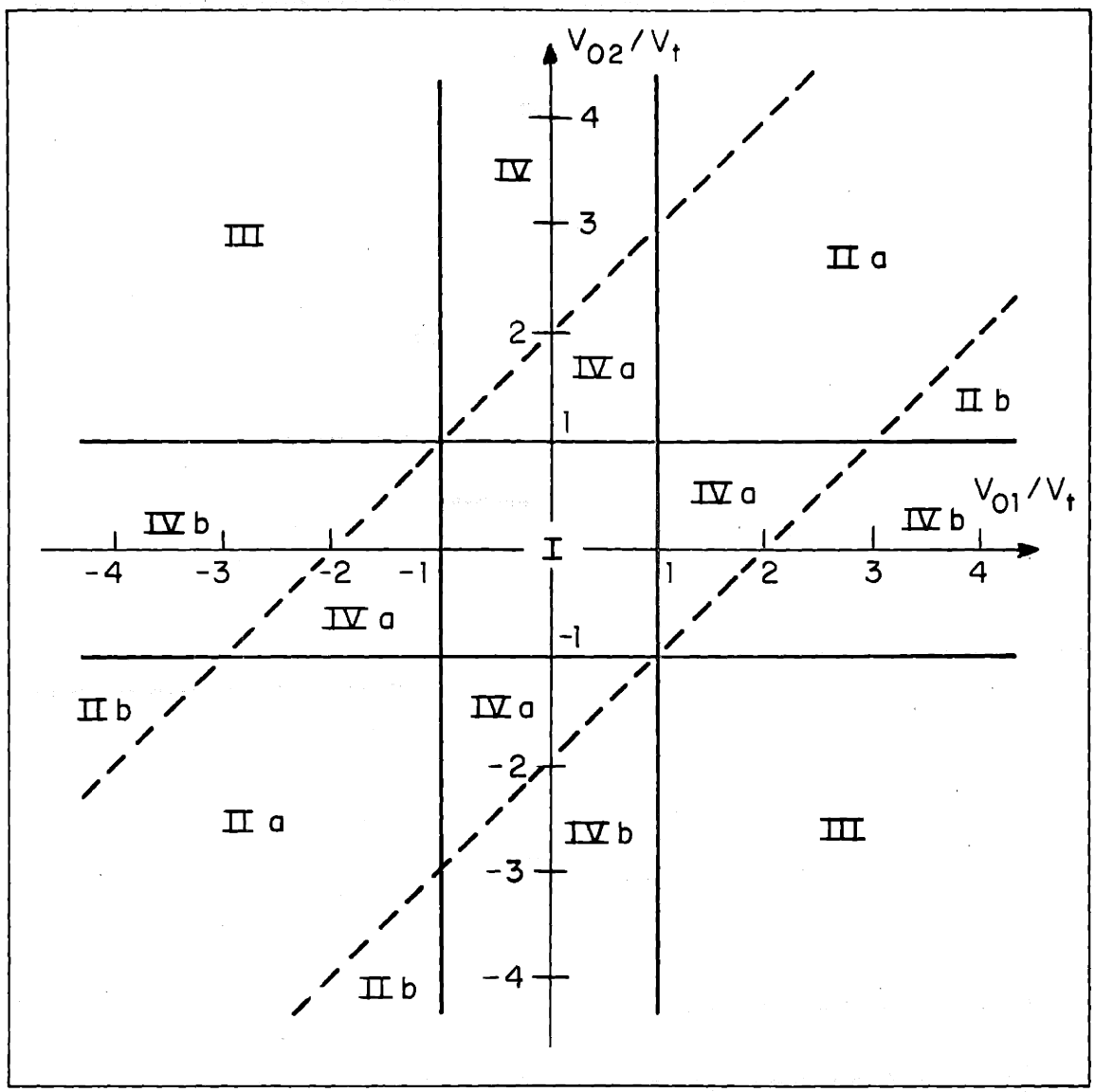

FIGURE 3.3 GRAPHICAL REPRESENTATION OF THE FLOW REGIMES FOR TWO STREAMS SHOWING THE FOUR DISTINCT CLASSES OF FLOW. THE REGIONS ARE SYMMETRIC ABOUT THE LINES $V_{o2} = \pm V_{o1}$.

similar jets, so that

$$V_{t_1} = V_{t_2} = V_t \quad \text{and} \quad \omega_{e_1} = \omega_{e_2} = \omega_e$$

and (3.5) simplifies, for electric field coupling, to

$$[(\bar{\omega} - M_1\bar{k})^2 - \bar{k}^2 + \tfrac{\eta}{2}][(\bar{\omega} - M_2\bar{k})^2 - \bar{k}^2 + \tfrac{\eta}{2}] - \tfrac{1}{4} = 0 \qquad (3.10)$$

where $\bar{\omega} = \omega/\omega_e$, $\bar{k} = \dfrac{kV_t}{\omega_e}$ and $M_{1,2} = \dfrac{V_{o1,2}}{V_t}$

The dispersion relation for magnetic coupling may be obtained simply by replacing ω_e^2 by $-\omega_h^2$ in (3.5).

$$[(\bar{\omega} - M_1\bar{k})^2 - \bar{k}^2 - \tfrac{\eta}{2}][(\bar{\omega} - M_2\bar{k})^2 - \bar{k}^2 - \tfrac{\eta}{2}] - \tfrac{1}{4} = 0 \qquad (3.11)$$

where now $\bar{\omega} = \omega/\omega_h$ and $\bar{k} = \dfrac{kV_t}{\omega_h}$.

A simple device for plotting higher order dispersion relations is to plot the uncoupled dispersion relations, which are simply quadratic expressions in k,ω for the systems considered here. The coupled dispersion relations will be altered appreciably only in regions where the curves intersect in the complex ω plane for real k or for complex k for real ω. These regions must be examined in detail, but the remaining regions are simply determined from the uncoupled curves. In the material to follow the uncoupled and exact dispersion relations are plotted to bring out the effect of the mutual coupling.

3.4.1 Class 1 - Subcapillary Jets

Electric Field Coupling: Two similar subcapillary jets will always have an intersection point as shown in Fig. 3.4a, independent of the flow velocities. The mutual coupling splits the curves effectively into two subcapillary jets, both having the same flow velocity but different surface tensions. We observe that there are no spatially growing waves for real frequencies. Also for large wavenumbers the frequency is real indicating the system is stable for short wavelengths. As the wavenumber is reduced two of the frequencies merge and become

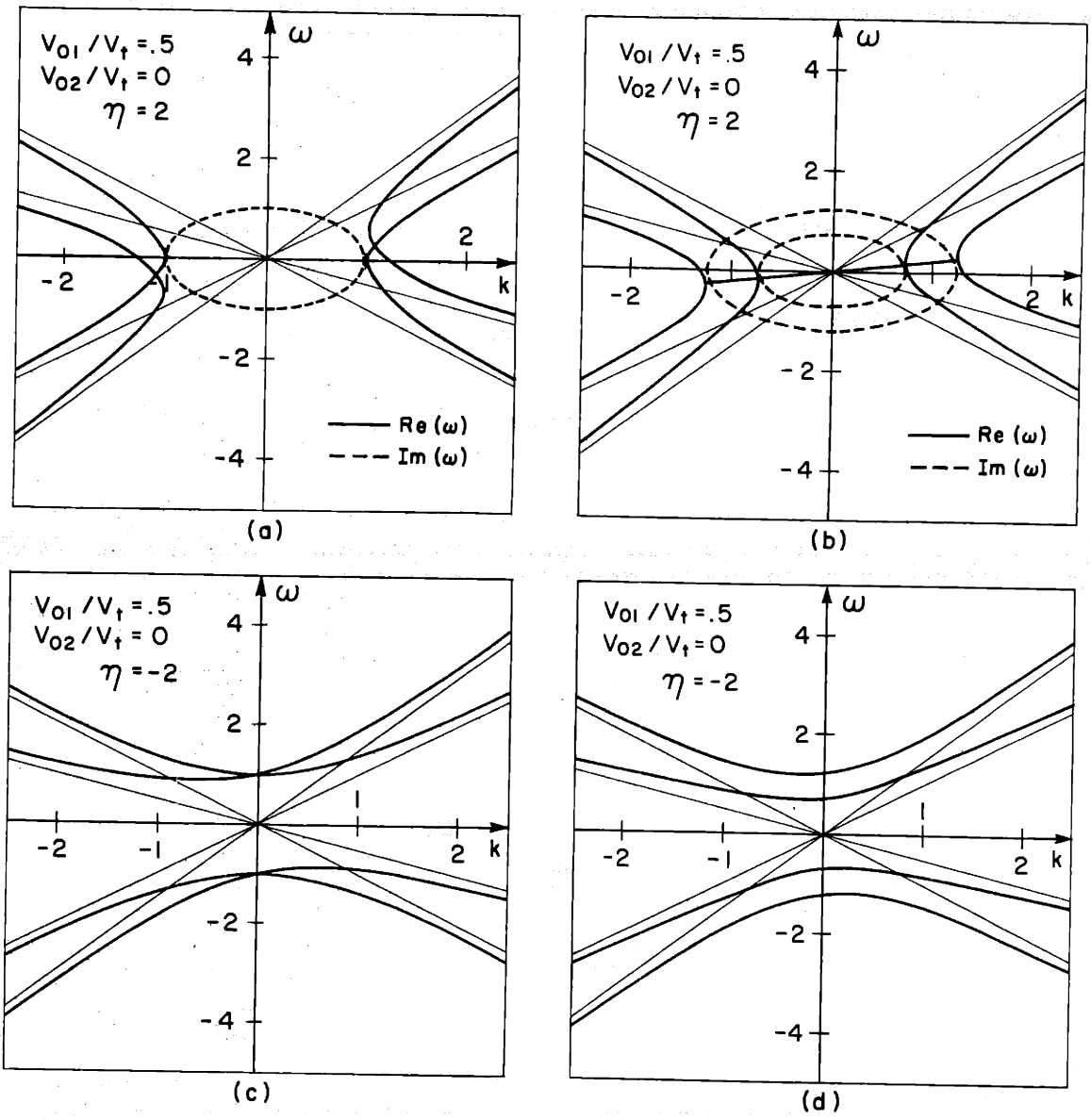

FIGURE 3.4 DISPERSION CURVES FOR CLASS I FLOW. THE MUTUAL COUPLING HAS BEEN SUPPRESSED IN (a) AND (c). THE ELECTRIC FIELD MODEL IS SHOWN IN (a) AND (b), THE MAGNETIC MODEL IN (b) AND (d).

complex indicating a potential instability and as k is reduced further, the second pair of frequencies also merge and become complex. This behavior is characteristic of a single subcapillary electric field coupled jet, which in Chapter 2 was shown to be absolutely unstable. We might expect then that in the absence of boundaries the system should exhibit two absolute instabilities, one being more unstable than the other. Indeed, if we examine the stability for the infinite system using the Bers-Briggs criterion, Fig. 3.5, we find two statically unstable saddle points. The corresponding wavenumbers are imaginary, indicating growth in space as well. These natural modes, if one can speak of natural modes of an infinite system, do not exhibit wavelike character, either spatial or temporal.

Magnetic Field Coupling: By contrast with electric field coupling, the magnetic field case features the coupling of two systems which by themselves exhibit a cutoff frequency below which the waves are evanescent. The splitting of the intersection point results in the formation of two curves which have similar appearance but have cutoff frequencies above and below the uncoupled value. As the frequency is reduced from some high value, the waves initially are all propagating, then two become evanescent and as the frequency is reduced further, all four waves become evanescent. The system exhibits no instabilities.

3.4.2 Class II - Supercapillary Jets: Co-streaming

Electric Field: If two supercapillary co-streaming jets are allowed to couple, there are two ways in which the dispersion curves can couple, shown in Fig. 3.6. If $V_{o1}/V_t > V_{o2}/V_t + 2$ there is no coupling except at zero frequency. The coupled dispersion curves retain essentially the original character as the uncoupled jets, i.e. both jets are convectively unstable at low frequencies, propagating at high frequencies. Because of the coupling at zero frequency, the spatial growth rates are split, one greater and one less than the uncoupled

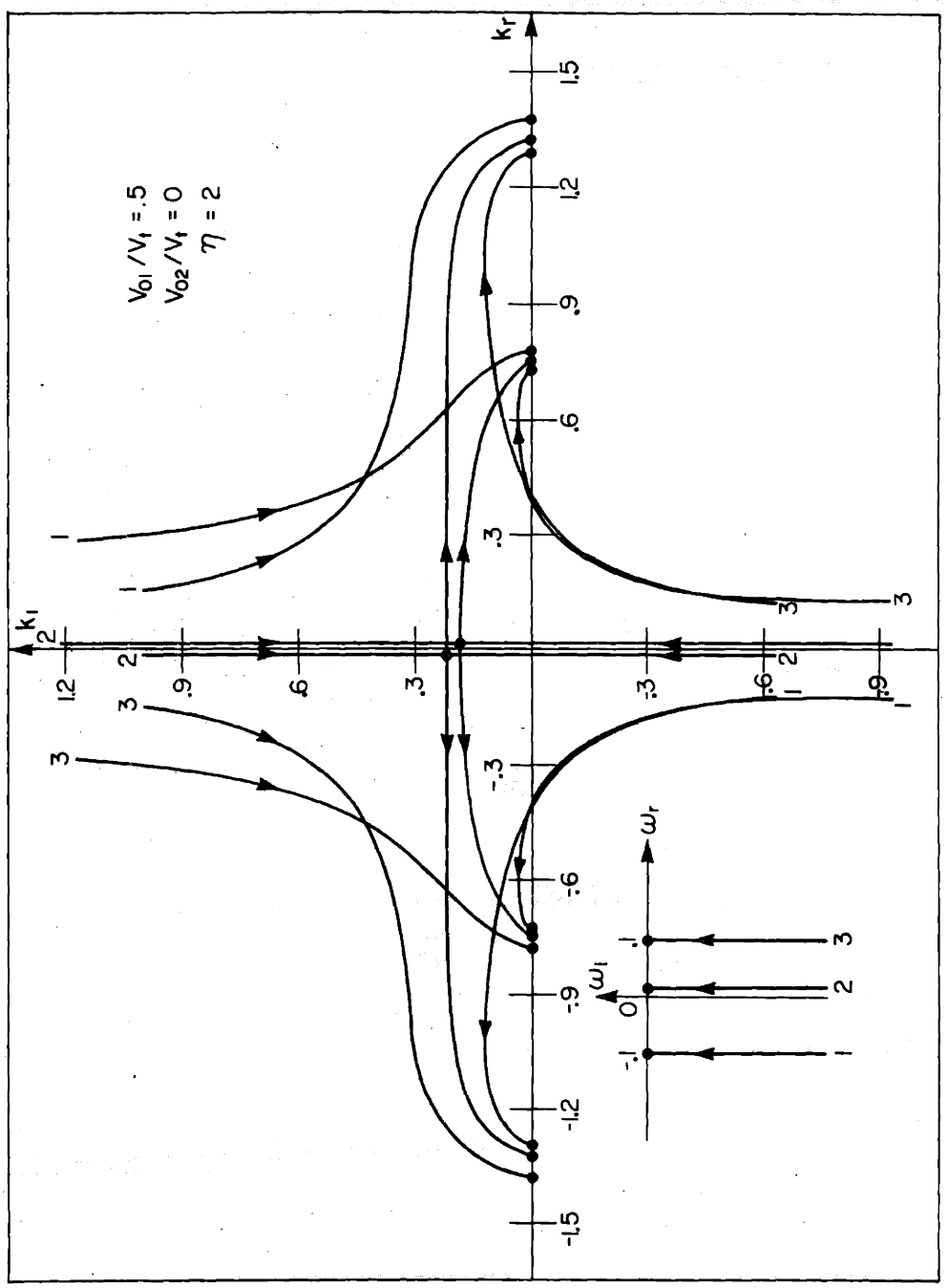

FIGURE 3.5 CLASS I STABILITY CURVES FOR ELECTRIC FIELD COUPLING. SYSTEM IS DOUBLY UNSTABLE.

-65-

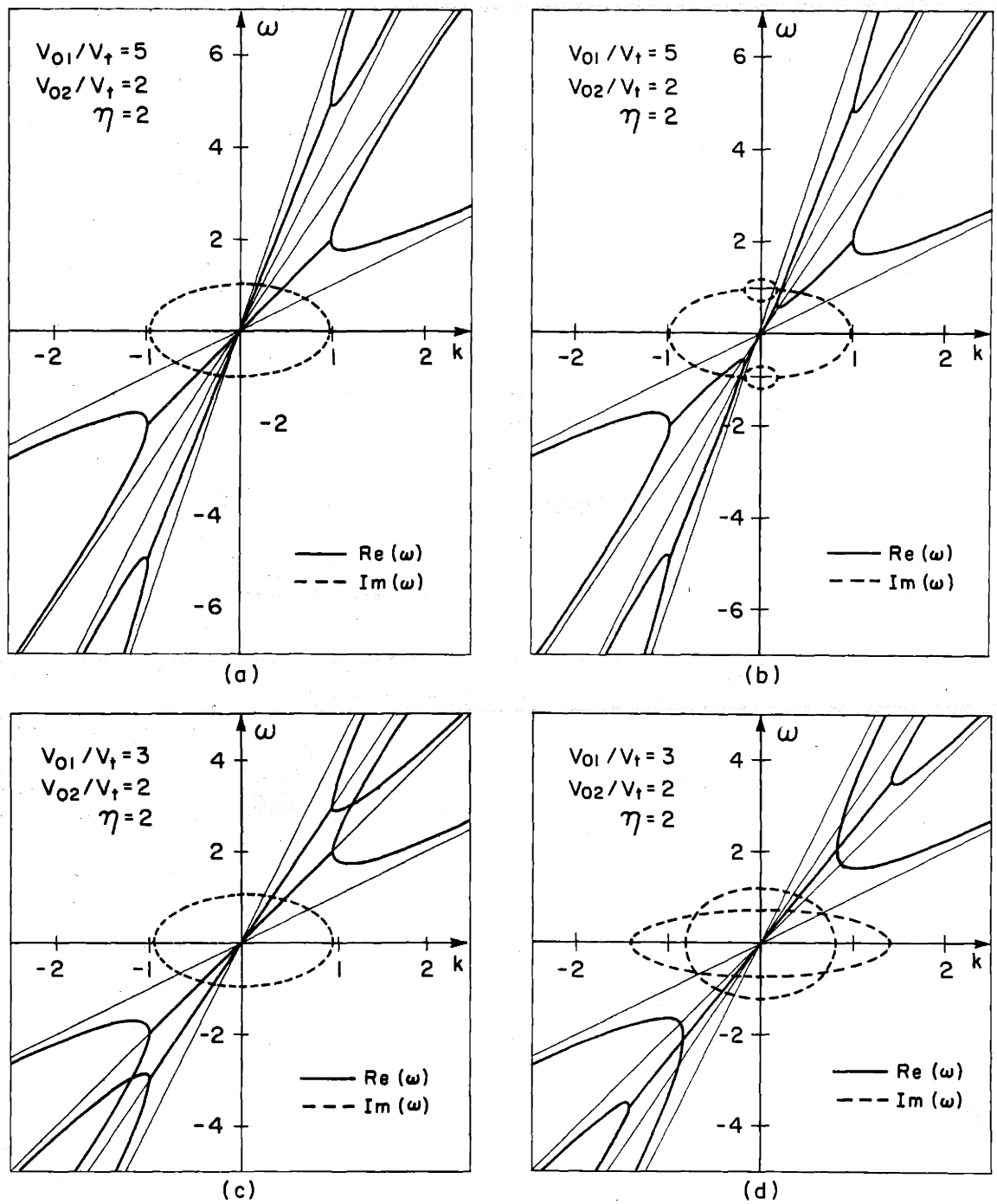

FIGURE 3.6 DISPERSION CURVES FOR CLASS II FLOW: ELECTRIC FIELD COUPLING. THE MUTUAL COUPLING HAS BEEN SUPPRESSED IN (a) AND (c).

growth rate. The real part of the frequency is the same for both of the growing and decaying waves. This has been designated class IIa in Fig. 3.3.

If $V_{o1}/V_t < V_{o2}/V_t + 2$ however, there is a crossing in the real ω,k plane. The result is to produce effectively two supercapillary jets of the same flow velocity but different surface tensions. The effectively different surface tensions result in two different cutoff frequencies for propagating waves. As the frequency is reduced, two waves become complex exhibiting a convective instability and below the lower cutoff frequency, all four waves become complex. The Bers-Briggs stability plot in Fig. 3.8 confirms the convectively unstable behavior. The essential behavior of both class IIa and IIb are similar.

Magnetic Field: If the co-streaming jets are magnetically coupled there again exists two subclasses of flow, but as observed in Fig. 3.7, the behavior is quite different for the two cases. For $V_{o1}/V_t > V_{o2}/V_t + 2$ (class IIa), the jets have nearly the same velocity and the effect of coupling is shown in Fig. 3.7b. Since there are no complex frequencies for real k, the system is stable. The dispersion curves, by analogy to the single stream magnetically coupled case, exhibit purely propagating wave behavior.

The case of two supercapillary streams having much different flow velocities ($V_{o1}/V_t > V_{o2}/V_t + 2$) is of some interest. From Fig. 3.7d there exists a band of wavelengths for which the system exhibits instability, and a band frequencies for which the wavenumbers are complex, suggesting convective unstable behavior. The Bers-Briggs stability plots shown in Fig. 3.8b verify the pass band amplification region. This system constrasts the electric field convective instabilities previously considered since in the electric field case the unstable region is at low frequencies.

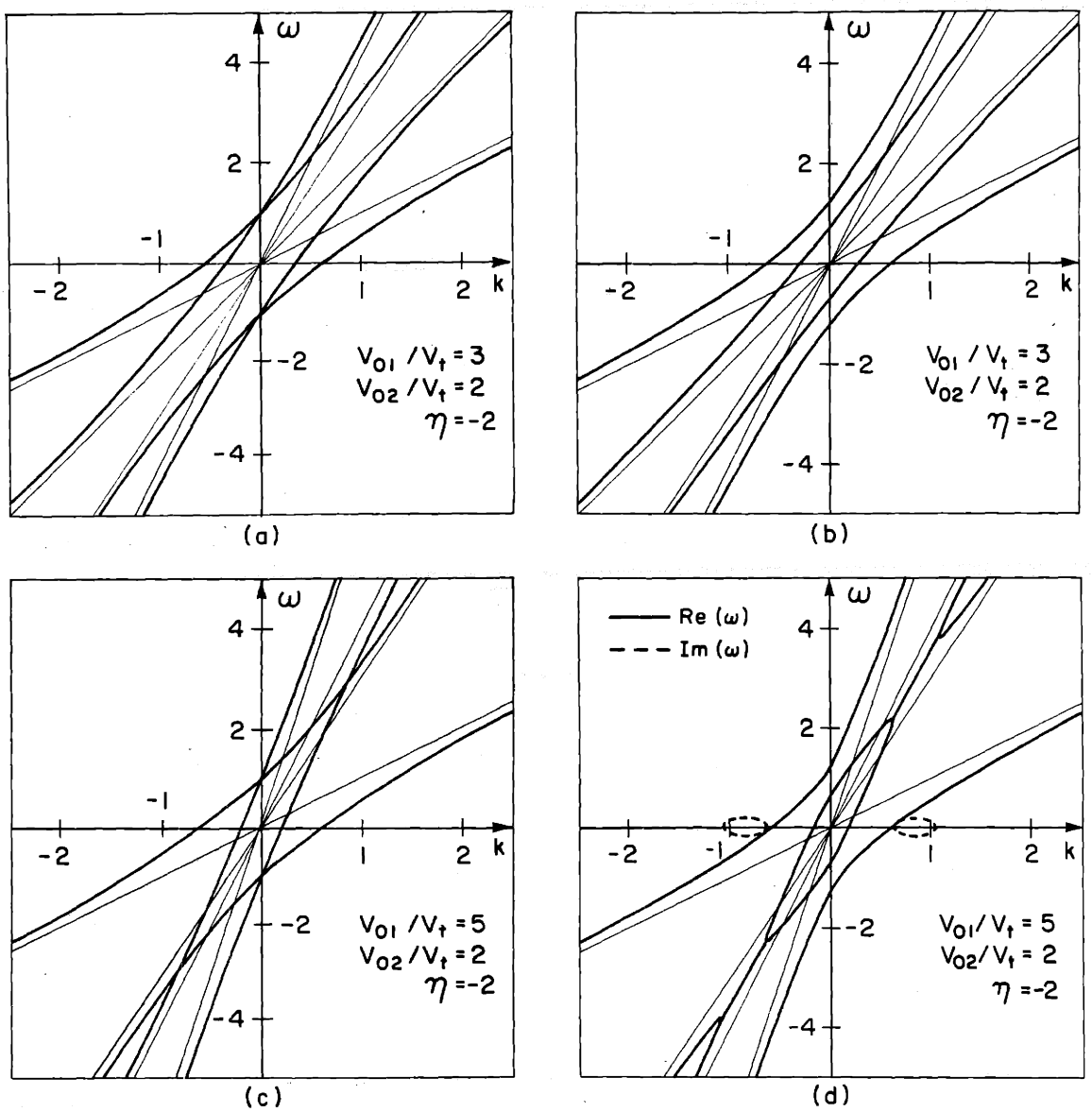

FIGURE 3.7 DISPERSION CURVES FOR CLASS II FLOW: MAGNETIC FIELD COUPLING. THE MUTUAL COUPLING HAS BEEN SUPPRESSED IN (a) AND (c).

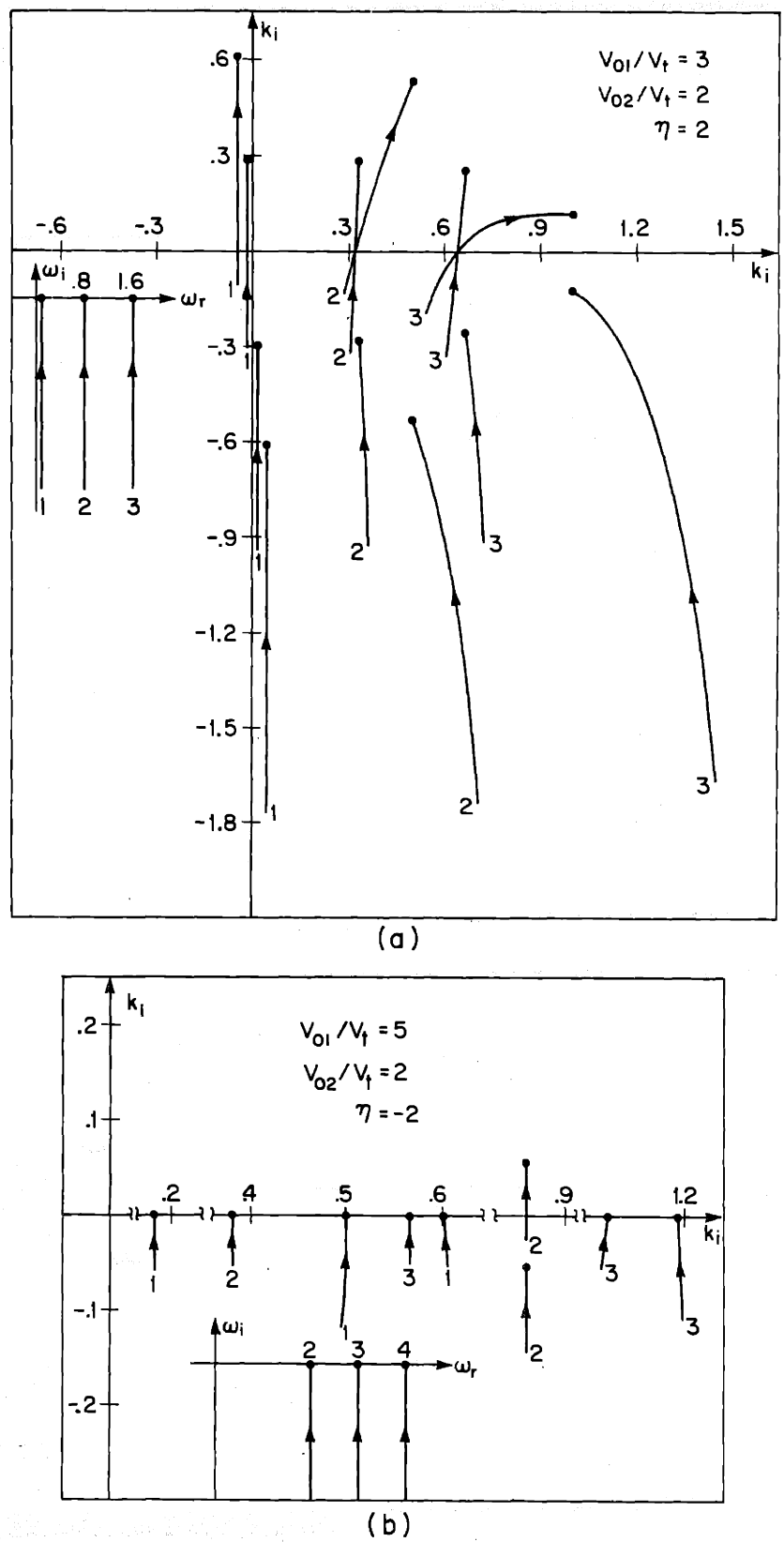

FIGURE 3.8 CLASS II STABILITY CURVES. THE CONVECTIVE INSTABILITY IS EVIDENT IN (a) ELECTRIC FIELD COUPLING AND (b) MAGNETIC FIELD COUPLING.

3.4.3 Class III Supercapillary Jets: Counter-Streaming

Electric Coupling: If two counter-streaming jets are coupled as in Fig. 3.9b it might appear that there is little coupling between the two jets, except for complex frequency near $\omega_r = 0$. This low frequency coupling behavior was also observed for weak coupling co-streaming jets, the effect there was to effect a splitting in the spatial growth from the single jet zero frequency value but the general behavior is unchanged. If we should draw the same conclusion in the present case, however, our conclusion would be entirely false. It is true that if the system were excited at any real frequency ω, the two jets would exhibit little mutual interaction, but we are assuming that the experiment can be performed, i.e. there are no absolute instabilities.

Because of the unusual character of the dispersion curves, one must exercise care in attempting to predict stability on the basis of these curves alone. A test of the infinite system stability in Fig. 3.10a, shows the presence of two saddle points, a static instability of large growth rate and a mild exponential spatial character and a weaker overstability occurring with a large spatial growth and long wavelength. The static instability is quite insensitive to flow velocity; however if the velocities of the two jets are equal but opposite, the growth rate of the overstability vanishes and the natural mode is purely oscillatory. The wavenumber becomes imaginary. The electric field coupled counter-streaming jets are convectively unstable as well for low frequencies.

Magnetic Coupling: If the counter-streaming jets are magnetically coupled the dispersion curves couple as shown in Fig. 3.9d. There is a band of wavelengths for which the system is unstable, and a band of frequencies for which the wavenumber is complex. Although convectively unstable systems also often exhibit this property one must again be careful. From the stability plot in

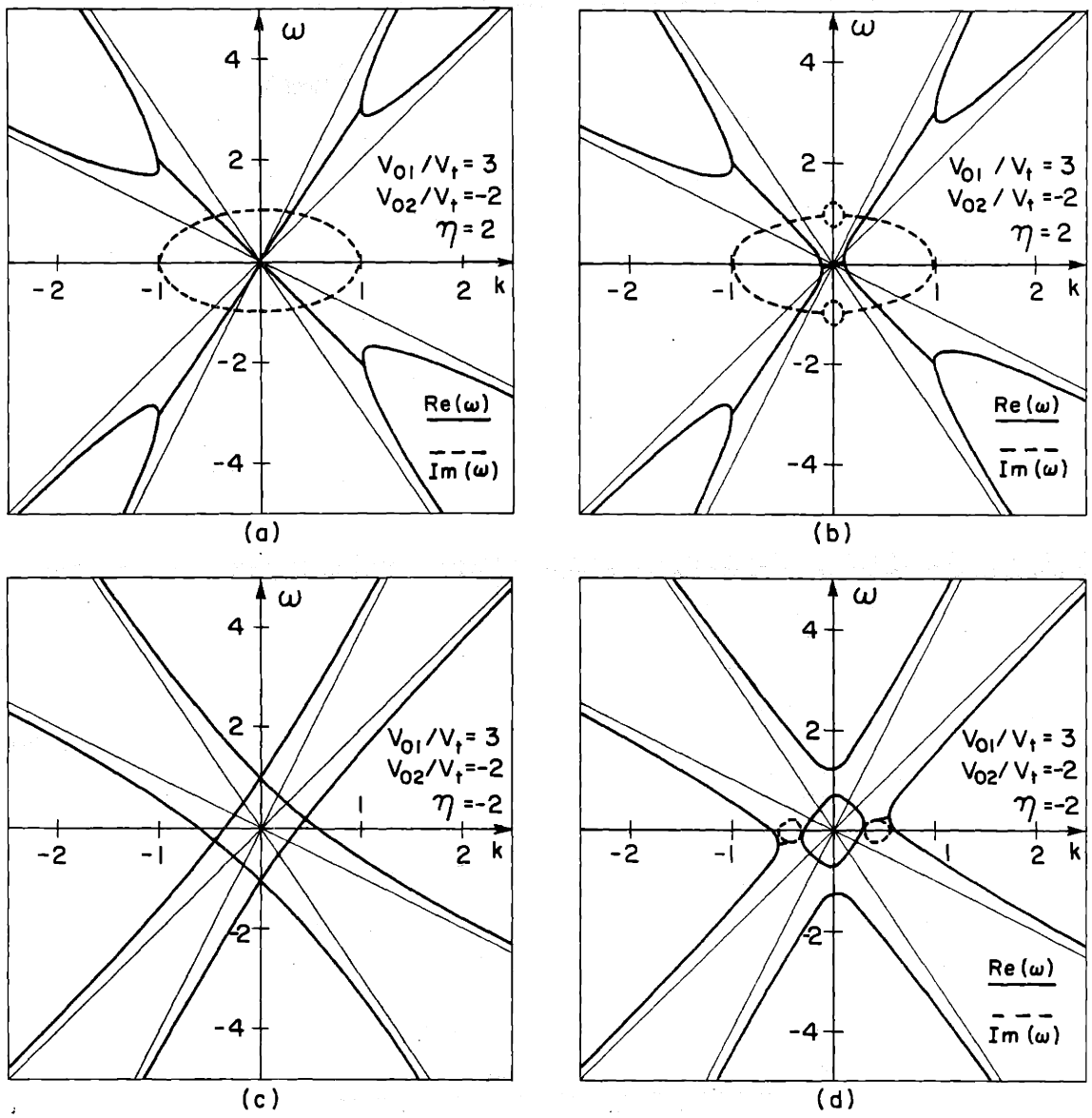

FIGURE 3.9 DISPERSION CURVES FOR CLASS III FLOW. THE MUTUAL COUPLING HAS BEEN SUPPRESSED IN (a) AND (c). THE ELECTRIC FIELD MODEL IS SHOWN IN (a) AND (b), THE MAGNETIC FIELD MODEL IN (c) AND (d).

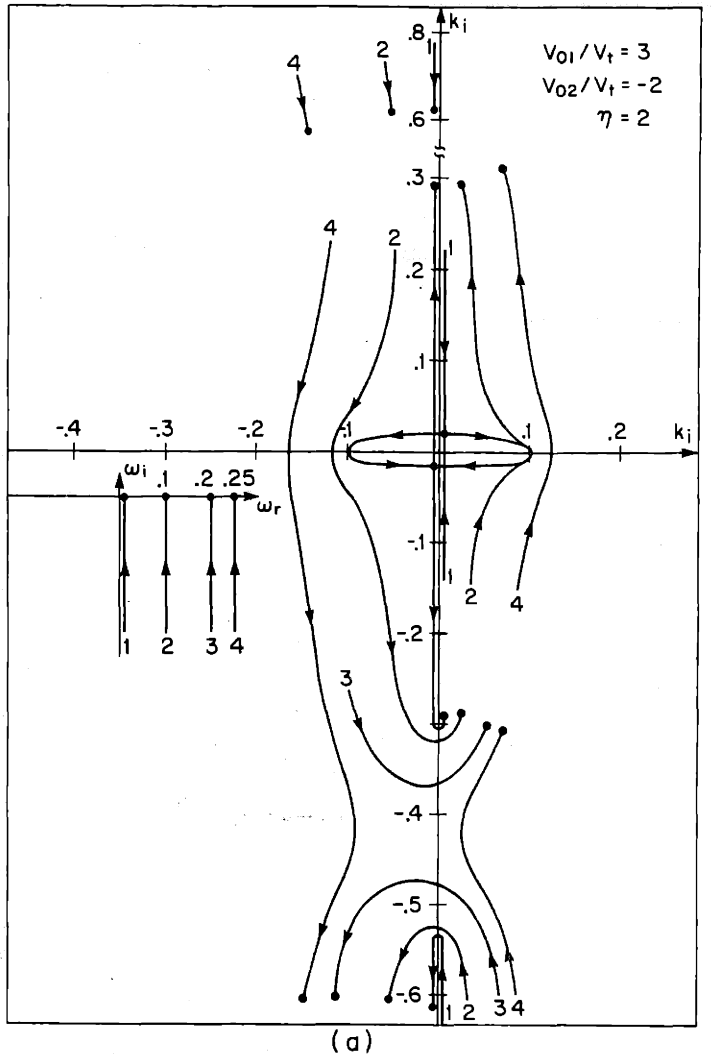

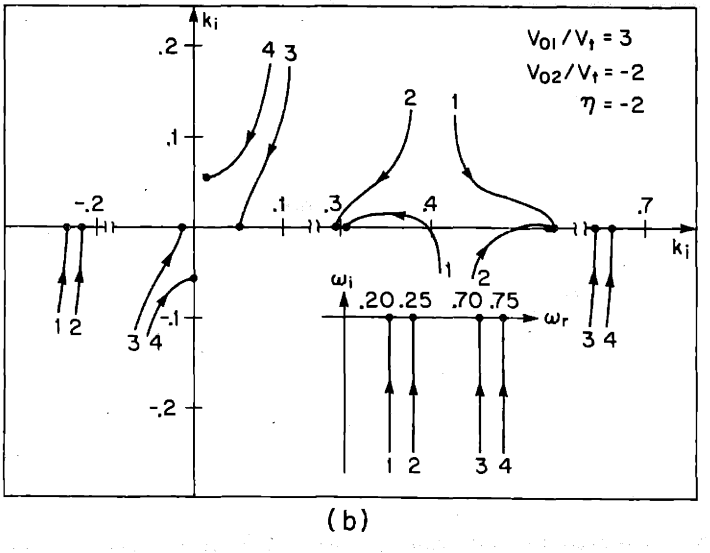

FIGURE 3.10 CLASS III STABILITY CURVES: (a) ELECTRIC FIELD COUPLING PRODUCES A STRONG STATIC INSTABILITY (CURVES 1) AND A WEAK OVERSTABILITY (CURVES 3 AND 4). (b) MAGNETIC FIELD COUPLING PRODUCES AN OVERSTABILITY (CURVES 1 AND 2).

Fig. 3.10b the system exhibits evanescence in the region where there is complex k for real ω. In addition there is a saddle point showing a mild overstability. The spatial character is wavelike and weakly exponential. If the velocities are made equal, the instability becomes static and the exponential part of the spatial character disappears.

It may seem strange that two supercapillary streams, each of which is stable, can couple to produce an absolute instability, but such is the case. Comparing the electric and magnetic field cases, one observes that both exhibit the same general behavior, although the details are different. It will be shown in Chapter 5 when counter-streaming jets are considered in detail, that the mutual coupling term is extremely important in determining system stability.

3.4.4 Class IV - Subcapillary-Supercapillary Streams

Electric Coupling: As in the case of co-streaming supercapillary jets, there are two subregions of flow. In Fig. 3.11b, in which $V_{o1}/V_t > V_{o2}/V_t + 2$, the jets exhibit strong coupling only near zero frequency. This system is quite unique in that it involves the coupling of a convectively unstable jet and an absolutely unstable jet. The result from the Bers-Briggs criterion verify that both types of instability exist when the jets are coupled, as in Fig. 3.12a.

If the jets are more nearly in synchronism such that $V_{o1}/V_t < V_{o2}/V_t$, then there exist two regions of wavenumbers in which the frequency is complex: the usual long wave region characteristic of a subcapillary jet, and a second region at slightly shorter wavelengths. By inspection of the dispersion curve it is not immediately evident what type of instability the latter region exhibits. The stability plot in Fig. 3.12b shows a static instability as expected and convective instability as well. Thus the two subregions both exhibit the same general character as seen in the class II subregions. It might seem that the convectively unstable behavior is inconsequential in the presence of an

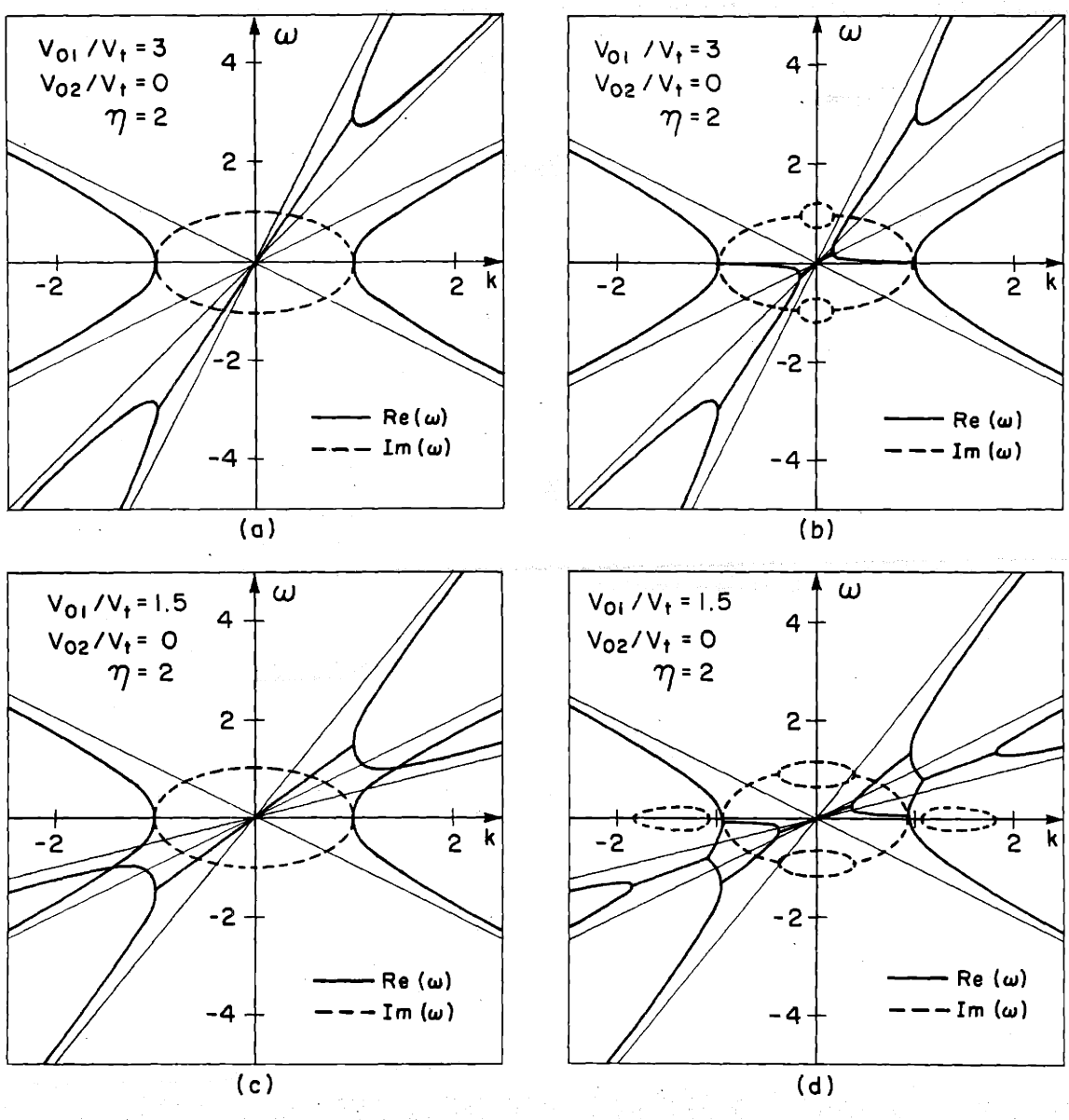

FIGURE 3.11 DISPERSION CURVES FOR CLASS IV FLOW: ELECTRIC FIELD COUPLING. THE MUTUAL COUPLING HAS BEEN SUPPRESSED IN (a) AND (c).

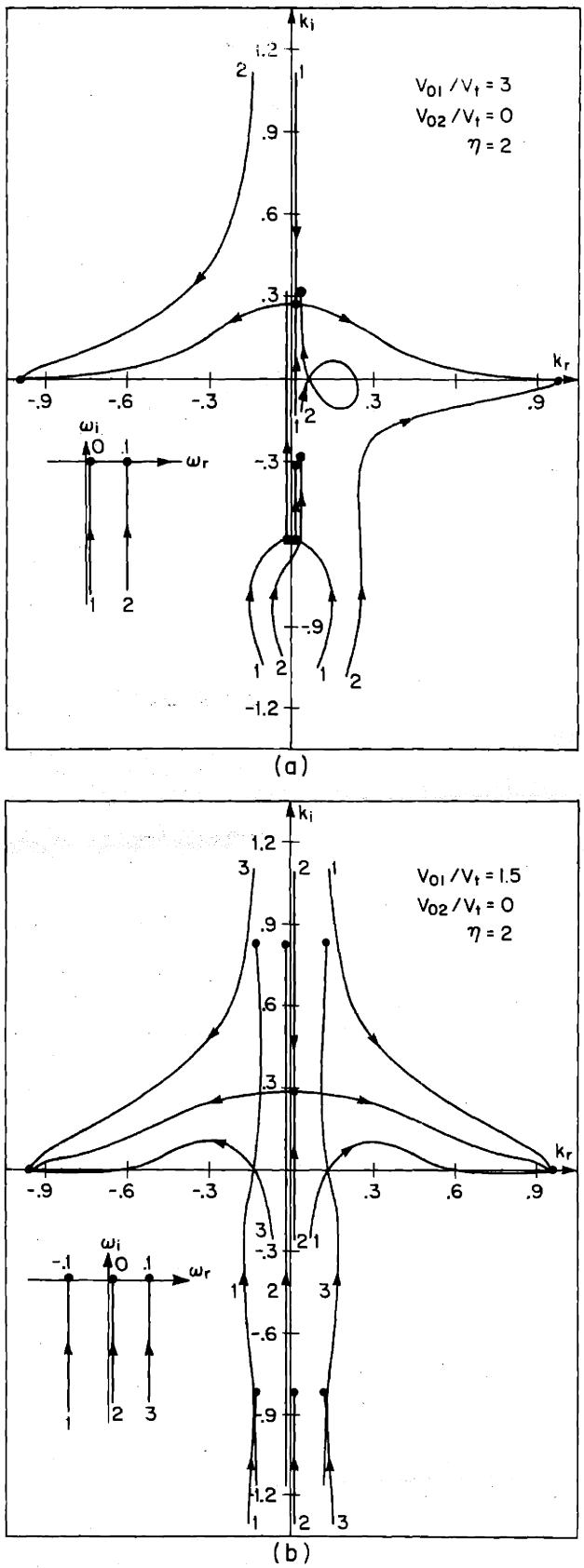

FIGURE 3.12 CLASS IV STABILITY CURVES FOR ELECTRIC FIELD COUPLING. STATIC AND CONVECTIVE INSTABILITIES ARE EVIDENT IN BOTH (a) AND (b).

absolute instability, but it is not difficult to imagine that the finite length system could provide the stabilizing mechanism to suppress the absolute instability and provide the feedback mechanism to transform the convective instability into an overstability. This behavior not only can occur but has been experimentally verified, as will be explained more fully in the discussion on class IV systems of finite length.

Magnetic Coupling: As in the electric field coupling there are again two subregions (Fig. 3.13). The subregion $V_{o1}/V_t < V_{o2}/V_t + 2$ (class IVa) retains the character of the individual jets, namely a purely propagating jet and an evanescent (at low frequencies) jet. For $V_{o1}/V_t > V_{o2}/V_t + 2$, the dispersion curve appears quite interesting. For a band of wavenumbers, the frequency is complex indicating unstable behavior. There is also a band of frequencies for which the wavenumber is complex. This system is in fact, somewhat analogous to the class IIb regime discussed earlier. A difference here is that in addition to the convective instability the system also exhibits evanescence. The stability plot is shown in Fig. 3.14. We shall find later, however, that the presence of boundaries produces a sharp discrimination between the co-streaming case, which retains its convectively unstable character and possesses no natural modes, and the present case, in which boundaries dictate the existence of eigenvalues. The presence of a downstream passive boundary is sufficient to turn a convectively unstable system into an overstability.

3.5 Propagation with Arbitrary Wavelength

Before concluding the chapter, a word should be said concerning the limitation imposed by the long wave model. The dispersion relations will now be rederived and coupling examined as a function of wavelength. As in the previous development, only the electric field coupled equations will be derived.

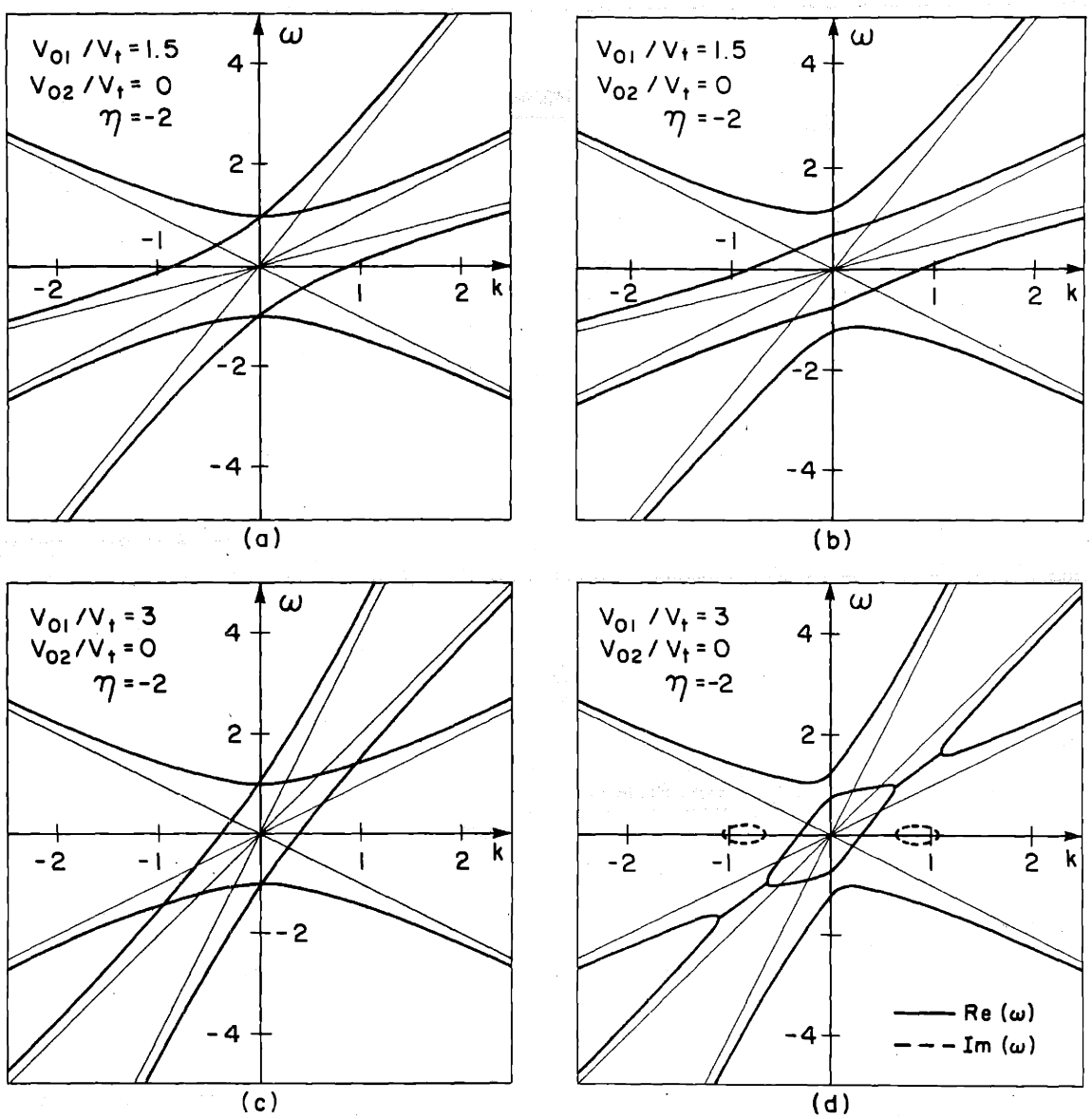

FIGURE 3.13 DISPERSION CURVES FOR CLASS IV FLOW: MAGNETIC FIELD COUPLING. THE MUTUAL COUPLING HAS BEEN SUPPRESSED IN (a) AND (c).

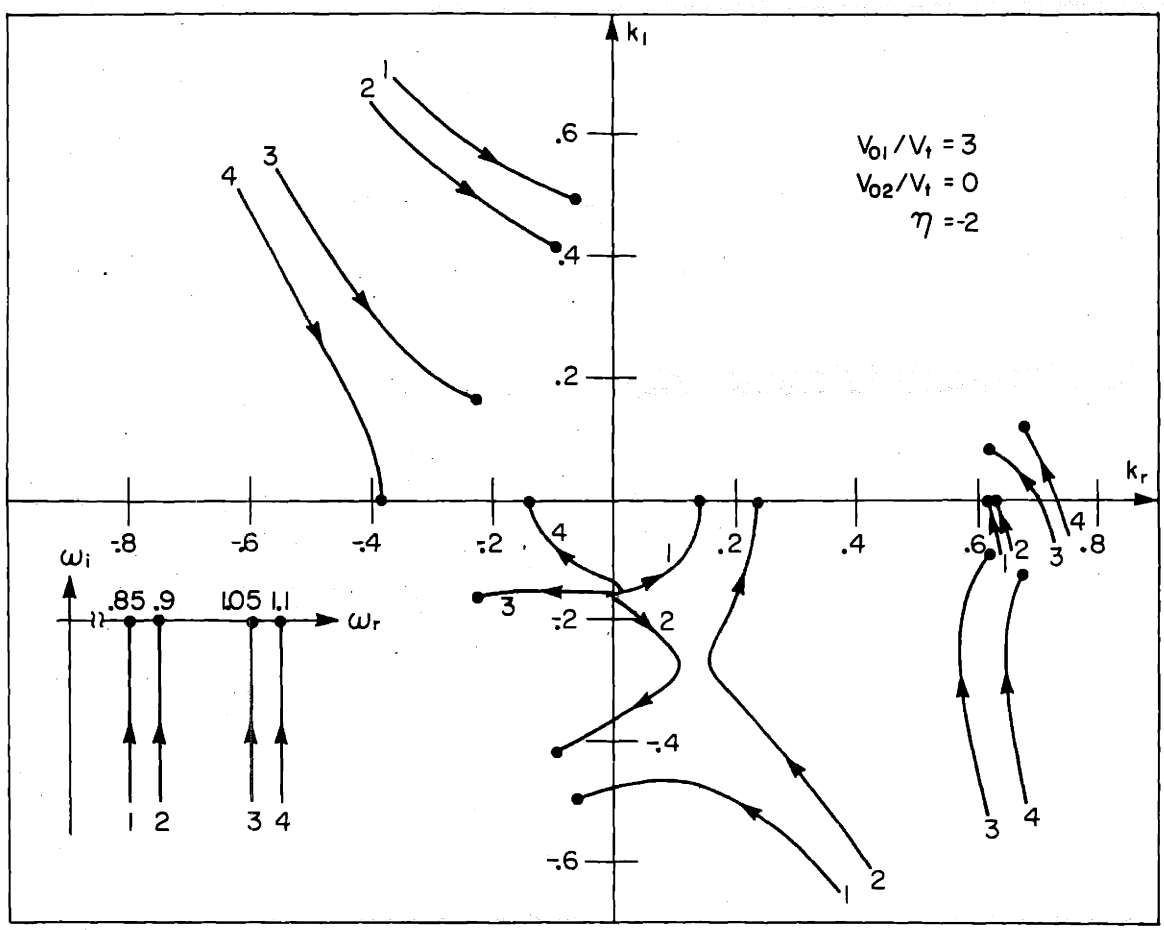

FIGURE 3.14 CLASS IV STABILITY CURVES. THE MAGNETIC FIELD COUPLING PRODUCES A CONVECTIVE INSTABILITY.

We shall use as a starting point the Laplace Equation for both the field and fluid regions and the irrotationality of the field and fluid variables:

Field Equations

$$\frac{\partial^2 E_1}{\partial x_1^2} + \frac{\partial^2 E_1}{\partial x_2^2} = 0$$

$$\frac{\partial E_1}{\partial x_2} - \frac{\partial E_2}{\partial x_1} = 0$$

Fluid Equations

$$\frac{\partial^2 V_2}{\partial x_1^2} + \frac{\partial^2 V_2}{\partial x_2^2} = 0$$

$$\frac{\partial V_1}{\partial x_2} - \frac{\partial V_2}{\partial x_1} = 0 \qquad (3.12)$$

$$\rho\left[\frac{\partial V_2}{\partial t} + V_o \frac{\partial V_2}{\partial x_1}\right] + \frac{\partial p}{\partial x_2} = 0$$

These equations were discussed in Chapter 2 and need no further explanation. If wavelike solutions are assumed of the form $q(x_1,x_2,t) = \mathrm{Re}[\tilde{q}(x_2)e^{j(\omega t-kx_1)}]$ where q is any field variable, the solution to the field equation of (3.12) is

Region 1.
$$\tilde{E}_1^{(1)} = A_1 \sinh k(b-x_2) + B_1 \sinh k(x_2-a-\Delta/2)$$
$$\tilde{E}_2^{(2)} = -j[A_1 \cosh k(b-x_2) - B_1 \cosh k(x_2-a-\Delta/2)]$$

Region 3.
$$\tilde{E}_1^{(3)} = A_3 \sinh k(a-\Delta/2-x_2) + B_3 \sinh k(x_2+a-\Delta/2)$$
$$\tilde{E}_2^{(3)} = -j[A_3 \cosh k(a-\Delta/2-x_2) - B_3 \cosh k(x_2+a-\Delta/2)]$$

Region 5.
$$\tilde{E}_1^{(5)} = A_5 \sinh k(x_2+b) + B_5 \sinh k(a+\Delta/2+x)$$
$$\tilde{E}_2^{(5)} = j[A_5 \cosh k(x_2+b) + B_5 \cosh k(a+\Delta/2+x)]$$

and in the field region

Region 2.
$$\tilde{V}_2^{(2)} = A_2 \sinh k(a+\Delta/2-x_2) + B_2 \sinh k(x_2-a+\Delta/2)$$
$$\tilde{V}_1^{(2)} = -j[A_2 \cosh k(a+\Delta/2-x_2) - B_2 \cosh k(x_2-a+\Delta/2)]$$

$$\tilde{p}^{(2)} = -j\frac{\rho(\omega-V_{o1}k)}{k}[A_2 \cosh k(a+\Delta/2-x_2) - B_2 \cosh k(x_2-a+\Delta/2)]$$

Region 4.
$$\tilde{V}_2^{(4)} = A_4 \sinh k(a+\Delta/2+x_2) + B_4 \sinh k(a-\Delta/2+x_2)$$
$$\tilde{V}_1^{(4)} = j[A_4 \cosh k(a+\Delta/2+x_2) + B_4 \cosh k(a-\Delta/2+x_2)]$$
$$\tilde{p}^{(4)} = j \frac{\rho(\omega-V_{o2}k)}{k}[A_4 \cosh (a+\Delta/2+x_2) + B_4 \cosh k(a-\Delta/2+x_2)]$$

Since there are five coupled regions, ten boundary conditions are required. In addition, the displacement amplitude of each interface is unknown, making a total of 14 constraints. Because each boundary is highly conducting, $\hat{n} \times \bar{E} = 0$ at each interface yields six relations, the equation of motion of each interface ($\frac{dF}{dt} = 0$) four more, and the transverse momentum boundary condition the final four conditions.

If the field boundary conditions at each of the six surfaces and the equation of motion of each of the four fluid interfaces are applied, the A and B coefficients defined above may be evaluated as a linear combination of the surface displacement amplitude.

$$A_1 = \frac{jkE_o\xi_1}{S_1} \qquad B_1 = 0$$

$$A_2 = \frac{j(\omega-V_{o1}k)\xi_2}{S_\Delta} \qquad B_2 = \frac{j(\omega-V_{o1}k)\xi_1}{S_\Delta}$$

$$A_3 = \frac{jkE_o\xi_3}{S_2} \qquad B_3 = \frac{jkE_o\xi_2}{S_2}$$

$$A_4 = \frac{j(\omega-V_{o2}k)\xi_3}{S_\Delta} \qquad B_4 = \frac{j(\omega-V_{o2}k)\xi_4}{S_\Delta}$$

$$A_5 = \frac{jkE_o\xi_4}{S_1} \qquad B_5 = 0$$

where

$$S_1 = \sinh k(b-a-\Delta/2)$$

$$S_2 = \sinh k(2a-\Delta)$$

$$S_\Delta = \sinh k\Delta$$

From Chapter 2, the momentum boundary condition is: $[\![p]\!] = T\frac{\partial^2 \xi}{\partial x^2} + [\![T_{22}]\!]$.

In order to evaluate the momentum boundary conditions it is necessary to compute the stress of electrical origin acting on each interface. Since $E_{tangential} \equiv 0$ at each interface, there can be no shear traction to first order terms, so that

$$T_{22} = \frac{1}{2}\varepsilon_o E_o^2 + \varepsilon_o E_o E_2(x_2) \text{ to linear terms.}$$

Applying the momentum equation at each interface and substituting the A's and B's from above the following set of coupled equations is obtained:

$$[\frac{(\omega-V_{o1}k)^2}{T_\Delta} - k^3\frac{T}{\rho} + \frac{\varepsilon_o E_o^2 k^2}{\rho\, T_1}]\xi_1 = \frac{(\omega-V_{o1}k)^2}{S_\Delta}\xi_2 \qquad (a)$$

$$[\frac{(\omega-V_{o1}k)^2}{T_\Delta} - k^3\frac{T}{\rho} + \frac{\varepsilon_o E_o^2 k^2}{\rho\, T_2}]\xi_2 = \frac{(\omega-V_{o1}k)^2}{S_\Delta}\xi_1 + \frac{\varepsilon_o E_o^2 k^2}{\rho\, S_2}\xi_3 \qquad (b)$$

$$[\frac{(\omega-V_{o2}k)^2}{T_\Delta} - k^3\frac{T}{\rho} + \frac{\varepsilon_o E_o^2 k^2}{\rho\, T_2}]\xi_3 = \frac{(\omega-V_{o2}k)^2}{S_\Delta}\xi_4 + \frac{\varepsilon_o E_o^2 k^2}{\rho\, S_2}\xi_2 \qquad (c)$$

$$[\frac{(\omega-V_{o2}k)^2}{T_\Delta} - k^3\frac{T}{\rho} + \frac{\varepsilon_o E_o^2 k^2}{\rho\, T_1}]\xi_4 = \frac{(\omega-V_{o2}k)^2}{S_\Delta}\xi_3 \qquad (d)$$

(3.12)

where $T_\Delta = \tanh k\Delta$, $T_1 = \tanh k(b-a-\Delta/2)$, $T_2 = \tanh k(2a-\Delta)$.

From inspection of (3.12) above, it is clear that the forces exerted on an interface come about either because of the motion of that interface (self coupling terms) or because of motion of the <u>adjacent</u> interfaces (mutual coupling terms). This is a result of the fact that the fluid regions are field

free and the field in one region is effectively screened from another.

Equations (3.12) may be combined to yield the following dispersion relation.

$$\{[\frac{(\omega-V_{o1}k)^2}{T_\Delta} - k^3\frac{T}{\rho} + \frac{\varepsilon_o E_o^2 k^2}{\rho\, T_1}][\frac{(\omega-V_{o1}k)^2}{T_\Delta} - k^3\frac{T}{\rho} + \frac{\varepsilon_o E_o^2 k^2}{\rho\, T_2}] - \frac{(\omega-V_{o1}k)^4}{S_\Delta^2}\}$$

$$\{[\frac{(\omega-V_{o2}k)^2}{T_\Delta} - k^3\frac{T}{\rho} + \frac{\varepsilon_o E_o^2 k^2}{\rho\, T_2}][\frac{(\omega-V_{o2}k)^2}{T_\Delta} - k^3\frac{T}{\rho} + \frac{\varepsilon_o E_o^2 k^2}{\rho\, T_1}] - \frac{(\omega-V_{o2}k)^4}{S_\Delta^2}\}$$

$$-(\frac{\varepsilon_o E_o^2 k^2}{\rho\, S_2})^2\,[\frac{(\omega-V_{o1}k)^2}{T_\Delta} - k^3\frac{T}{\rho} + \frac{\varepsilon_o E_o^2 k^2}{\rho\, T_1}][\frac{(\omega-V_{o2}k)^2}{T_\Delta} - k^3\frac{T}{\rho} + \frac{\varepsilon_o E_o^2 k^2}{\rho\, T_1}] = 0 \qquad (3.13)$$

This dispersion relation as it stands is not very useful. In order to make the analysis more tractable, we will assume, on physical grounds, the jets to be thin compared to the other transverse dimensions; i.e. $\frac{\Delta}{2a} << 1$ and $\frac{\Delta}{b-a} << 1$. This assumption allows one to think of each jet as composed of a symmetric and antisymmetric mode as in the single jet case. If the jet is thin, then, we would expect that the two interfaces would move in phase (kink mode) or in opposition (sausage mode) with about the same amplitude.

Kink Modes: If we add (3.12a) to (3.12b) and (3.12c) to (3.12d) and make the approximation that $\xi_+ \tilde{\sim} \xi_1 \tilde{\sim} \xi_2$ and $\xi_- \tilde{\sim} \xi_3 \tilde{\sim} \xi_4$, (3.13) becomes

$$\{(\omega-V_{o1}k)^2\, T\,\frac{\Delta}{2} - k^3\frac{T}{\rho} + \frac{\varepsilon_o E_o^2 k^2}{2\rho}[\frac{1}{T_1}+\frac{1}{T_2}]\}\xi_+ = \frac{\varepsilon_o E_o^2 k^2}{2\rho S_2}\,\xi_-$$

$$\{(\omega-V_{o2}k)^2\, T\,\frac{\Delta}{2} - k^3\frac{T}{\rho} + \frac{\varepsilon_o E_o^2 k^2}{2\rho}[\frac{1}{T_1}+\frac{1}{T_2}]\}\xi_- = \frac{\varepsilon_o E_o^2 k^2}{2\rho S_2}\,\xi_+ \qquad (3.14)$$

Sausage Modes: If (3.12a) and (3.12c) are subtracted from (3.12b) and (3.12d) respectively, and the approximation $\xi_+ \tilde{\sim} \xi_2 \tilde{\sim} \xi_1$ and $\xi_- \tilde{\sim} \xi_3 \tilde{\sim} \xi_4$ is made, we get

$$\left\{\frac{(\omega-V_{o1}k)^2}{T_{\Delta/2}} - k^3\frac{T}{\rho} + \frac{\varepsilon_o E_o^2 k^2}{2\rho}\left[\frac{1}{T_1}+\frac{1}{T_2}\right]\right\}\xi_+ = \frac{\varepsilon_o E_o^2 k^2}{2\rho S_2}\xi_-$$

$$\left\{\frac{(\omega-V_o k)^2}{T_{\Delta/2}} - k^3\frac{T}{\rho} + \frac{\varepsilon_o E_o^2 k^2}{2\rho}\left[\frac{1}{T_1}+\frac{1}{T_2}\right]\right\}\xi_- = \frac{\varepsilon_o E_o^2 k^2}{2\rho S_2}\xi_+ \qquad (3.15)$$

The above approximation is not a long wave assumption, but rather a statement that the two fluid boundaries of a given jet are much more strongly influenced by each other than by the rigid plates or the other jet. If the mutual coupling terms are suppressed in (3.14) the equations decouple and become the dispersion relation for a single jet (2.21).

To simplify (3.14) and (3.15) further, consider the asymptotic behavior at short and long wavelength. Since there are two transverse dimensions, there are several possible limiting cases. For very short waves, $k\Delta \gg 1$ and as in the case of a single jet, the two surfaces of the jet decouple from each other and of course decouple from the other transverse boundaries. From (3.14) and (3.15) it is evident that the mutual coupling becomes exponentially important as the waves become long. For short waves the coupling approaches zero and each jet behaves independent of the other.

Long Wave Approximation: Since the interest here is to study the interaction of one stream on another, the long wave region is especially important. If the approximation is then made that the wavelengths of interest are long compared to all transverse dimensions, then the hyperbolic functions in (3.14) and (3.15) can be replaced by their argument and we obtain

Kink modes

$$[(\omega-V_{o1}k)^2 - k^2V_t^2 + \frac{\omega_e^2\eta}{2}]\xi_+ = \frac{\omega_e^2}{2}\xi_-$$

$$[(\omega-V_{o2}k)^2 - k^2V_t^2 + \frac{\omega_e^2\eta}{2}]\xi_- = \frac{\omega_e^2}{2}\xi_+ \qquad (3.16)$$

Sausage modes

$$[(\omega-V_{o1}k)^2 - k^2V_t^2\,(\frac{k\Delta}{2})^2 + \frac{\omega_e^2\eta}{2}\,(\frac{k\Delta}{2})^2]\xi_+ = \frac{\omega_e^2}{2}\,(\frac{k\Delta}{2})^2\xi_-$$

$$[(\omega-V_{o2}k)^2 - k^2V_t^2\,(\frac{k\Delta}{2})^2 + \frac{\omega_e^2\eta}{2}\,(\frac{k\Delta}{2})^2]\xi_- = \frac{\omega_e^2}{2}\,(\frac{k\Delta}{2})^2\xi_+ \qquad (3.17)$$

where $V_t^2 = \frac{2T}{\rho\Delta}$, $\omega_e^2 = \frac{2\varepsilon_o E_o^2}{\rho\Delta(2a-\Delta)}$, and $\eta = \frac{b+a-\frac{3\Delta}{2}}{b-a-\frac{\Delta}{2}}$.

The equations for the sausage and kink modes are similar in form except for the factor $(\frac{k\Delta}{2})^2$ appearing in the force terms of the sausage mode. Since now $k\Delta << 1$ the forces are small. Equations (3.16) and (3.17) are the same as (3.4) if a wavelike solution is assumed. There are thus two points of view which one can take in deriving the equations of motion. One can postulate a long wave model and solve the considerably simplified field equation. It might be mentioned that the nonlinear equations are available from (3.3). Alternately the linear two dimensional model may be solved exactly and regions of interest examined. In this light the long wave limit is simply the first term in an infinite expansion of the transverse eigenmodes. In either case the long wave kink modes will be the subject of interest for the remainder of this thesis.

CHAPTER 4

CO-STREAMING SUBCAPILLARY AND SUPERCAPILLARY FLOW

In the previous chapter it was found that the various two stream flow regimes could be divided into four classes. Two of these regimes, co-streaming supercapillary jets and two subcapillary jets, will be presently investigated. It was shown that for two subcapillary jets, causal solutions are obtained only when one boundary condition is applied at each end of each jet. This is the same conclusion that would have been reached if the jets were uncoupled. In fact, it was shown that for spring-type coupling (characterized by either electric or magnetic field coupling) the coupling plays no role in the specification of boundary conditions. For supercapillary co-streaming jets two boundary conditions are appropriate at the upstream end of the jets.

Boundary conditions at more than one point in space imply that the system possesses eigenvalues. If both jets have the same flow velocity, the system splits into two symmetry modes, each mode possessing dynamics similar to that of a single jet of the same flow velocity but different coupling co-efficients. The special cases of two stationary jets and two supercapillary jets of the same flow velocity are studied here. Experiments which support the model for the former case will be discussed.

We shall use as a starting point the long wave quasi-one-dimensional model of two streaming similar jets, equation (3.4).

$$\left[\left(\frac{\partial}{\partial t} + V_{o1}\frac{\partial}{\partial x}\right)^2 - V_t^2\frac{\partial^2}{\partial x^2} - \omega_e^2\frac{\eta}{2}\right]\xi_1 = -\frac{\omega_e^2}{2}\xi_2 \qquad (4.1)$$

$$\left[\left(\frac{\partial}{\partial t} + V_{o2}\frac{\partial}{\partial x}\right)^2 - V_t^2\frac{\partial^2}{\partial x^2} - \omega_e^2\frac{\eta}{2}\right]\xi_2 = -\omega_e^2\xi_1$$

If we now set $V_{o1} = V_{o2} = V_o$, we observe that both equations of (4.1) are identical if $\xi_2 = \pm \xi_1$. These then are general solutions and represent the symmetry modes of the system. The + sign will be called the symmetric mode while the - sign refers to the antisymmetric mode (hereafter for convenience the S and A modes respectively) and are shown in Fig. 4.1. Equation (4.1) becomes

$$\left[\left(\frac{\partial}{\partial t} + V_o \frac{\partial}{\partial x}\right)^2 - V_t^2 \frac{\partial^2}{\partial x^2} - \omega_e^2 \frac{\eta \pm 1}{2}\right] \xi_{\substack{S \\ A}} = 0 \qquad (4.2)$$

When the symmetry modes are being discussed together, the upper sign will refer to the S mode. We recognize that this equation is of the same form as (2.38) for a single jet between rigid plates, with the modification that the coupling coefficient is altered, becoming larger for the S mode and smaller for the A mode than in the single jet case. This type of behavior is quite common in lumped parameter systems in which two identical components (two oscillators, for example) are coupled together, producing symmetry modes whose behavior lies on either side of that of one component by itself.

Since the equations of motion decouple into two second-order systems, all of the techniques described in Chapter 2 are valid. In particular, there are two distinct flow regimes, $V_o < V_t$ (subcapillary flow) and $V_o > V_t$ (supercapillary flow). The dispersion relation corresponding to (4.2), (assuming solutions of the form $e^{j(\omega t - kx)}$) is given by:

$$(\omega - V_o k)^2 - V_t^2 k^2 + \omega_e^2 \frac{\eta \pm 1}{2} = 0 \qquad (4.3)$$

and is of the same form as the one stream interaction of Chapter 2. We observe that at point a of Fig. 2.3, the two values of ω merge as k is varied. Solving (4.3) for ω,

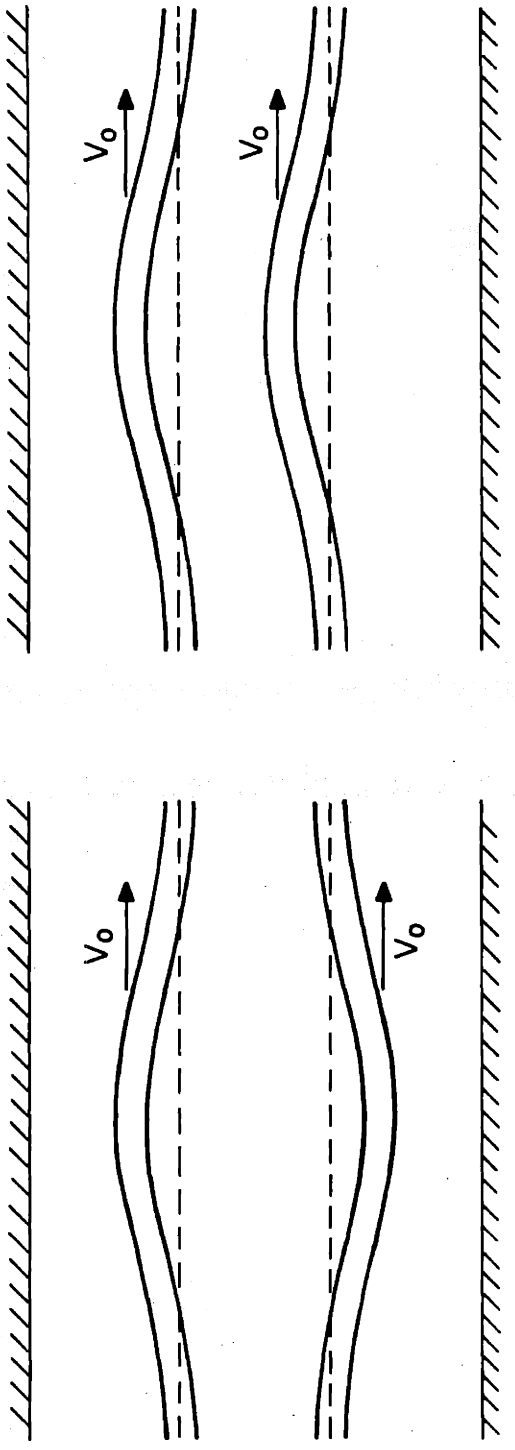

FIGURE 4.1 SYMMETRY MODES FOR SIMILAR CO-STREAMING JETS

$$\omega = V_o k \pm \sqrt{V_t^2 k^2 - \omega_e^2 \frac{\eta \pm 1}{2}}$$

so that at the cutoff frequency the radical must vanish, or

$$k_a = \frac{\omega_e}{V_t} \sqrt{\frac{\eta \pm 1}{2}}$$

and

$$\omega_a = V_o k_a = \frac{V_o}{V_t} \omega_e \sqrt{\frac{\eta \pm 1}{2}}$$

For values of k below this critical value the frequency becomes complex. From the discussion of the previous chapter, for subcapillary flow the system exhibits a static instability. Since the k values are the same at the saddle point, solving (4.3) for k

$$k = \frac{V_o}{V_o^2 - V_t^2} \pm \sqrt{\omega^2 V_t^2 - (V_o^2 - V_t^2)\omega_e^2 \frac{\eta \pm 1}{2}} \; / \; (V_o^2 - V_t^2) \qquad (4.4)$$

we obtained at the saddle point,

$$\omega_s = -j\omega_e \sqrt{(1 - V_o^2/V_t^2)\frac{\eta \pm 1}{2}}$$

and

$$k_s = \frac{j\omega_e V_o}{\sqrt{1 - V_o^2/V_t^2}} \sqrt{\frac{\eta \pm 1}{2}}$$

We observe that the symmetric mode is more unstable than the antisymmetric mode.

The effect of jet velocity on the saddle point is interesting. At zero velocity the system is at maximum instability and the wave number is zero (infinite wavelength.) As the velocity is raised to V_t, the temporal growth rate is decreased to zero but the spatial growth rate is increased to infinity as V_o approaches V_t.

For $V_o > V_t$, the Bers-Briggs plots exhibit a convective instability for the

range of frequencies $0 \leq \omega < \frac{\omega_e V_o}{V_t} \sqrt{(1-V_t^2/V_o^2)\frac{n\pm1}{2}}$. The maximum spatial growth rate occurs at zero frequency and is given by

$$k_{max} = \frac{j\omega_e \frac{n\pm1}{2}}{\sqrt{V_o^2 - V_t^2}}$$

As the jet velocity is decreased to V_t, the spatial growth rate becomes infinite. The point $V_o = V_t$ then physically represents a transition at which spatial growth is transformed into temporal growth.

4.1 Boundary Conditions for Identical Jets

We may take advantage of the symmetry of the system to state that the boundary conditions must apply in the same way for each jet; i.e. for subcapillary jets, one boundary condition is applied at each end of each jet, while for supercapillary flow two boundary conditions are applied at the upstream end of the jet.

The solution of (4.2) may be written:

$$\xi = e^{j\omega t}\left[A_1 e^{-jk_1 x} + A_2 e^{-jk_2 x}\right]$$

Applying the B.C. for subcapillary flow that $\xi(o,t) = \xi(L,t) = 0$ we obtain the following determinantal equation

$$\begin{bmatrix} 1 & 1 \\ e^{-jk_1 L} & e^{-jk_2 L} \end{bmatrix} \begin{bmatrix} A_1 \\ A_2 \end{bmatrix} = \begin{bmatrix} 0 \\ 0 \end{bmatrix}$$

For a nontrivial solution, the determinant must vanish, or $e^{-jk_1 L} = e^{-jk_2 L}$

This means that $k_1 = k_2 + \frac{2n\pi}{L}$ (4.5)

Combining (4.5) with the dispersion relation yields the eigenfrequencies and eigenvalues. Inserting (4.5) into (4.4) we have

$$\left(\frac{n\pi}{L}\right)^2 = \left(\frac{\omega V_o}{V_o^2-V_t^2}\right)^2 - \frac{\omega^2+\omega_e^2\,\frac{\eta\pm1}{2}}{V_o^2-V_t^2}$$

Solving for ω^2:

$$\omega^2 = (1-V_o^2/V_t^2)\left[(V_t^2-V_o^2)\left(\frac{n\pi}{L}\right)^2 - \omega_e^2\,\frac{\eta\pm1}{2}\right] \tag{4.6}$$

At zero electric field the resonant frequency is given simply by

$$\omega_o = \frac{V_t^2-V_o^2}{V_t}\,\frac{n\pi}{L}$$

As the electric field is increased, the resonant frequency is decreased to zero at the critical field value given by

$$\omega_{ec}\sqrt{\frac{\eta\pm1}{2}} = \omega_o \tag{4.7}$$

We observe that the fundamental mode is the first to go unstable and that the symmetric mode becomes unstable at a lower critical field than the antisymmetric mode. The complex eigenfrequencies are plotted in Fig. 4.2, where ω and L have been normalized to

$$\bar{\omega} = \frac{\omega}{\omega_e}\,\frac{V_t}{\sqrt{V_t^2-V_o^2}} \quad \text{and} \quad \bar{L} = \frac{L\omega_e}{\sqrt{V_t^2-V_o^2}}$$

and (4.6) becomes

$$\bar{\omega}^2 = \left(\frac{n\pi}{\bar{L}}\right)^2 - \frac{\eta\pm1}{2} \tag{4.8}$$

4.2 The Two Spring Experiment

In order to test out the theory presented in the previous sections, an experiment was devised to simulate two identical jets of zero velocity making use of weak springs (having approximately the same linear density although a considerably higher tension than the surface tension of liquid jets). This experiment

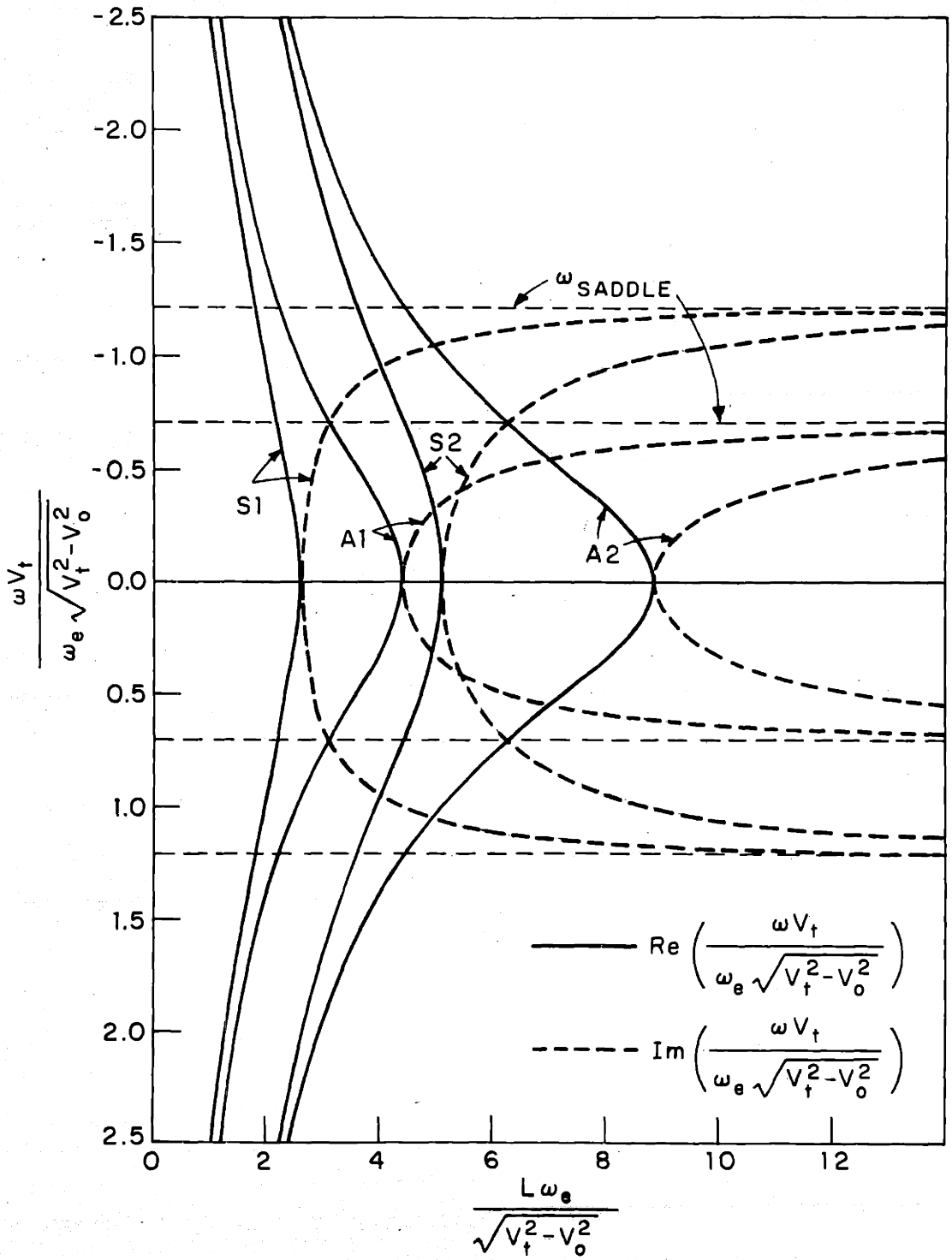

FIGURE 4.2 COMPLEX EIGEN FREQUENCIES VERSUS NORMALIZED LENGTH FOR ELECTRIC FIELD COUPLED SUBCAPILLARY JETS. ONLY THE TWO LOWEST SYMMETRIC AND ANTISYMMETRIC MODES ARE SHOWN.

serves the additional purpose of providing a quantitative evaluation of the coupling parameters to be used in the experiments of later chapters. Two springs of the same spring constant and mass were stretched to the same tension between horizontal rigid supports. Rigid rods were placed on either side in order to establish electrical equilibrium. A d.c. voltage was then applied to the springs and plates. By carefully adjusting the outer plates, it was possible to establish electrical equilibrium using a single voltage source. The positions of the springs were detected by means of phototubes placed above the springs; the springs were illuminated from below by a single small but intense source of light. The phototubes were calibrated and it was found that the voltage output versus spring displacement was linear over the useful range of the phototube (about 75% of the cathode length or 3 cm.) which allowed for a maximum peak to peak spring amplitude of about 1.0 cm. before the output waveform would be sharply clipped.

The question of whether springs can be used to provide verification for a planar model is well taken. What will be shown below, in fact, is the the dynamics are predicted properly, but to provide quantitative agreement, that self and mutal coupling co-efficients must be measured experimentally. Since the two-spring experiment can be performed quite accurately, this experiment will be used to dynamically measure these co-efficients for the experiments to be described in this and later chapters.

The theoretical model used to predict the experimental behavior, is strictly speaking, incorrect. The effect of gravity cannot be ignored, even though the springs are stretched in the horizontal plane. Since the springs were stretched only slightly the sag in the springs is appreciable. To eliminate this, each spring was supported by fine insulating strings at several points along its length to make the springs line up horizontally with the plates. The support strings,

however, introduced a restoring force given by $-\rho\pi r^2 g/_{\ell}\xi$ since then a spring acts as a continuum of pendulums as well as a vibrating string.

If this term is included into the equations of motion, (4.1), we get, after setting $V_{o1} = V_{o2} = 0$

$$\left[\frac{\partial^2}{\partial t^2} - V_t^2 \frac{\partial^2}{\partial x^2} - \omega_e^2 \frac{\eta}{2} + \frac{\pi r^2 g}{\ell}\right] \xi_1 = -\frac{\omega_e^2}{2} \xi_2$$

$$\left[\frac{\partial^2}{\partial x^2} - V_t^2 \frac{\partial^2}{\partial x^2} - \omega_e^2 \frac{\eta}{2} + \frac{\pi r^2 g}{\ell}\right] \xi_2 = -\frac{\omega_e^2}{2} \xi_1 \qquad (4.9)$$

It is evident that the pendulum correction term does not affect the symmetry of the system. The dispersion relation for these modes then becomes

$$\omega^2 - V_t^2 k^2 + \omega_e^2 \frac{\eta \pm 1}{2} - \frac{\pi r^2 g}{\ell} = 0 \qquad (4.10)$$

Combining with the determinantal equation, (4.5)

$$\omega^2 = V_t^2 \left(\frac{n\pi}{L}\right)^2 - \omega_e^2 \frac{\eta \pm 1}{2} + \frac{\pi r^2 g}{\ell} \qquad (4.11)$$

The most accurate dynamical measurement which can be made on the springs is that of the resonant frequency. From (4.6) we observe that $\omega^2 \sim -\omega_e^2(\eta \pm 1)$; a plot of the frequency squared vs. voltage squared should yield two straight lines of negative slope. The experimental data is shown on Fig. 4.3 and is seen to follow the predicted behavior. At high voltage the equilibrium positions of the springs were displaced, which account for the deviation of the curve from a straight line. It might be mentioned in passing that the Q of a spring is high ($O(10^3)$). As a result the resonant frequency is sharp, so sharp in fact that drift in the oscillator and voltage supply and the error in reading the frequency from the oscillator dial become the limiting factors in determining the resonant frequency.

From Fig. 4.3, we may determine the values of the coupling parameters ω_e and η.

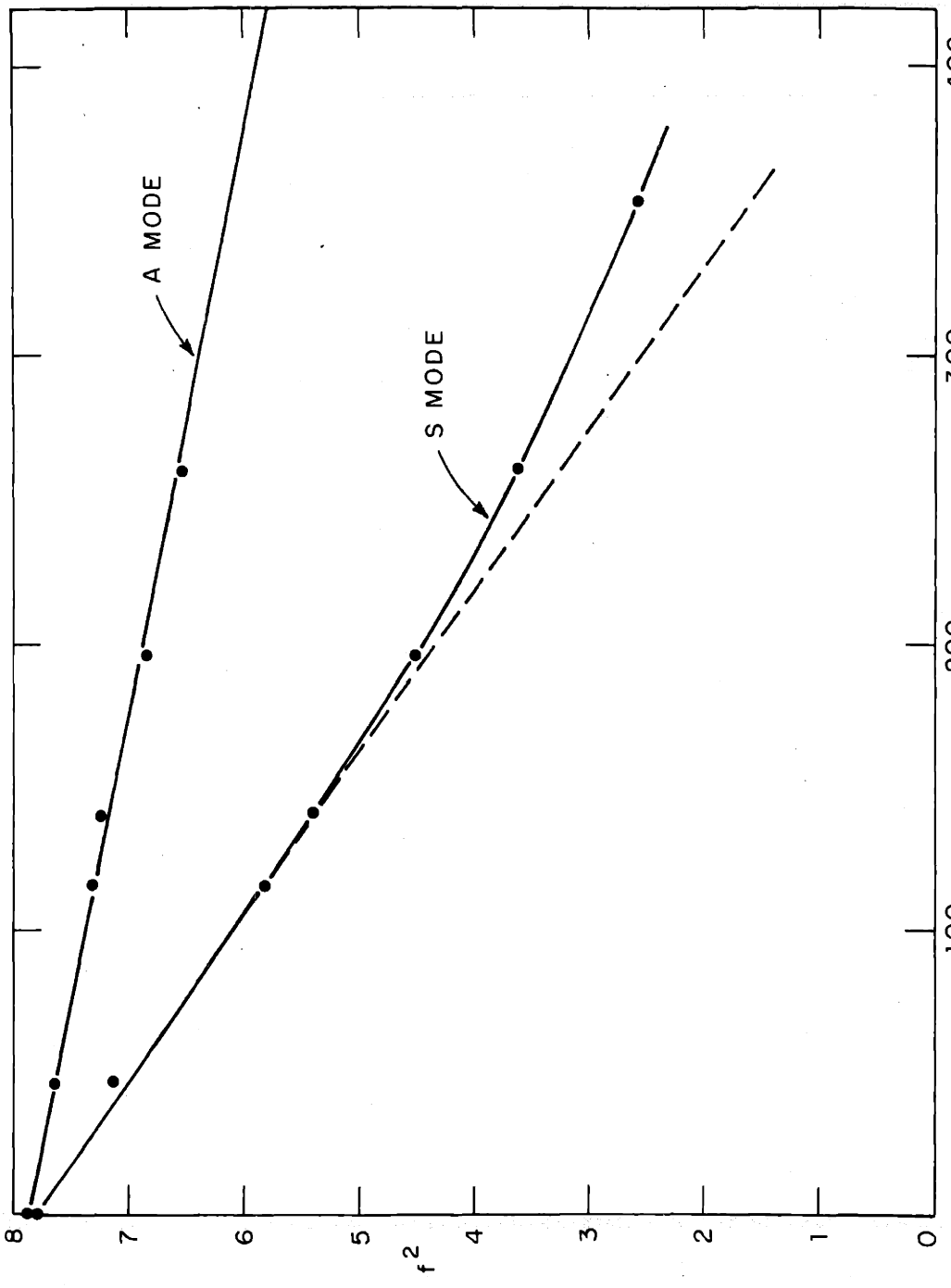

FIGURE 4.3 FUNDAMENTAL SYMMETRIC AND ANTISYMMETRIC MODE FREQUENCY SHIFT DATA FOR TWO SPRINGS STRESSED BY A TRANSVERSE ELECTRIC FIELD.

From (4.11)

$$f^2 = V_t^2 \frac{n^2}{4L^2} - \omega_e^2 \frac{\eta \pm 1}{2} \frac{1}{(2\pi)^2} + \frac{r^2 f}{4\pi \ell} \qquad (4.12)$$

Setting $\omega_e/2\pi = AV$, the slopes of the curves become $A^2 \frac{\eta \pm 1}{2}$.

If the slopes are defined as S_s and S_a then

$$\eta = \frac{S_s/S_a + 1}{S_s/S_a - 1} = 1.765$$

and

$$A = \frac{2S_s}{\eta+1} = .1101 \quad \frac{cps}{kV}$$

These may be compared to the theoretical values for the experiment

$$\eta = \frac{b+a-\frac{3\Delta}{2}}{b-a-\frac{\Delta}{2}} = 1.915$$

$$A = \frac{1}{2\pi}\sqrt{\frac{2\varepsilon_o}{\rho\Delta(2a-\Delta)^3}} = .0671 \quad \frac{cps}{kV}$$

One should not expect these theoretical values of η and A based on a planar jet theory to agree with experimental values, since the geometry here is considerably different.

From the above discussion, the inclusion of the pendulum term had no effect on the determination of the coupling parameters ω_e and η. This is not to say that it can be ignored, however. If f^2 is plotted vs n^2, for example, with no electric field, it is found that the experimental data does in fact lie on a straight line but not passing through the origin, verifying (4.12). The pendulum effect will become important in spring-jet interactions, discussed in Chapter 8.

4.3 Co-Streaming Supercapillary Jets:

If the two jets have $V_o > V_t$ the dynamics are entirely changed. In this case, the jets can exhibit spatial growth but not temporal growth, since disturbances

which would tend to grow on the jet are swept downstream faster than they would propagate upstream. The solution of (4.2) may be written

$$\xi = \mathrm{Re}\left\{e^{j\omega t}\left[A_1 e^{-jk_1 x} + A_2 e^{-jk_2 x}\right]\right\} \tag{4.13}$$

Since there are no absolute instabilities, the system may be excited in the sinusoidal steady state. If we now impose the boundary conditions

$$\xi_1(0,t) = 0 \qquad \xi_2(0,t) = 0$$

$$\frac{\partial \xi_1}{\partial x}(0,t) = \theta e^{j\omega t} \qquad \frac{\partial \xi_2}{\partial x}(0,t) = 0$$

If (4.4) is used to eliminate k_1 and k_2, there are two forms of the solution depending on whether the driving frequency is above the cutoff frequency (k's real) or below the cutoff frequency (k's complex). Then

$$\xi_1 = \mathrm{Re}\left\{\frac{\theta}{2}\left[\frac{\sin\beta_S x}{\beta_S} + \frac{\sin\beta_A x}{\beta_A}\right] e^{j(\omega t - \beta_o x)}\right\}$$

$$\xi_2 = \mathrm{Re}\left\{\frac{\theta}{2}\left[\frac{\sin\beta_S x}{\beta_S} + \frac{\sin\beta_A x}{\beta_A}\right] e^{j(\omega t - \beta_o x)}\right\} \quad \omega > \omega_a$$

$$\xi_1 = \mathrm{Re}\left\{\frac{\theta}{2}\left[\frac{\sinh\beta_S x}{\beta_S} + \frac{\sinh\beta_A x}{\beta_A}\right] e^{j(\omega t - \beta_o x)}\right\} \tag{4.14}$$

$$\xi_2 = \mathrm{Re}\left\{\frac{\theta}{2} - \left[\frac{\sinh\beta_S x}{\beta_S} + \frac{\sinh\beta_A x}{\beta_A}\right] e^{j(\omega t - \beta_o x)}\right\}$$

where

$$\beta_o = \frac{\omega V_o}{V_o^2 - V_t^2}$$

and

$$\beta_{\substack{S \\ A}} = \sqrt{\frac{\omega^2 V_t^2 - (V_o^2 - V_t^2)\omega_e^2 \frac{n\pm 1}{2}}{V_o^2 - V_t^2}}$$

As can be seen, the symmetric and antisymmetric modes are equally excited at $x = 0$. For $\omega < \omega_a$, however, the S mode exhibits a larger spatial growth and for large x the system has the appearance of the symmetric mode only. This has been observed experimentally.

4.4 Physical Interpretation of S and A Mode Instabilities

The cause of the S and A mode instabilities can be explained by a simple physical picture. Suppose in Fig. 4.1 that jet 1 is displaced upward from equilibrium while jet 2 is fixed. Then the electric field in region 1 is increased, in region 2 decreased and the net traction on jet 1 is given by $\tau = \frac{1}{2}\epsilon_o[E_2^{(1)2} - E_2^{(2)2}]$ or

$$\tau = \frac{1}{2}\,\epsilon_o E_o^2 \left[\frac{1}{1-\left(\frac{\xi_1}{b-a-\frac{\Delta}{2}}\right)^2} - \frac{1}{\left(1+\frac{\xi_1}{2a-\Delta}\right)^2} \right] \approx \frac{\epsilon_o E_o^2}{(2a-\Delta)}\,\frac{\eta}{2}\,\xi_1$$

to linear terms. This is the traction on a single jet between rigid plates. If jet 2 moves downward the same amount that jet no. 1 moves up (S mode) then the electric field in region 2 is decreased further and the electrical traction becomes

$$\tau_S = \frac{1}{2}\,\epsilon_o E_o^2 \left[\frac{1}{1-\left(\frac{\xi_1}{b-a-\frac{\Delta}{2}}\right)^2} - \frac{1}{1+\left(\frac{2\xi_1}{2a-\Delta}\right)^2} \right] \approx \frac{2\epsilon_o E_o^2}{2a-\Delta}\,\frac{\eta\pm 1}{2}\,\xi_1$$

Similarly if $\xi_2 = \xi_1$ (A mode) the field in region 2 is unperturbed and the traction is

$$\tau_A = \frac{1}{2}\,\epsilon_o E_o^2 \left[\frac{1}{1-\left(\frac{\xi_1}{b-a-\frac{\Delta}{2}}\right)^2} \right] \approx \frac{2\epsilon_o E_o^2}{2a-\Delta}\,\frac{\eta-1}{2}\,\xi_1$$

If each field region is of equal width, $\eta = 2$ and

$$\tau_S/\tau = \frac{\eta+1}{\eta} = 1.5$$

$$\tau_A/\tau = \frac{\eta-1}{\eta} = 0.5$$

This represents a sizable change in the electric traction on a jet. Since this term is responsible for the destabilization of the jets, whether subcapillary or supercapillary, the symmetric mode will be more unstable, the antisymmetric less unstable, than the single jet between rigid plates.

4.5 Magnetic Field Coupling

The previous sections have been devoted to electric field coupling primarily because the effects are physically more interesting and the theory can be compared with experiment. Much of what has already been said can be equally well applied to magnetic field coupling. Since the magnetic field equations can be derived simply by replacing ω_e^2 by $-\omega_h^2$ (4.1) becomes

$$[(\frac{\partial}{\partial t} + V_{o1}\frac{\partial}{\partial x})^2 - V_t^2\frac{\partial^2}{\partial x^2} + \omega_h^2\frac{\eta}{2}]\xi_1 = \omega_h^2\frac{\xi_2}{2}$$

$$[(\frac{\partial}{\partial t} + V_{o2}\frac{\partial}{\partial x})^2 - V_t^2\frac{\partial^2}{\partial x^2} + \omega_h^2\frac{\eta}{2}]\xi_2 = \omega_h^2\frac{\xi_1}{2} \qquad (4.15)$$

letting V_{o1} and $V_{o2} = V_o$ we obtain

$$[(\frac{\partial}{\partial t} + V_o\frac{\partial}{\partial x})^2 - V_t^2\frac{\partial^2}{\partial x^2} + \omega_h^2\frac{\eta\pm1}{2}]\xi_{S\atop A} = 0 \qquad (4.16)$$

and the dispersion relation becomes

$$[\omega - V_o k]^2 - V_t^2k^2 - \omega_h^2\frac{\eta\pm1}{2} = 0 \qquad (4.17)$$

We observe that the equations are similar to the single jet case so that there is evanescence for subcapillary flow and purely propagating waves for supercapillary flow. The cutoff frequencies for subcapillary flow is given by:

$$\omega_{co} = \pm \omega_h \sqrt{\frac{\eta \pm 1}{2}} \sqrt{1 - \frac{V_o^2}{V_t^2}}$$

and the corresponding wavenumber is

$$k_{co} = \pm \frac{2V_o \omega_{co}}{V_t^2 - V_o^2}$$

Since what has been said about the single magnetic field coupled stream and the co-streaming electric field coupled jets carries over to the present case, it requires no further discussion.

CHAPTER 5

COUNTER-STREAMING JETS

As pointed out in Chapter 1, the problem of counter-streaming flow arises in several areas of research. The well known Kelvin-Helmholtz instability in fluid mechanics is an example that occurs when two incompressible fluids are in relative motion. In electronics the problem of counter-streaming electron beams is being investigated and in solid state plasma research counter-streaming flow of holes and electrons is at least the subject of speculation. In this chapter, the dynamics of two counter-streaming supercapillary jets will be considered. In all the situations of which the author is aware, counter-streaming flow leads to absolute instabilities. It will be shown later that for spring-type coupling the mechanism for instability is the counter-streaming convected momentum.

The dispersion relations and stability will be discussed using the Bers-Briggs criterion. Since the instabilities are long wave, we should expect the effect of longitudinal boundaries to exert a large influence on the stability of the system. The boundary value problem is formulated for the particular case of equal but opposite flow velocities. This choice leads to symmetric and antisymmetric modes (the symmetry here is different from that discussed in the previous chapter) and the complex eigenfrequencies and the corresponding eigenfunctions computed. It is found that boundaries do indeed play a large role in predicting the stability of the system. Because the problem is of current interest, the eigenfrequencies for longitudinal oscillations of counter-streaming electron beams are also presented.

To show the dynamic behavior and development of an instability, the method of characteristics has been used to compute the transient response for both stable and unstable conditions.

The starting point will again be the long wave model equations derived in Chapter 3.

In order to simplify the analysis, we shall restrict ourselves to the case $V_{o1} = -V_{o2} = V_o$ in order to take advantage of the symmetry of the system, and (3.4) becomes

$$\left[\left(\frac{\partial}{\partial t} + V_o \frac{\partial}{\partial x}\right)^2 - V_t^2 \frac{\partial^2}{\partial x^2} - \frac{\omega_e^2 \eta}{2}\right]\xi_1 = -\frac{\omega_e^2}{2}\xi_2$$

$$\left[\left(\frac{\partial}{\partial t} - V_o \frac{\partial}{\partial x}\right)^2 - V_t^2 \frac{\partial^2}{\partial x^2} - \frac{\omega_e^2 \eta}{2}\right]\xi_2 = -\frac{\omega_e^2}{2}\xi_1 \qquad (5.1)$$

We observe that if $\xi_2 = \pm\xi_1$, (5.1) reduces to the single equation

$$\left[\left(\frac{\partial}{\partial t} + V_o \frac{\partial}{\partial x}\right)^2 - V_t^2 \frac{\partial^2}{\partial x^2} - \frac{\omega_e^2 \eta}{2}\right]\xi_1(x,t) = \pm\frac{\omega_e^2}{2}\xi_1(-x,t). \qquad (5.2)$$

These represent the symmetry modes of the system, designated the symmetric mode for $\xi_2(x) = -\xi_1(-x)$ and antisymmetric mode, $\xi_2(x) = \xi_1(-x)$, (hereafter the S and A modes respectively). As observed in Figure 5.1, the symmetry is about the origin in contrast with the longitudinal axis symmetry of co-streaming jets discussed in the previous chapter. Since two boundary conditions are to be specified at $x = -L$ for jet 1 and two at $x = L$ for jet 2, the boundary conditions also satisfy the symmetry condition.

The dispersion relation corresponding to (5.1) is:

$$\left[(\omega - V_o k)^2 - V_t^2 k^2 + \omega_e^2 \frac{\eta}{2}\right]\left[(\omega + V_o k)^2 - V_t^2 k^2 + \frac{\omega_e^2 \eta}{2}\right] - \frac{\omega_e^4}{4} = 0$$

or in powers of k,

$$(V_o^2 - V_t^2)k^4 + k^2[\omega_e^2 \eta (V_o^2 - V_t^2) - 2\omega^2(V_o^2 + V_t^2)] + \omega^4 + \omega^2\omega_e^2 + \omega_e^4 \frac{\eta^2 - 1}{4} = 0 \qquad (5.3)$$

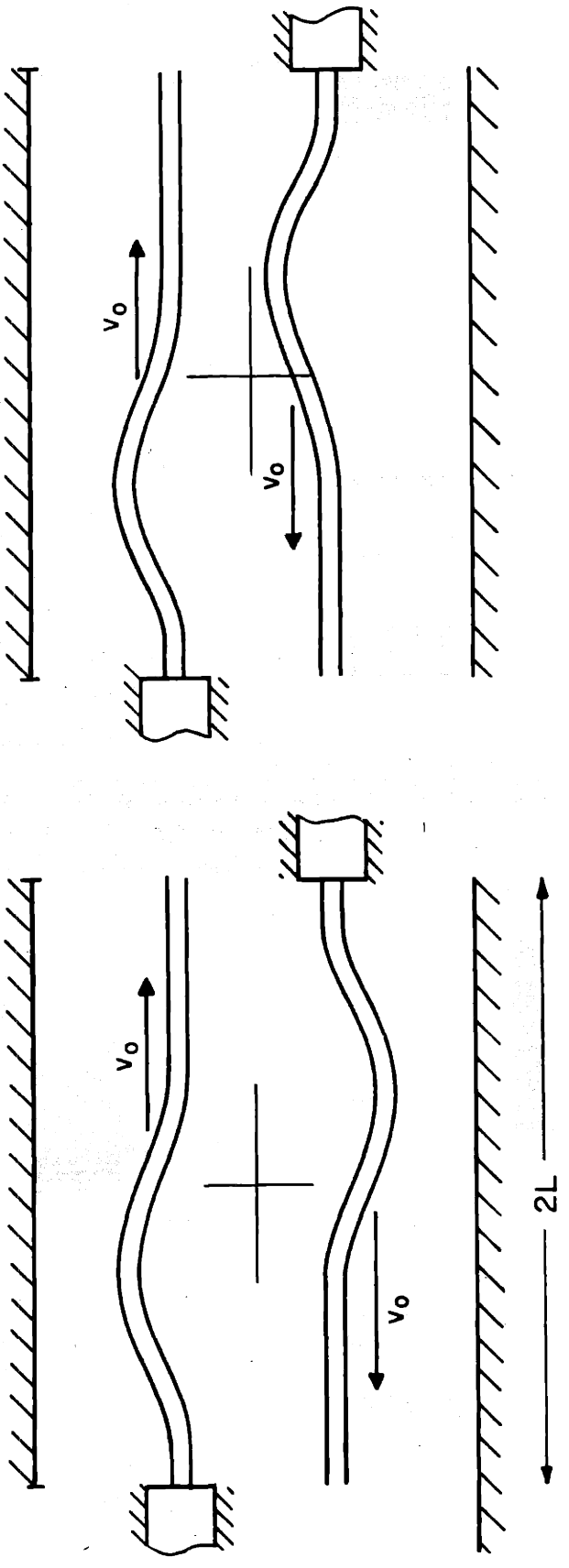

FIGURE 5.1 SYMMETRY MODES FOR SIMILAR COUNTER-STREAMING JETS.

We observe that the dispersion equation is biquadratic in both ω and k; this is a consequence of the two flow speeds being equal. The character of the dispersion relation is similar to Fig. 3.9. There appears to be little interaction of the two streams except near zero frequency.

From a sketch of complex ω for real k shown below, the ω values are at first purely real, join, and branch out in the complex ω plane as k is increased from $-\infty$ to 0. Point a represents a joining of two waves on the same jet. As k is decreased further, a second joining occurs, at $\omega_r = 0$ and the roots become pure imaginary at $k = 0$. This second splitting is a result of strong coupling between the waves of one jet and those on the other near zero frequency. The locus for $k > 0$ is the same as shown with the arrows reversed. Point a represents the maximum real frequency at which instability can occur, while $\omega_s = -j\,\omega_e\sqrt{\frac{n+1}{2}}$ represents the maximum possible rate of growth of instability for the system.

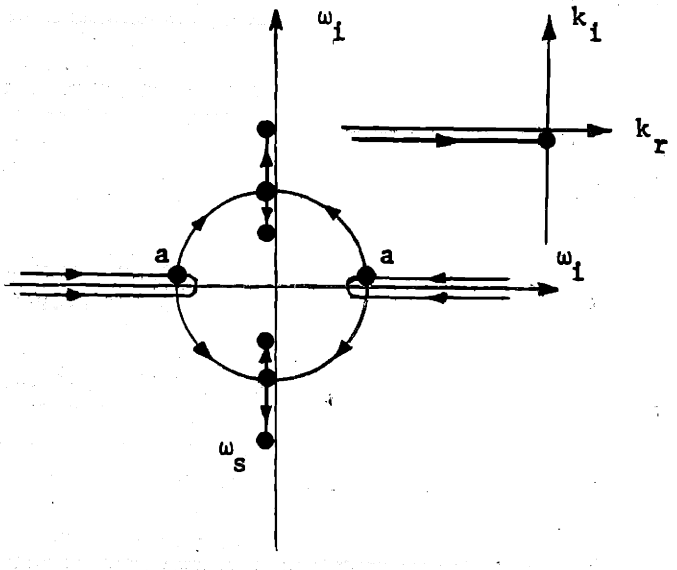

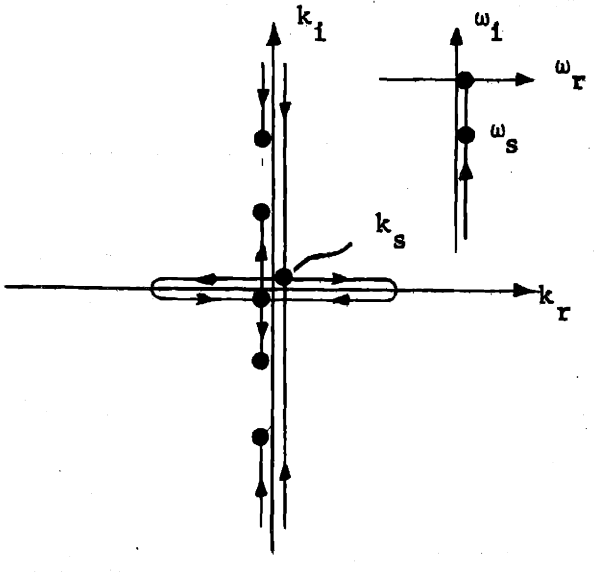

From the Bers-Briggs stability plot at right, the saddle point frequency corresponds to this maximum growth rate. The instability is static and the corresponding $k_s = 0$. To observe the effect of different jet velocity, compare this sketch with Fig. 3.10a. Because the instability wavelength is infinite, we would expect longitudinal boundaries to have a significant effect on the stability of the system. We observe further that as the voltage is decreased to zero the temporal growth is reduced to zero, but the system is statically unstable for any value of applied field. This should be expected since there is no stabilizing force for long waves.

If two counter-streaming jets are stressed by a small E field no instability is observed experimentally; the stabilization must come, therefore, from the boundaries.

5.1 The Eigenvalue Problem, Electric Field Coupling

Since boundary conditions must be imposed at two different points in space the system possesses eigenmodes. This system is peculiar, however, in that each jet is free to move at its downstream end. Furthermore, two counter-streaming jets is an example of a system each component of which does not possess eigenvalues but when combined leads to eigenvalues.

To determine the natural modes of the system, each jet will be assumed to enter the interaction region unexcited. The boundary conditions are

$$\begin{aligned} \xi_1(-L,t) &= \xi_2(L,t) = 0 \\ \frac{\partial \xi_1}{\partial x}(-L,t) &= \frac{\partial \xi_2}{\partial x}(L,t) = 0 \end{aligned} \tag{5.4}$$

Because the boundary conditions involve both ξ_1 and ξ_2 at different points in space, the solution of the determinantal equation appears difficult. However, since this equation satisfies the symmetric and antisymmetric mode

requirements of p.101 the symmetric and antisymmetric modes exist for the bounded problem. This results in splitting the determinantal equation into two second order sets of two boundary condition equations.

From (5.1), assuming a solution $\xi(x,t) = \mathrm{Re}\{\hat{\xi}(x)e^{j\omega t}\}$, we have

$$\xi_1(x,t) = \mathrm{Re}\{[B_1 e^{-jk_1x} + B_2 e^{-jk_2x} + B_3 e^{jk_1x} + B_4 e^{jk_2x}]e^{j\omega t}\}$$

where the k's are determined from the biquadratic dispersion relation, (5.3). The solution for jet 2 is obtained from (5.1)

$$\xi_2(x,t) = \mathrm{Re}\{-\frac{2}{\omega_e^2}[(j\omega + V_o\frac{d}{dx})^2 - V_t^2\frac{d^2}{dx^2} - \frac{\eta\omega_e^2}{2}]\hat{\xi}_1(x)e^{j\omega t}\}$$

To obtain the solutions in simpler form, ξ_1 and ξ_2 may be written as a linear combination of odd and even functions of x.

$$\hat{\xi}_1(x) = A_1\delta_{e1}(x) + A_2\delta_{o1}(x) + A_3\delta_{e2}(x) + A_4\delta_{o2}(x)$$

and
$$\hat{\xi}_2(x) = \frac{2}{\omega_e^2}\{\omega^2 - (V_o^2 - V_t^2)\frac{d^2}{dx^2} + \frac{\eta}{2}\omega_e^2\}\hat{\xi}_1(x) - \frac{2}{\omega_e^2}(2j\omega V_o)\frac{d\hat{\xi}_1(x)}{dx} \qquad (5.5)$$

where

$$\delta_{e1,2}(x) = \cos\beta_{1,2}x\cosh\alpha_{1,2}x - j\sin\beta_{1,2}x\sinh\alpha_{1,2}x$$

$$\delta_{o1,2}(x) = \cos\beta_{1,2}x\sinh\alpha_{1,2}x - j\sin\beta_{1,2}x\cosh\alpha_{1,2}x$$

and
$$k_{1,2} = \beta_{1,2} + j\alpha_{1,2}$$

This is a consequence of the biquadratic dependence of k on ω.

Applying the symmetry conditions $\hat{\xi}_2(x) = \mp\hat{\xi}_1(-x)$ $(^{S}_{A})$ mode we get

$$\hat{\xi}_1(x) = A_1[\delta_{e1}(x) + \Gamma_1\delta_{o1}(x)] + A_3[\delta_{e2}(x) + \Gamma_2\delta_{o2}(x)]$$

where (5.6)

$$\Gamma_{1,2} = \frac{\omega^2 + k_{1,2}^2(V_o^2 - V_t^2) + \omega_e^2\frac{\eta\pm1}{2}}{2\omega V_o k_{1,2}}$$

Substituting the boundary conditions (5.4) into (5.6), the following eigenvalue equation is obtained:

$$k_1[\Gamma_1\delta_{e1}(L)-\delta_{o1}(L)][-\Gamma_2\delta_{o2}(L)+\delta_2(L)]-k_2[-\Gamma_1\delta_{o1}(L)+\delta_{e1}(L)][\Gamma_2\delta_{e2}(L)-\delta_{o2}(L)]=0 \tag{5.7}$$

This equation combined with the dispersion relation yields an expression $\Delta(\omega,V_o,V_t,\omega_e,\eta,L) = 0$ which in principle can be solved to obtain the complex eigenfrequencies as a function of the parameters of the system. If we restrict our analysis for the moment to investigating only imaginary eigenfrequencies then (5.7) can be reduced to an equation of purely real quantities. From the dispersion relation, the k values are either real or imaginary, divided into three subregions.

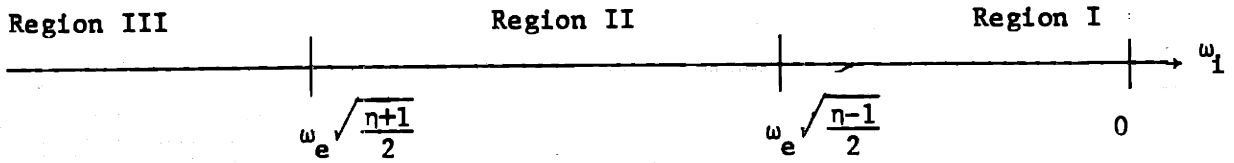

4 imaginary roots	2 imaginary roots 2 real roots	4 imaginary roots
$k = \pm j\alpha_1, \pm j\alpha_2$	$k = \pm j\alpha, \pm \beta$	$k = \pm j\alpha_1, \pm j\alpha_2$
<u>Regions I and III</u>	$\delta_e(L) \rightarrow \cosh \alpha L$ $\delta_o(L) \rightarrow \sinh \alpha L$	

and (5.7) becomes

$$\alpha_1[\Gamma_1-T(\alpha_1L)][-\Gamma_2T(\alpha_2L) + 1]-\alpha_2[\Gamma_1T(\alpha_1L) + 1][\Gamma_2-T(\alpha_2L)] = 0 \tag{5.8}$$

where

$$T(x) \equiv \tanh x$$

and

$$\Gamma_{1,2} = \frac{\omega_i^2 + \alpha_{1,2}^2 (V_o^2 - V_t^2) - \omega_e^2 \frac{\eta\pm1}{2}}{2V_o\omega_i\alpha_{1,2}}$$

Region II $\quad \delta_{o1} \to -j \sin \beta L \qquad \delta_{o2}(L) \to \sinh(\alpha L)$

$\quad \delta_{o2} \to \cos \beta L \qquad \delta_{e2}(L) \to \cosh(\alpha L)$

and (5.7) reduces to

$$\beta\left[\frac{\Gamma_1}{j}\cos\beta L - \sin\beta L\right][-\Gamma_2 T(\alpha L)+1]-\alpha\left[-\frac{\Gamma_1}{j}\sin\beta L + \cos\beta L\right][\Gamma_2 - T(\alpha L)] = 0 \qquad (5.9)$$

where

$$\Gamma_1 = j\,\frac{\omega_i^2-\beta^2(V_o^2-V_t^2)-\omega_e^2\,\frac{n\pm1}{2}}{2V_o\omega_i\beta} \quad \text{and} \quad \Gamma_2 = \frac{\omega_i^2+\alpha^2(V_o^2-V_t^2)-\omega_e^2\,\frac{n\pm1}{2}}{2V_o\omega_i\alpha}$$

These limiting cases provide a check on the general solution found by solving (5.7) using the dispersion relation (5.4). The results are shown in Fig. 5.2. The numerical techniques used are described in the next section. For very small fields, all modes represent decay, the decay rate $\to \infty$ as $\omega_e \to 0$. For very large values of ω_e, the modes which are unstable approach two asymptotic values, the more unstable of which is the saddle point predicted by the Bers-Briggs criterion. The asymptotic behavior at strong field (or large length) and weak field seems physical and in agreement with the Bers-Briggs criterion.

However, there are several facts which cannot be predicted from the dispersion relation alone. The lowest S and A mode eigenfrequencies are purely imaginary; the A mode remains a decay mode, while the S mode becomes unstable as $\omega_e L/V_o$ is increased and finally approaches the saddle point. The second and higher S and A modes, are of different character. These are dynamic modes ($\omega_r \neq 0$) until $\omega_e L/V_o$ reaches a critical value for each mode at which ω_r becomes zero and the modes represent pure exponential growth or decay. Modes A2, S3, A4, etc. are particularly interesting, since they represent overstabilities, i.e. sinusoidal variations with exponential growth, in time. It is also

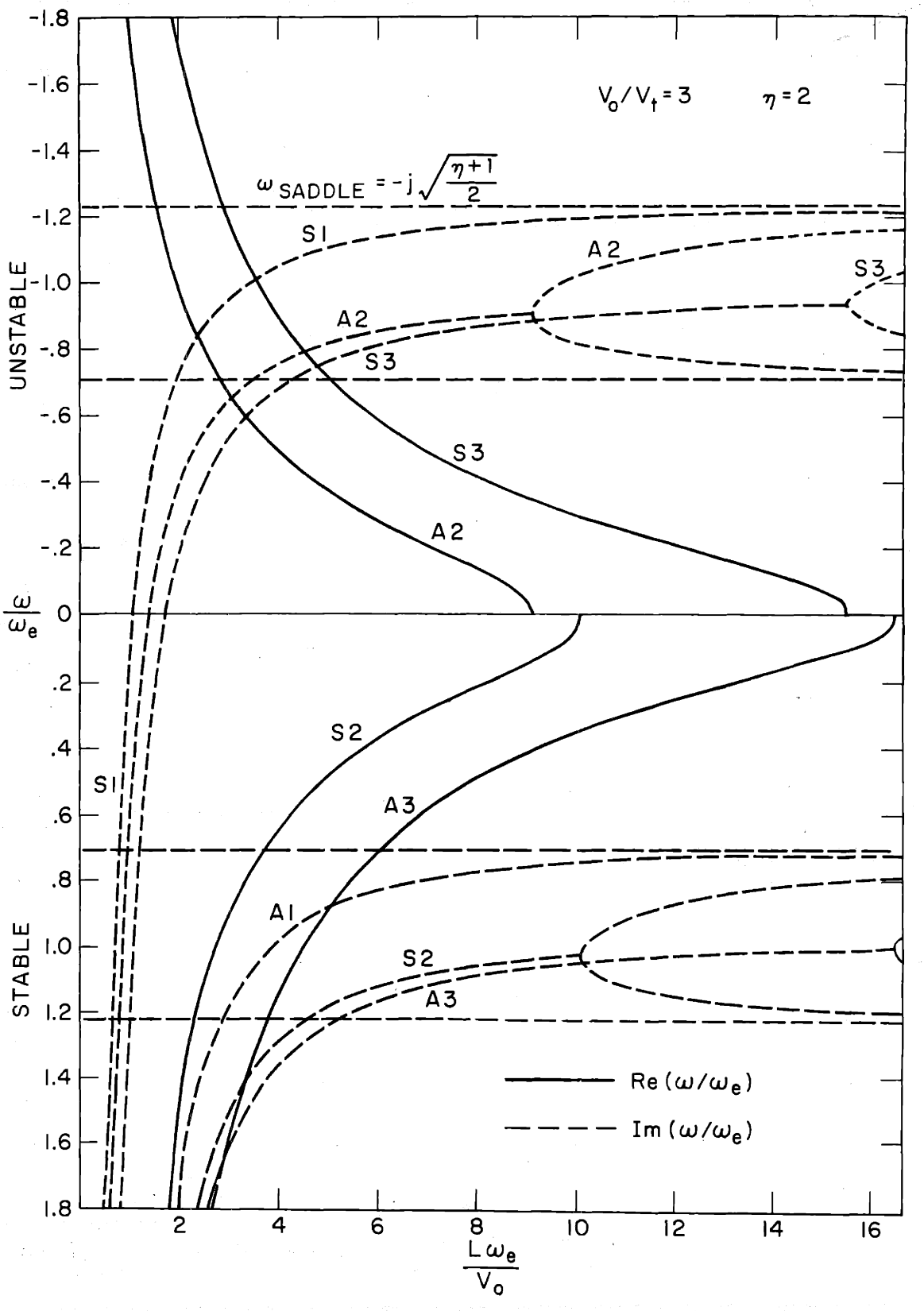

FIGURE 5.2 COMPLEX EIGENFREQUENCY VS. NORMALIZED LENGTH FOR ELECTRIC FIELD COUPLED COUNTER-STREAMING JETS. THE REAL PART OF THE EIGENFREQUENCY IS SYMMETRIC ABOUT THE ABSCISSA AND ONLY ONE BRANCH IS SHOWN.

interesting that only half of the modes are unstable; the others represent underdamping in the lumped parameter sense until a critical value of $\omega_e L/V_o$ is reached, when each mode becomes overdamped. Mode A1 is always overdamped.

Since the S1 mode is the most unstable and becomes unstable for the smallest value of $\omega_e L/V_o$, it is this mode which will dominate the transient behavior of the system. At the point of impending instability for this mode, $\omega = 0$ and the constraint on the parameter values may be calculated from (5.8) and the dispersion relation. From (5.3) at $\eta = 0$,

$$(V_o^2-V_t^2)^2\, k^4 + k^2\, \omega_e^2(V_o^2-V_t^2) + \omega_e^4\, \frac{\eta^2-1}{4} = 0$$

Solving for k,

$$k = \pm\, j\, \frac{\omega_e}{\sqrt{(V_o^2-V_t^2)}}\, \sqrt{\frac{\eta\pm1}{2}}$$

Therefore

$$\alpha_{2,1} = \sqrt{\frac{\eta\pm1}{2}}\ \ \frac{\omega_e}{\sqrt{V_o^2+V_t^2}}$$

From (5.8) Γ_1 and Γ_2 become indeterminate at $\omega = 0$, but if the limit is used as $\omega_i \to 0$, then, Γ_1 and Γ_2 are of the order $1/\omega_i$ and ω_i respectively so that Γ_2 may be ignored. This simplification yields

$$\tanh\left[\sqrt{\frac{\eta+1}{2}}\ \ \frac{\omega_e L}{\sqrt{V_o^2-V_t^2}}\right] \tanh\left[\sqrt{\frac{\eta-1}{2}}\ \ \frac{\omega_e L}{\sqrt{V_o^2-V_t^2}}\right] = \sqrt{\frac{\eta-1}{\eta+1}} \qquad (5.10)$$

Equation (5.10) is plotted in Fig. 5.3 as $\frac{\omega_e L}{\sqrt{V_o^2-V_t^2}}$ vs. a/b, the ratio of jet spacing to plate spacing. For parameter values lying above the curve, the system is unstable, below the curve stable. With regard to the transverse dependence, the system is in the most stable condition when $a/b \to 0$, or the external plates are far apart (but within the limitation of the long wave

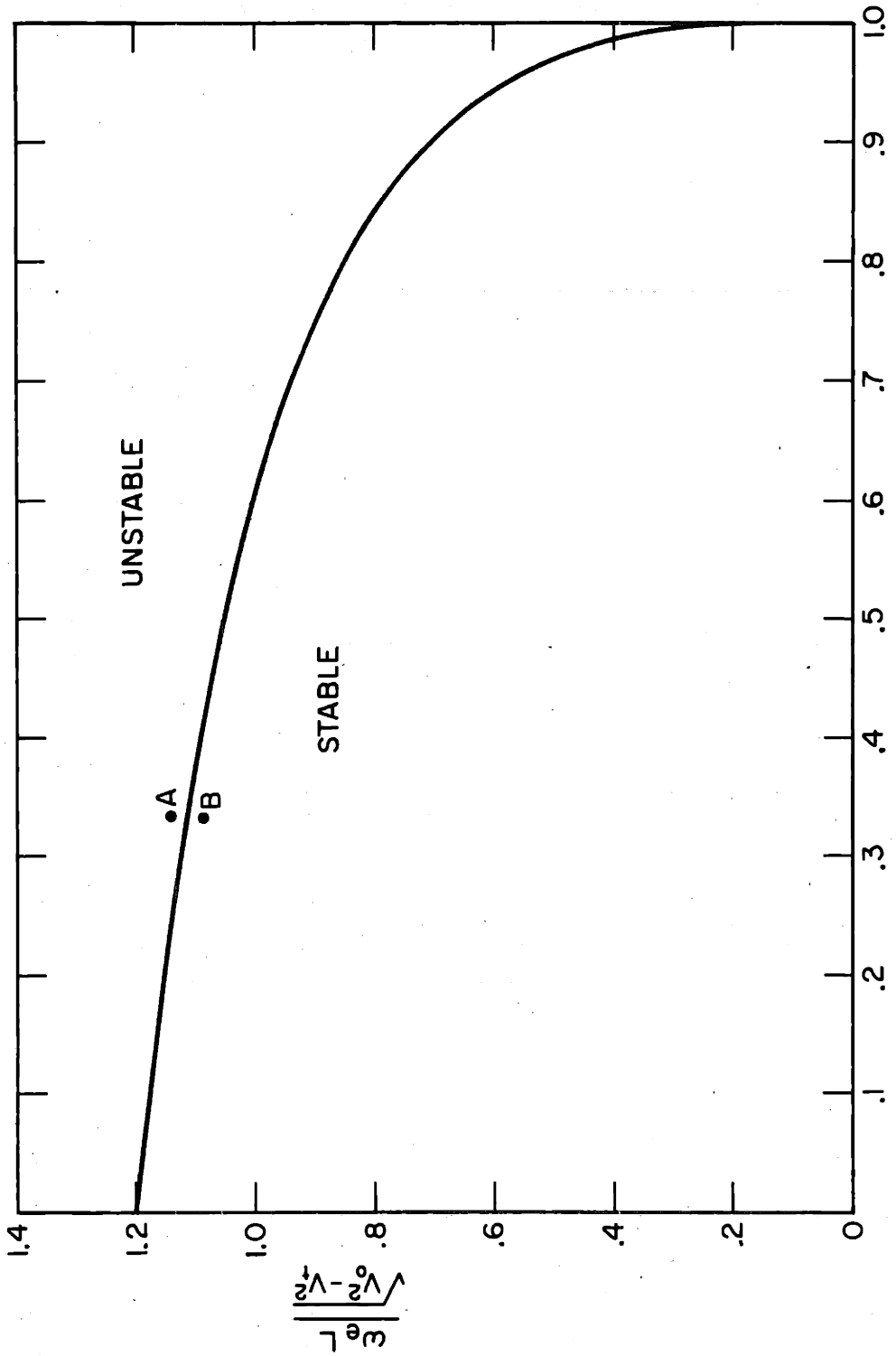

FIGURE 5.3 EFFECT OF PLATE SPACING ON THE NORMALIZED ELECTRIC FIELD REQUIRED FOR THE STATIC INSTABILITY OF COUNTER-STREAMING JETS. THE INSTABILITY WHICH OCCURS FIRST IS THE FUNDAMENTAL SYMMETRIC MODE.

model). Bringing the external plates sufficiently close to the jets can have a large effect in destabilizing the jets. This may be explained intuitively on the basis that a small displacement on a jet will lead to a large change in the electric traction .

The role of surface tension is also clear from Fig. 5.3. As long as the jet velocity is not approximately equal to the capillary velocity, the point of impending stability is practically independent of surface tension. This is interesting since for a single jet between parallel rigid plates, the role of surface tension was to determine the cutoff frequency between propagating and spatially growing waves. It might be thought that the static instability considered here is somehow related. Such is not the case, however. It will be shown later that for jets sufficiently supercapillary, the surface tension has little effect on the dynamics, and that the counter-streaming convected momentum term and the mutual coupling term in the equations of motion are the cause of the instability.

The eigenfunctions for the point of impending instability are easily calculated. From (5.8), for $\omega_1 \longrightarrow 0$, and the value of Γ above,

$$\hat{\xi}_1(x) = A \sinh \alpha_1 x + B \cosh \alpha_2 x$$

and

$$\hat{\xi}_2(x) = - \hat{\xi}_1(-x) = A \sinh \alpha_1 x - B \cosh \alpha_2 x$$

Applying the boundary conditions at $x = - L$ for ξ_1

$$0 = - A \sinh \alpha_1 L + B \cosh \alpha_2 L$$

$$0 = \alpha_1 A \cosh \alpha_1 L - \alpha_2 B \sinh \alpha_2 L$$

The above equations yield (5.10) and

$$B/A = \frac{\sinh \alpha_1 L}{\cosh \alpha_2 L}$$

so that

$$\hat{\xi}_1(x) = \xi_o\left\{ \frac{\sinh\alpha_1 x}{\sinh\alpha_1 L} + \frac{\cosh\alpha_2 x}{\cosh\alpha_2 L} \right\}$$

$$\hat{\xi}_2(x) = \xi_o\left\{ \frac{\sinh\alpha_1 x}{\sinh\alpha_1 L} - \frac{\cosh\alpha_2 x}{\cosh\alpha_2 L} \right\} \qquad (5.11)$$

where

$$\alpha_1 = \frac{\omega_e\sqrt{\frac{\eta-1}{2}}}{\sqrt{V_o^2 - V_t^2}}, \quad \alpha_2 = \frac{\omega_e\sqrt{\frac{\eta+1}{2}}}{\sqrt{V_o^2 - V_t^2}}$$

The open-endedness of the jets is clearly evident in (5.11), and contrasts the displacement of the fundamental mode of the two spring system. The plot of (5.11) is essentially the same as that shown in Fig. 5.3(a) and Figs. (5.6) and (5.7). It is interesting that the point of instability of the counter-streaming jets and the fundamental S mode of two springs are roughly the same if the tension velocity is replaced by the jet velocity.

5.1.1 Numerical Computation

The solution of (5.8) to yield the complex eigenfrequencies as a function of the parameters, while it can be done formally, requires the use of a computer to arrive at useful solutions. The difficulty, which is a general one for eigenvalue problems, lies in not having explicit expressions for the wave numbers from the dispersion relation to substitute into the determinantal equation. In the present case explicit expressions can be obtained without much difficulty, but the resulting analytical expression is of little use.

An iteration technique was developed to automatically compute the complex eigenfrequency curves once the computation was properly started. The algorithm is a two dimensional Newton-Raphson iteration method, in which the complex frequency is considered as two independent variables.

The computation proceeds as follows: the parameter values and the complex frequency is initially assumed and the wavenumbers computed. The complex boundary conditions determinantal function (the left hand side of (5.8)) is then evaluated. For eigenfrequencies this determinant is identically zero, but in general it is not. The real and imaginary parts of the frequency are subsequently incremented and the four partial derivatives $\partial\Delta_{r,i}/\partial\omega_{r,i}$ evaluated numerically. From these a new complex frequency is determined by following the slope of the intersection curve of the Δ_r and Δ_i surfaces to the frequency at which the curve intersects the ω_r vs. ω_i plane. Mathematically this may be written:

$$\begin{aligned}
&\Delta_r(\omega_r,\omega_i) + \frac{\partial\Delta_r(\omega_r,\omega_i)}{\partial\omega_r}\ \delta\omega_r + \frac{\partial\Delta_r(\omega_r,\omega_i)}{\partial\omega_r}\ \delta\omega_i = 0 \\
&\Delta_i(\omega_r,\omega_i) + \frac{\partial\Delta_i(\omega_r,\omega_i)}{\partial\omega_r}\ \delta\omega_r + \frac{\partial\omega_i(\omega_r,\omega_i)}{\partial\omega_r}\ \delta\omega_r = 0
\end{aligned} \tag{5.12}$$

Solving for the new value of the complex frequency,

$$\omega_r^{new} = \omega_r - \frac{1}{J}\begin{vmatrix} \Delta_r & \frac{\partial\Delta_r}{\partial\omega_i} \\ \Delta_i & \frac{\partial\Delta_i}{\partial\omega_i} \end{vmatrix} \qquad \omega_i^{new} = \omega_i - \frac{1}{J}\begin{vmatrix} \frac{\partial\Delta_r}{\partial\omega_r} & \Delta_r \\ \frac{\partial\Delta_i}{\partial\omega_r} & \Delta_i \end{vmatrix}$$

where

$$J = \begin{vmatrix} \frac{\partial\Delta_r}{\partial\omega_r} & \frac{\partial\Delta_r}{\partial\omega_i} \\ \frac{\partial\Delta_i}{\partial\omega_r} & \frac{\partial\Delta_i}{\partial\omega_i} \end{vmatrix}$$

The iteration is continued until a convergence test is satisfied or a preset number of interations exceeded and that particular computation terminated. Once a convergence has been achieved, a parameter (usually the normalized length) is incremented, the starting value for the next computation automatically computed

using a three point extrapolation formula and the process continued until a branch of the eigen-frequency curve is completed or a non-convergence occurs. This technique has several advantages: (1) it is a simple technique conceptually and easy to program and debug (2) the convergence is very rapid in most cases. Once an eigenfrequency has been computed, the starting value for subsequent calculations is usually close and convergence to 5 digits is achieved within 3 iterations (3) computing time is short (4) the method is completely general in that the roots of any differentiable function can be found.

The principle disadvantage is that the convergence is a strong function of the starting value and an initial trial and error period is necessary to find the first eigenfrequency of each branch.

The important parameters of the system are V_o, ω_e, and L; by suitable scaling

$$\bar{\omega} = \omega/\omega_e \qquad \text{and} \qquad \bar{L} = \frac{L\omega_e}{V_o}$$

the number of parameters may be reduced and the determinantal equation becomes $\Delta(\bar{\omega}, V_t/V_o, \eta, \bar{L}) = 0$. The effect of V_t/V_o and η are small, so that $\bar{\omega} \sim \bar{\omega}(\bar{L})$ is the functional dependence desired.

5.1.2 Eigenfunctions

The eigenfunctions for $\bar{L} = 3$ and 9 have been computed for the first three symmetric and antisymmetric modes for several values of time and are shown in Fig. 5.4 and 5.5. The symmetry and stability are apparent. The eigenfrequency for the fundamental modes is purely imaginary, representing static instability for the symmetric mode and decay for the antisymmetric mode. The trajectories exhibit no shift in phase for increasing time, typical of a standing wave pattern. From the physical argument given in Chapter 4 concerning the stability of the symmetric and antisymmetric modes for co-streaming jets, we may explain why the S1 mode is stable and the A1 mode unstable.

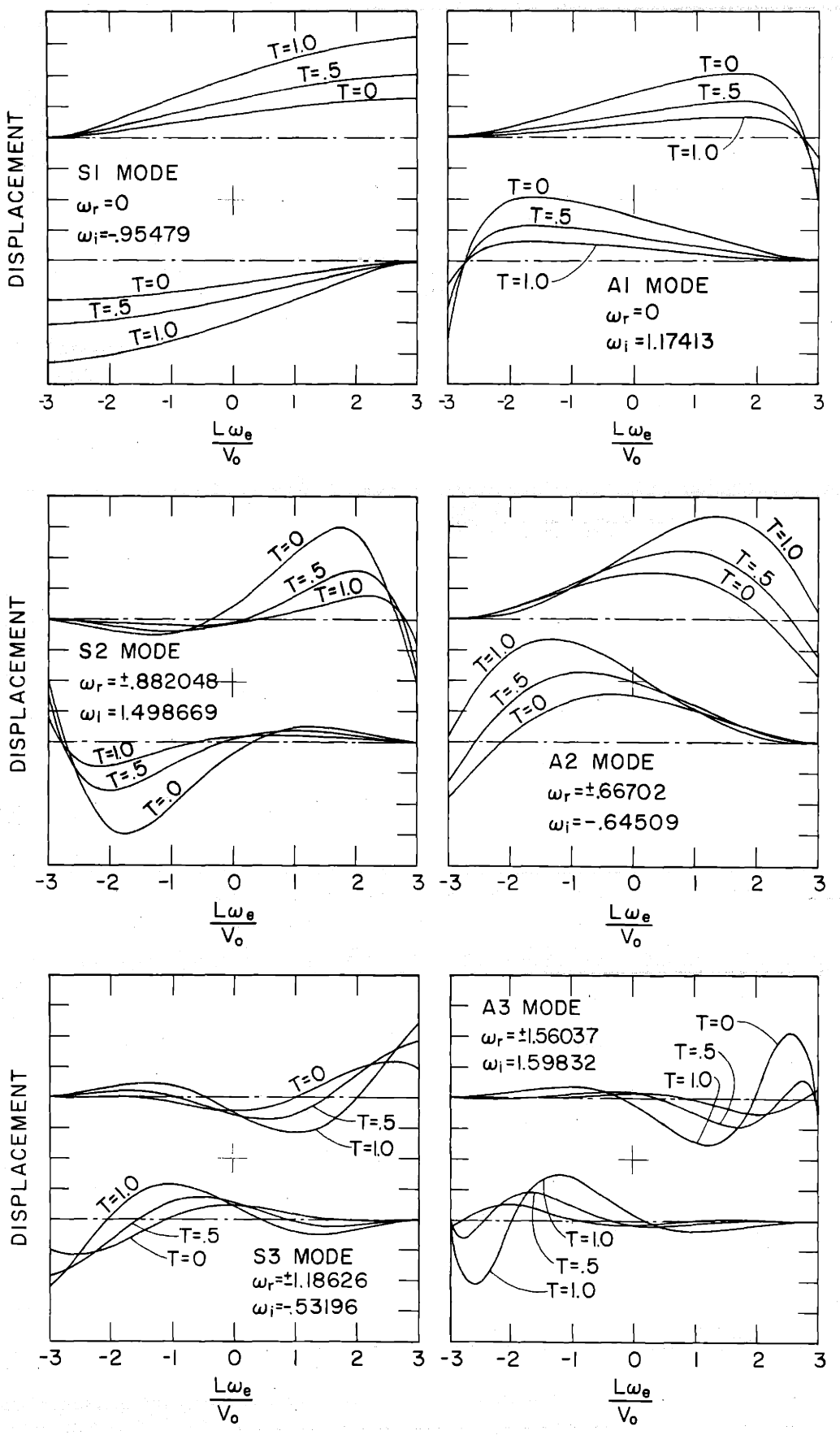

FIGURE 5.4 EIGENFUNCTIONS FOR THE THREE LOWEST SYMMETRIC AND ANTISYMMETRIC MODES OF FIGURE 5.2 THE NORMALIZED LENGTH $\frac{L\omega_e}{V_o} = 3$.

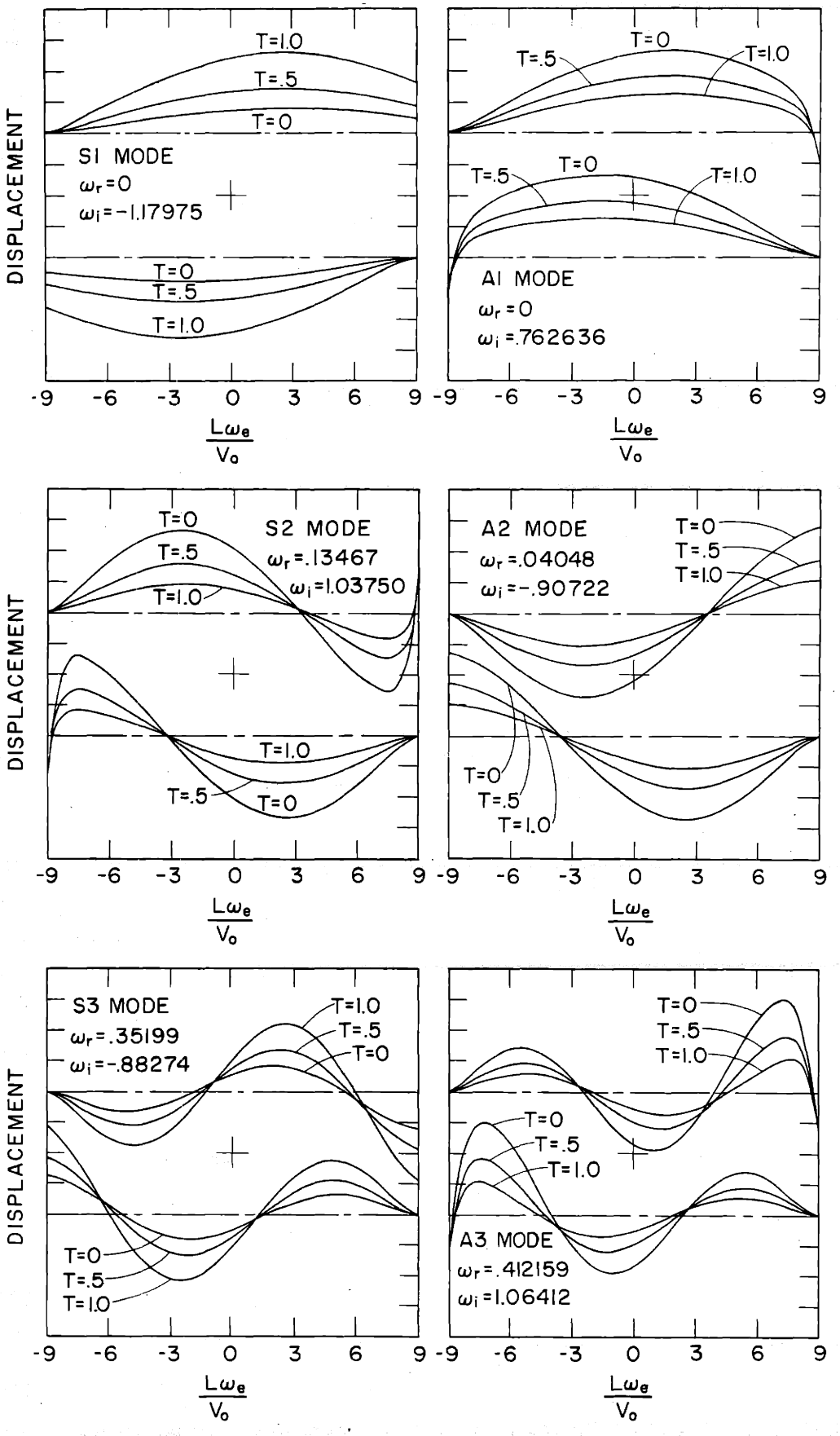

FIGURE 5.5 EIGENFUNCTIONS SIMILAR TO FIGURE 5.4 FOR ELECTRIC FIELD COUPLED COUNTER-STREAMING JETS. THE NORMALIZED LENGTH $\frac{L\omega_e}{V_o}$ = 9

5.1.3 Physical Argument

Consider the S1 mode at time T = 0 (T here is nondimensional time; it is the time required for a jet traveling with velocity V_o to travel a distance of one unit in Fig. 5.4 or 1/6 of the total length of the jet). The electric field between the plate and each jet has increased from its equilibrium value while between the jets the field has decreased. Each particle of the jet experiences a transverse electric force tending to accelerate it towards the adjacent plate while it is being convected along. Surface tension is not an important mechanism in determining the eigenfrequencies or eigenfunctions of counter-streaming jets. Its main importance is to serve as a lower bound on the jet velocity for which the characteristics go downstream for each jet. As a result the trajectory would look like that shown in Fig. 5.4 for $T_2 = 0.5$. The situation is now no different from before, except now the electric traction is even stronger and the jet departure from equilibrium increases. The process continues and the jets exhibit exponential growth in time. It should be apparent to the reader that if the initial deflection of the jets was inward, the same argument applies and the jets will pull together. For planar jets, which way the jets can go unstable is equally likely.

It might appear at first that a single jet between parallel plates is also absolutely unstable, since if it were given the trajectory of, say, the right moving jet at time T = 0, the electric traction is such as to deflect each particle in the jet further. A short time later, the particles which were in the jet at time T = 0 have indeed been convected along and experienced a larger deflection. However, new particles have been injected into the stream and since the external plates are rigid, these particles see an equilibrium electric field and are not deflected. The result is that the original disturbance is swept downstream out of the interaction region and equilibrium is restored.

The essential ingredient for absolute instability of counter-streaming jets is that there be a means of returning the downstream disturbance to a point upstream in order that the disturbance may be sustained. In this case the feedback is internal, returning on the opposite jet. Whether or not the S1 mode is unstable will depend on the length of time a particle remains in the interaction region ($\sim L/V_o$) and on the electric traction the particle experiences ($\sim\omega_e$) so that intuitively the important measure of stability is $\frac{L\omega_e}{V_o}$. The quantity $\frac{L\omega_e}{V_o}$ may be thought of as a ratio of the transit time to the E folding time for instability. It is interesting that $\frac{L\omega_e}{V_o} \gtrsim 1$ is the condition for impending instability of counter-streaming jets.

If we apply the above argument to the lowest antisymmetric mode in Fig. 5.4, the traction on most of the jet is such as to pull the jet back toward equilibrium. This process is slowed down by the fact that the incoming particles receive a short destabilizing pull because of the overshoot near the exit of the other jet. A short time later the jet has the trajectory shown in Fig. 5.4 for T = 0.5. The electrical traction has become weaker, but still stabilizing in character. As in the case of the symmetric mode, if the initial displacement were inward the situation is unaltered and the jets are stable.

It is more difficult to predict the stability of the higher modes, because of their more complicated trajectories. Further, in Fig. 5.4 for the A2 mode, we observe the first example of an eigenfunction presenting an overstability and whose phase is not constant but progresses downstream on each jet, giving the system the character of traveling waves instead of the common standing wave behavior. The velocity of the zero crossings appears to be about one unit in length per one unit in time, which is just the velocity of the jet. The same is true for the S2, A3, and S3 for $\bar{L} = 3$. This does not appear to be true,

however, for the modes at $\bar{L} = 9$, shown in Fig. 5.5. Comparing Fig. 5.4 with 5.5, we may observe that the slopes of the eigenfunctions are not appreciably altered by a large change in $\bar{L}$, indicating that the eigenfunctions are fairly insensitive to parameters.

5.1.4 Transient Behavior by the Method of Characteristics

While a complete knowledge of the eigenmodes is sufficient to determine the dynamical behavior of the system, it does not leave the reader with a very clear physical picture of the transient behavior to some arbitrary initial distrubance. To provide this picture and to verify that the eigenmodes (at least the lowest mode) are indeed correct, the differential equations, (5.1) were programmed using the method of characteristics. The boundary conditions postulated that the jets enter the interaction region unexcited. Jet 1 was given an initial distrubance; jet 2 was initially unexcited. The resulting transient is shown in Fig. 5.6 and 5.7 for two values of electric field very close to but on either side of the point of impending instability, marked points A and B in Fig. 5.3.

The initial disturbance propagates downstream and grows spatially in so doing, illustrating the convectively unstable character of the jets. As it propagates it exerts a traction on jet 2 pulling it away from equilibrium (T = 5). At the end of 10 units of time, the initial disturbance has been swept out of the interaction region and the shape of the fundamental symmetric mode begins to appear. As time progresses, the displacement grows in time and the S1 mode dominates completely. Since point A is so close to the point of impending instability, the growth rate is quite slow.

In Fig. 5.7, the same conditions were used with the exception that the electric field was reduced slightly to just below the instability point. The initial transient up to T = 10 is the same as in Fig. 5.6. However, the electric

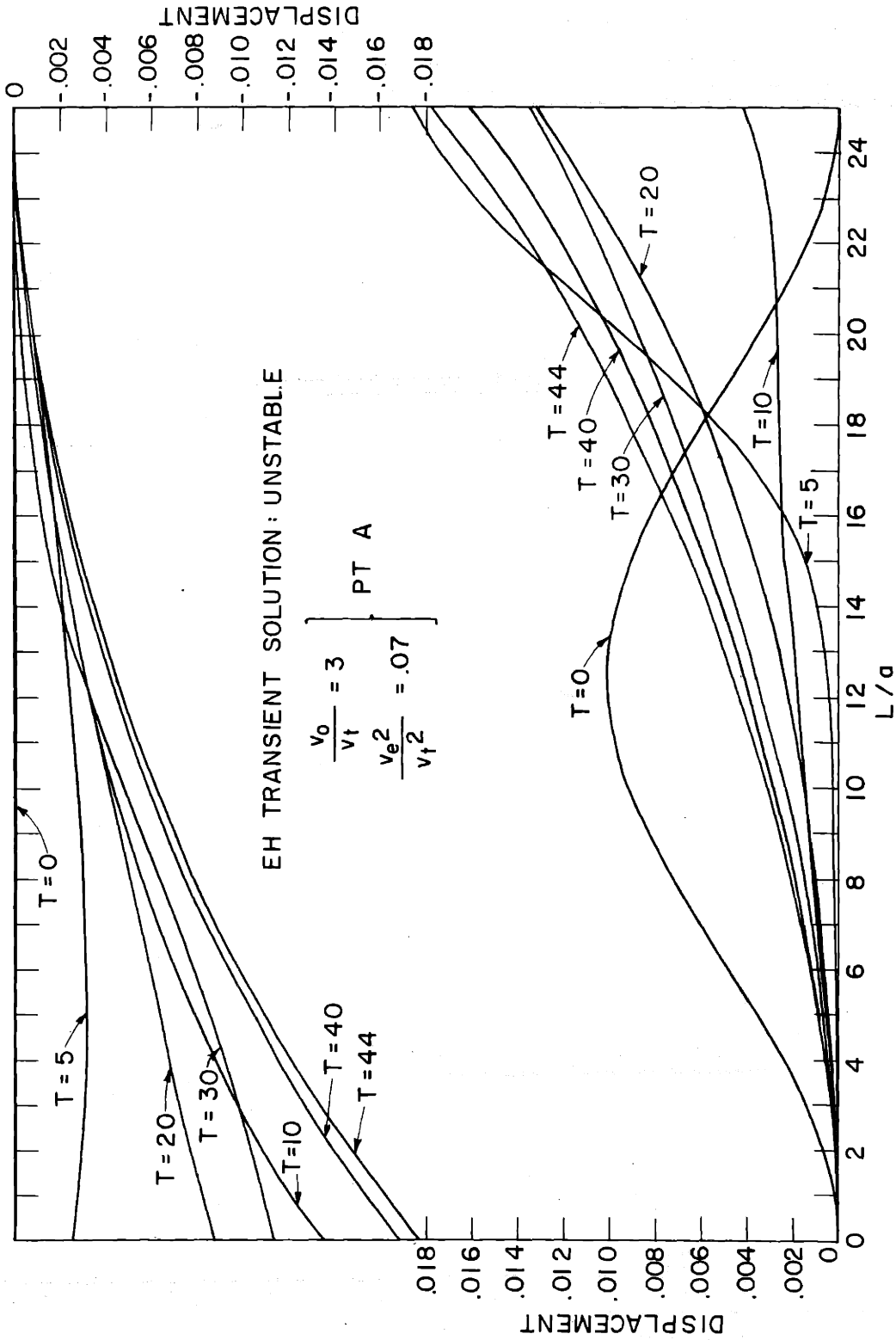

FIGURE 5.6 TRANSIENT SOLUTION TO AN INITIAL EXCITATION ON THE LOWER JET. STABLE COMPONENTS OF THIS PULSE PROPAGATE AWAY, LEAVING ONLY THE FUNDAMENTAL SYMMETRIC MODE WHICH SLOWLY BECOMES UNSTABLE. POINT A IS SHOWN IN FIGURE 5.3.

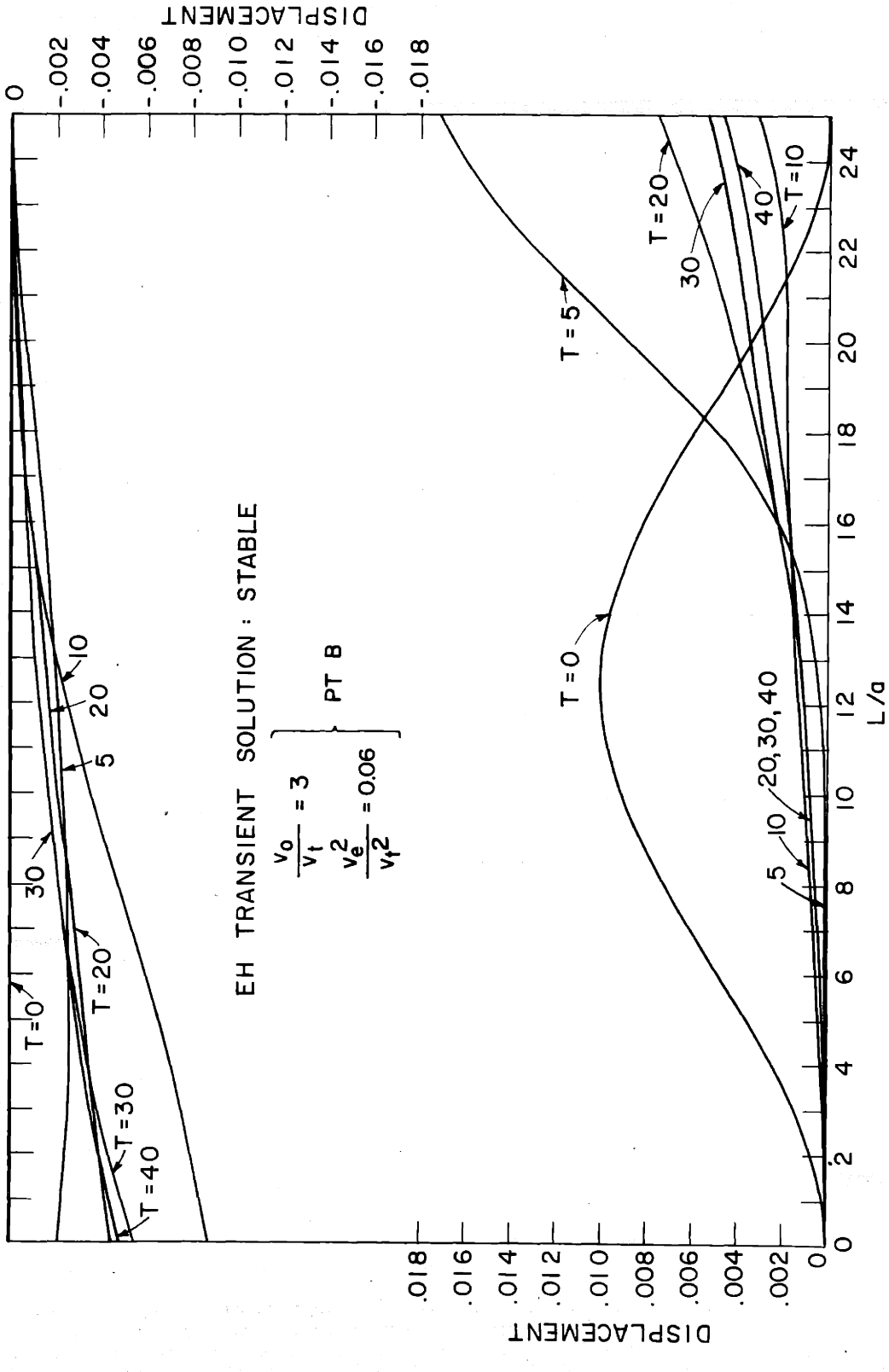

FIGURE 5.7 TRANSIENT SOLUTION SIMILAR TO FIGURE 5.6 WITH THE ELECTRIC FIELD SLIGHTLY REDUCED. POINT B IS SHOWN IN FIGURE 5.3.

traction is not quite large enough to allow particles originating at the nozzle of jet 1 to grow to sufficient amplitude to exert sufficient traction on the returning jet to sustain the disturbance, and the disturbance decays slowly in time. In both cases the initial transient was swept away and the system settled down after a brief period to the fundamental symmetric mode. If sufficient electric field is applied to the system so that the A2 mode is also unstable and the same initial and boundary conditions applied, indeed it is found that after a short transient in which the initial disturbance is swept downstream, the system settles down to a combination of the two unstable modes, but since the S1 mode is more unstable, this mode dominates the behavior of the system.

5.2 Magnetic Field Coupling

As mentioned earlier the magnetic field and electric field coupled systems are closely analogous, the principle difference being the perturbation magnetic field behaves like a distributed spring of positive constant, the electric field of negative spring constant. This shows up in the equation of motion simply as a replacement of ω_e^2 by $-\omega_h^2$. This change however, has had a dramatic effect on the dynamics of all the systems considered so far. A principle exception was the class III systems which exhibited absolute instability for both electric and magnetic field coupling. An essential difference between the two systems is that the electric field coupled jet is naturally convectively unstable and should enhance any tendency of the counter-streaming flow to produce absolute instability, whereas the magnetic field coupled jet would not. The effect of boundaries on the counter-streaming electric field case was stabilizing. We shall now consider the finite length magnetic field coupled system.

The dispersion relation, from (5.3) is essentially that shown in Fig. 3.9d. The Bers-Briggs stability plot shows that the system is statically unstable,

the saddle point wavenumber is real, contrasting the electric field case which is imaginary. One might expect that if the longitudinal boundaries were more than a few wavelengths apart that they would not play an important role in determining the stability of the system. This is misleading, however, since the saddle point wavelength depends on the applied magnetic field, approaching infinity as the field tends to zero. The longitudinal boundaries again should be expected to play an important role in the dynamics of the system. Two other saddle points exist, for real frequencies and infinite wavelength, but since $\omega_i = 0$ for both, these represent oscillatory natural modes. The physical interpretation of these natural modes is that if the system were plucked, the jets would resonate at either of these frequencies with every point along the jet in phase and the same amplitude, since $k = 0$, assuming no other natural modes were excited. The reason for two resonant frequencies is clear since the jets can resonate in either a symmetric or antisymmetric manner. In any case the system possesses an unstable natural mode and hence is the one to be considered.

5.2.1 Complex Eigenfrequencies

The boundary conditions equation is formulated in the same way as for electric field coupling and (5.7) is valid if ω_e^2 is replaced by $-\omega_h^2$ in the expression for $\Gamma_{1,2}$.

The complex eigenfrequencies are plotted vs. $L\omega_h/V_o$ in Fig. 5.8. As in the electric field case, for small magnetic field, all modes are decay modes, the decay rate $\rightarrow \infty$ as $\omega_r \rightarrow 0$. For large $L\omega_h/V_o$ the unstable modes asymptotically approach the saddle point frequency. The lowest S and A modes are static modes.

By constrast with the electric field coupling here the S and A modes have nearly the same eigenfrequency. As the magnetic field is increased each mode in turn becomes unstable whereas only half the electric modes were unstable. Also no overstabilities are observed for the higher modes, since $\omega_i > 0$ as

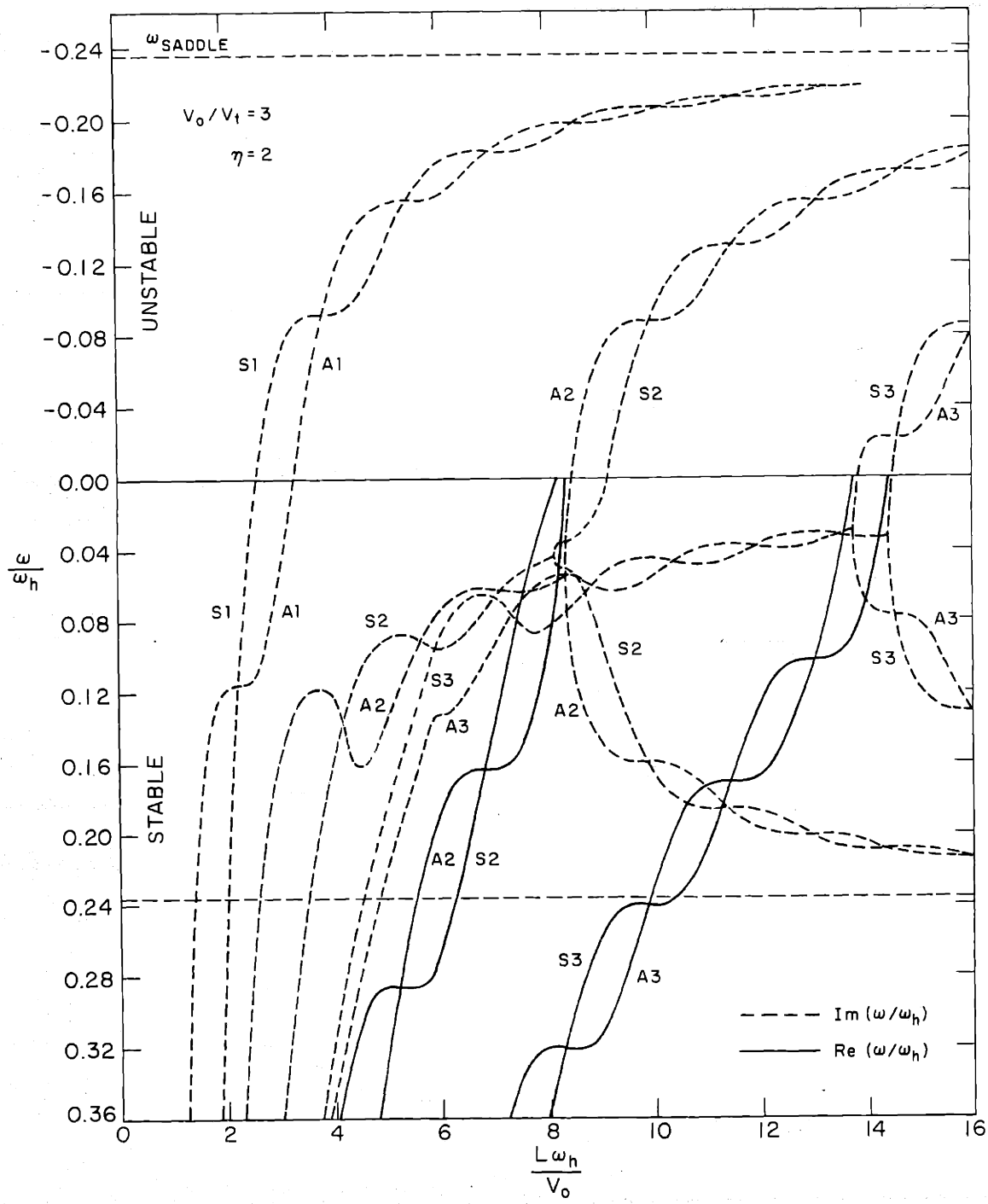

FIGURE 5.8 MH2f COUNTER STREAMING JET EIGENFREQUENCIES

$\omega_r \to 0$. As in the electric field case the fundamental mode will dominate the dynamics, being the most unstable and becoming unstable for the smallest value of $\omega_h L/V_o$. Here, however, both S and A modes must be considered.

At the point of impending instability, $\omega = 0$, and carrying out an analysis similar to the derivation of (5.10), we obtain

$$\tan\left[\sqrt{\frac{n+1}{2}}\ \frac{\omega_h L}{\sqrt{V_o^2-V_t^2}}\right]\ \tan\left[\sqrt{\frac{n-1}{2}}\ \frac{\omega_h L}{\sqrt{V_o^2-V_t^2}}\right] = -\sqrt{\frac{n-1}{n+1}}$$

symmetric mode

$$\tan\left[\sqrt{\frac{n+1}{2}}\ \frac{\omega_h L}{\sqrt{V_o^2-V_t^2}}\right]\ \tan\left[\sqrt{\frac{n-1}{2}}\ \frac{\omega_h L}{\sqrt{V_o^2-V_t^2}}\right] = -\sqrt{\frac{n+1}{n-1}}$$

antisymmetric mode (5.13)

These are plotted in Fig. 5.9. The general trend is similar to that for electric field coupling, but here transverse boundaries have an important effect in determining whether the S or A mode will be the first to go unstable as the magnetic field is increased. The effect of the transverse plate spacing is opposite to the electric field case. Since the magnetic field is inherently stabilizing, bringing the plates in close to jets will impede any destabilizing mechanism.

5.2.2 Eigenfunctions

The eigenfunctions may be found analytically for the point of impending instability as in the development of (5.11).

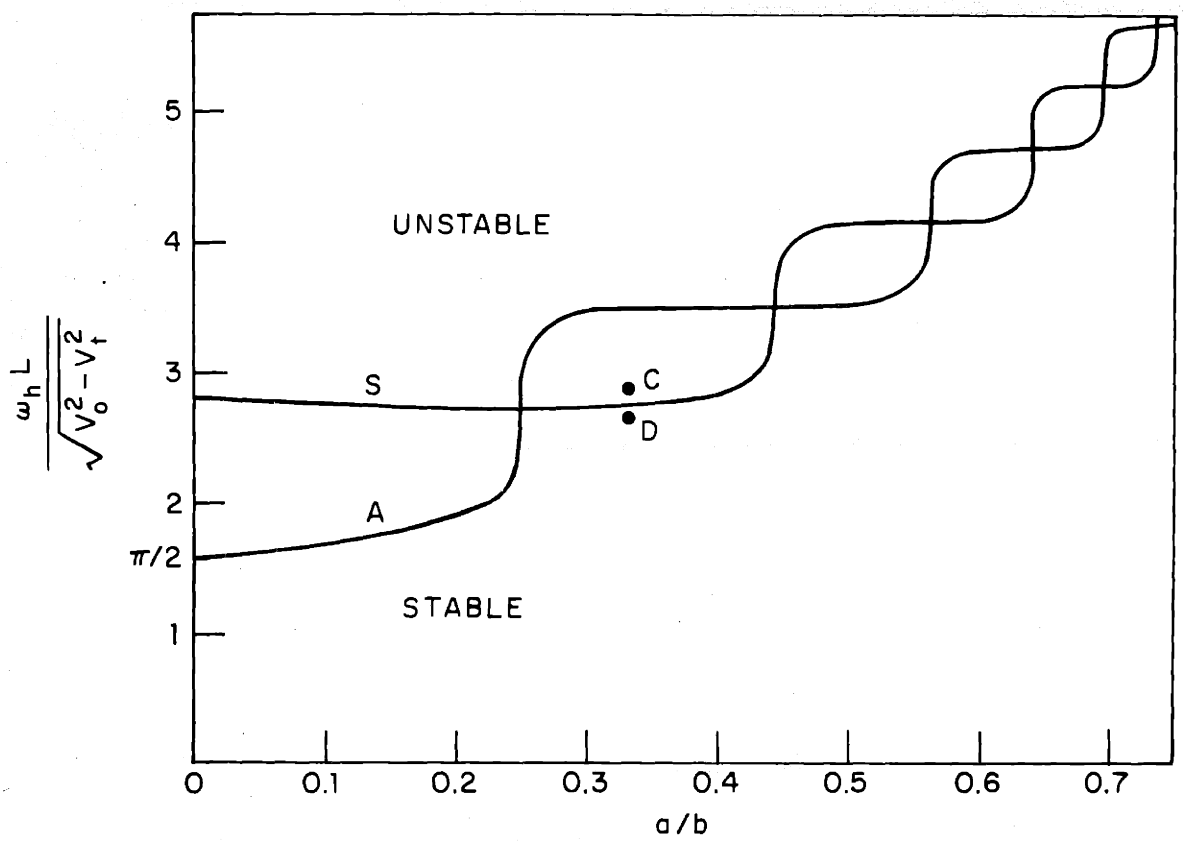

FIGURE 5.9 EFFECT OF PLATE SPACING ON THE NORMALIZED MAGNETIC FIELD REQUIRED FOR THE STATIC INSTABILITY OF COUNTER-STREAMING JETS. S AND A ARE THE SYMMETRIC AND ANTISYMMETRIC MODES.

The equations are

$$\hat{\xi}_1(x) = \xi_o \left\{ \frac{\sin\beta_1 x}{\sin\beta_1 L} + \frac{\cos\beta_2 x}{\cos\beta_2 L} \right\}$$

$$\hat{\xi}_2(x) = \xi_o \left\{ \frac{\sin\beta_1 x}{\sin\beta_1 L} - \frac{\cos\beta_2 x}{\cos\beta_2 L} \right\} \qquad \text{S mode}$$

$$\hat{\xi}_1(x) = \xi_o \left\{ \frac{\cos\beta_1 x}{\cos\beta_1 L} + \frac{\sin\beta_2 x}{\sin\beta_2 L} \right\} \qquad (5.14)$$

$$\hat{\xi}_2(x) = \xi_o \left\{ \frac{\cos\beta_1 x}{\cos\beta_1 L} - \frac{\sin\beta_2 x}{\sin\beta_2 L} \right\} \qquad \text{A mode}$$

where $$\beta_1 = \frac{\omega_h\sqrt{\frac{\eta-1}{2}}}{\sqrt{v_o^2-v_t^2}}, \quad \beta_2 = \frac{\omega_h\sqrt{\frac{\eta+1}{2}}}{\sqrt{v_o^2-v_t^2}}$$

Because of the sinusoidal dependance, the eigenfunctions are strongly affected by the transverse spacing.

In Fig. 5.10, the eigenfunctions for $\bar{L} = 4$ are plotted for the first three modes as a function of time. Because of the spatial oscillatory character of the trajectories it is more difficult to predict the stability of the mode than in the electric field case.

5.2.3 Transient Behavior

The equations of motion (5.1) were programmed for magnetic field coupling in exactly the same way as for the electric field case for points C and D of Fig. 5.9. These results are shown in Figs. 5.11 and 5.12. The initial disturbance on jet 1 is swept downstream and one can observe the push exerted by jet 2 as it is swept along. As the downstream section of jet 1 moves below the equilibrium it starts to pull on jet 2, giving it an initial downward deflection. As it moves to the left it is given an upward push by jet

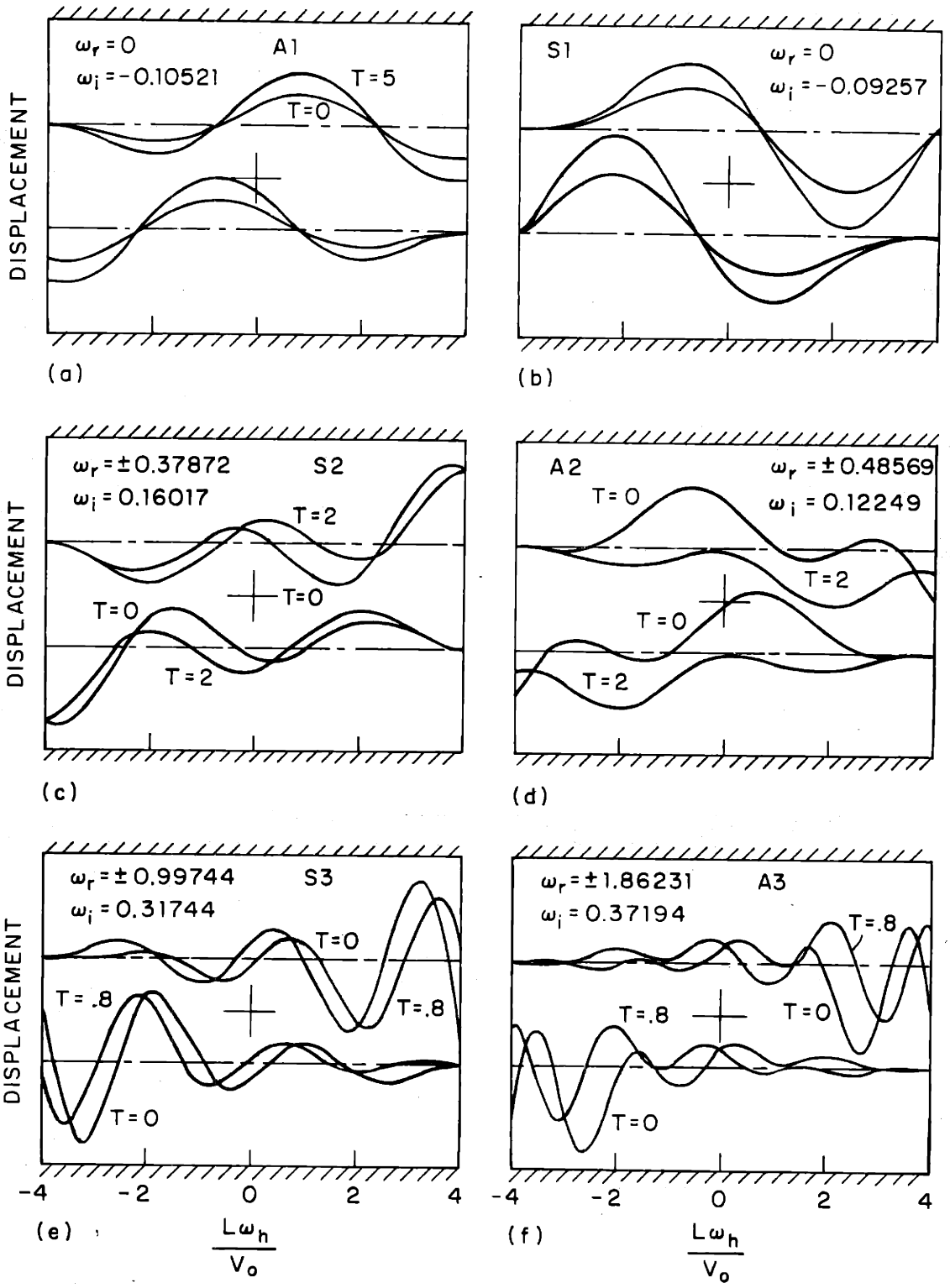

FIGURE 5.10 EIGENFUNCTIONS FOR THE THREE LOWEST SYMMETRIC AND ANTISYMMETRIC MODES OF FIGURE 5.8. THE NORMALIZED LENGTH $\frac{L\omega_e}{V_o} = 4.$

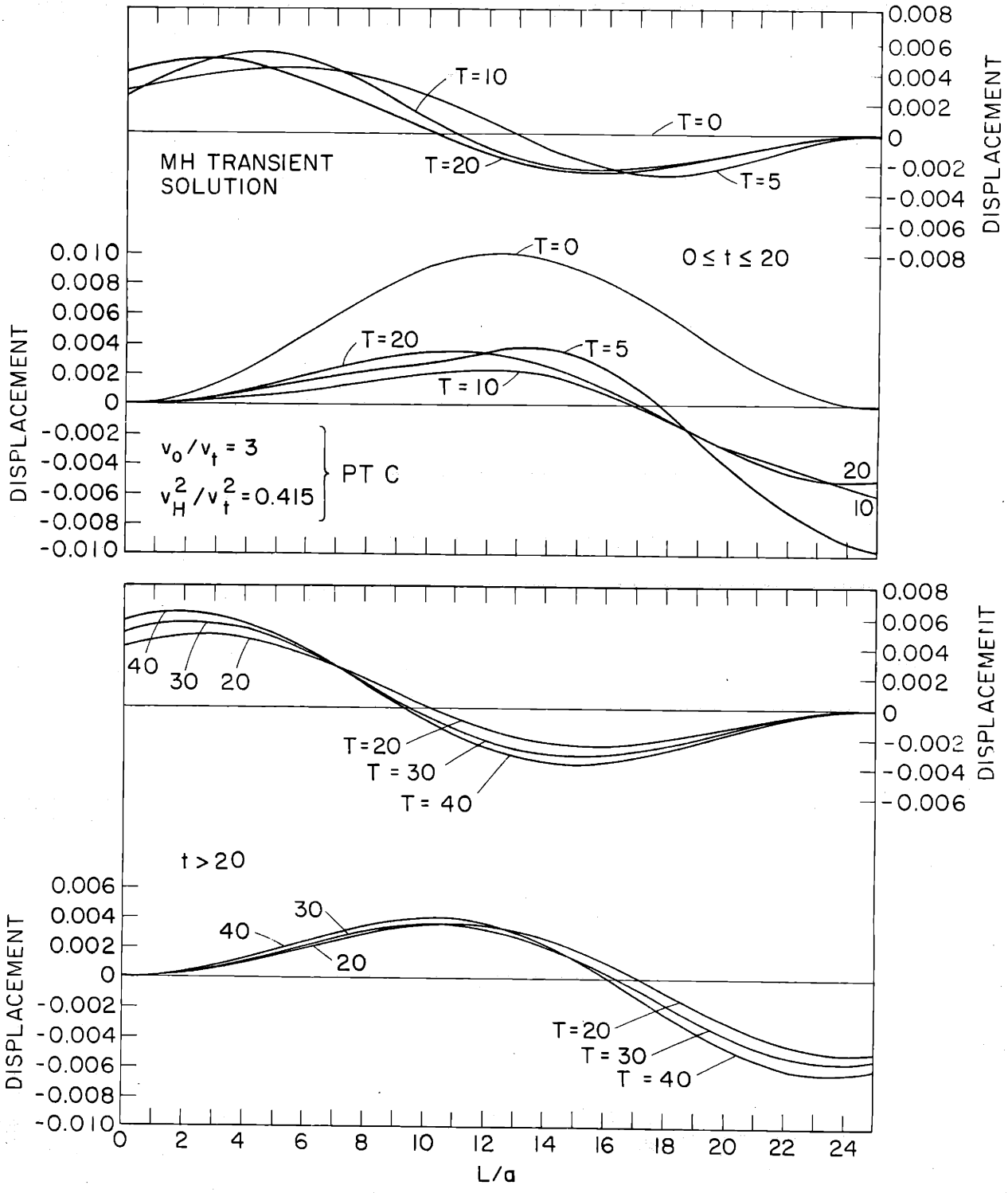

FIGURE 5.11 TRANSIENT SOLUTION TO AN INITIAL EXCITATION ON THE LOWER JET. STABLE COMPONENTS OF THIS PULSE PROPAGATE AWAY, LEAVING ONLY THE FUNDAMENTAL SYMMETRIC MODE WHICH SLOWLY BECOMES UNSTABLE. POINT C IS SHOWN IN FIGURE 5.9.

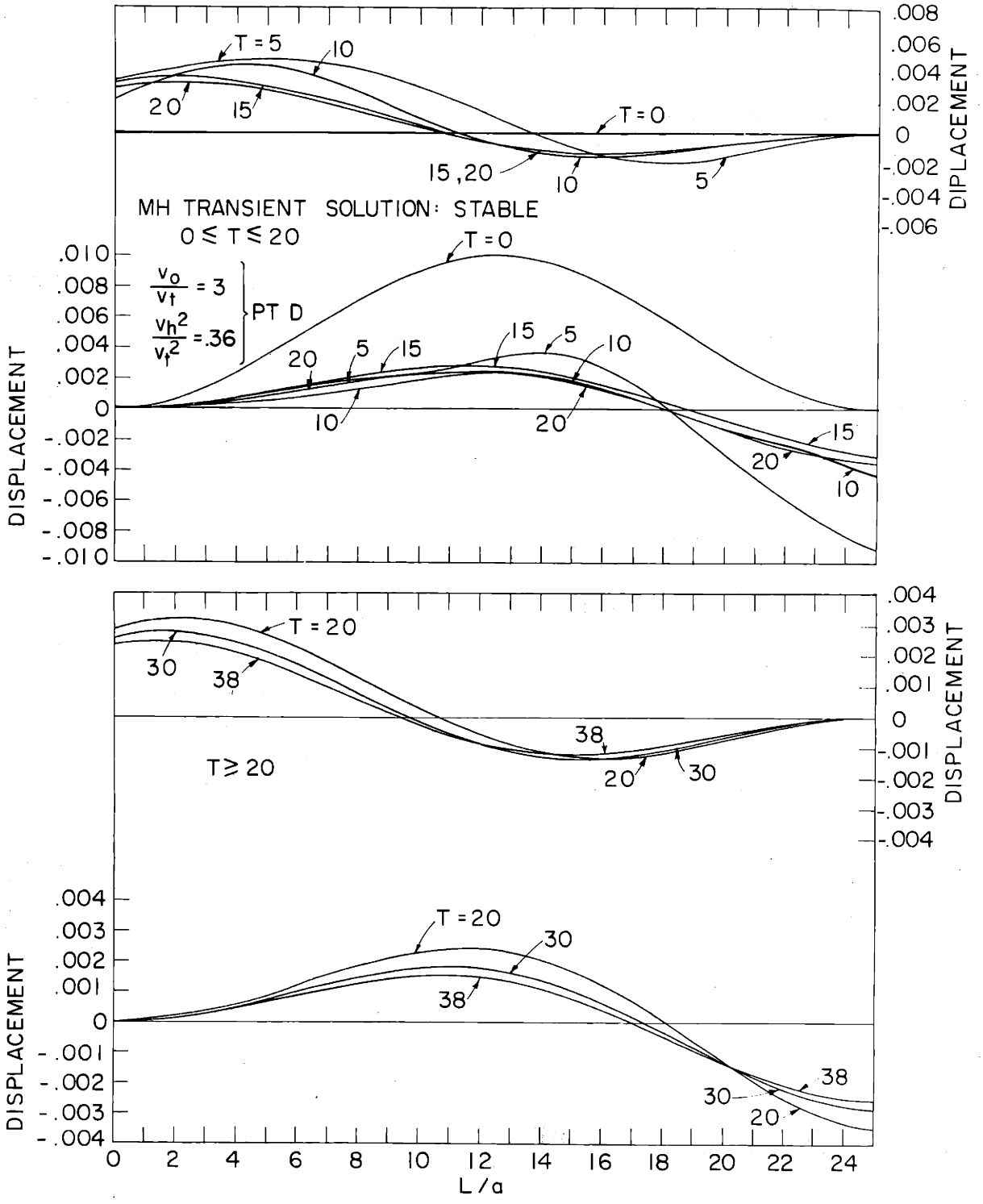

FIGURE 5.12 TRANSIENT SOLUTION SIMILAR TO FIGURE 5.11 WITH THE MAGNETIC FIELD SLIGHTLY REDUCED. POINT D IS SHOWN IN FIGURE 5.9

1 due to its trajectory now lying above the axis. Jet 2 now overshoots the axis and is given a final push back by the external plate, resulting in the trajectory for T = 5. The fundamental symmetric mode has already begun to take shape. As time progresses the higher modes propagate away and the system settles down into the S1 mode and this case begins to exhibit temporal growth. In Fig. 5.12 the magnetic field is slightly less than that required for instability and after an initial transient settles down to the S1 mode and slowly decays in time. The trajectory agrees with the analytical expression shown in (5.14). A similar analysis, performed at different value of η so that the antisymmetric mode would be the first mode of instability, showed in fact a similar initial transient, the system settling down into the A1 mode and slowly growing or decaying in time depending on the magnitude of the magnetic field.

5.3 The Case of Counter-Streaming Degenerate Jets

It has been mentioned earlier that the convection and mutual coupling terms in the equations of motion are responsible for the instability of counter-streaming jets for both electric and magnetic field coupling. One might suspect this to be true on the basis that much of the stability behavior of the two systems is quite similar, in spite of the fact that the dynamics of class I and class II systems are entirely different for electric and magnetic field coupling. To show the importance of convection and mutual coupling a little more clearly let us postulate a hypothetical system in which the surface tension is zero and the self coupling term negligible (this last restriction is unphysical). The equations of motion reduce to

$$\left(\frac{\partial}{\partial t} + V_o \frac{\partial}{\partial x}\right)^2 \xi_1 = \frac{\omega_o^2}{2} \xi_2$$

$$\left(\frac{\partial}{\partial t} - V_o \frac{\partial}{\partial x}\right)^2 \xi_2 = \frac{\omega_o^2}{2} \xi_1 \qquad (5.15)$$

where $\omega_o^2/_2$ can represent either the electric or magnetic mutual coupling. The dispersion relation is

$$\omega^4 - 2\omega^2 V_o^2 k^2 + V_o^4 k^4 - \omega_o^4/_4 = 0$$

and is the plotted in Fig. 5.13a. Solving for k,

$$k = \pm \sqrt{\frac{\omega^2 \pm \omega_o^2/_2}{V_o^2}} \qquad (5.18)$$

We can immediately see that a saddle point exists at $\omega_s = -j\frac{\omega_o}{\sqrt{2}}$, $k_s = 0$ indicating the existence of a static instability of zero wavenumber. Since the value is independent of the sign of ω_o^2 the saddle point is the same for both electric and magnetic field coupling.

5.3.1 Eigenfrequencies and Impending Instability

The boundary condition equation is simply (5.7) with V_t and η set to zero in the expression for $\Gamma_{1,2}$. The eigenfrequencies which are imaginary are plotted in Fig. 5.14 and are the same for both electric and magnetic coupling, except for an interchange of symmetric and antisymmetric modes. The complex branches of the eigenfrequencies are not shown. The system exhibits static instability for all modes. The point of impending instability may be obtained from (5.10) or (5.14) by setting $\eta = V_t = 0$.

Electric S Mode or Magnetic A Mode

$$\tan \alpha L \tanh \alpha L = 1 \quad \text{or} \quad \alpha L = .93755 \quad \text{mode 1}$$

$$\alpha L \approx (n + \tfrac{1}{4})\pi, n = 1,2 \quad \text{higher modes}$$

Electric A Mode or Magnetic Mode

$$\tan \alpha L \tanh \alpha L = -1 \quad \text{or} \quad \alpha L = 2.34705 \quad \text{mode 1} \qquad (5.18)$$

$$\alpha L \approx (n + \tfrac{3}{4})\pi, n = 1,2 \quad \text{higher modes}$$

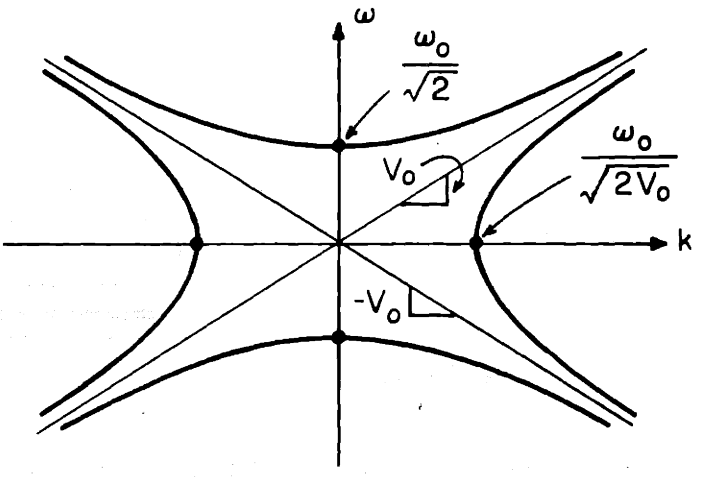

(a) DISPERSION CURVE

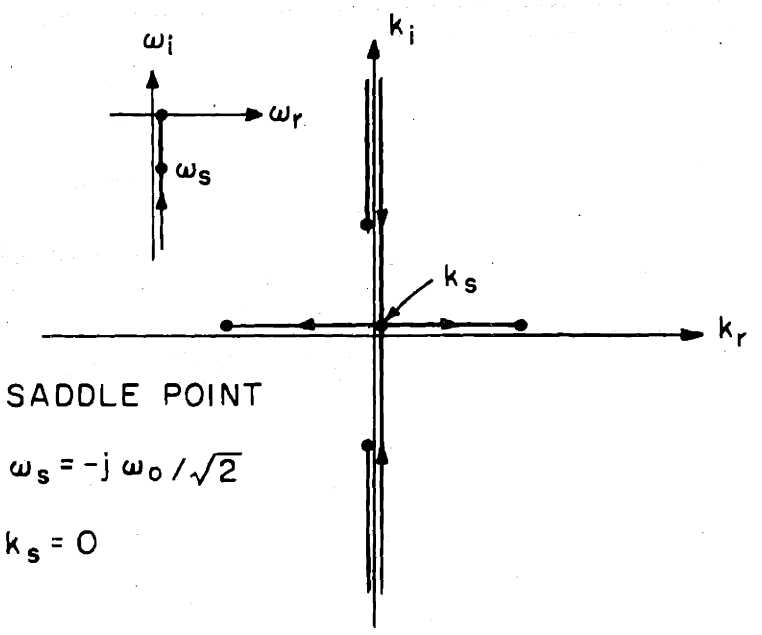

(b) STABILITY PLOT

FIGURE 5.13 DISPERSION CURVE AND STABILITY PLOT FOR DEGENERATE COUNTER-STREAMING JETS, SHOWING THE STATIC INSTABILITY AT INFINITE WAVELENGTH.

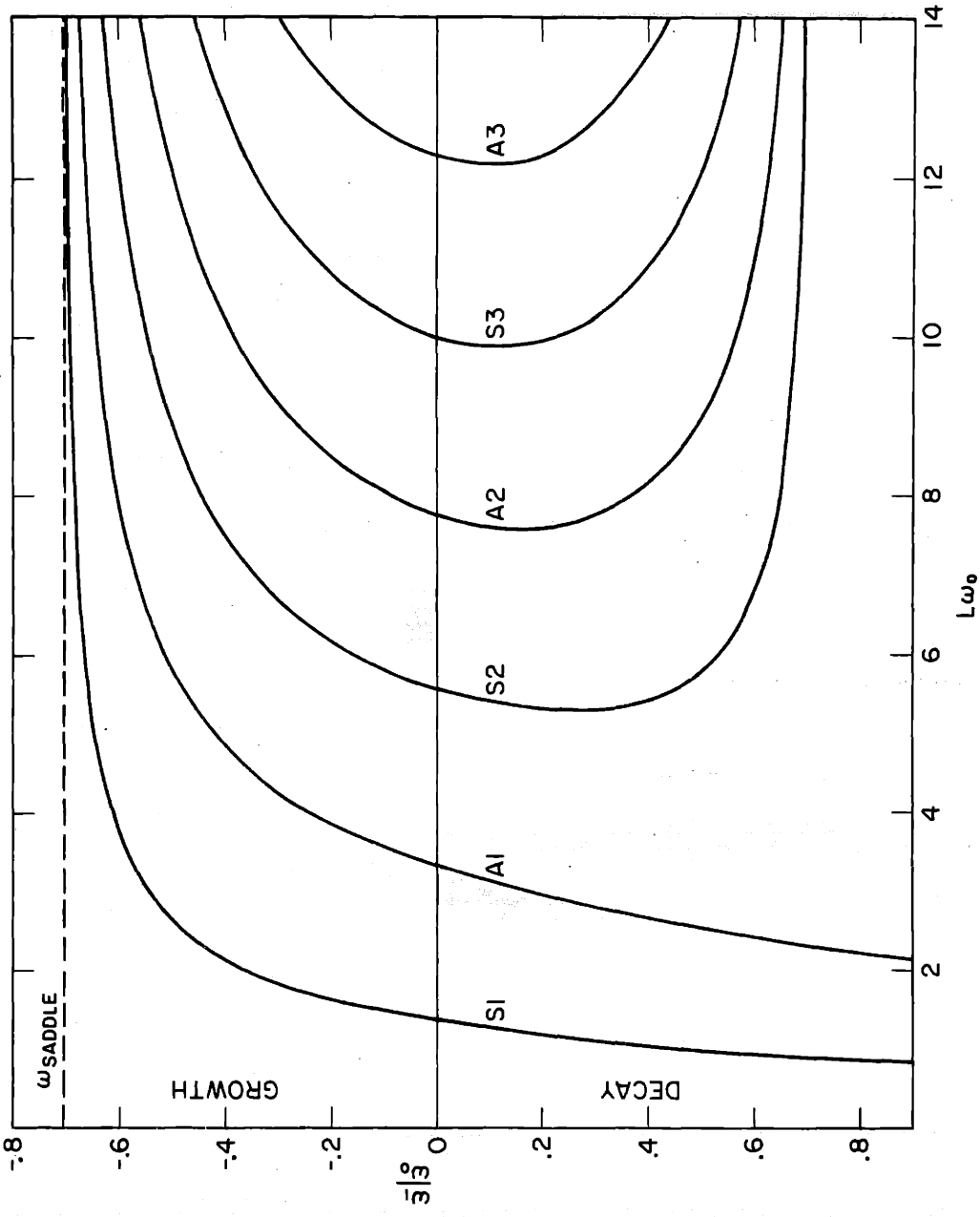

FIGURE 5.14 IMAGINARY EIGENFREQUENCIES VERSUS NORMALIZED LENGTH FOR THE DEGENERATE COUNTER-STREAMING JETS. ALL MODES ARE STATICALLY UNSTABLE.

where $\alpha L = \dfrac{\omega_o L}{\sqrt{2} V_o}$

(Care must be taken in setting $\eta = 0$ to preserve the proper sign). The eigenfunctions at the point of impending instability can be obtained from (5.11) and (5.15).

	Electric Coupling	Magnetic Coupling
S Mode	$\dfrac{\hat{\xi}_1(x)}{\xi_o} = \dfrac{1}{2}\left\{\dfrac{\sin \alpha x}{\sin \alpha L} + \dfrac{\cosh \alpha x}{\cosh \alpha L}\right\}$	$\dfrac{\hat{\xi}_1(x)}{\xi_o} = \dfrac{1}{2}\left\{\dfrac{\cos \alpha x}{\cos \alpha L} + \dfrac{\sinh \alpha x}{\sinh \alpha L}\right\}$
	$\dfrac{\hat{\xi}_2(x)}{\xi_o} = \dfrac{1}{2}\left\{\dfrac{\sin \alpha x}{\sin \alpha L} - \dfrac{\cosh \alpha x}{\cosh \alpha L}\right\}$	$\dfrac{\hat{\xi}_2(x)}{\xi_o} = \dfrac{1}{2}\left\{-\dfrac{\cos \alpha x}{\cos \alpha L} + \dfrac{\sinh \alpha x}{\sinh \alpha L}\right\}$
A Mode	$\dfrac{\hat{\xi}_1(x)}{\xi_o} = \dfrac{1}{2}\left\{\dfrac{\cos \alpha x}{\cos \alpha L} + \dfrac{\sinh \alpha x}{\sinh \alpha L}\right\}$	$\dfrac{\hat{\xi}_1(x)}{\xi_o} = \dfrac{1}{2}\left\{\dfrac{\sin \alpha x}{\sin \alpha L} + \dfrac{\cosh \alpha x}{\cosh \alpha L}\right\}$
	$\dfrac{\hat{\xi}_2(x)}{\xi_o} = \dfrac{1}{2}\left\{\dfrac{\cos \alpha x}{\cos \alpha L} - \dfrac{\sinh \alpha x}{\sinh \alpha L}\right\}$	$\dfrac{\hat{\xi}_2(x)}{\xi_o} = \dfrac{1}{2}\left\{-\dfrac{\sin \alpha x}{\sin \alpha L} + \dfrac{\cosh \alpha x}{\cosh \alpha L}\right\}$

(5.19)

These eigenfunctions are plotted in Fig. 5.15.

5.3.2 Eigenfunctions and Physical Explanation

Examination of these stationary eigenfunctions will shed some light on the role the convected momentum and mutual coupling terms play. Consider in Fig. 5.15a that the lower jet (jet 2) has the deflection shown and a particle from the upper jet (jet 1) enters the interaction region. It will be deflected upward due to the reduced electric traction in the field region between the jets. The net traction exerted on jet 1 is upward but tends to zero as the particle progresses to the exit plane. Since there is no time variation of the trajectory, the particle will follow the path shown in Fig. 5.15a. Note there is no traction on a jet because of its own displacement from the assumption of the model.

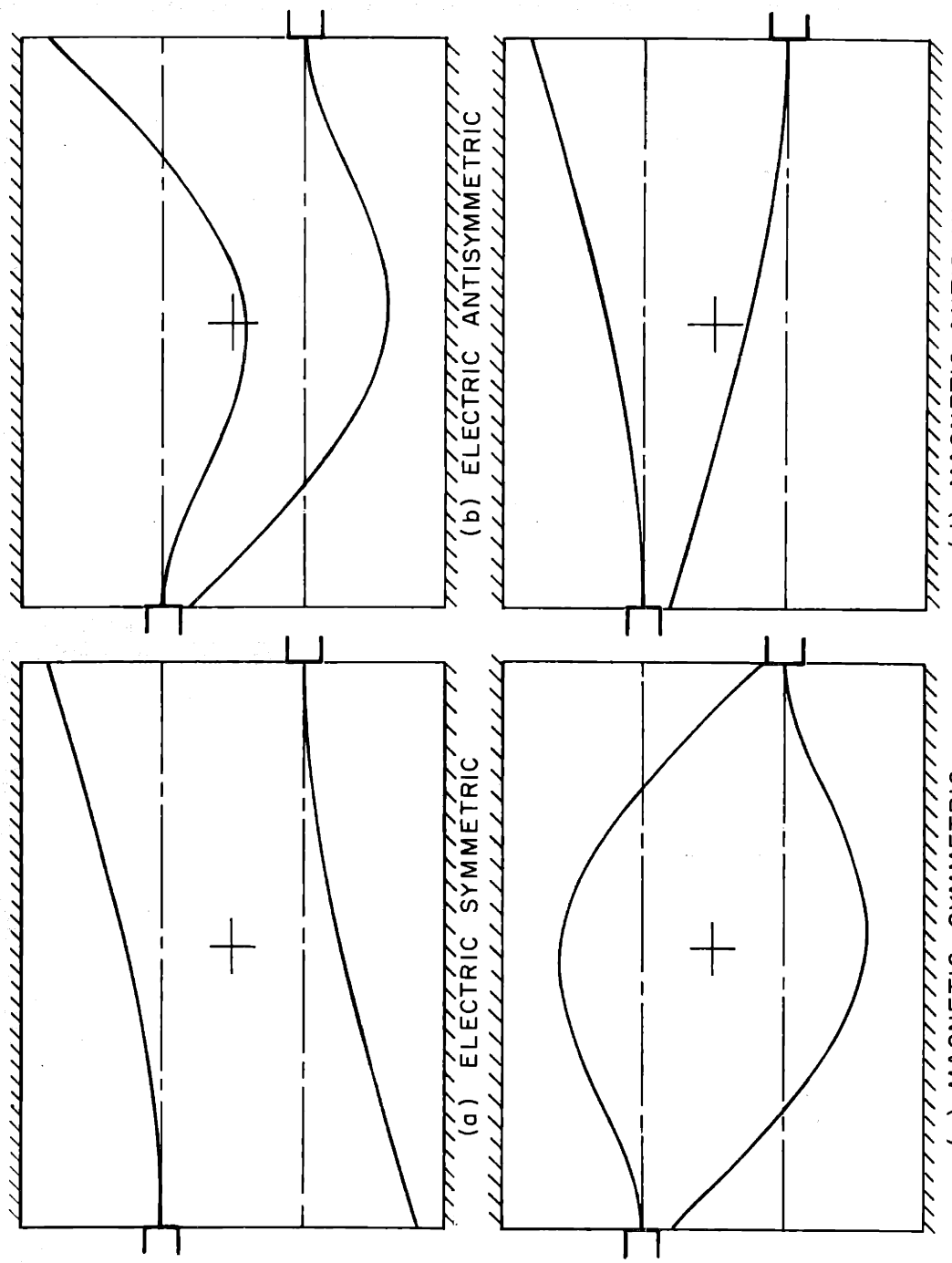

FIGURE 5.15 EIGENFUNCTIONS AT IMPENDING INSTABILITY FOR DEGENERATE COUNTERSTREAMING JETS.

The question of instability then is, can the deflection of jet 1 caused by the assumed deflection of jet 2 be sufficient to produce a displacement of jet 1 as large or larger than that assumed? This will depend on the value of $L\omega_o/V_o$.

If the electric S mode and magnetic A mode are compared, although the symmetry is opposite, the traction exerted by jet 2 on jet 1 is the same for both systems. This is because a compression of the magnetic field lines resulting in an upward push, is equivalent to an extension of the electric field lines, which results in an upward pull on jet 1. Both systems then have the same eigenfunction (but opposite symmetry) and the same $L\omega_o/V_o$ for instability.

Jet 1 for the electric A mode in Fig. 5.15b shows an initial downward traction due to the upward deflection of jet 2, followed by an upward traction as a particle travels downstream. The effect of the convected momentum is evident, since the particle continues its downward deflection for a considerable distance downstream before it is turned around by the upward force exerted by jet 2. Because jet 1 experiences first a downward force and then an upward force, we might intuitively expect that a larger $L\omega_o/V_o$ would be required for instability. Indeed, the value of $L\omega_o/V_o$ is about 2.5 times that for the symmetric mode. The antiduality between the magnetic S mode and the electric A mode is evident.

Finally if the eigenfrequencies and eigenfunctions of the degenerate problem are compared with the original electric and magnetic field coupled problems, we can learn something about the role of the self coupling term in the instability. From the results of Chapter 2 concerning the single jet interactions between rigid walls, electric self coupling resulted in a convective instability for long waves, the short wavelength cutoff depending on the surface tension. Since the present instability is definitely long wave, surface tension should not play an important role in the behavior of the system. The result is that in the degenerate electric S mode, given the same jet 2 trajectory, jet 1 would now experience a considerably

larger upward force, producing a larger displacement, and hence a larger traction on jet 2. Self coupling aids the mutual coupling and requires a smaller $L\omega_o/V_o$ for instability. Comparing the eigenfrequencies for the two cases shows that this is in fact true.

For the electric A mode, however, the self term interferes with the mutual coupling term. Consider the same jet 2 deflection in Fig. 5.15b as before. Jet 1 will now achieve a larger downward deflection than before. At the point jet 2 changes sign, for example, the net traction on jet 1 is downward. The result is that jet 1 will have little or no upward deflection at the exit, and jet 2 will experience little initial traction and hence cannot sustain the given trajectory. Indeed the self term so effectively interferes that the lowest electric A mode is quite stable for all values of $L\omega_o/V_o$.

The magnetic systems are not so strongly affected by the self coupling term, since the single jet behavior exhibits only propagating waves. From the magnetic S mode in Fig. 5.15c, the self term of jet 1 produces a downward traction, resulting in a larger overshoot than before. This causes a larger initial downward displacement of jet 2 and hence reinforces the instability as is, in fact, observed. The self coupling term for the magnetic A mode clearly interferes with the mutal coupling term, making it less unstable. The higher modes may be similarly explained but are more difficult because of the more complex trajectory.

5.4 Counter Streaming Electron Beams

As a matter of interest, the eigenfrequencies for coupled counter streaming electron beams with longitudinal oscillations is shown in Fig. 5.16. As mentioned earlier, electrostatic oscillations on an electron beam model as the magnetic surface wave if the surface tension is suppressed and the rigid plates are moved to infinity ($\eta = -1$). As can be observed the system exhibits only static

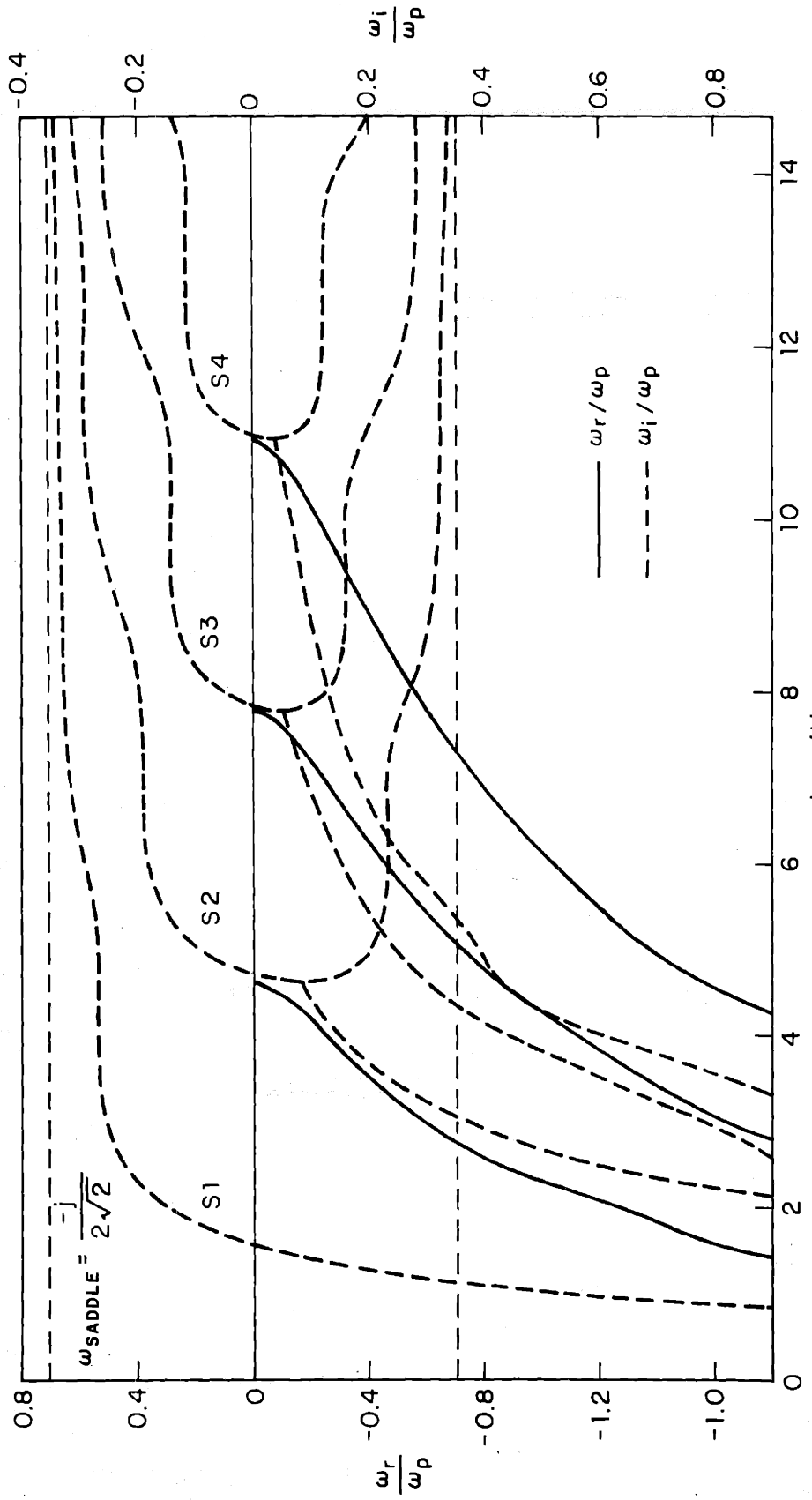

FIGURE 5.16a COMPLEX EIGENFREQUENCY VERSUS NORMALIZED LENGTH FOR COUNTER-STREAMING ELECTRON BEAMS: SYMMETRIC MODE.

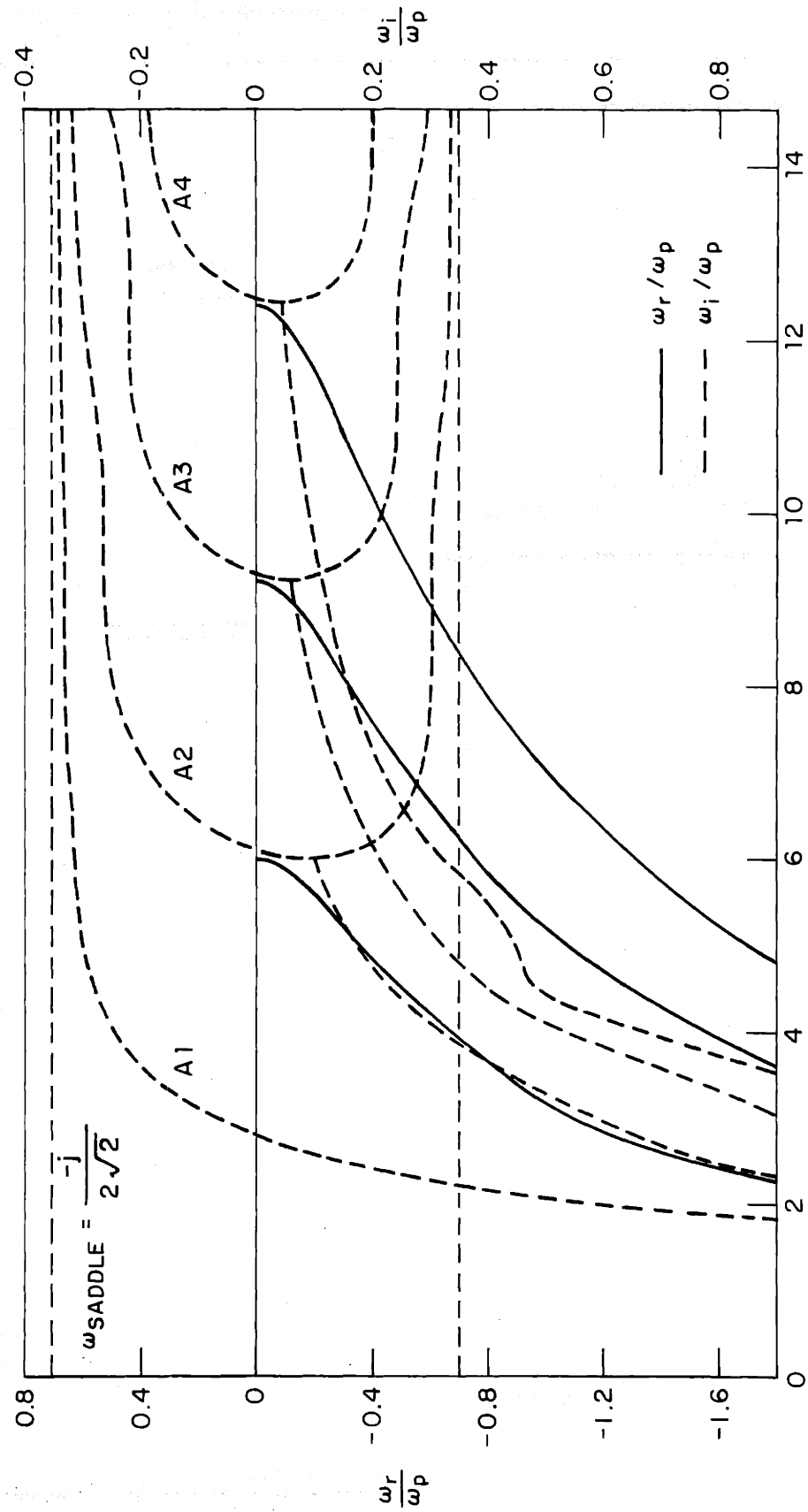

FIGURE 5.16b COMPLEX EIGENFREQUENCY VERSUS NORMALIZED LENGTH FOR COUNTERSTREAMING ELECTRON BEAMS: ANTISYMMETRIC MODE.

instabilities and the results are quite similar to the degenerate magnetic field case.

This problem has been investigated experimentally by Kofoid,[27] who in fact did observe absolute instabilities. However the instabilities were not static instabilities as predicted in our model, but rather standing waves at a frequency of the order of the plasma frequency. Kofoid found that the oscillations are a strong function of the background plasma, so that another ingredient is necessary in the model. Gerwin and Nelson[20] in studying the theoretical aspects of this problem, have computed the statically unstable eigenfrequencies for the model assumed here and the results are the same as the upper half plane of Fig. 5.16a and b, except for the factor $\sqrt{2}$ which enters from the definition of ω_p.

CHAPTER 6

COUNTER-STREAMING ELECTRIC FIELD COUPLED JET EXPERIMENT

6.1 Introduction

In order to verify the theoretical results of the previous chapter, an experiment was constructed to measure complex eigenfrequencies for the electric field coupled model. A brief discussion of experimental detail will be given and the experimental results discussed. Experimental agreement with the theoretical model of the previous chapter has been obtained for the fundamental symmetric mode, the only mode which could be investigated.

6.2 Experimental Description

The experiment was constructed using the same apparatus as in the two-spring experiment, simply replacing the springs by jets for counter-streaming flow. The length between nozzles and the transverse spacings were carefully kept the same as for the springs so that the calibration of the electrical coupling parameters performed in Chapter 4 was valid. The jets and springs were the same diameter. The external plates were bent to the same vertical curvature as the jets. A considerable amount of care is required to align the jets parallel and to provide the proper spacing while at the same time insuring that the jets have the same elevation. The external plate alignment is also critical since a slight unbalance in electric traction produces a large deflection and shifts the equilibrium. This is especially serious since an equilibrium shift and the fundamental symmetric mode eigenfunction have similar spatial dependence. With the jets properly aligned, it is possible to position the plates so that the equilibrium is not disturbed by a large electric field, using a single voltage source.

It might be mentioned that because the plates and jets are non-planar, the relative polarity of the electric field in the field regions is important. This is

because a jet is now influenced by the non-adjacent plate. In all of the experiments described, the voltage of the elements was of alternate polarity. This minimized the effect of the non-adjacent plate and secondly allows the use of a single power supply.

Because one jet is required to be at high voltage, two electrically isolated, closed loop systems were used. The loop consisted of a pump, filter, overhead tank, nozzle, collector, and return tank. A simple overflow device in the overhead supply tanks insured constant level for the jets. A single double shaft motor with insulating drive belt and pulleys was sufficient to provide electrical isolation for the two centrifugal pumps. At the highest voltages used (about 15 kv) leakage current from the power supply to the whole apparatus was maintained below 0.1 ma. This is important since corona discharge and other sources of leakage currents have a degrading effect on the quality of the jets.

A few words are in order concerning the formation of 1 meter long laminar jets. Everyone has observed the breaking up of a water jet into droplets when a faucet is slowly turned on, due to the surface tension of the jet tending to constrict the jet. A planar jet should not exhibit this instability, since there is no transverse curvature. A finite width planar jet, however, exhibits a sharp pulling in of the outer edges and it is extremely difficult to produce a jet that remains planar for any appreciable length. Planar jets have been studied by G. I. Taylor,[50] but jets such as those described are unsuitable for our purposes.

This natural pinch mode instability of a circular jet has been observed to be convective, and its electric field dependence studied by Melcher,[34] who has shown that the spatial growth rate of the $m = 0$ mode increases with electric fields and competes very well with the kink ($m = 1$) mode for a cylindrical jet for even a large electric field. Since only small displacements are required for the sausage mode

to be nonlinear and effectively make the jet unsuitable for kink mode measurements, it is essential that the sausage mode be suppressed. Mechanical vibrations, unsteady flow, vorticity and acoustical noise are all fine sources of excitation of the sausage mode. An early experiment by Rayleigh[29] showed that by transmitting the mechanical vibrations set up by a pinched off jet hitting the collecting container back to the nozzle that the jet broke into oscillation and was absolutely unstable. This effect was observed quite frequently and it was necessary to shock mount the nozzle and collector separately to destroy the natural feedback paths in the supporting structure. The whole apparatus was also shock mounted to minimize building noise and the motor and pump assembly separately shock mounted. Each of these modifications improved the quality of the jets.

To improve flow conditions, the overhead supply tanks were provided with large sponges which served two purposes: (1) to filter out fine air bubbles which do not convect sufficiently fast to the surface to be removed and (2) to act as a damper to settle the flow. These were quite effective. Finally the lead-in hose must be of smooth wall and free of any kinks and the nozzle was especially constructed to provide smooth entrance flow. With all these inovations it was possible to obtain a jet of about 80 cm. useful length with some unsteadiness but not reproducibility. The final touch was a result of adding glycerine to the water in about equal proportion. This has little effect on conductivity and density but a large effect on viscosity. Since the wavelength of instability for the sausage mode is at least an order of magnitude less than for the kink modes to be investigated the addition of viscosity should preferentially damp the sausage mode. The effect of large viscosity on the transverse wave motion of jets has been studied by Middleman and Javis[38]. A sufficient amount of glycerine was added to produce quiet jets 1 meter long in the absence of electric field.

6.3 Results

In addition to the coupling parameters the other constants of the system were measured, and the experimental coefficients used to compute the low mode eigenfrequencies as a function of $L\omega_e/V_o$. Since the lowest mode is static ($\omega_r = 0$), the measurement of this eigenfrequency consisted in measuring the decay rate. A small d.c. voltage was impressed on the normally grounded plate to deflect the jets, with a large d.c. voltage on. With the jets deflected, the plate was grounded and the decay transient recorded. The results are shown in Fig. 6.1, and the theoretical results are seen to be in agreement with the experiment.

For low applied voltage, the decay transient is quite rapid and a bit difficult to interpret. In order to measure the fundamental mode unambiguously it is assumed that all higher modes have damped before the usable portion of the decay curve has been reached. This was near the end of the transient but before the transient became noise limited. As the voltage is increased, the decay curves are more accurate, but near the point of instability the jets become quite noisy and the signals of poor quality. Because of the jet breakup at the highest voltages, the planar model is no longer valid and the experimental data is not in agreement with the theoretical value.

The second mode should be of some interest, since it has a real component of the frequency. At low voltages it decays, but for sufficiently high voltages the mode becomes overstable. It would not be possible to experimentally measure the overstability with the existing system because of the fundamental mode instability at lower field. The 2nd mode decay is greater than the fundamental for the same voltage and is therefore more difficult to measure. At the higher voltages where 2nd mode decay rates are feasible, the n = 0 mode noise was too great to permit useful measurements.

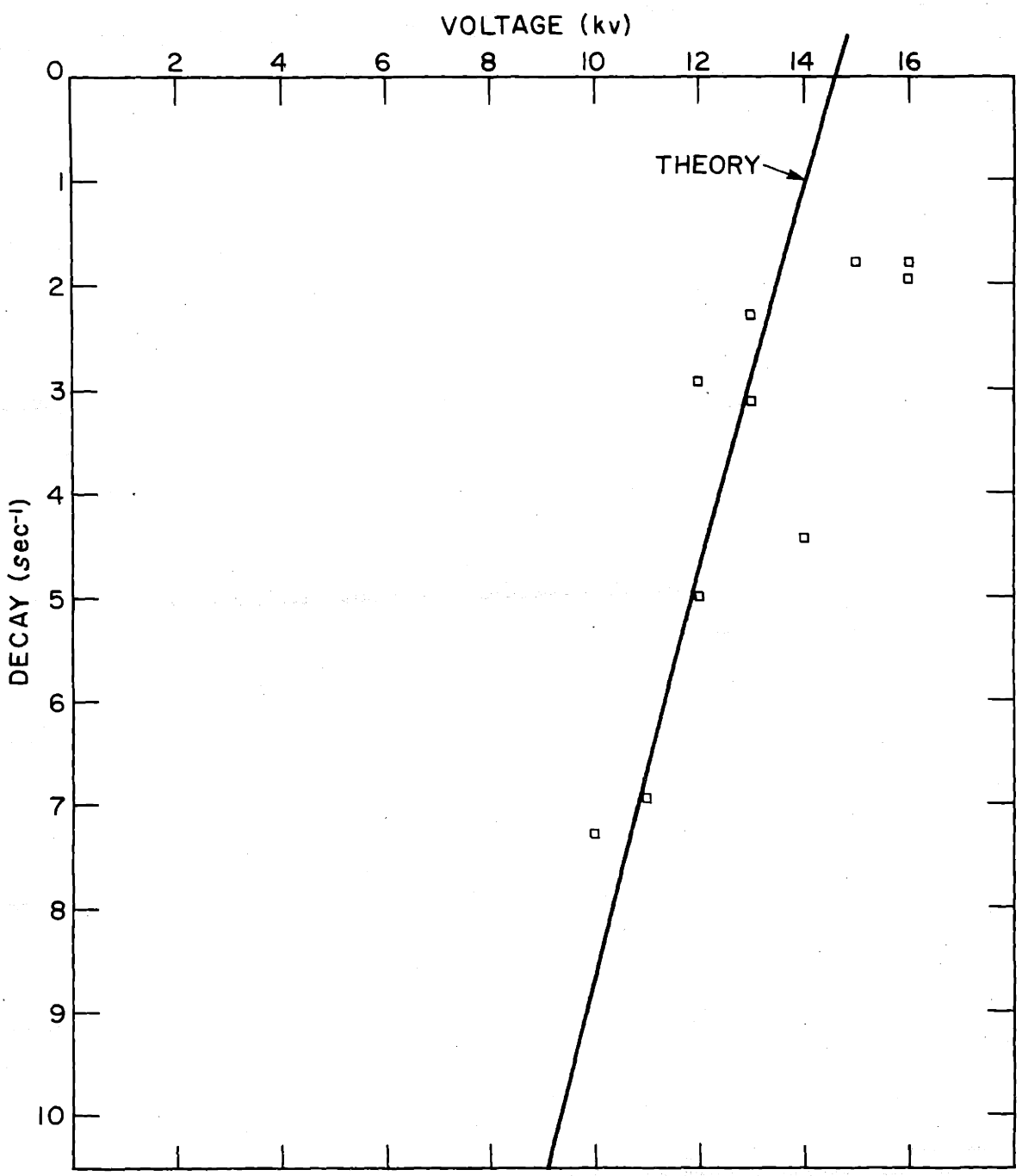

FIGURE 6.1 FUNDAMENTAL SYMMETRIC MODE DECAY RATE VERSUS VOLTAGE FOR ELECTRIC FIELD COUPLED COUNTER-STREAMING JETS.

In conclusion the experimental eigenfrequencies of two circular counter-streaming, electric field coupled jets agree with theoretical values when the experimentally determined values of the system parameters are used in the analysis. It might be mentioned that the jet velocity is about 30 times the capillary velocity and since the important system parameter is V_t^2/V_o^2 compared to unity, the effect of surface tension is completely negligible.

CHAPTER 7

STREAM-STRUCTURE INSTABILITIES

7.1 Summary

The eigenvalue equations are formulated for a special case of the class IV systems, namely the interaction of a supercapillary jet with a stationary structure. The complex eigenfrequencies are numerically computed for both electric field and magnetic field coupling. The electric field coupling produces the expected statically unstable behavior characteristic of the structure by itself stressed by an electric field. In addition, it exhibits overstable behavior at smaller $\omega_e L/V_o$ than required for static instability. These overstabilities are found only for modes higher than the fundamental and for jet velocities greater than the natural wave velocity on the structure. The fundamental mode exhibits electrical damping. The computed eigenfunctions show that the structure resonates essentially in its natural modes of oscillation, the jet exhibits its characteristic convective instability, and there is a delicate interplay between the jet and the structure.

The magnetic field coupled system also exhibits overstability for the higher modes, damping for the fundamental and for the same range of parameters as in the electric field case. The asymptotic behavior for both types of field coupling for large $\omega_{e,h} L/V_o$ is predicted by the Bers-Briggs stability criterion for the infinite system.

To examine the common features of electric and magnetic field coupled stream-structure interactions, the degenerate jet-structure model is examined and compared with the former systems. Physical arguments are given to explain the overstabilities for the higher modes, damping of the fundamental, and the dependence on the ratio of spring tension to jet velocity.

7.2 Introduction

The last main topic, and perhaps the most interesting one from the standpoint of physical realizability, possible practical usefulness, and variety of interactions, is the investigation of the class IV systems described in Chapter 3 for the infinite system. The attention will be given to the special case in which the subcapillary stream is stationary and hence can be modeled by a mechanical structure. This class of interactions in the (mathematically) related area of electron beams has achieved a considerable degree of sophistication, and such devices as the traveling wave amplifier and the backward wave oscillator are common hardware to the microwave engineer. Because of the similarity between the surface wave stream-structure discussed here and the electron beam-cavity devices (extended region klystron) system, the former devices will occasionaly be referred to as surface wave klystrons. While the behavior is understood qualitatively, it is only recently that effort has been made to analytically compute the complex eigenfrequencies for a stream-structure device [7,20] of finite length. Experiments on the electric field coupled spring-jet system will be described in the next chapter and the quantitative agreement with theory discussed.

7.3 The Eigenvalue Problem

Let us again return to the long wave equations of motion, (3.4)

$$\left(\frac{\partial}{\partial t} + V_{o1}\frac{\partial}{\partial x}\right)^2 \xi_+ - V_{t1}^2 \frac{\partial^2}{\partial x^2}\xi_+ - \frac{\eta\omega_{e1}^2\xi}{2}_+ = -\frac{1}{2}\omega_{e1}^2\xi_-$$

$$\left(\frac{\partial}{\partial t} + V_{o2}\frac{\partial}{\partial x}\right)^2 \xi_- - V_{t2}^2 \frac{\partial^2}{\partial x^2}\xi_- - \frac{\eta\omega_{e2}^2}{2}\xi_- = -\frac{1}{2}\omega_{e2}^2\xi_+ \qquad (7.1)$$

Since the structure is stationary, $V_{o1} = V_o$, $V_{o2} = 0$, and assuming solutions of the form $e^{j(\omega t - kx)}$

$$[(\bar{\omega}-\bar{k})^2 - \bar{k}^2 G + \frac{\eta}{2}]\xi_+ = \frac{1}{2}\xi_-$$

$$[\bar{\omega}^2-\bar{k}^2 G_1 + \frac{\eta}{2} G_2]\xi_- = \frac{G_2}{2}\xi_+$$

where

$$\bar{\omega} = \frac{\omega}{\omega_{e1}} \quad , \quad \bar{k} = \frac{kV_o}{\omega_{e1}} \quad , \quad G = \left(\frac{V_{t1}}{V_o}\right)^2 \quad , \quad G_1 = \left(\frac{V_{t2}}{V_o}\right)^2 \quad , \quad G_2 = \left(\frac{V_{e2}}{V_{e1}}\right)^2$$

Combining $$[(\bar{\omega}-\bar{k})^2-\bar{k}^2 G+ \frac{\eta}{2}][\bar{\omega}^2-\bar{k}^2 G_1+ \frac{\eta}{2} G_2] - \frac{G_2}{4} = 0 \qquad (7.2)$$

Equation(7.2) is the dispersion relation for stream-structure systems and is a general fourth degree polynomial in both $\bar{\omega}$ and $\bar{k}$. There do not appear to be any useful special cases and since the model does not possess symmetry, it is necessary to determine the solutions numerically. As a guide in computing the complex eigenfrequencies, it is useful to start with the uncoupled eigenfrequencies of the structure. Hereafter, the structure will be assumed to be a spring.

Recalling the results of Chapter 3, the class IV systems could be divided into two regions depending on the number of crossings of the uncoupled dispersion relation curves. Class IVa represented the case where the jet was slightly supercapillary. The electric field case exhibited a convective instability and static instability characteristic of the uncoupled elements. The magnetic system exhibited propagating wave and evanescent wave behavior, also characteristic of the uncoupled interactions. Class IVb systems (jet very supercapillary), on the other hand, showed the same general behavior for electric field coupling, but exhibited a convective instability for magnetic field coupling for a band of frequencies as well as the usual propagating and evanescent behavior.

We should now like to consider how these systems behave with boundaries imposed. The system to be considered is a supercapillary jet which enters the interaction region unexcited, and a stationary jet (structure) fixed at the ends.

The boundary conditions are:

$$\xi_+(o,t) = \frac{\partial \xi_+}{\partial x}(o,t) = 0$$

and $$\xi_-(o,t) = \xi_-(L,t) = 0$$

From (7.1) assuming $\underline{\xi}_+(x,t) = \mathrm{Re}[\hat{\underline{\xi}}_+(x)e^{j\omega t}]$ and setting $x = \frac{V_o}{\omega_e}\bar{x}$

$$[(j\bar{\omega} + \frac{d}{d\bar{x}})^2 - G\frac{d^2}{d\bar{x}^2} - \frac{\eta}{2}]\hat{\xi}_+ = -\hat{\xi}_-/_2 \tag{7.3}$$

and $$[-\omega^2 - G_1\frac{d^2}{d\bar{x}^2} - \frac{\eta G_2}{2}]\hat{\xi}_- = -\frac{G_2}{2}\hat{\xi}_+$$

The solution to this 4th order equation may be written

$$\hat{\xi}_-(\bar{x}) = \sum_{i=1}^{4} B_i e^{-j\bar{k}_i\bar{x}}$$

and $$\hat{\xi}_+(\bar{x}) = \sum_{i=1}^{4} Q_i B_i e^{-j\bar{k}_i\bar{x}} \tag{7.4}$$

where $Q_i = -\frac{2}{G_2}\{-\bar{\omega}^2 + G_1\bar{k}_i^2 - \frac{\eta G_2}{2}\}$

If the boundary conditions are evaluated, the following determinantal equation is obtained

$$\begin{bmatrix} 1 & 1 & 1 & 1 \\ e^{-jk_1L} & e^{-jk_2L} & e^{-jk_3L} & e^{-jk_4L} \\ Q_1 & Q_2 & Q_3 & Q_4 \\ k_1Q_1 & k_2Q_2 & k_3Q_3 & k_4Q_4 \end{bmatrix} \begin{bmatrix} B_1 \\ B_2 \\ B_3 \\ B_4 \end{bmatrix} = 0 \tag{7.5}$$

By manipulating (7.4), a somewhat simpler expression results.

$$
\begin{aligned}
& e^{-j(k_2-k_1)L}\,\frac{(k_3-k_4)}{(k_2-k_1)}\left\{\omega^2+\frac{\eta G_2}{2}+G_1(k_3k_4+k_1k_4+k_1k_3)\right\} \\
& +e^{-j(k_3-k_1)L}\,\frac{(k_1-k_2)}{(k_3-k_1)}\left\{\omega^2+\frac{G_2}{2}+G_1(k_2k_4+k_1k_4+k_1k_2)\right\} \\
& +e^{-j(k_4-k_1)L}\,\frac{(k_2-k_3)}{(k_4-k_1)}\left\{\omega^2+\frac{G_2}{2}+G_1(k_2k_3+k_1k_3+k_1k_2)\right\}=0
\end{aligned}
\tag{7.6}
$$

Equation (7.6), combined with the dispersion relation, (7.2) forms the eigenvalue equation to be solved. This combined equation (formally speaking) is a function of $\bar{\omega}$, $\bar{L}$, and the system parameters. As in the case of counter-streaming jets, the computational procedure will be to assume $\bar{L}$ and $\bar{\omega}$, compute the $\bar{k}$ values from (7.2), and evaluate (7.6), and by a suitable iteration process, vary $\bar{\omega}$ until (7.6) is satisfied. The $\bar{\omega}$ thus computed is the normalized complex eigenfrequency and the corresponding $\bar{k}$ values the normalized eigenvalues. The details of this procedure are the same as described in Sec. 5.1.1.

The eigenfrequencies for two similar jets, one stationary, the other with a velocity $\frac{V_t}{V_o}=\frac{1}{2}$, are shown in Fig. 7.1. This is on the edge between the class IVa and b regions. To interpret the curves, it is useful to compare the eigenfrequencies for the uncoupled case, namely a single spring between rigid plates. The determinantal equation reduces simply to $\bar{k}=\frac{n\pi}{\bar{L}}$ and the eigenvalue equation becomes

$$
\bar{\omega}^2=G_1\left(\frac{n\pi}{\bar{L}}\right)^2-1 \tag{7.7}
$$

The real part of the eigenfrequencies shown in Fig. 7.1 are essentially those of the spring alone (compare Figs. 4.2 and 7.1). In addition, the point of instability

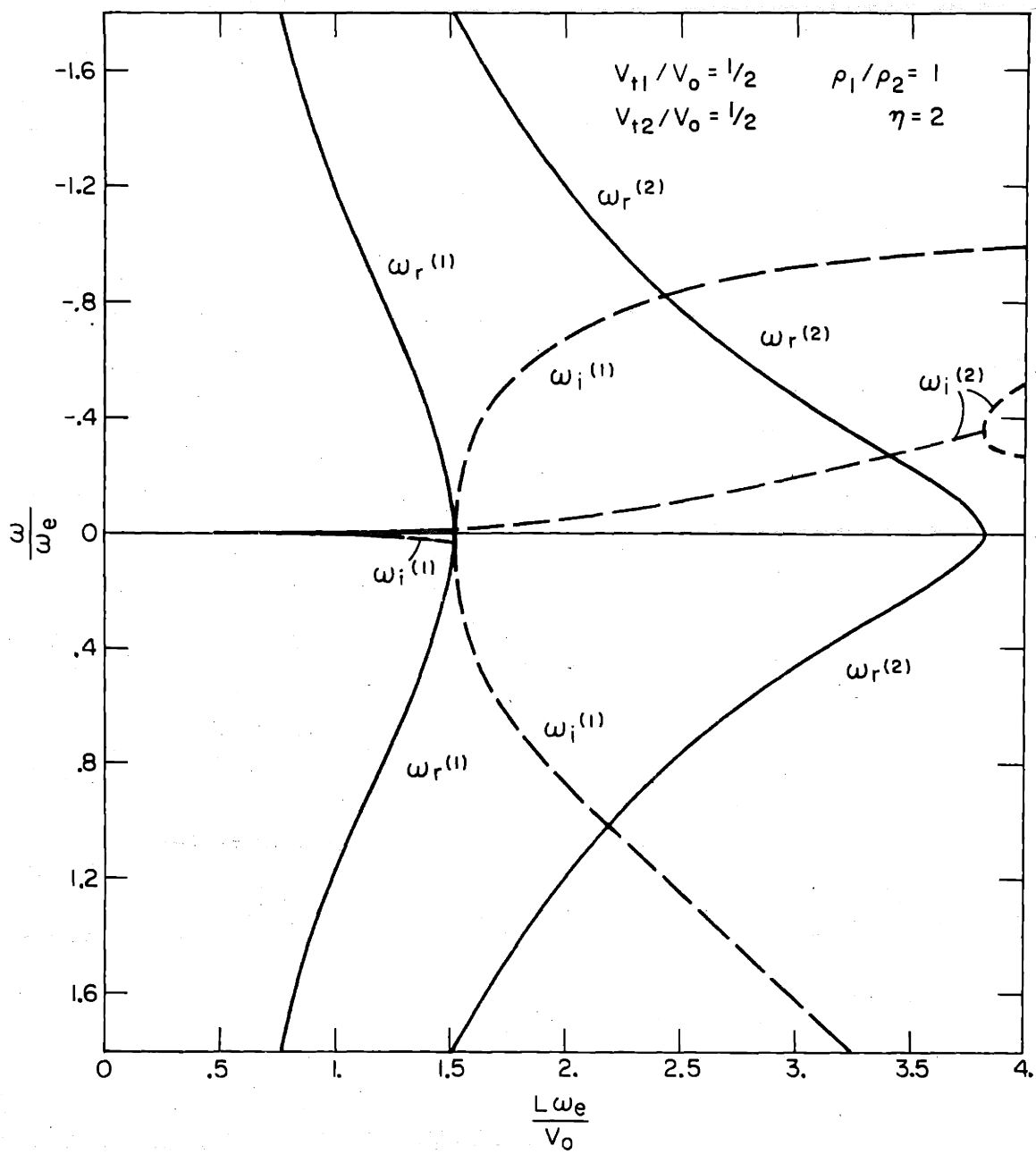

FIGURE 7.1 COMPLEX EIGENFREQUENCY VS. NORMALIZED LENGTH FOR AN ELECTRIC FIELD COUPLED SURFACE WAVE KLYSTRON.

for the first mode is very nearly that for a spring coupled to rigid walls. The effect of the coupling is to produce electrical damping of the spring. Above the instability point the growth rate also agrees quite well with the uncoupled case and approaches the same asymptotic limit. The decay branch, however, exhibits an increased decay rate.

The effect of coupling on mode 2, however, is quite significant. Mode 2 exhibits overstability for a wide range of $\bar{L}$, and becomes unstable (theoretically) as soon as the slightest electric field is applied. As $\bar{L}$ is increased, the normalized growth rate increases to quite a large value until the real part of the eigenfrequency becomes zero and the curve splits into two statically unstable modes. The deviation from the uncoupled eigenfrequency case becomes larger with increasing $\bar{L}$. The overstable behavior of mode 2 is exhibited by higher modes as well although not shown in Fig. 7.1.

7.3.1 Eigenfunctions

The eigenfunctions may be computed using (7.4) and (7.5). If we assume $B_1 \neq 0$ for the moment, then the ratios of the coefficients to B_1 may be computed from

$$\begin{bmatrix} 1 & 1 & 1 \\ Q_2 & Q_3 & Q_4 \\ k_2Q_2 & k_3Q_3 & k_4Q_4 \end{bmatrix} \begin{bmatrix} \frac{B_2}{B_1} \\ \frac{B_3}{B_1} \\ \frac{B_4}{B_1} \end{bmatrix} = \begin{bmatrix} -1 \\ -Q_1 \\ -Q_1k_1 \end{bmatrix} \tag{7.8}$$

Since B_1 is arbitrary, it may be set equal to the determinant of the coefficient matrix of (7.8). This allows the B's to be written in a symmetric form and the restriction that $B_1 \neq 0$ can be removed. Manipulating (7.8), we get

$$
\begin{aligned}
B_1 &= (k_3-k_4)(k_3-k_2)(k_4-k_2)\{A+G_1(k_3k_4+k_3k_2+k_4k_2)\} \\
B_2 &= (k_4-k_3)(k_4-k_1)(k_3-k_1)\{A+G_1(k_3k_4+k_1k_3+k_1k_4)\} \\
B_3 &= (k_2-k_4)(k_2-k_1)(k_4-k_1)\{A+G_1(k_4k_2+k_4k_1+k_2k_1)\} \\
B_4 &= (k_3-k_2)(k_3-k_1)(k_2-k_1)\{A+G_1(k_3k_2+k_3k_1+k_2k_1)\}
\end{aligned}
\tag{7.9}
$$

where $A = \omega^2 + \frac{\eta G_2}{2}$ and the bar (-) has been omitted from the k's and ω. From (7.4) the spatial dependence of the eigenfunctions can be calculated and finally the eigenfunctions follow from

$$\xi(x,t) = \mathrm{Re}\{\hat{\xi}(x)e^{j\omega t}\}$$

The eigenfunctions for $\bar{L} = 1.75$, of Fig. 7.1 are displayed in Fig. 7.2. The fundamental mode for both the growth and decay branches exhibit the behavior of the uncoupled jet and spring. The relative phasing is as expected, since a downward deflection of the spring weakens the field in the midregion and produces an upward traction on the jet. The phase amplitude of the spring is very slightly shifted downstream. The spring eigenfunction of mode 2 is also the same as in the uncoupled case. For $\bar{x} < \frac{\bar{L}}{2}$ the traction on the jet is downward; for $\frac{\bar{L}}{2} < \bar{x} < \bar{L}$, upward. But a certain length is required for the jet to reverse its direction of motion and cross the axis. The amplitude grows fairly rapidly since the self and mutual coupling terms are reinforcing.

For small $\bar{L}$, the spring behaves as in the uncoupled case and the jet trajectory may conveniently be thought of as determined by the behavior of the spring. As $\bar{L}$ is increased (by increasing the length, for example) the jet and spring have a longer time to interact and the jet deflections increase to a point where the jet can exert an influence on the motion of the spring, shown in Fig. 7.3.

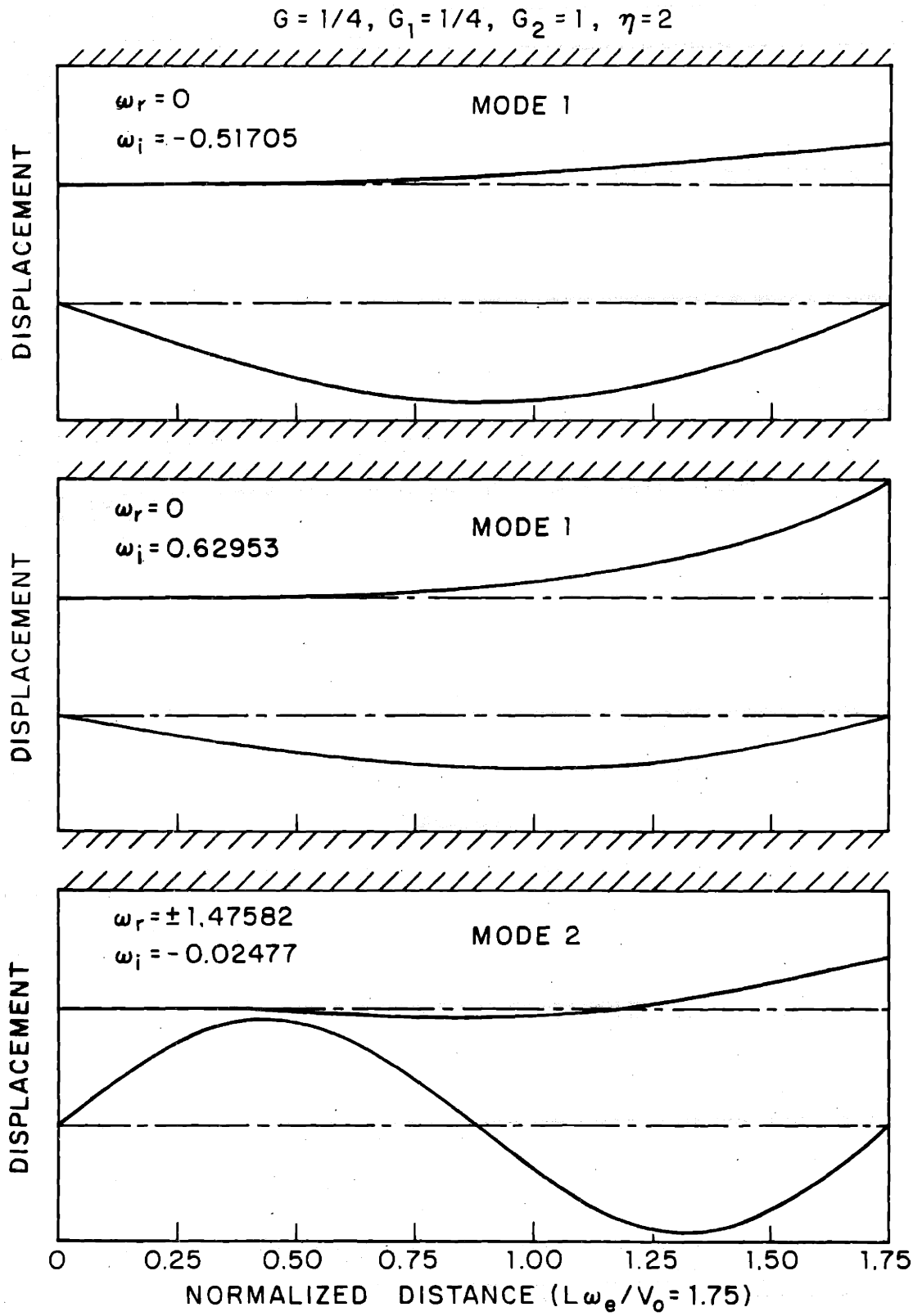

FIGURE 7.2 EIGENFUNCTIONS FOR THE MODES OF FIGURE 7.1

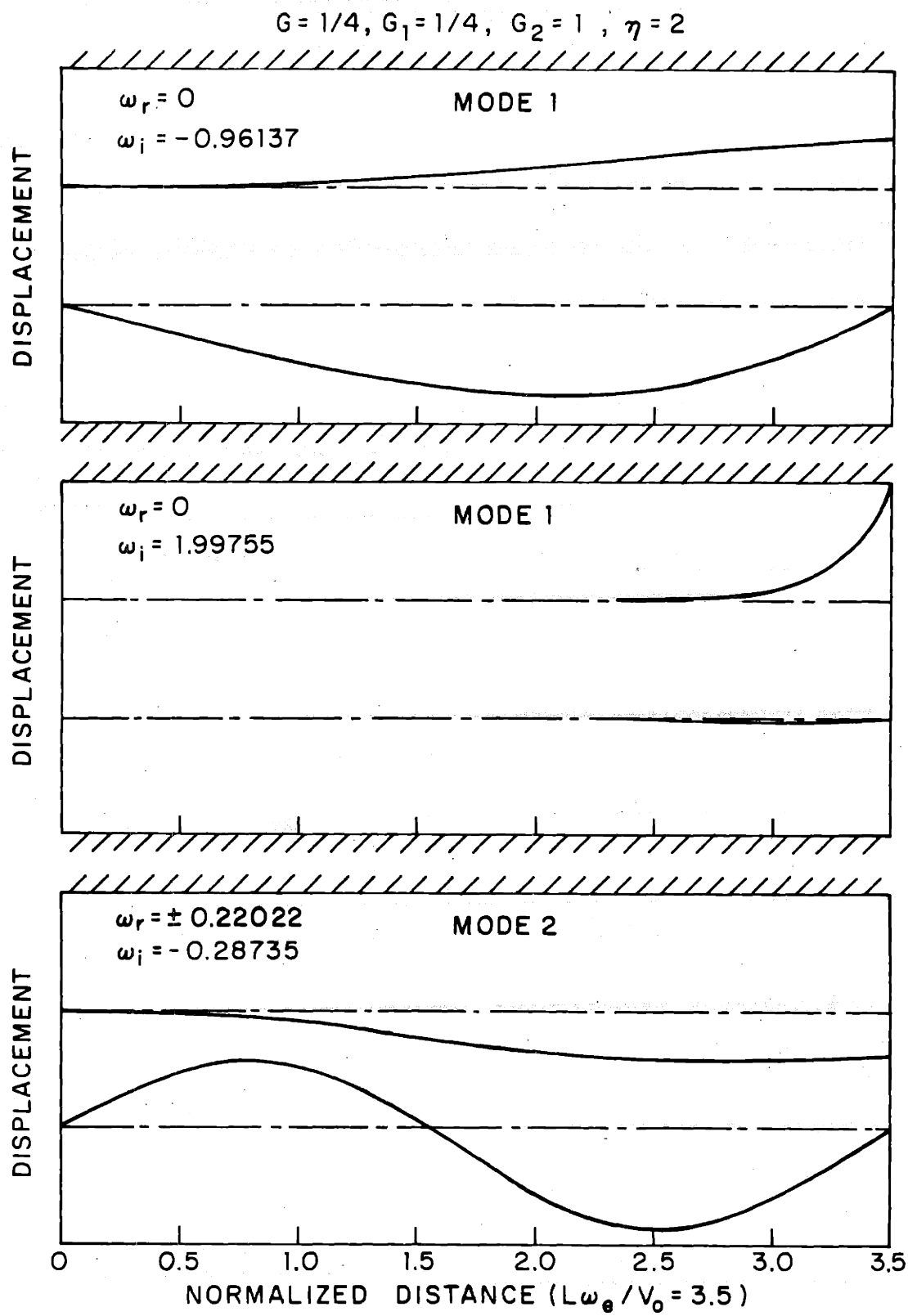

FIGURE 7.3 EIGENFUNCTIONS SIMILAR TO FIGURE 7.2 FOR THE MODES OF FIGURE 7.1

One might intuitively expect that the jet velocity would play an important role in the dynamics of the system. If the jet and spring are again assumed to be similar, but the jet velocity is increased (or perhaps better, V_t reduced since $\bar{\omega}$ and $\bar{L}$ are scaled to V_o), the resulting eigenfrequencies are shown in Fig. 7.4. The general behavior is similar to Fig. 7.1. The curves are shifted to smaller $\bar{L}$ because of the reduced tension of the spring. This implies a lower value of electric field required for fundamental mode instability. The system exhibits overstability for higher modes and damping of the fundamental as previously described. Eigenfunctions plotted for this system do not exhibit essentially different behavior than shown in Figs. 7.2 and 7.3.

The magnetic field coupled system eigenfrequencies for the same parameters as in the case just mentioned are shown in Fig. 7.5 for the lowest three modes. The real parts of the eigenfrequencies are typical of a magnetically coupled spring. The imaginary parts exhibit the same decay of the fundamental mode and growth of higher modes as for electric field coupling. It is interesting that each higher mode exhibits a peak growth rate, the 2nd mode for $\bar{L} = 2.6$ and the 3rd mode for $\bar{L} \lesssim 3.9$. The maximum growth rates are about equal. This implies an optimum length if one wished to design an oscillator using a particular mode (neglecting the adverse effects of other modes). That such a peak should occur is reasonable if one recalls from Chapter 3 that no absolute instabilities exist in the infinite system.

The eigenfunctions for $\bar{L} = 1.75$ are shown for the three lowest modes in Fig. 7.6. The same spring-like behavior is observed as in the electric field case, but the jet is more wavelike. Recall that the magnetic self coupling term is stabilizing so that the field coupled jet by itself exhibits purely propagating waves in contrast to the electric field coupling case.

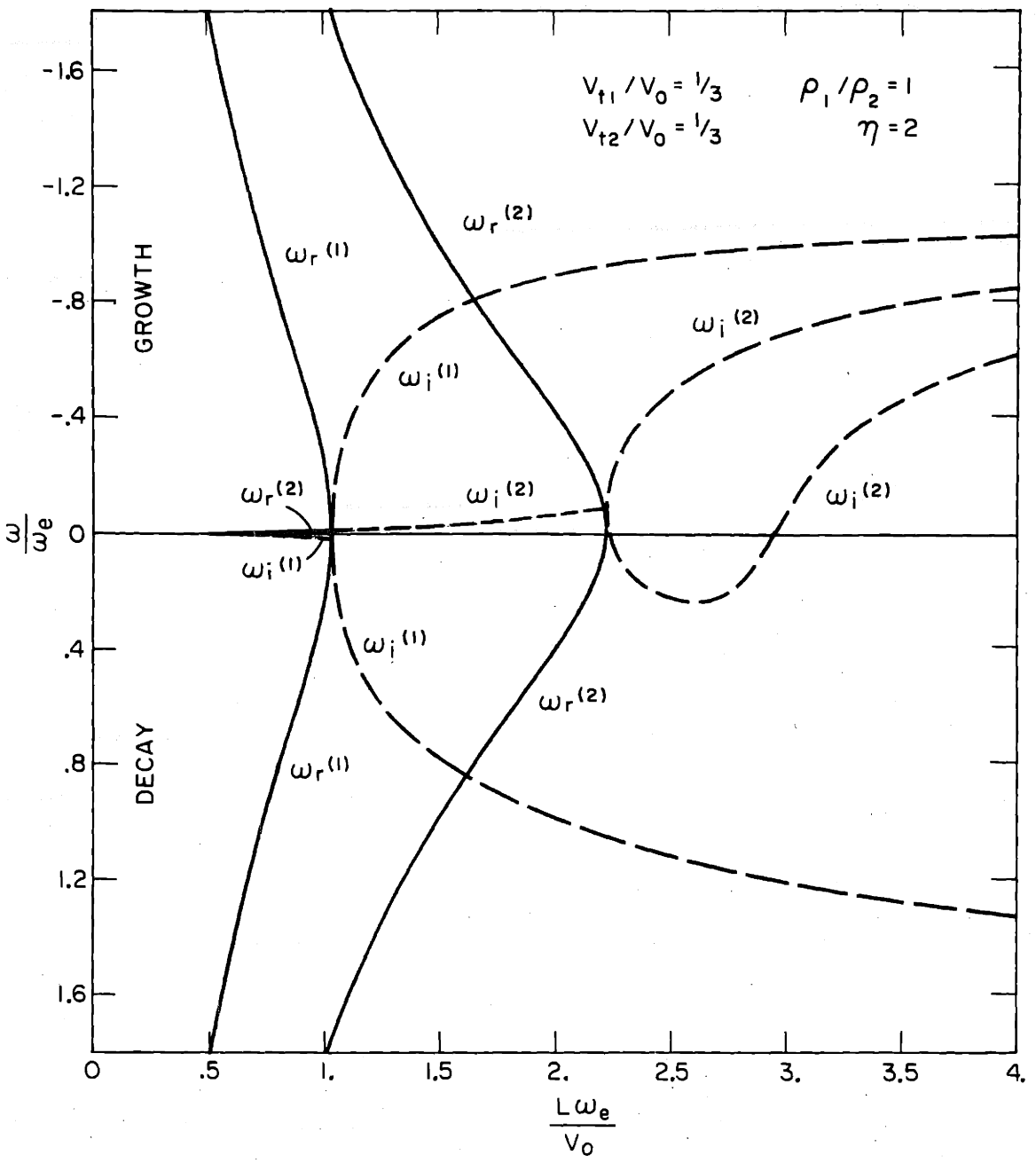

FIGURE 7.4 COMPLEX EIGENFREQUENCY VS. NORMALIZED LENGTH FOR AN ELECTRIC FIELD COUPLED SURFACE WAVE KLYSTRON: EFFECT OF PARAMETERS.

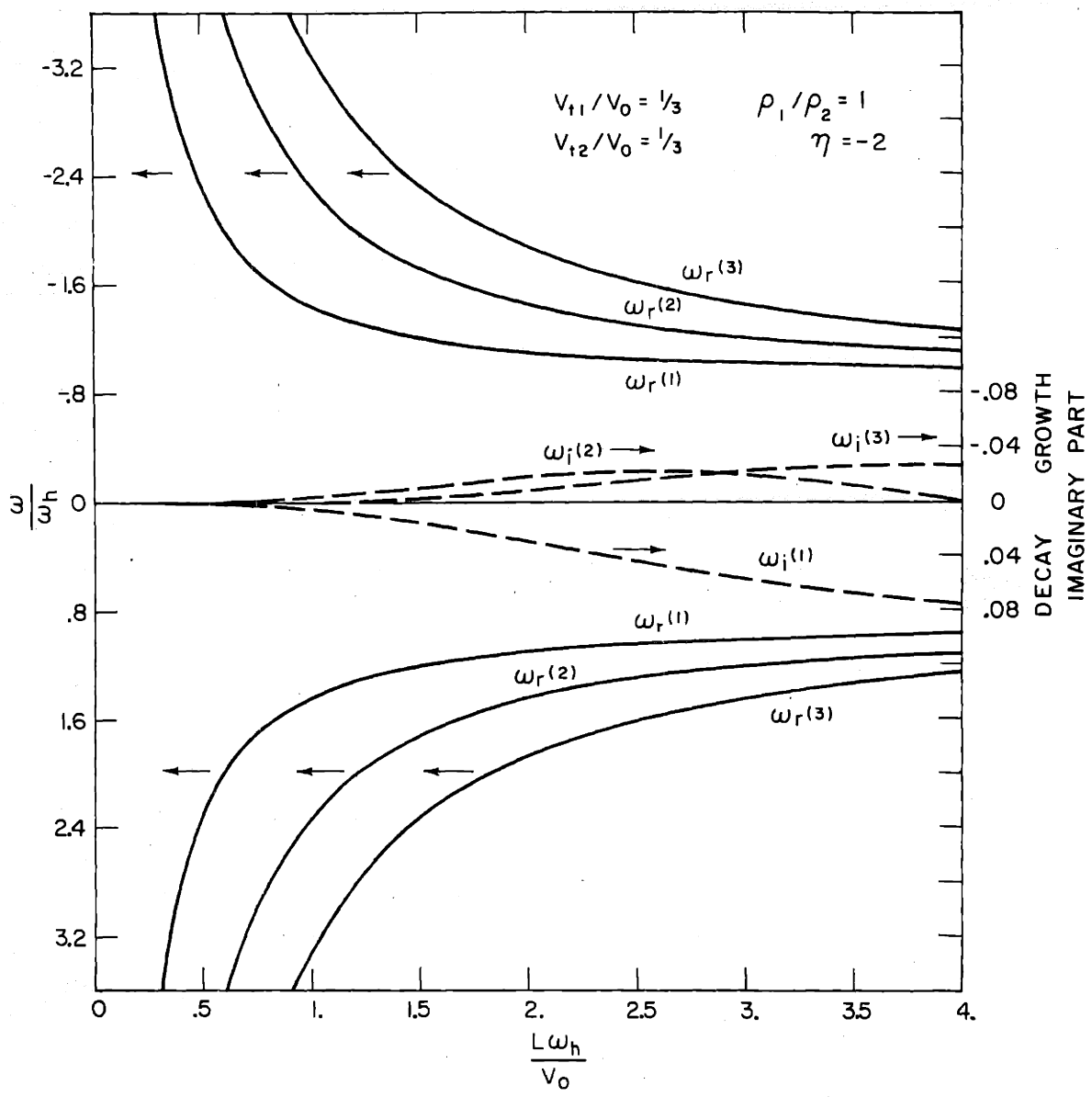

FIGURE 7.5 COMPLEX EIGENFREQUENCY VS. NORMALIZED LENGTH FOR A MAGNETIC FIELD COUPLED SURFACE WAVE KLYSTRON SHOWING THE LOWEST THREE MODES

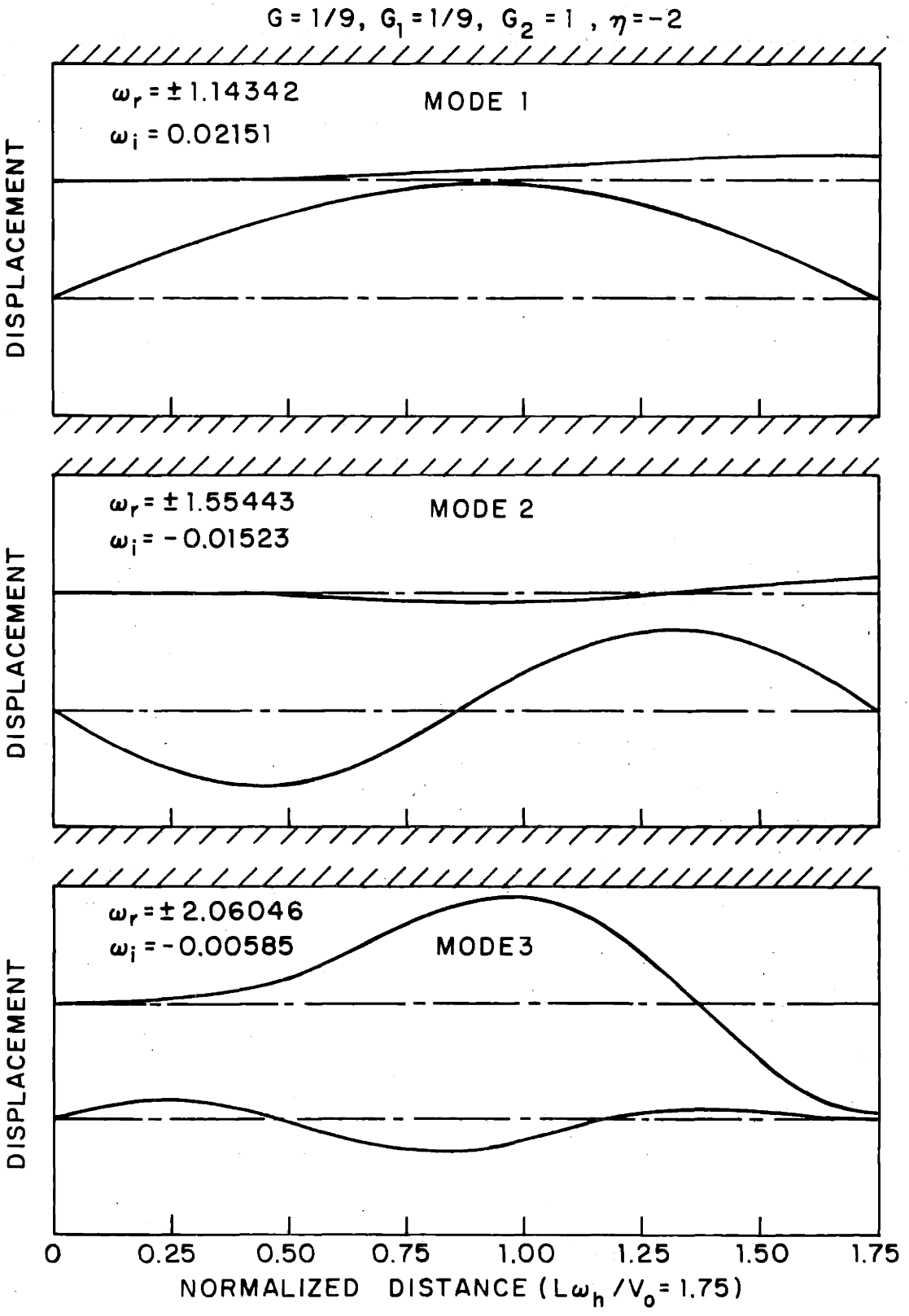

FIGURE 7.6 EIGENFUNCTIONS FOR THE MODES OF FIGURE 7.5

7.4 The Degenerate Stream-Structure Model

It is evident from the previous discussion of electric and magnetic field stream-structure interactions that the electric and magnetic systems have many common features. The same conclusion was reached in Chapter 5 in the discussion of counter-streaming jets, where it was found that the mutual coupling and convective terms were of primary importance, with the surface tension unimportant, and the self coupling term either enhanced (electric field) or depressed (magnetic field) instabilities. It is worthwhile to speculate if the dynamical terms in the equations of motion play the same role in the present case.

Let us postulate here that the jet is without surface tension and that the self coupling field terms are unimportant. This is equivalent to setting V_{t1}(or G) and η to zero in (7.1) and (7.2). Unfortunately, this degeneracy still does not permit an appreciable simplification in the dispersion or eigenvalue equations, and one must continue to use numerical solutions. The complex eigenfrequencies for a jet traveling with a velocity three times the structure wave velocity is shown in Fig. 7.7. Comparing with Figs. 7.4 and 7.5 for the electric and magnetic field cases respectively, we observe that the curve appears to be a hybrid of the two cases.

The system exhibits both static instability and overstabilities similar to the case with electric field coupling. Since the self coupling term is absent, however, the point of static instability is shifted to a larger value of $L\omega_o/V_o$. Below this value the first mode is stable, and the higher modes overstable, characteristic of both electric and magnetic field coupling. In addition, these higher modes exhibit peakes in growth rate. We may conclude, as in the case of counter-streaming jets, that the mutual coupling term is of fundamental importance.

With the surface tension suppressed the jet is supercapillary for all flow velocities and one wonders if the general behavior of this system is unaltered as

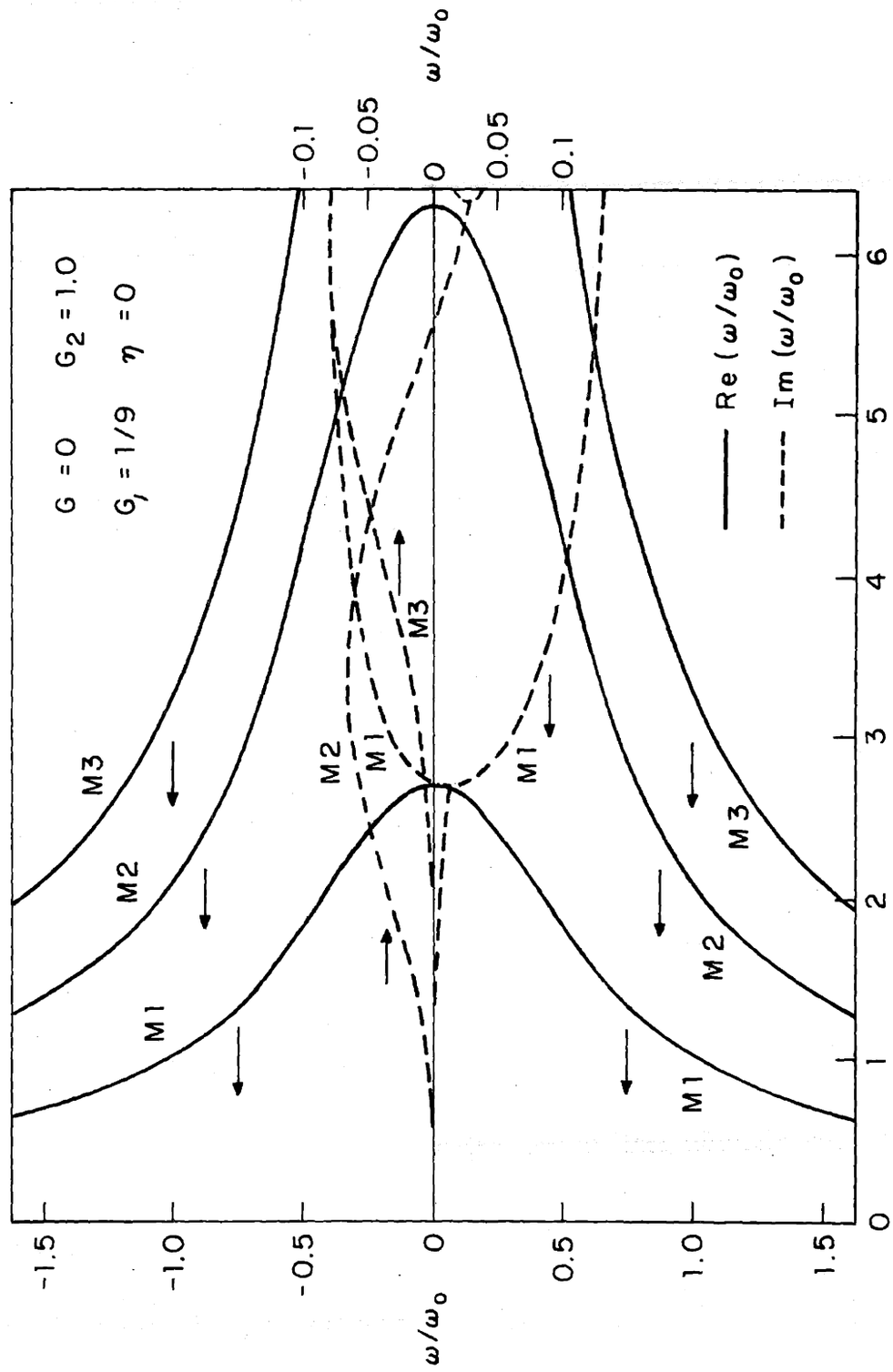

FIGURE 7.7 COMPLEX EIGENFREQUENCY VS. NORMALIZED LENGTH FOR THE DEGENERATE SURFACE WAVE KLYSTRON.

the flow velocity (or tension of the spring) is varied. A particular case of interest is the point where the flow velocity and spring tension velocity are equal. One might suspect that in these circumstances the spring and jet should couple strongly and expect instabilities to be large. The results are shown in Fig. 7.8. Comparing with Fig. 7.8, we observe first that the point of static instability has been shifted to higher $L\omega_o/V_o$ as one might expect if the spring is under increased tension. Secondly and more significantly, perhaps, is that the higher modes are damped until a large value of $L\omega_o/V_o$ is reached. It appears then that if the jet velocity is comparable to the spring tension velocity, it is difficult to produce instability. If one could achieve large $L\omega_o/V_o$ and somehow suppress the fundamental mode instability, then larger growth rates could be achieved.

7.5 Physical Description of Class IV Overstability

In the foregoing sections detailed eigenfrequency curves were presented for several cases and the results briefly discussed. One might wonder if there is a simply physical argument which might be given to explain the mechanism of overstability as there was for the case of counter-streaming jets. In fact, there is. The argument must be modified from that used for the counter-streaming jets, however, since the instability is dynamical in character.

Consider in the spring jet electric field coupled system that the spring is vibrating in its second natural mode of oscillation, with the displacement given by $\sin(\omega t + \frac{\pi}{8})\sin\frac{2\pi x}{L}$. To simplify the physical argument we shall consider a sampling of small pieces of fluid and investigate two effects: The traction exerted and the power delivered by the spring to the jet in the left half region, and the traction exerted and power delivered by the jet to the spring in the right half region. An essential ingredient in the analysis is that the power supplied by the spring to the jet in the left half region is more than offset by the power supplied by the jet to

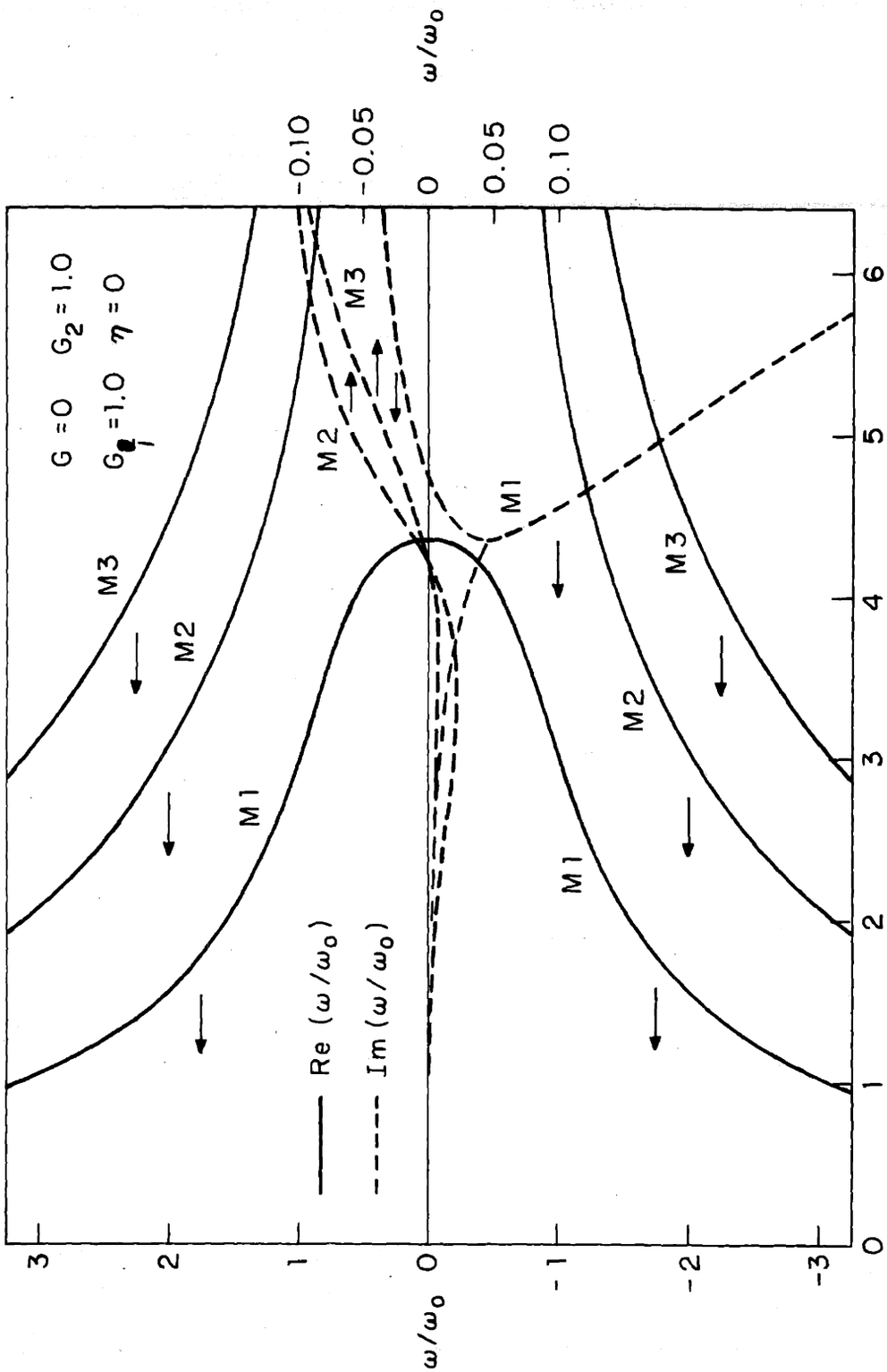

FIGURE 7 8 COMPLEX EIGENFREQUENCY VS NORMALIZED LENGTH FOR THE DEGENERATE SURFACE WAVE KLYSTRON: EFFECT OF PARAMETERS.

the spring in the right half region. The net power transfer must be from the jet to the spring since the spring is a passive element and cannot supply time average power. A second essential ingredient for oscillation is that even if the jet supplies net power to the spring, the mechanism must be present for the spring to feedback some of this power to the upstream section of the jet to sustain the oscillations. Otherwise we have an amplifier and not an oscillator. To simplify the discussion, surface tension on the jet will be ignored and the only force acting on the pieces of fluid to be studied are due to the mutual coupling.

It will be assumed for the convenience of the argument that the jet velocity is twice the wave velocity on the spring, or alternatively, the transit time of the jet is half the period of oscillation. It is necessary to consider only two elements of fluid, labeled elements A and B of the sketch below.

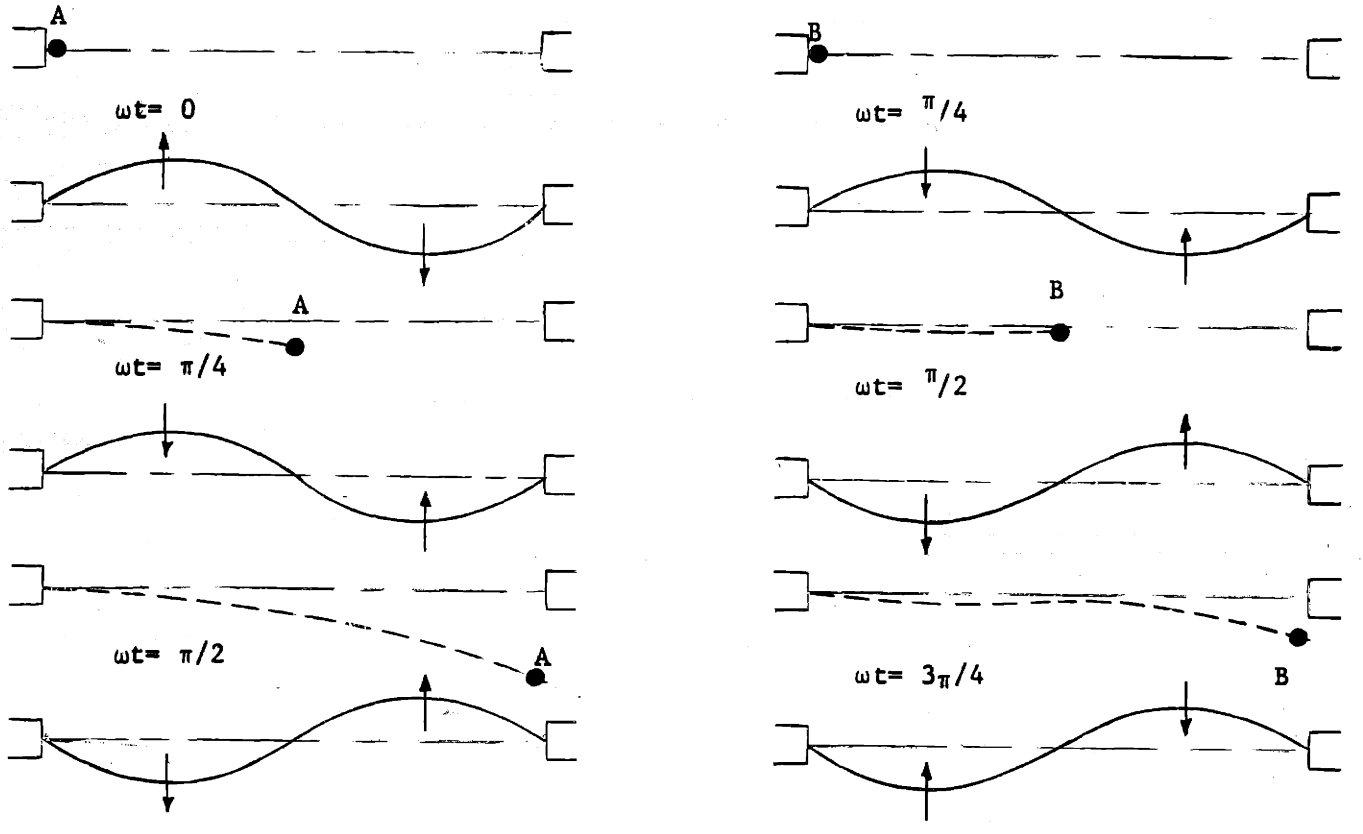

Element A enters the interaction region unexcited at $t = 0$ when the spring is about half amplitude. As time advances, the spring exerts a strong traction on A; as A travels to the right and the spring amplitude increases toward its peak value. At $\omega t = \frac{\pi}{8}$, the spring is at peak amplitude and A is directly opposite the peak, but now deflected downward slightly 1/4 the distance downstream from the nozzle. As ωt increases to $\frac{\pi}{4}$, the downward traction on A is still strong and A deflects even further due to the downward acceleration. The spring has exerted a large traction on A, but supplied only a modest amount of kinetic energy because of the small transverse jet velocity.

If we now focus our attention on the downstream half, the deflection of the spring is downward (at half amplitude) at $\omega t = \frac{\pi}{4}$, but is rising. The mutual coupling term provides an upward traction on the spring, but the important effect is the upward force exerted by the element on the spring during the entire time until it exits the interaction region. Further this upward force occurs when the spring is at near maximum velocity, so that the kinetic energy transferred is large, much larger than that delivered to the element by the spring during the 1st quarter cycle. This shows then that element A at least satisfies both requirements for overstability, having been excited by the spring during the 1st quarter cycle and delivering net kinetic energy to the spring. It is necessary, however, to show that other fluid elements do not degrade the overstable effect of element A.

Consider element B which enters the interaction region at $\omega t = \frac{\pi}{4}$. The left half of the spring is at half amplitude and traveling downward. At $\omega t = \frac{3\pi}{8}$, the spring is at the equilibrium and exerts no traction on the fluid element. The net deflection of B at $\omega t = \frac{3\pi}{8}$ is slightly downward during the next $\frac{\pi}{8}$ interval, the mutual traction is upward and essentially restores B to the equilibrium position. The net effect is that B arrives at the midplane virtually unexcited. Between

$\frac{\pi}{2} < \omega t < \frac{5\pi}{8}$ the traction exerted on the spring by the jet is very weak. The spring on the other hand exerts a strong downward force on the jet although there is little power transfer. Finally, for $\frac{5\pi}{8} < \omega t < \frac{3\pi}{4}$, the jet is now moving downward, as is the spring and the spring transfers some kinetic energy back to the jet. The net result of element B is that the spring loses a modest amount of energy to the jet.

If we consider another entering element at $\omega t = \frac{\pi}{2}$, the situation is symmetrical to that for fluid element B, with the jet and spring rotated 180^{o} about its axis. The result is the same as for fluid element B, large amounts of kinetic energy are transfered from the jet to the spring. For elements which enter midway between elements A and B, say, or B and C, there is a modest power gain by the spring. If we make a qualitative sketch of kinetic energy versus entrance time for fluid elements, the results would look like that shown below.

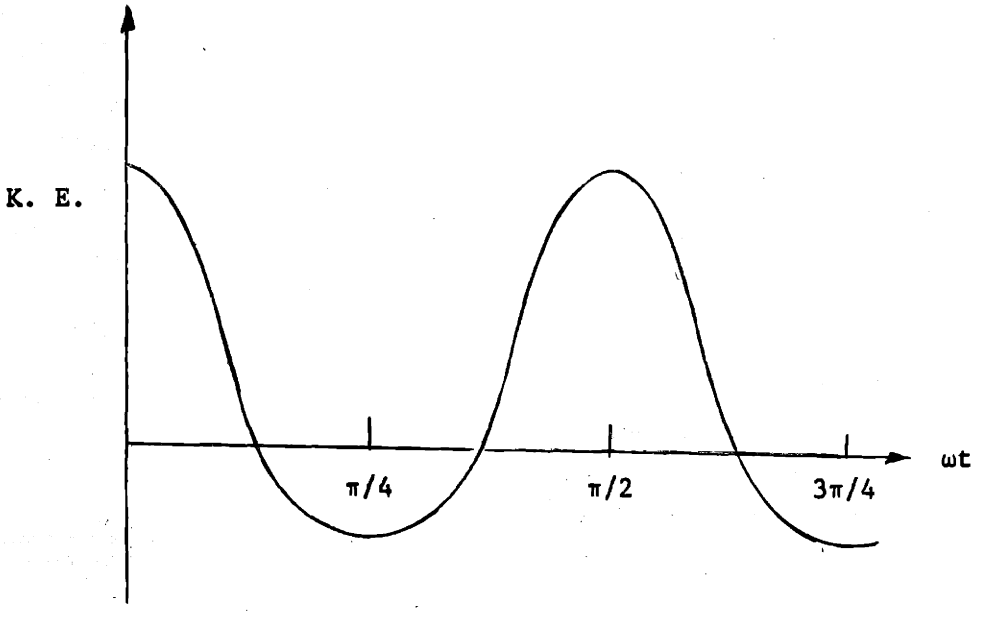

Time average power is then transferred from the jet to the spring.

If the same argument is used for the case $V_o = V_t$, it is concluded that there is little or no power transferred, and for $V_o < V_t$, the spring delivers power to the jet. Since the spring is a passive element, the conclusion is that the mode is damped. The argument may be extended to the third or higher modes without conceptual difficulty, although the details become involved.

In all of the modes higher than the first, the mechanism for instability depended on the spring exciting the jet upstream and the jet in turn transferring net power back to the spring. The fundamental mode is peculiar, however, since each point on the spring has essentially the same phase, and no feedback mechanism is available.

The Extended Region Klystron : As a final example which may be of some interest, consider an electron beam streaming through a microwave cavity. This may be modeled as a special case of the magnetically coupled spring-jet system, in the same way that the counter-streaming electron beam case could be considered. Such a device is called a klystron for short length, or an extended region klystron if the device is long. In any case it is a simple matter to compute the complex eigenfrequencies as a function of length, as shown in Fig. 7.9. The eigenfrequency curves are very similar to Fig. 7.5 for the magnetically coupled surface wave case. The characteristic fundamental mode damping and higher mode overstability is evident. These latter modes also exhibit peak growth rates as in the magnetically coupled case.

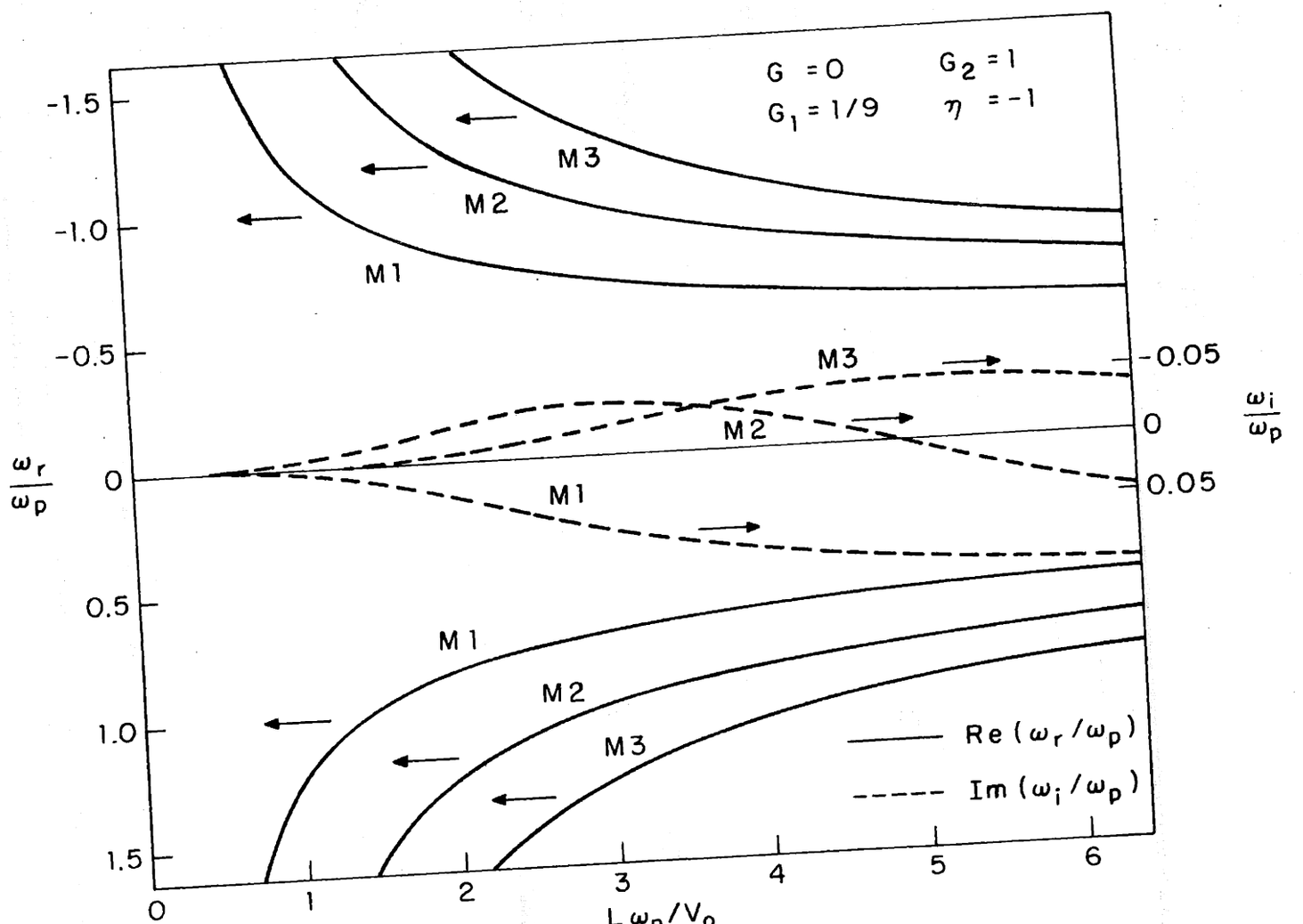

FIGURE 7.9 COMPLEX EIGENFREQUENCY VS NORMALIZED LENGTH FOR AN ELECTRON BEAM EXTENDED REGION KLYSTRON.

CHAPTER 8

SPRING JET EXPERIMENT

8.1 Introduction

In the previous chapter the theoretical framework for a membrame interacting with a supercapillary jet was established. The results of Chapter 3 suggested that, for the electric field coupled system of infinite length, both convective and non-convective instabilities exist. The appearance of longitudinal boundaries had the effect of shifting the imaginary part of the eigenfrequency so that the fundamental mode decayed in time while the 2nd mode became overstable. We would like to find out whether in fact it is experimentally possible to produce unstable oscillations at electric fields below the critical field for the static fundamental mode instability.

8.2 Experimental Description

As mentioned in the discussion of the two spring experiment, the stationary jet model is physically realized by a spring under small tension. The same apparatus was used as in earlier experiments, the deformable elements here are a spring and a jet, supported in the horizontal plane to minimize gravitational effects, which would produce a non-uniform jet velocity and a non-uniform spring tension. This presents a difficulty since a jet is concave downward, a spring concave upward. It was found that the vertical separation was too great for a planar model to be valid. To correct this, the spring was supported by fine insulating strings at a sufficient number of stations to give the spring the same curvature as the jet. The external plates also had the same curvature. The spacing of the strings was also kept small compared to wavelengths of interest (the shortest wavelength is the fourth mode of the spring, 44 cm.) so that the effect of the support strings could be modeled by a continuum of pendulums. For convenience the jet was electrically grounded, the spring then was allowed to be at high voltage.

To detect the existance of absolute instabilities, the d.c. voltage is increased from zero until either an instability or electrical breakdown occurs. At low voltages, the spring and jet are effectively uncoupled, disturbances on the spring appear as standing wave oscillations which very slowly decay in time, while jet disturbances appear as pulses traveling downstream at about the jet velocity. As the voltage is increased, the spring and jet begin to couple. The oscillation frequencies of the spring are not affected significantly by the presence of the electric field; the damping, however, is significantly altered. The fundamental mode decays more rapidly while higher modes decay more slowly. Disturbances on the jet exhibit spatial growth for longer waves (characteristic of a single jet interacting with rigid plates).

As the voltage is increased further, a critical electric field is reached when the spring-jet system spontaneously breaks into oscillation and the amplitudes increase slowly with time, building up to such an amplitude that the spring and jet collide, terminating the experiment. The trajectory of the spring is unmistakably the third mode. The jet, however, exhibits a traveling wave behavior with an exponential envelope which grows in time at the same rate as the spring. The critical voltage is reproducible. If this voltage is exceeded by a modest amount, the temporal growth rate is increased, but the spatial character of the system is unchanged. Further increase of the voltage results in other modes becoming unstable, first the 4th mode, then others. The spring-jet system is now tightly coupled, the unstable modes grow, beating against each other, until non-linear effects couple the modes and can even tend to limit the amplitude. This last effect is not understood.

8.3 Results

The frequency of the third mode of instability is 7.1 cps, which is a bit high for visual observation of the phase relationships between the spring and jet. The

physical arrangement of the experiment makes taking photographs quite difficult. As a result, a second apparatus was constructed (simplier in design) and the spring, jet, and plates mounted in a vertical plane to eliminate the curvature difficulties explained earlier. The transverse spacing was increased and the longitudinal dimension shortened. Because of the large transverse spacing, the instability voltage is correspondingly increased and it was necessary to perform the experiment in an atmosphere of Freon or sulfurhexafluoride to prevent corona and breakdown. As the voltage is raised to the critical point, the system becomes unstable as before, but now the first unstable mode is the second mode as shown in Fig. 8.1. This photograph was taken with a shutter speed adjusted to the period of oscillation to show the amplitude envelope.

High speed motion pictures† were taken to observe the phase relationships of the spring and jet during an oscillation and to observe the oscillation buildup. A sequence of four frames one sixth of a cycle apart in time are shown in Fig. 8.2a. The second natural mode of the spring and the convective instability character of the jet at the same frequency as the spring are apparent. The relationship of the jet deformation to that of the spring lends support to the physical arguments of the previous chapter concerning the mechanism for overstability.

To the best of the author's knowledge, this is the first stream-structure device which couples a convecting fluid exhibiting amplifying waves in the uncoupled state to a passive propagating structure to produce overstabilities. The complex eigenfrequencies were computed for the experimental conditions and for the time sequence shown in Fig. 8.2a. The theoretical eigenfunctions provide an excellent picture of the dynamics, as can be seen by a comparison with the photographs. The non-linear

---

†These motion pictures were taken by Educational Services, Inc., Watertown, Mass., for use in the film "Electromechanical Waves and Instabilities", sponsored by the National Science Foundation under the supervision of the National Committee on Electrical Engineering Films.

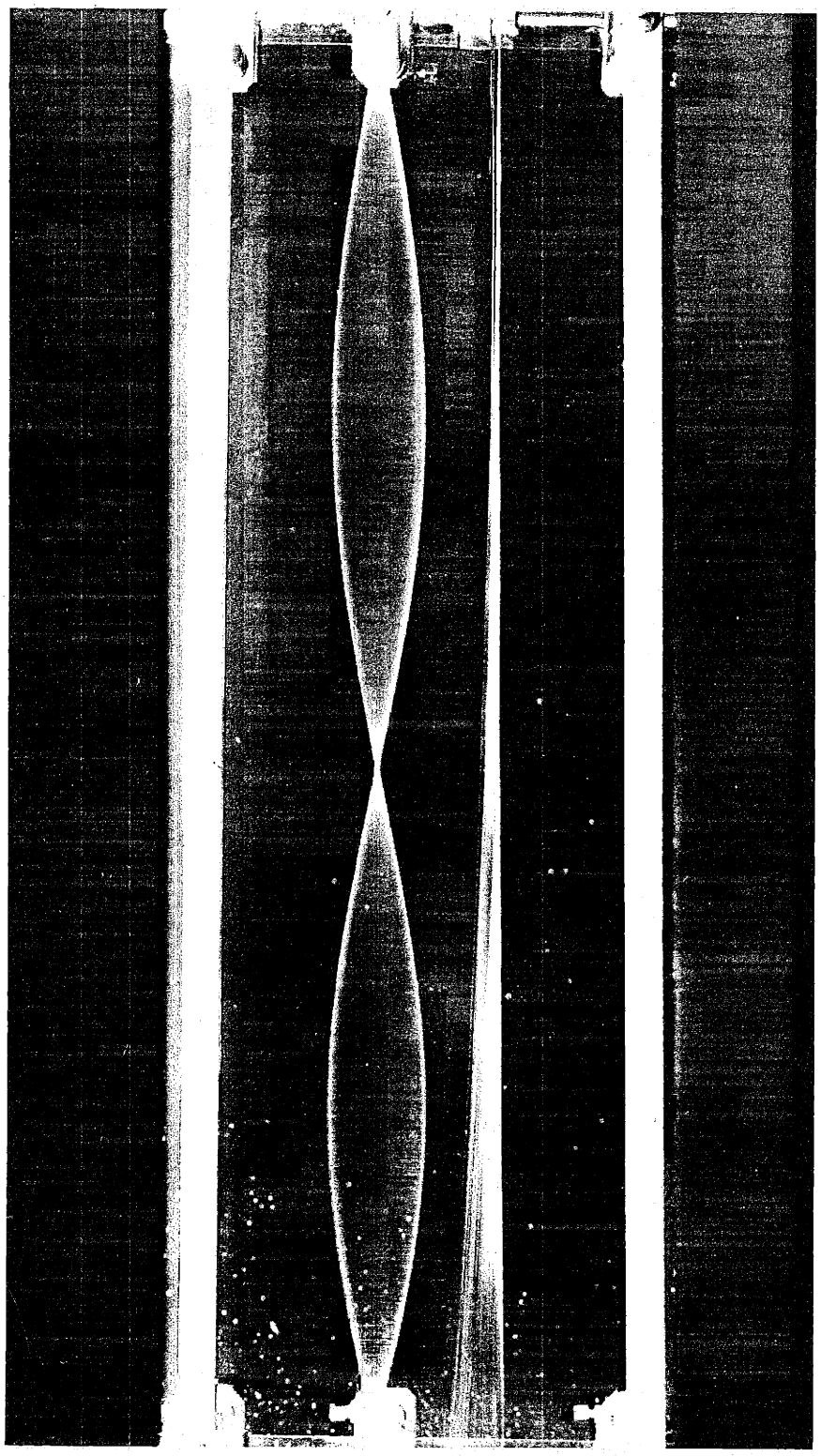

FIGURE 8.1 TIME EXPOSURE FOR ONE PERIOD OF OSCILLATION DURING BUILDUP OF ELECTRIC FIELD COUPLED STREAMING OVER-STABILITY. SPRING (LEFT) AND JET (RIGHT) ARE RESONATING AT THE SECOND EIGENFREQUENCY.

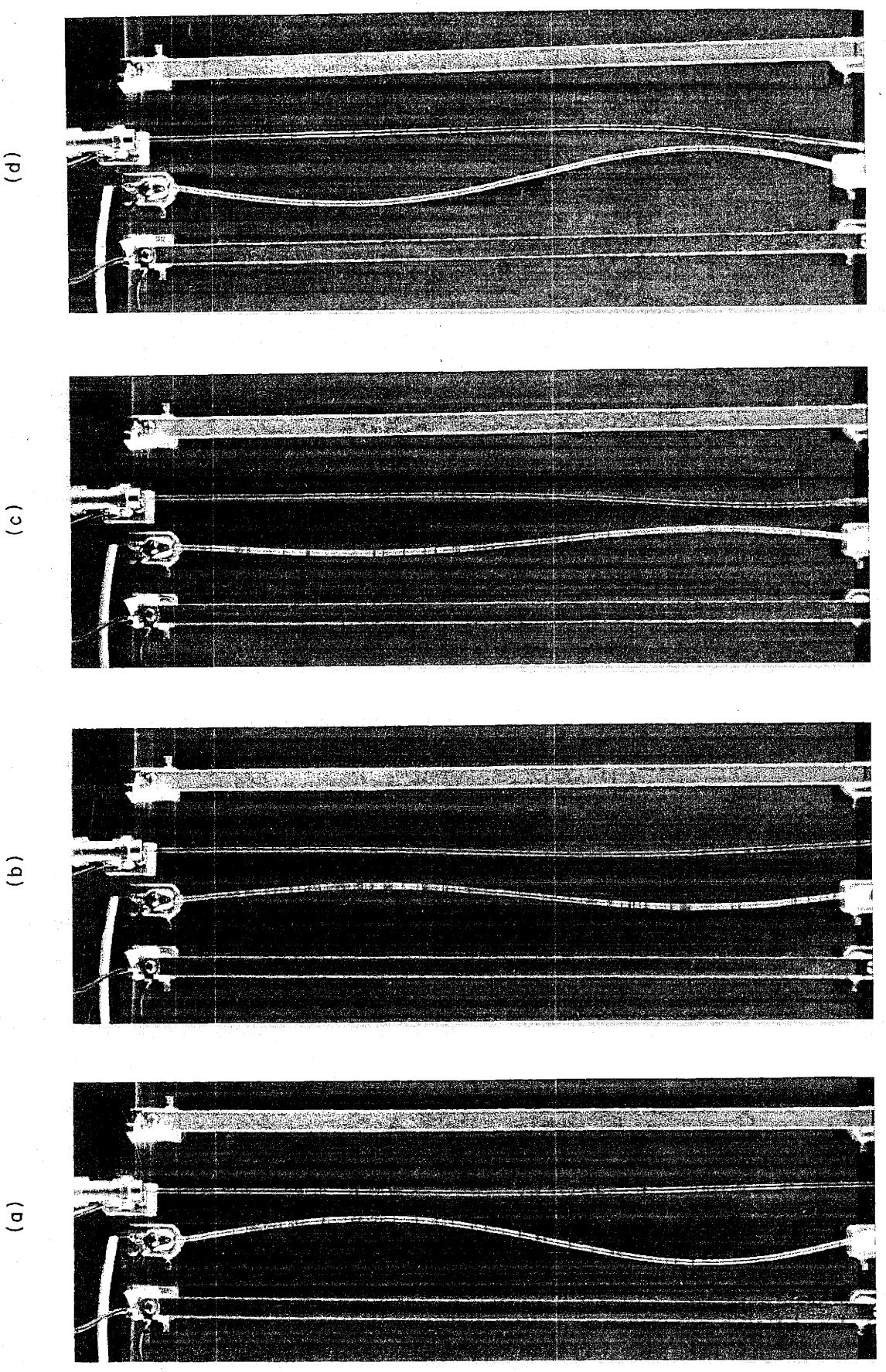

FIGURE 8.2a HIGH SPEED PHOTOGRAPHS OF A KELVIN-HELMHOLTZ OR STREAMING OVERSTABILITY

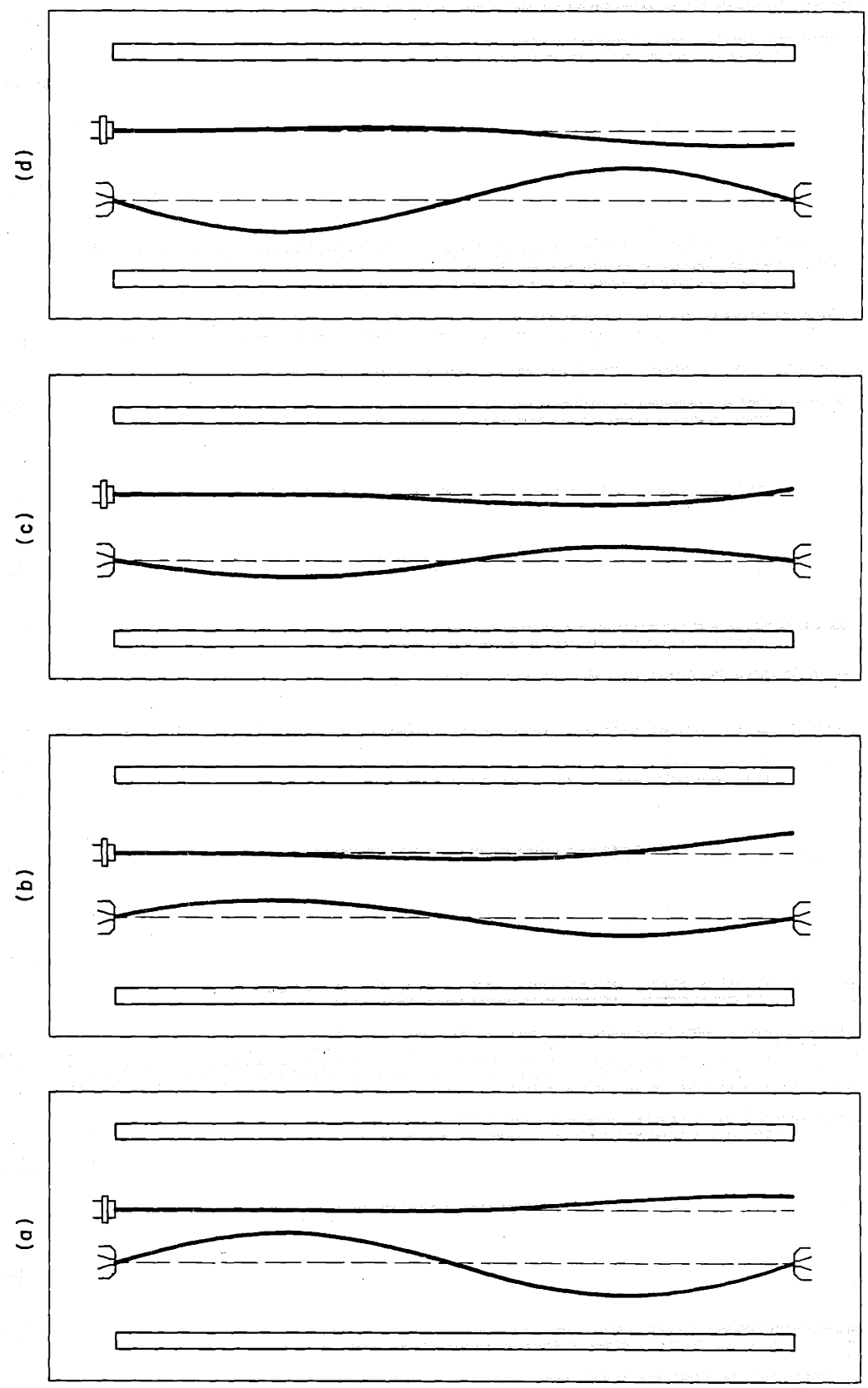

FIGURE 8.2b THEORETICAL EIGENFUNCTIONS FOR EXPERIMENTAL CONDITIONS OF FIGURE 8.2a

displacement of the jet is evident in (d) of Fig. 8.2a, and exhibits the same behavior as the single jet nonlinear transient.

The complex eigenfrequencies using the experimental parameters are shown in Fig. 8.3a and b. According to theory, the fundamental mode should be increasingly damped until a critical $L\omega e/V_o$ is reached and static instability sets in. All of the higher modes computed are overstable, however, even for the lowest values of $L\omega e/V_o$. From Fig. 8.3a the second and third mode eigenfrequency curves lose their spring-like character for large $L\omega e/V_o$. As can be seen, the growth rates for the higher modes, particularly the second mode can be quite large. If a means were available to suppress the fundamental mode (perhaps by constraining the midpoint of the spring), large growth rates are possible at low frequency. Such a device could be of practical use.

In order to determine the dynamics of the system quantitatively, the first four complex resonant frequencies were measured as a function of applied voltage. The real part of the frequency was measured by applying a small alternating voltage to the previously grounded plate adjacent to the spring and the frequency for maximum amplitude displacement was determined. This voltage was then removed and the subsequent decay transient recorded. The decay constants were obtained from a semilog plot of the envelope measurements for the recordings, and are plotted in Fig. 8.4 a to d for the first four modes. The theoretical growth and decay rates from Fig. 8.3b are shown as the curves marked SJP. The trend of the results appears to be correct although the quantitative disagreement is much too large to be explained by experimental error of the measurements. As can be observed the scatter of the data is quite small except for mode 4. The difficulty in obtaining good results here lies in the competing effects of mode 3 which modulates the envelope. Attempts to suppress or impede the third mode were unsuccessful since in so doing the 4th mode decay was also disturbed.

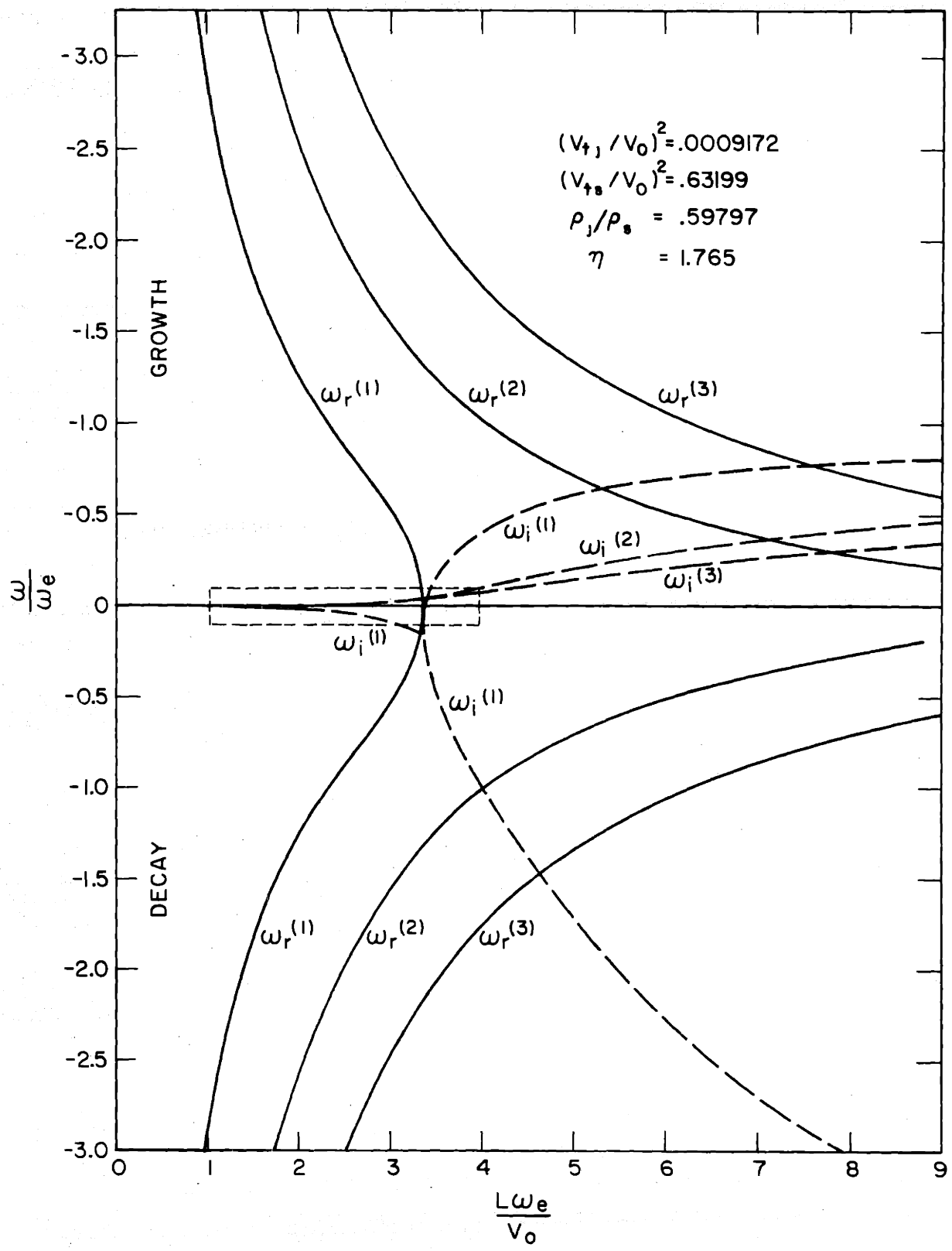

FIGURE 8.3a COMPLEX EIGENFREQUENCY VS. NORMALIZED LENGTH FOR EXPERIMENTAL CONDITIONS SHOWING THE THREE LOWEST MODES. SEE FIGURE 8.3b FOR AN EXPANDED VIEW OF THE ENCLOSED RECTANGLE.

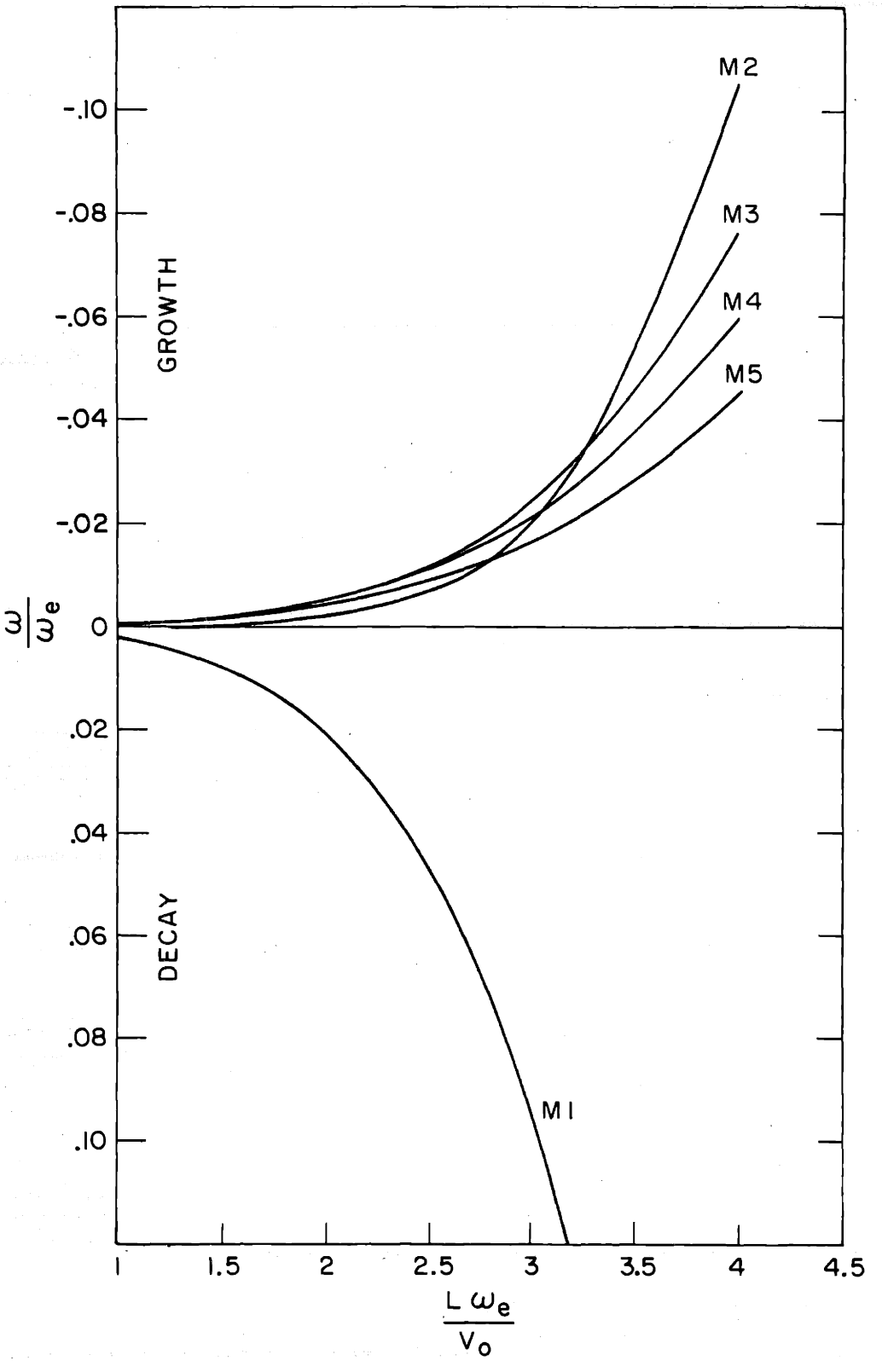

FIGURE 8.3b GROWTH AND DECAY RATES OF FIGURE 8.3a FOR THE LOWEST FIVE MODES.

The agreement of the SJP curves with experiment is quite good if an allowance is made for a zero voltage shift. The solid unmarked lines in Fig. 8.4 are the SJP curves shifted down an amount equal to the zero voltage shift for each mode. This means there must exist another mechanism which has a strong effect on damping rate; this matter will be discussed in Sec. 8.5.

8.4 The Pendulum Effect

Before discussing this discrepancy, let us consider the real part of the eigenfrequencies. The theoretical values of the real part of the resonant frequencies at zero voltage should be exact multiples of the fundamental if we ignore the effect of the support strings on the springs. This, however, was not observed, as seen in Fig. 8.5 (recall that resonant frequency measurements are accurate to ± .01 cps, so that the deviation from a straight line in Fig. 8.5 is significant).

Let us postulate then, as in Chapter 4, that in addition to the spring behaving as a vibrating string, it also experiences a continuum gravitational restoring force through the support strings holding the spring. The restoring force on a section of spring of unit length is simply given by $-\rho\pi r^2 g/\ell$. The dispersion relation derived in Chapter 4 for two springs, simply becomes

$$\omega^2 - V_t^2 k^2 + \omega_e^2 - \frac{\pi r^2 g}{\ell} = 0 \qquad (8.1)$$

Since the ends of the spring are fixed, $k = \frac{n\pi}{\ell}$ and the functional dependence of the frequency on mode number becomes

$$f^2 = an^2 + b \qquad (8.2)$$

The parameters a and b were calculated from the data and (8.2) drawn as the solid curve of Fig. 8.5. The data is predicted quite well by an equation of the form of (8.2).

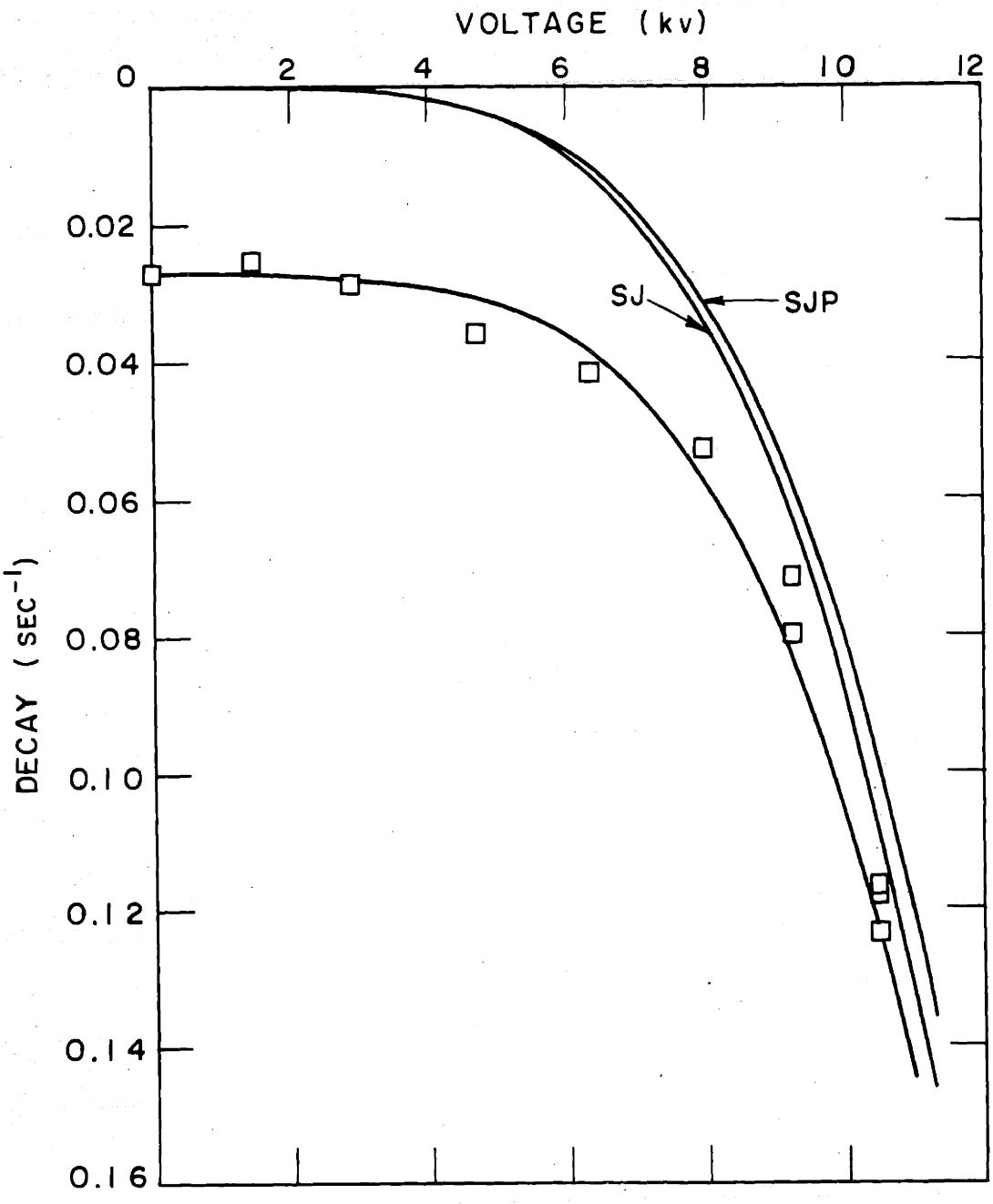

FIGURE 8.4a. DECAY VS. VOLTAGE, MODE #1

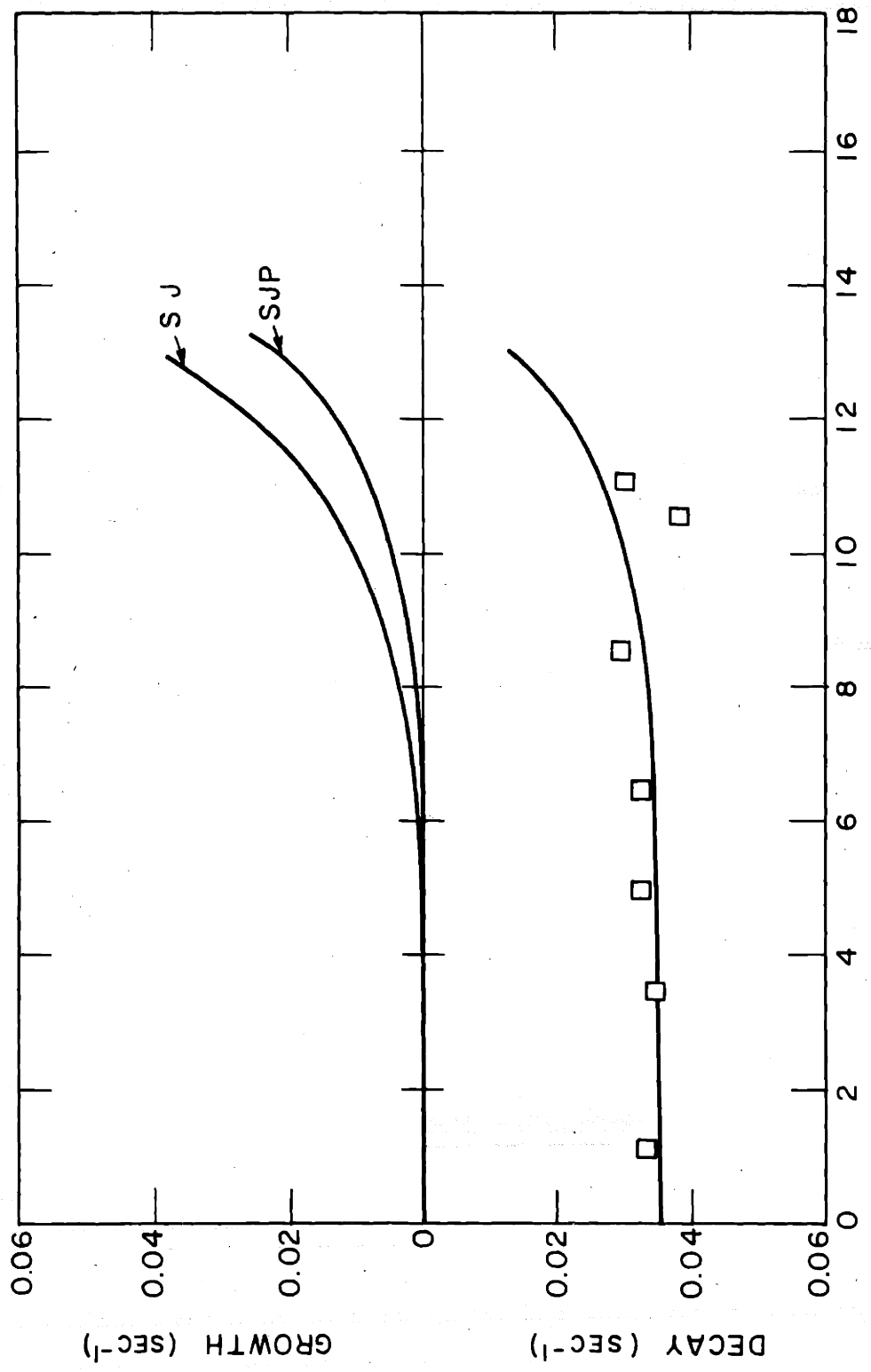

FIGURE 8.4b DECAY VS VOLTAGE, MODE #2

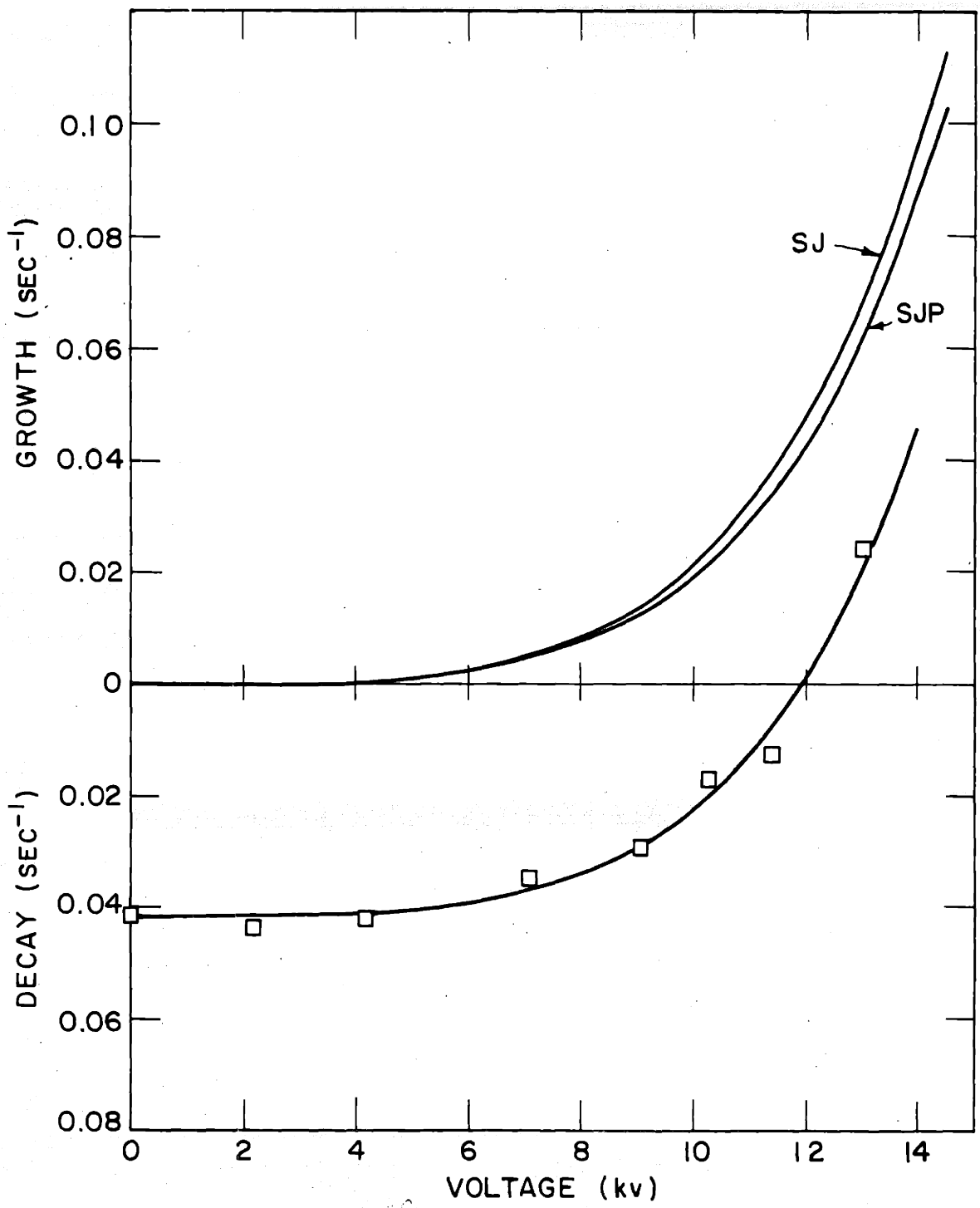

FIGURE 8.4c DECAY VS VOLTAGE, MODE #3

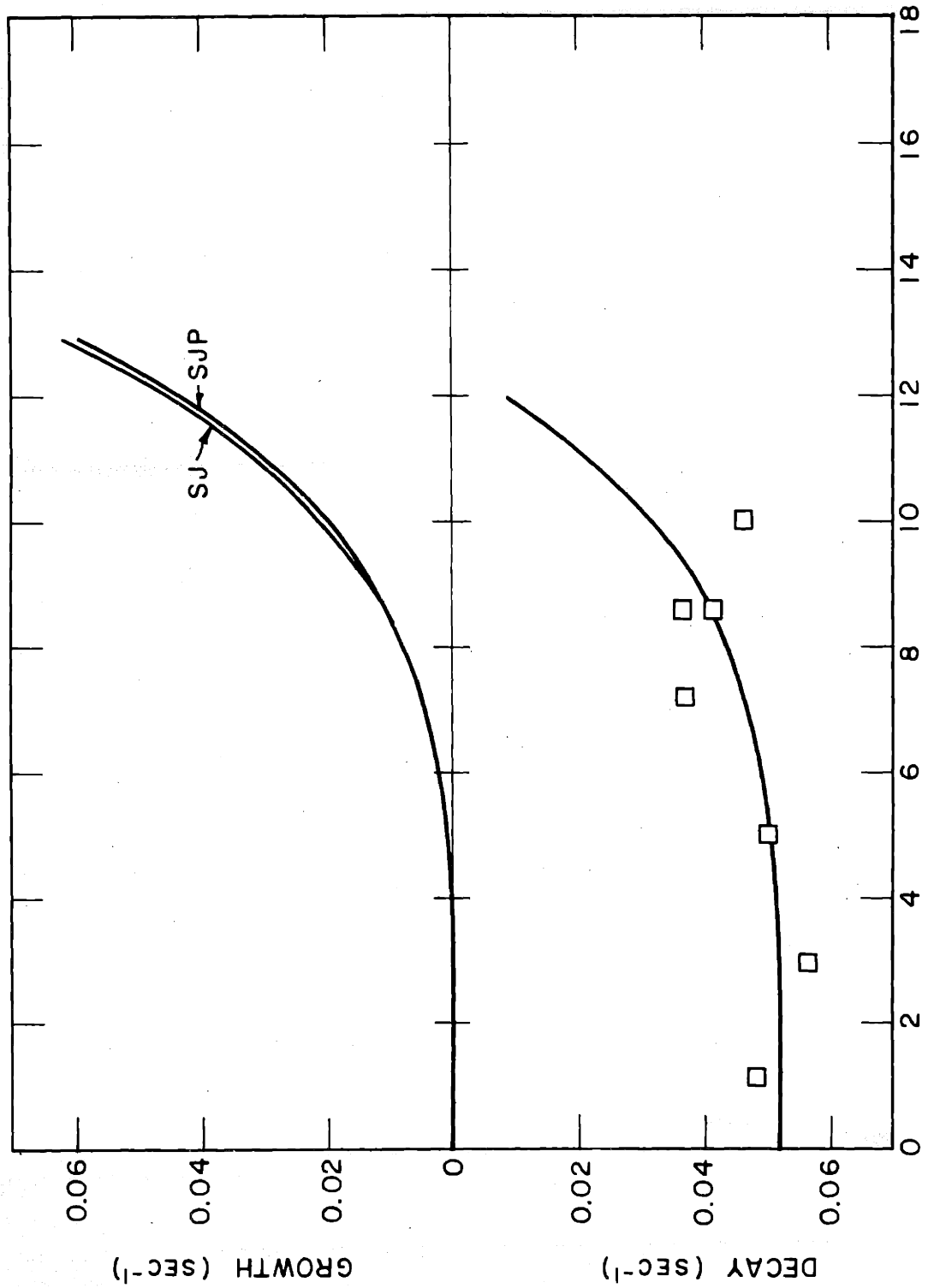

FIGURE 8.4d DECAY VS. VOLTAGE, MODE #4

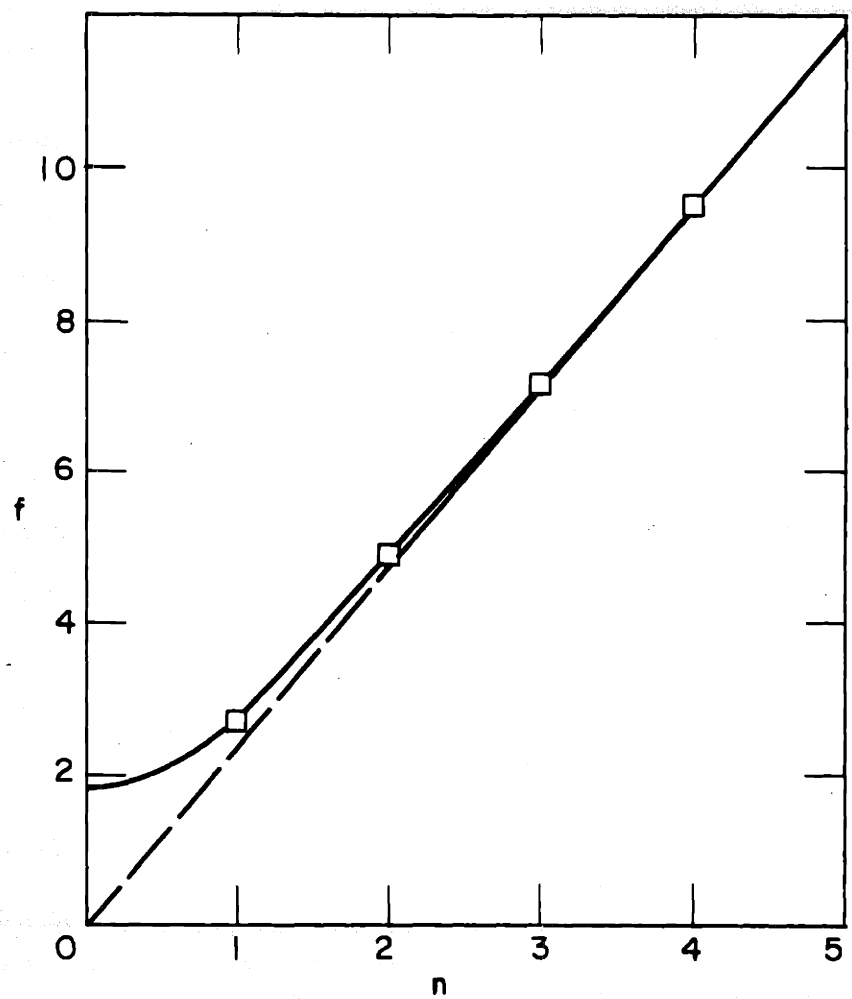

FIGURE 8.5 FREQUENCY VS MODE NUMBER
FOR ZERO VOLTAGE

To determine the effect of the support strings on the growth and decay rates, the complex eigenfrequencies were recomputed with the pendulum term omitted; the results are the curves marked SJ in Fig. 8.4a to d. The pendulum term has little effect at low voltages, but as the voltage is raised its effect becomes more pronounced, especially for the lower modes. The effect of adding the support strings is to shift the system toward a position of neutral equilibrium for all the modes considered. This appears intuitively reasonable since the natural frequency of the pendulum is considerably smaller than the lowest mode of the system and would interfere with all the eigenfrequencies.

8.5 Losses

Let us now return to the question of loss mechanisms mentioned previously to explain the disparity between theory and experiment in the decay and growth rates. If the zero voltage shift is plotted versus the real part of the resonant frequency, as in Fig. 8.6, the damping mechanism is seen to be a linear function of frequency, and from the agreement between theory and experiment, is not a function of voltage.

8.5.1 Air drag

There are several possible mechanisms for mechanical damping; one which appears likely and is amenable to calculation is air drag. Suppose the oscillatory motion of the spring is modeled by a stationary cylindrical rod in a uniform velocity (V_o) air stream moving at 1/2 the maximum transverse velocity of the spring.[†] If the Reynolds number of the flow is sufficiently low, then the drag coefficient is quite closely given by:[††]

[†]The factor of 2 is included here for space and time averaging. For the Reynolds numbers of interest, the drag force is nearly proportional to V_o^2.

[††]Rouse, Elementary Mechanics of Fluids, Wiley and Sons, p. 247.

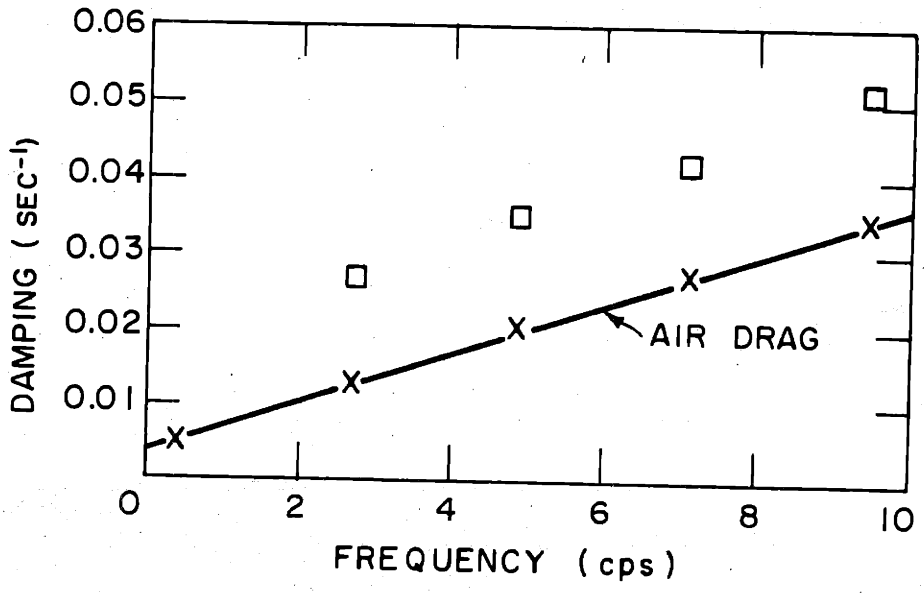

FIGURE 8.6 DAMPING AT ZERO VOLTAGE

$$C_D \approx C/R_e \qquad R_e = \text{Reynolds number} = \frac{\rho V_o 2r}{\mu}$$

C = constant

A = projected area = $2r\ell$

μ = viscosity

where the drag force $F_D = C_D A \rho V_o^2/2$

Under these conditions, the drag force is proportional to velocity. The equation of motion for a spring with air drag may then be written:

$$\rho \pi r^2 \frac{\partial^2 \xi}{\partial t^2} = T \frac{\partial^2 \xi}{\partial x^2} - \rho \pi r^2 g/_\ell \xi - \gamma \frac{\partial \xi}{\partial t}$$

where γ is the damping constant in newt.-sec/m^2

The resonant frequencies are given by:

$$\omega = \frac{j\gamma}{2\rho\pi r^2} \pm \sqrt{\left(\frac{\gamma}{2\rho\pi r^2}\right)^2 + \frac{T}{\rho\pi r^2}\left(\frac{n\pi}{\ell}\right)^2 + g/_\ell}$$

For small damping,

$$\omega_i \approx \frac{\gamma}{2\rho\pi r^2} = \frac{\gamma}{2\lambda} \qquad \lambda = \text{mass}/_{\text{length}} \text{ of spring}$$

The drag force in terms of flow quantities is:

$$F_D = \frac{C\mu}{2rV_o\rho_{air}} \, 2r\ell \, \rho_{air} \frac{V_o^2}{2}$$

so that

$$\omega_i = \frac{C\mu}{4\lambda}$$

We see that under the assumed conditions the mechanical decay constant is independent of frequency. However, the empirical data of Rouse indicates that, for

the Reynolds numbers of the experiment ($O(10^2)$), C is in reality C = C(Re). Using the values of C_D tabulated corresponding to the four measured modes, the damping constants are computed as shown in Fig. 8.6. Air drag, then appears to be the predominant mechanical loss mechanism. The slope of the curve of Fig. 8.7 is characteristic of drag force nearly proportional to the square of the velocity.

8.6 Other Results

Before concluding the chapter, it is worthwhile to point out the results of two recent experiments by Herba[22] using the same apparatus previously described. The first was the measurement of growth and decay rates with the spring tension increased to $V_{ts}/V_o \gtrsim 1$. The effect of this increased tension was to suppress the second and third mode instability and require a considerably larger voltage to produce the fourth and fifth mode overstabilities. Theoretical calculations using his experimentally measured parameters showed no overstabilities for the range of voltages considered, but a numerical sensitivity test of the parameters indicated that in the neighborhood of unity the parameter V_{ts}/V_o had a strong effect on growth and decay rate. A reduction was made in this parameter (but within the experimental error of the measurement) and the observed overstabilities were predicted. This lends support to the physical arguments of the previous chapter concerning the dependence of overstability on V_{ts}/V_o.

The second experiment consisted in driving the jet in the sinusoidal steady state at a voltage below the start oscillation point. The measurements were made on the fundamental mode. For fixed voltage and fixed amplitude of excitation, the frequency of excitation was varied through the resonant frequency and the displacements of the spring and jet recorded. The jet amplitude remained constant except in a small band near the resonant frequency when the amplitude dropped to a minimum at the resonant frequency. The spring amplitude was small and relatively

constant except near the resonant frequency when the amplitude rose sharply. The relative phase between the jet and spring changed very rapidly by 180^{o} as the frequency was increased through the resonant frequency. The frequency band for phase reversal was smaller than the amplitude bandwidth. This behavior is common in lumped parameter circuits.

The second mode was also investigated, but the Q of the system was so high that the structure of the resonance could not be measured. A conclusion is inescapable, however. The amplitude of both the spring and jet increased markedly at resonance, in contrast to the fundamental mode. The explanation is proposed that the second mode is actually overstable but is limited to very small amplitude by the mechanical loss mechanisms, notably air drag. Since this is a nonlinear process, the effect of driving the unstable mode would be for the system to settle to a new operating point with a larger amplitude for both jet and spring.

CHAPTER 9

CONCLUSION AND SUGGESTIONS

This work has been devoted to the intensive study of two fluid streams in relative motion, coupled by an electric or magnetic field. The author has not pursued the usual procedure of ignoring end effects and only examining the stability of the eigenmodes produced by the imposition of boundaries transverse to the direction of flow, by means of the dispersion relation. Such a procedure is valid provided the wavelengths of importance are short compared to the length of the device. Often, however, the stability is determined more by the long waves than the higher order transverse modes, and end conditions become of primary concern. This has been true in all of the cases investigated. The various flow regimes have been have been examined with careful attention to the effects of longitudinal boundaries. Experiments have been performed which verify this procedure, so that a complete picture of the system dynamics is possible.

In addition to this work expanding the area of knowledge of two-stream electromechanical surface waves, the results shed light on the nature of two-stream interactions generally. An important advantage of the problems studied here is that the models are free of the difficulties usually encountered in other areas.

This work is by no means complete; quite the contrary, it serves as an introduction to the general problem of the effects of longitudinal boundary conditions which are consistent with causality. For example, the problem of two-stream sausage modes, while practically perhaps not as interesting as the kink modes, has yet to be formulated.

There are several suggestions which the author would like to propose concerning future research. The question of whether stream-structure interactions,such as described in Chapters 7 and 8, could be put to practical use is intriguing. Possible uses might be energy conversion from flowing fluid energy to electrical power, or as devices such as low frequency oscillators and amplifiers.

The problem of continuum feedback control is just now receiving attention. Work by Melcher[35,36] and Crowley[12] has been concerned with the control of a liquid interface and a fluid jet by means of field coupling. The implications of continuum feedback control are immense; one such application is the control of thermonuclear machines. Since many instabilities observed in plasmas are Kelvin-Helmholtz in character, the electromechanical models described here provide an excellent medium for studying the processes of continuum feedback control.

It was shown briefly that analogies exist between field coupled surface waves and electron beams. Electron beam devices have reached a fairly degree of sophistication, but are not well understood analytically in the sense described here. It appears that both of the areas would benefit if the analogies were exploited.

In chapter 2 the nonlinear transient problem for a single jet was investigated. Experiments have not been done to correlate the theory, and no work has been done to consider the non-long-wave case. The nonlinear dynamics of the spring-jet experiments are apparant from observations of the large amplitude motions of a single mode, the eigenmode mixing observed between two unstable modes, and the nonlinear damping. This needs further study.

The large area of electromechanical stream-structure interactions is virtually unexplored. The only structure studied here was a spring fixed at the ends. Simply changing the terminations can have a large effect on the system dynamics. When one imagines the number of both continuum and lumped parameter elements which can be used as a structure, the list is large indeed. If more than one stream is considered, the use of structures as space filters provides yet more interesting configurations.

As a final suggestion, it might be remarked that the equilibrium field for all cases studied was constant. The effect of using a low frequency electric field coupling to produce parametric oscillations is now under study by Devitt. The problem of an alternating field on a single fluid jet has not been studied, and the application to two streams appears exciting indeed.

REFERENCES

1. Allis, W.P., Buchsbaum, S.J., and Bers, A. Waves in Anisotropic Plasmas, The M.I.T. Press, Cambridge, Mass., 1963.

2. Akao, Y. and Ida, Y. "Resonance of Surface Waves on a Cylindrical Plasma Column", J.A.P. 34, 7, 2119 (1963).

3. Alterman, F., Phys. Fluids 4, 1207 (1961).

4. Barnes, C.W., "Conservative Coupling between Modes of Propagation - A Tabular Summary", Proc. I.E.E.E., January, 1964.

5. Basset, A.B., "Waves and Jets in a Viscous Liquid", J. of Math. 16, 93 (1894).

6. Bers, A. and Briggs, R. "Criteria for Determining Absolute Instabilities and Distinguishing between Amplifying and Evanescent Waves", QPR No. 71, RLE, M.I.T., October 16, 1963, pp. 122-130.

7. D.L. Bobroff, "The Buildup of Oscillations in an Electron Beam Backward-Wave Oscillator", I.E.E.E. Transactions on Electron Devices, June, 1965, p. 307.

8. Bohm, D. and Gross, E.P., Theory of Plasma Oscillations, Phys. Rev., 75, 1851 and 1864 (1949).

9. Briggs, R., Electron Stream Interactions with Plasmas, The M.I.T. Press, 1964 Chapter 2.

10. Chandrasekhar, S., Hydrodynamic and Hydromagnetic Stability, Oxford at the Clarendon Press, 1961.

11. Courant, R. and Friedrichs, K., Supersonic Flow and Shock Waves, Vol. 1, Interscience Publishers, 1948.

12. Crowley, J.M., "Feedback Control of a Convective Instability", Ph.D Thesis M.I.T., May, 1965.

13. Crowley, J.M., "Excitation and Growth Rate of EHD Instabilities", S.M. Thesis, E.E. Department, M.I.T., August, 1963.

14. Devitt, E.B., "Surface Coupled Electromechanics in Time Varying Fields", February, 1966, M.I.T.

15. Devitt, E.B. and Melcher, J.R., "Surface Electrohydrodynamics with High Frequency Fields", Phys. Fluids, Vol. 8, No. 6, p. 1193, June, 1965.

16. Fejer, J.A., "Hydromagnetic Stability at a Fluid Velocity Discontinuity between Compressible Fluids", Phys. Fluids 7, 499 (1964).

17. Fox, L., Numerical Solution of Ordinary and Partial Differential Equations, Pergamon Press, 1962.

18. Friedberg, J.P., "Nonlinear Effects in the Two-Stream Instability", Phys. Fluids, Vol. 8, No. 6, p. 1031, June, 1965.

19. Frieman, Goldberger, Watson, Weinberg, "Two Stream Instability in Finite Beams", Phys. Fluids 5, 196 (1962).

20. Gerwin, R. and Nelson, D.J., "Two Stream Instability in a Finite Length" Boeing Scientific Research Lab., Plasma Physics, March, 1964.

21. Harleman, D.R.F., Handbook of Fluid Dynamics, Chapter 26 on "Stratified Flow", McGraw-Hill, (1961).

22. Herba, F., "Experimental Study of Electromechanical Two Stream Instabilities", S.B. Thesis, E.E. Department, M.I.T., 1965.

23. Ippen, A.T. and Harleman, D., "Steady-State Characteristics of Subsurface Flow", Gravity Waves (Symposium), NBS Cir. 521, November, 1952, p. 79.

24. Johnson, H.R., "Backward-Wave Oscillators", Proc. IRE, 43, 684-697, June, 1955.

25. Keulegan, G.H., "Interfacial Instability and Mixing in Stratified Flows", Natl. Bur. Standards, J. Research 43, 487, (1949).

26. Keulegan, G.H., Natl. Bur. Standards, J. Research 32, 303, (1944).

27. Kofoid, M.J., "Experimental Two Beam Excitation of Plasma Oscillations", Boeing Scientific Research Lab., December, 1961.

28. Lofquist, K., "Flow and Stress near an Interface between Stratified Liquids", Phys. Fluids 3, 158, (1960).

29. Lamb, H., Hydrodynamics, Dover Publications, 1945.

30. Louisell, W.H., Coupled Mode and Parametric Electronics, John Wiley and Sons, 1960.

31. Lucken, J.A. and Turner, C.W., "An Experimental Study of Passive Parametric Interactions between Transverse Electron Beam Waves", J. Electronics and Control XV, 5, 479, November, 1963.

32. Lyon, J.F., "Electrohydrodynamic Kelvin-Helmholtz Instability", S.M. Thesis, E.E. Department, M.I.T., Cambridge, Mass. (1962).

33. Maxum, B.J. and Trivelpiece, A.W., "Two Stream Cyclotron and Plasma Wave Interactions", JAP Vol. 36, #2, February, 1965, pp. 481-494.

34. Melcher, J.R., Field Coupled Surface Waves, The M.I.T. Press, 1963.

35. Melcher, J.R., "An Experiment to Stabilize an Electromechanical Continuum", to be published in Trans. on Automatic Control, I.E.E.E.

36. Melcher, J.R., "Control of a Continuum Electromechanical Instability", Proc. I.E.E.E., May, 1965, 53, 5, 460-473.

37. Michael, D.H., Proc. Cambridge Phil. Soc. 51, 528 (1955).

38. Middleman, S. and Javis, J. "Transverse Wave Motion on a Thin Capillary Jet of a Viscous Liquid", Phys. Fluids, Vol. 8, No. 2, p. 222, February, 1965.

39. Morse, P.M. and Feshbach, H., Methods of Theoretical Physics, McGraw-Hill, (1953).

40. Nayyer, N.K. and Murtz, G.S., "The Stability of a Dielectric Liquid Jet in the Presence of a Longitudinal Electric Field", Proc. Phys. Soc. 75. 369 (1960).

41. Nayyer, N.K. and Trehan, S.K., "Oscillations of a Capillary Jet of Finite Electrical Conductivity in the Presence of a Uniform Axial Magnetic Field", Phys. Fluids 6 11, 1587, November, 1963.

42. Northrop, T.G., Phys. Rev. 103, 1150 (1956).

43. Pierce, J.R., Traveling Wave Tubes, Van Nostrand, 1950, Chapter 4.

44. Sen, A.K., "Stability of Hydromagnetic Kelvin Helmholtz Discontinuity", Phys. Fluids, 6, 8, 1154 (August, 1963).

45. Shapiro, A., The Dynamics and Thermodynamics of Compressible Fluid Flow, Vol. 1, Ronald Press, 1953.

46. Steutzer, O.M., "Magnetohydrodynamics and Electrohydrodynamics", Phys. Fluids 5, 534 (1962).

47. Stix, T.H., The Theory of Plasma Waves, McGraw-Hill (1962).

48. Stoker, J.J., Water Waves, Interscience Publishers, Inc., (1957).

49. Taylor, G.I. and McEwan, A.D., "The Stability of a Horizontal Fluid Interface in a Vertical Electric Field", J. Fluid Mech. 22, 1, 1-15 (1965).

50. Taylor, G.I., "The Dynamics of Thin Sheets of Fluid", Proc. Royal Soc. A253, 289 (1959).

51. Wessel-Berg, T., "A General Theory of Klystrons with Arbitrary, Extended Interaction Fields", ML Report No. 376, Lab. of Phys., Stanford University, March, 1957.

BIOGRAPHY

The author was born in Philadelphia, Pennsylvania in 1932. After graduating from the Roxborough High School in 1950, he studied at the University of Pennsylvania on a Philadelphia Board of Education Scholarship and received a BA in Physics in 1954. While in school, he captained the varsity golf team and was a member of Pi Mu Epsilon.

After four years of employment with the DuPont Company, he returned to The More School of Electrical Engineering of the University of Pennsylvania and received an MSEE in 1960. Summer employment included the Autonetics Division of North American Aviation and the Missile and Space Vehicle Division of the General Electric Company. In 1960, he entered MIT, and assumed the duties of Research Assistant, Research Laboratory of Electronics, and Instructor of Electrical Engineering. He received an award for teaching in 1964 and is a member of Tau Beta Pi, Sigma Xi, and the A.P.S.

He is married to the former Barbara Mitchell of Sharon Hill, Pennsylvania and has two daughters and a son.